

# **Development of biomarkers for the risk stratification and targeted therapy of Barrett's oesophagus and oesophageal adenocarcinoma**

---

**Mohammed Adil Butt**

**A thesis to be submitted in fulfilment of the requirements for  
the degree of Doctor of Philosophy**

**(Ph.D.)**

**2018**

**Research Department of Tissue and Energy**

**Division of Surgery and Interventional Science, UCL**

## Statement of originality

I, Mohammed Adil Butt confirm that the work in this thesis is my own and that this thesis has not been submitted for a higher degree to any other University or institutions. Where assistance has been required and when work has been carried out with others, this will be acknowledged below. Where information has been derived from other sources, I confirm that this has been indicated in the thesis.

Professor Laurence Lovat reviewed all aspects of my thesis and its development. He was directly involved in the selection of patients and their consent through his various research studies that enabled the collection of biomarker material. I was further assisted in the selection of patients, their consent and with tissue acquisition by my friend and colleague Dr Rehan Haidry.

Professor Marco Novelli reported the human and animal slides immunostained in this thesis with Dr Manuel Rodriguez-Justo. He additionally signed off the DNA cytometry work which was first analysed automatically using computer software and by myself. The DNA cytometry preparation was primarily done with and under the supervision of Dr Dahmane Oukrif. Professor Novelli and Mr Dahmane Oukrif supervised the optimisation of my immunohistochemistry experiments, and the direction they took, particularly with the mucin glycoprotein-1 antibodies where this thesis initially began. Dahmane also primarily conducted the clinical image cytometry experiments which I then collated and analysed in this thesis. Image cytometry is part of the service he offers. Later experiments when the techniques had been optimised and upscaled were carried out by myself with the assistance of our research technicians Mr Saif Khan and Mr Ignazio Puccio when the workload was particularly intense. Mr Ignazio Puccio also supervised and conducted the in vivo immunohistochemical studies detailed in chapter 7. Some CT2 antibody slides were kindly immunostained with the paid assistance of Mr Mohammed Rashid using his established protocols. Later these experiments were repeated by me and further optimised with the assistance of Mr Saif Khan. I am grateful

for the advice from Professor Dallas Swallow (UCL) who originally suggested on the selection of the antibody CT2 and helped me acquire it from her collaborator Professor Sandra Gendler (Mayo Clinic, USA) for this section of the experiments.

Immunostaining of replication licencing factors for the prediction of aneuploidy were re-optimised on a small number of slides using the automated immunostaining Leica BOND max platform by Mr Colin Tristram's team in Leica Biosystems, Newcastle after my initial benchtop immunohistochemical studies. The majority of slides were then immunostained on the Leica BOND max platform in UCL Advanced Diagnostics facilities under the guidance of Mr Michael Gandy (UCL-AD Laboratory Manager). Mike conducted the HER2 in situ hybridisation experiments, the data from which I collated and analysed. Furthermore, without his permission to allow me access into the clinical histology facilities, often very late in the evening, much of the immunohistochemistry and image analysis data would not have been feasible. The laser capture dissection experiments were performed by Dr Jason Dunn with the assistance of Mr Dahmane Oukrif.

Mr Haroon Miah kindly assisted with processing the paperwork for consent and with the financial management of the grants we were awarded through the experiments in my thesis.

Dr Mahendra Deonarain and Dr Ioanna Stamati assisted with the guidance and supervision of photochemistry experiments conducted in this thesis. Dr Gokhan Yahiloglu provided the photosensitisers used for these experiments and supervised their handling.

Dr Hayley Pye was the main scientist supervising my training in flow cytometry, confocal studies and had a major role in undertaking the development of the antibody drug conjugate photochemistry and photophysical studies. These experiments were part of a grant that required a small team of people full time to undertake the amount of work required. The photochemistry studies in Chapter 6 were further assisted by, Ms

Halla Reinert, our laboratory technician. Without this collaborative effort, these experiments would not have been possible to meet the objectives of our grant.

The flow cytometry facility used to acquire the data was managed by Tomas Adejumo (Wolfson Institute, University College London, UK). The laser and light delivery systems were loaned from Antikor BioPharma and calibrated using equipment from Sandy (Dr Charles A. Mosse) (University College London, UK).

Datasets where gene expression had been published from patients with normal squamous oesophageal epithelium, Barrett's epithelium and oesophageal adenocarcinoma were identified. Microarray data was then extracted from Gene Expression Omnibus. Gene set enrichment analysis (GSEA), pathway analysis and microarray data mining using this data was then conducted by Dr Rifat Hamoudi.

Digital image analysis algorithms were trained by myself after initial tuition on the method by Dr Marco Loddo. As the work in this section escalated, the scanning, processing and analysis of the slides was assisted by our gap year research technician Miss Eleanor Bloom.

In vivo studies were undertaken by and with our in vivo technician Dr Laura Funnel. Laura helped guide and perform most of the in vivo studies under my supervision and with my assistance. Without her help, these studies would not have been possible.

Dr Mohammed Adil Butt

## Acknowledgements

I will always be grateful to my first supervisor Dr Laurence Lovat who saw potential in me years ago, offering me the opportunity to work in his group and develop ideas to improve the outcomes of our patients with upper gastrointestinal cancer into a coherent story for this thesis. His astute guidance and critical appraisal both inside and outside of my studies has helped me develop into the researcher I have become.

I am indebted to my second supervisor Prof Marco Novelli for his guidance when difficulties arose, and conversations on life outside of the work environment, putting all the work carried out into perspective. Marco with Dr Manuel Rodriguez Justo, to whom I am also indebted, spent many afternoons of their free time to introduce me to the field of pathology and its crucial aspect within gastroenterology. My histology experiments would not have even started without my green fingered friend and colleague Mr Dahmane Oukrif. This was later supported by our research technicians Mr Saif Khan and Mr Ignazio Puccio who additionally carried forward projects spinning out from work undertaken in this thesis.

I am thankful to Dr Mahendra Deonarain, Dr Gokhan Yahioglu and Dr Ioanna Stamati Antisoma (previously PhotoBiotics). Deno and Gokhan are exceptional scientists and their approachable nature, generous personalities and astute guidance have been instrumental in the work described in this thesis. Without their collaboration, often at the eleventh hour, we would not have been awarded the research grants required to undertake the studies and spin off projects that developed from my thesis.

Dr Hayley Pye requires a special mention. I can still remember the day I met Hayley in the biochemistry building of Imperial College London. She was a PhD student at the time and I was completely new to the laboratory environment. Despite her own experiments and pressures, Hayley made the time to mentor me on how things worked in the laboratory, and how to conduct oneself as a scientist. Both were quite alien to me as a clinician but with her guidance I certainly learnt quickly! Her meticulous manner

and strict adherence to protocol was instrumental in enabling me to develop the scientific mindset needed to develop the experiments formulated in this thesis and troubleshoot when things didn't often go to plan. I will forever be appreciative for her friendship, patience and guidance.

In the same vein, I am grateful for the support, guidance and friendship of Dr Rifat Hamoudi. Rifat is a phenomenal scientist who seemed to produce Nature papers in his sleep during our time working together. There was rarely a month that went by without him helping another struggling clinician or scientist to take their experiments to another level. I am just waiting for the day I see him on the news for winning the Nobel prize or similar accolade which he thoroughly deserves.

I am forever grateful to Mr Michael Gandy, Head of UCL advanced diagnostics at the time, for his assistance, friendship and guidance on the business behind research and how to run an efficient laboratory service. Although 'RAMgen' didn't come to pass, I know Mike has carried his flame for entrepreneurship on after leaving research to work in industry.

I would like to thank Professor Marilena Louizidou, Royal Free Hospital, UCL and Professor Rhonda Souza, UT Southwestern Medical Centre, Texas USA and Dr Stuart McDonald and Dr Sebastian Zeki, Blizzard Institute, Bart's and the London School of Medicine for their kind gift of cell lines in this thesis. Mrs Noreen Farooqi requires a special mention for the many hours she spent teaching me cell culture and answering my late-night weekend calls when my cells became ill.

Although not directly involved in my experiments, I am grateful to all of the National Medical Laser Centre team who supported me with experiments in the labs, troubleshooting when issues arose, maintaining the laboratories we shared together and conversations outside of work, particularly during late evenings and weekends when it seemed the world was asleep. That is until someone from the team turned up at 3am to set up a cell kill! These include Dr Rehan Haidry, Dr Elnaz Yaghini, Dr

Josephine Woodhams, Dr Melissa Bovis, Dr Derick Kofi-Adigbli, Dr Ahmed Sultan, Dr Julie Tzu-Wen Wang, Dr Sandy Mosse, Dr Sinan Battah, Professor Sandy MacRobert and Professor Stephen Bown.

I thank Ms Faith Hanstater, Bloomsbury Campus Administrator for the division of surgery and Ms Nalini Singh, Rockefeller laboratory administrator in the Cancer Institute for their kindness, friendship and assistance in facilitating the logistics of conducting scientific experimentation in this thesis.

It is difficult to thank everyone involved in the development of my thesis but on a personal note, I must thank my parents Ali Mohommed Butt and Shamim Butt, and brother Mohammed Ashraf Butt for their endless encouragement, prayers and for willing for me to always strive for the best possible outcome no matter how difficult the task. Finally, I must thank my wife Aisha and children Akbar, Azhar, Ambar and more recently Umar, who gave me the inspiration to conduct these studies. Without Aisha's patience and support to persevere, particularly when everything seemed to be going wrong, none of this work would have been possible.

## Abstract

Barrett's oesophagus is the most important risk factor for the development of oesophageal adenocarcinoma (OA), but progression is unpredictable. Dysplasia predicts which Barrett's patients are at greatest risk for OA but achieving the diagnosis can be challenging. Immunohistochemistry with p53 is recommended as an adjunct to assist with dysplasia diagnosis. This thesis will examine if replication licensing factors and DNA ploidy status are as good if not better than p53 to assist in the diagnosis of dysplasia.

Overexpression of HER2 in foregut cancer is an indication for HER2 targeted treatments. Its influence on prognosis is less understood. The relationships between clinicopathological variables, HER2 overexpression and prognosis will next be evaluated.

Current ablative techniques for Barrett's neoplasia are limited to superficial disease. Photodynamic therapy was a treatment for Barrett's that could penetrate more deeply into diseased tissue but was limited by the side effects of off-target photosensitivity. Combining targeting vehicles such as antibodies to newer and more deeply penetrating photosensitiser drugs, may overcome the previous limitations of this technology.

A photosensitive ADC against HER2 will be created and its efficacy in vitro and in vivo evaluated. However, even the most effective ADC against HER2 will not treat the majority of cancers, as we will show HER2 is only expressed in the minority of foregut tumours.

The final experiments will look to characterise the mucin MUC1 in Barrett's and associated neoplasia. Studies have previously shown it to be present in up to 100% of cancers while others say far fewer. We will show proof of principle data for the development of a MUC1 targeting photosensitive ADC in vitro and postulate how it may in future enable treatment of locoregional invasive tumours endoscopically.



## Impact statement

The five-year survival rate for oesophageal cancer remains abysmal at <15% despite advances in treatment. This has led Cancer Research UK to highlight it as a top priority.

To perhaps impact this worrying statistic, this thesis will look to identify changes in the cells lining the gullet known as Barrett's oesophagus, the most important risk factor for the development of oesophageal adenocarcinoma. Barrett's oesophagus alone does not qualify a patient for treatment. Which patients will progress to cancer is also uncertain? At present, some patients are offered endoscopic surveillance to identify early neoplasia, though the evidence for surveillance is still being gathered.

Identification of tissue biomarkers that can be used to predict which patients with Barrett's are at risk of malignant progression, and which patients already have changes that put them at greater risk of cancer will be examined. In some circumstances, this may qualify patients for ablative endoscopic therapy earlier perhaps than they would have in current clinical practice.

Current ablative technologies limit therapy to superficial mucosal neoplasia.

Endoscopically delivered photodynamic therapy had potential to treat deeper into diseased tissue but its application was limited by unacceptable protracted side effects. More targeted photosensitising drugs could overcome these issues.

The next phase of this thesis will look to develop targeted tissue biomarkers as candidates for endoscopic therapy in oesophageal neoplasia. It will first examine the established biomarker HER2 for this aim, but later develop a first in class MUC1 targeting antibody drug conjugate and show proof of principle data of the potential for this approach. No other endoscopic modalities offer treatment for locally advanced esophageal neoplasia, which is what these targeted drugs may offer in the future.

## **Grant support**

Funding for this thesis was acquired from the UK government Technology Strategy Board (now called Innovate UK, project reference 101444) and Antikor Biopharma. Work was further supported by the CRUK UCL Experimental Cancer Medicine Centre and the Department of Health's National Institute for Health Research Biomedical Research Centre's funding scheme (Reference: C12125/A15576). The views expressed in this publication are those of the authors and not necessarily those of the Department of Health.

## Abbreviations

ADC	Antibody-Drug Conjugates
ADP	Antibody Directed Phototherapy
APS	Ammonium Persulphate
ARID1A	AT-rich interactive domain-containing protein 1A
ATCC	American Type Culture Collection
AUC	Area under the curve
BE	Barrett's Epithelium
BMI	Body mass index
BSA	Bovine serum albumin
BSG	British Society of Gastroenterology
C & M	Circumferential and mucosal
CBE	Complete Barrett's Excision
CDC	Cell division cycle
Cdk1	Cyclin-dependent kinase 1
CDT1	Chromatin licensing and DNA replication factor 1
CEA	Carcinoma-embryonic antigen
CELLO	Columnar epithelium lined lower oesophagus
CI	Confidence interval
CT	Cytoplasmic tail
D	Diffuse type
DAB	3,3'-Diaminobenzidine
DAPI	4',6-diamidino-2-phenylindole
DDISH	Dual-silver in-situ hybridisation
DI	DNA index
DIA	Digital Image Analysis
DMSO	Dimethyl Sulphoxide (a colourless solvent)
DNA CA	DNA content abnormalities
DPX	Distyrene Plasticizer Xylene
E	Extent
ECASP	European Society of Analytical Cellular Pathology
EDRN	Early Detection Research Network
EDTA	Ethylenediaminetetraacetic acid
EGFR	Epidermal Growth Factor Receptor
ER	Oestrogen receptor
EXPAND	Erbix in Combination with Xeloda and Cisplatin in Advanced Esophagogastric Cancer
F/DDISH	Fluorescent/Dual-silver in-situ hybridisation
FAB	Fragment antigen-binding
FACS	Fluorescence-activated cell sorting
FCS	Foetal calf serum
FDA	US Food and Drugs Administration
FFPE	Formalin fixed paraffin embedded
FISH	Fluorescent in-situ hybridisation
FITC	Fluorescein isothiocyanate
FOX F1	Forkhead box F1
FOX M1	Forkhead box M1

G	Geminin
GI	Gastrointestinal
GOJ	Gastro-oesophageal junction
GORD	Gastro-oesophageal reflux disease
GSEA	Gene Set Enrichment Analysis
HATU	1-[Bis(dimethylamino)methylene]-1H-1,2,3-triazolo[4,5-b] pyridinium-3-oxid hexafluorophosphate, N-[(Dimethylamino)-1H-1,2,3-triazolo[4,5-b] pyridin-1-ylmethylene]-N-methylmethanaminium hexafluorophosphate N-oxide. A reagent used in peptide coupling chemistry to generate an active ester from COOH
H&E	Haematoxylin and eosin
HCL	Hydrochloric acid
HER2	Human Epidermal Growth Factor Receptor 2
HGD	High grade dysplasia
HH	Hiatus hernia
HPP1	Hyperplastic polyposis 1 gene
HT-29	Colon cancer cell line
HuHMFG1	Humanised Human Milk Fat Globule 1
I	Intensity
IC	Image capture
IC50	Concentration required to reduce cells by half
IFD	Indefinite for dysplasia
IHC	Immunohistochemistry
IM	Intestinal metaplasia
IMC	Intramucosal carcinoma
INT	Intestinal type
ISH	In-situ hybridisation
IWGCO	International Working Group for Classification of Oesophagitis
Ki-67	Protein encoded by MKI67 gene. The name Ki-67 is derived from the city of origin (Kiel) and the clone number in the original 96-well plate
L	Polo Like Kinase 1 (Leica)
LCM	Laser capture microdissection
LGD	Low Grade Dysplasia
LOH	Loss of heterozygosity
M	Polo Like Kinase 1 (Millipore)
M: F	Male to Female ratio
MCM	Mini chromosome maintenance proteins
MFI	Median fluorescence intensity
MHC	Major histocompatibility complex
MPF	Maturation-promoting factors
MTT	(3-(4,5- <a href="#">dimethylthiazol</a> -2-yl)-2,5-diphenyltetrazolium) A calometric assay to measure cell metabolic activity.
MUC1	Mucin 1
MUC1-CT	MUC1-cytoplasmic tail
NDBE	non-dysplastic Barrett's epithelium
OA	Oesophageal adenocarcinoma
OE19	Oesophageal adenocarcinoma cell line for gastroesophageal junction
ORC	Origin recognition complex
PBS	Phosphate buffered saline

PCR	Polymerase chain reaction
PDT	Photodynamic therapy
PLK1	Polo-like kinase 1
pre-RC	Pre-Replication Complex
PSA	prostate specific antigen
PVDF	Polyvinylidene difluoride
RLF	Replication Licencing Factors
ROC	Receiver Operator Curves
ROI	Region of interest
RPMI-1640	Roswell Park Memorial Institute - 1640 media
RUNX3	Runt-related transcription factor 3
scFv	Single-chain variable fragment
scFv	Single chain variable fragment
SCOPE1	Chemoradiotherapy with or without cetuximab in patients with oesophageal cancer
SD	Standard deviations
SDS-PAGE	Sodium dodecyl sulfate–polyacrylamide gel electrophoresis. A biochemical methods to separate charged molecules in mixtures by their molecular masses in an electric field.
SKOV3	Ovarian cancer cell line
STAT3	Signal transducer and activator of transcription 3
SURF	SURveillance vs RadioFrequency ablation for LGD
T	Total Allred score
TAA	Tumour associated antigens
TAT	Turn-around time
TBS	Tris-buffered saline
TBS-Tween	Tris-buffered saline with Tween 20
TCT	Fully human anti-HER2 single-chain Fv re-engineered with T7 tag on the C-terminus.
TCC	Tumour cell cluster
TCR	T cell receptors
TEMED	Tetramethylethylenediamine
TM	Total modified Allred
TM Allred	Total modified Allred
ToGA	Trastuzumab in combination with chemotherapy versus chemotherapy alone for treatment of HER2-positive advanced gastric or gastro-oesophageal junction cancer
TRA	tumour related antigen
Tris	Tris(hydroxymethyl)aminomethane
TSA	Tumour specific antigens
TSA	Tumour specific antigens
TSG	Tumour suppressor genes
UCH	University College Hospital
UK	United Kingdom
UKBOR	UK Barrett's Oesophagus Registry
US	United States of America
VNTR	Variable number of tandem repeats

## Contents

Statement of originality .....	2
Acknowledgements.....	5
Abstract .....	8
Impact statement .....	9
Grant support.....	10
Abbreviations.....	11
Contents .....	14
Tables.....	23
Figures .....	25
Chapter 1: Barrett's oesophagus .....	30
1.1. Barrett's oesophagus.....	31
1.2 Association of Barrett's with oesophageal adenocarcinoma and importance	32
1.3 Epidemiology and risk factors for Barrett's progression .....	33
1.3.1 Prevalence .....	33
1.3.2 Reflux .....	33
1.3.3 Age and sex .....	33
1.3.4 Ethnicity.....	34
1.3.5 Obesity .....	34
1.3.6 Helicobacter Pylori.....	35
1.3.7 Lifestyle factors; smoking, alcohol and diet.....	35
1.3.8 Endoscopic risk .....	36

1.4	Pathology .....	37
1.4.1	Oesophageal metaplasia .....	39
1.4.2	Dysplasia.....	40
1.5	Endoscopic classification of Barrett's.....	45
1.5.1	Prague C & M Criteria.....	45
1.5.2	Reporting Barrett's segments .....	45
1.6	Screening .....	46
1.6.1	Unsedated transnasal endoscopy.....	48
1.6.2	Wireless capsule endoscopy .....	50
1.6.3	Capsule sponge.....	52
1.7	Surveillance.....	55
1.8	Registries .....	56
1.9	Medical Management .....	57
1.9.1	The role of GORD.....	57
1.9.2	Proton pump inhibitor therapy.....	58
1.9.3	Bile acids .....	60
1.9.4	Pepsin .....	62
1.9.5	COX-2 .....	62
1.10	Endoscopic management.....	64
1.10.1	Photodynamic therapy .....	64
1.10.2	Radiofrequency ablation .....	67
1.10.3	Endoscopic Resection .....	70
1.11	Surgery .....	75

Chapter 2: Tissue biomarkers for the risk stratification and therapy of Barrett's neoplasia .....	78
2.1. Tissue biomarkers for progression in Barrett's oesophagus.....	79
2.2. DNA content abnormalities (aneuploidy and tetraploidy).....	81
2.3. Loss of tumour suppressor loci – p16 and p53.....	83
2.4. Epigenetic changes .....	85
2.5. Cell cycle biomarkers.....	86
2.5.1 Initiation of DNA replication (G1 phase): Pre-replication complex .....	86
2.5.2 Cyclins.....	87
2.5.3 Cell cycle biomarkers as a surrogate for DNA content abnormalities .....	88
2.6. Therapeutic biomarkers .....	92
2.6.1. Targeting and classification of Tumour Related Antigens .....	92
2.6.2. Diagnostic and prognostic role for TRA in abdominal malignancy.....	93
2.6.3. Human Epidermal growth factor Receptor 2 .....	94
2.6.4. Epidermal Growth Factor Receptor.....	95
2.6.5. The glycoprotein Mucin 1 .....	97
2.7. Summary .....	101
Chapter 3: Research aims and hypothesis.....	102
3.1. Overview of research aims and hypothesis.....	103
3.2. Risk stratification of Barrett's oesophagus .....	104
3.2.1. Is abnormal p53 the most accurate biomarker for dysplasia in BE? .....	104
3.2.2. Replication licencing factors as surrogates for DNA-CA .....	105
3.2.3. Biomarkers to predict neoplastic progression .....	106



3.2.4.	Field cancerisation of BE surrounding OA .....	106
3.3.	HER2 expression in the squamous-metaplasia-dysplasia-adenocarcinoma sequence .....	108
3.4.	Development of HER2 targeting Antibody Directed Phototherapy (ADP) for OA	108
3.5.	MUC1 as a therapeutic target for antibody directed therapy .....	109
3.6.	Development and characterisation of MUC1 targeting photoactive ADC.....	111
Chapter 4: Biomarkers associated with Barrett's risk of progression to oesophageal adenocarcinoma .....		112
4.1	Introduction.....	113
4.2	Materials and methods .....	116
4.2.1	Tissue specimens.....	116
4.2.2.	Microtome sequence .....	119
4.2.3.	Haematoxylin and Eosin staining.....	120
4.2.4.	Image cytometry.....	121
4.2.5.	Immunohistochemistry.....	124
4.2.6.	Protein expression profile analysis.....	127
4.2.7.	Laser capture microdissection .....	127
4.2.8.	Digital Image Analysis .....	128
4.2.9.	Statistical analysis .....	130
4.3.	Results .....	131
4.3.1.	Relationship between biomarkers and pathological grade.....	131
4.3.2.	Association between clinicopathological variables and dysplasia .....	135
4.3.3.	Association between clinicopathological variables and DNA content ...	140

4.3.4.	Are replications licensing factors overexpressed prior to dysplasia or cancer?	144
4.3.5.	Is polo-like kinase 1 upregulated in Barrett's progressors?	146
4.3.6.	Inter-observer agreement between pathologists reporting IHC biomarkers	148
4.3.7.	Audit of specialist clinical image cytometry service to identify relationship between predicted DNA CA and pathological grade	150
4.3.8.	Digital Image Analysis of immunostained slides	152
4.4.	Discussion	157
Chapter 5: Evaluation of the therapeutic biomarker HER2 and relationships with prognosis in oesophagogastric adenocarcinoma		
		164
5.1.	Introduction	165
5.2.	Materials and methods	166
5.2.1.	Tissue specimens and patient cohorts	166
5.2.2.	Immunohistochemistry	167
5.2.3.	In situ hybridisation	168
5.2.4.	Clinicopathological detail	170
5.2.5.	Statistics	171
5.3.	Results	172
5.3.1.	Analysis of HER2 protein expression and amplification	172
5.3.2.	Clinicopathological relationships with HER2 expression	173
5.3.3.	HER2 diagnostics and HER2 status relationships with survival	175
5.3.4.	Clinicopathological relationships with survival	178

5.3.5. Clinicopathological relationships with survival when stratified by HER2 status	179
5.4. Discussion	184
Chapter 6: Development of a HER2 targeting photoactive antibody drug conjugate against oesophageal adenocarcinoma	
6.1. Introduction	190
6.2. Materials and methods	192
6.2.1. Patient cohort	192
6.2.2. HER2 immunohistochemistry, and scoring	192
6.2.3. HER2 gene set enrichment analysis	193
6.2.4. Chemical synthesis of the photosensitiser Chlorin e6-anhydride (Ce6-Anhydride)	193
6.2.6. Cell culture	195
6.2.7. Flow cytometry	196
6.2.8. In vitro Photodynamic therapy (PDT)	196
6.2.9. In vivo mouse tumour model protocol	197
6.2.10. Pharmacokinetics and biodistribution of TCT-Ce6 and Ce6	198
6.2.11. HER2 immunohistochemistry, and scoring	198
6.2.12. T7 Immunohistochemistry	199
6.3. Results	199
6.3.1. HER2 protein expression as a biomarker in oesophageal adenocarcinoma	199
6.3.2. HER2 mRNA expression as a biomarker in oesophageal adenocarcinoma	202

6.3.3.	Production of the HER2 targeted phototherapy drug; TCT-Ce6.....	212
6.3.4.	Selective binding of TCT-Ce6 to HER2 positive oesophageal cells in vitro 214	
6.3.5.	Light dependent cytotoxicity of TCT-Ce6 in vitro.....	215
6.3.6.	Mouse xenograft model of human OA .....	218
6.3.7.	Pharmacokinetics and biodistribution of Ce6 and TCT-Ce6 in vivo .....	220
6.3.8.	Expression of HER2 in tumour and surrounding skin in vivo .....	223
6.3.9.	Development of laser parameters.....	225
6.3.10.	Effective photodynamic therapy using TCT-Ce6 in vivo .....	228
6.4.	Discussion .....	231
Chapter 7: Upregulation of MUC1 in the progression to oesophageal adenocarcinoma and therapeutic potential with a targeted photoactive antibody drug conjugate.....		
7.1.	Introduction.....	235
7.2.	Methods.....	237
7.2.1.	Gene set enrichment analysis.....	237
7.2.2.	Tissue panel .....	237
7.2.3.	Immunohistochemistry .....	238
7.2.4.	Cell culture .....	239
7.2.5.	Flow cytometry .....	240
7.2.6.	Confocal microscopy .....	240
7.2.7.	Production and characterization of HuHMFG1:PS1 .....	241
7.2.8.	Cytotoxicity studies.....	242
7.3.	Results .....	243
7.3.1.	Identification of MUC1 as a biomarker in the development of OA .....	243

7.3.2.	MUC1 glycoprotein tissue staining.....	247
7.3.3.	HuHMFG1 potential as a therapeutic antibody in living cells.....	256
7.3.4.	Development of HuHMFG1:PS1 antibody drug conjugate .....	258
7.3.5.	Cytotoxic efficacy of HuHMFG1:PS1 antibody drug conjugate.....	262
7.4.	Discussion .....	264
Chapter 8: Discussion and future experiments.....		268
8.1.	Future biomarker studies for the risk stratification of BE .....	269
8.1.1.	Validation of DNA-CA in the prediction of dysplasia.....	269
8.1.2.	Evaluation of serial RLFs in tissue samples from patients who have progressed during Barrett's screening.....	270
8.1.3.	Utility of targeting RLF to prevent malignant progression in Barrett's in high risk populations .....	270
8.1.4.	Validation of RLF immunohistochemistry results and investigation into the relationships between other recently established biomarkers of progression ....	270
8.1.5.	Expansion of DNA-CA clinical studies .....	271
8.1.6.	Digital Image Analysis .....	271
8.2.	Future studies for the translation of biomarkers targeting into clinical practice	273
8.2.1.	Future of HER2 targeting TCT-Ce6 .....	273
8.2.2.	MUC1 as a therapeutic target in OA .....	274
8.1.1.1.	Validation and completion of MUC1 characterisation studies .....	274
8.1.1.2.	Characterisation of HuHMFG1 internalisation kinetics.....	275
8.1.1.3.	Evaluation of serum tumour markers in MUC1 positive OA cancers.	275

8.1.1.4. Development of MUC1 targeted therapies against oesophageal adenocarcinoma .....	276
8.2.3. Summary .....	276
References .....	278

## Tables

Table 1: Modified Vienna classification of oesophageal dysplasia & neoplasia <sup>40</sup> .....	38
Table 2: Institution and population based Barrett's registries .....	57
Table 3: Summary of evidence for potential PPI-associated adverse effects <sup>95</sup> .....	59
Table 4: Indications for clinical evaluation of DNA content abnormalities. ....	83
Table 5: Functions of Geminin in cytokinesis <sup>208</sup> . ....	91
Table 6: Methods for tumour associated antigen creation in MUC1 and antibodies to detect them adapted from <sup>247,248</sup> .....	99
Table 7: Clinical projects providing tissue for biomarker research.....	117
Table 8: Patient cohorts and characteristics.....	119
Table 9: Summary of immunohistochemical antibodies evaluated .....	126
Table 10: Relationship between biomarker expression and pathological grades.....	132
Table 11: Relationship between biomarker expression and dysplasia.....	137
Table 12: Sensitivity and specificity analysis of PLK-1 (Millipore) and PLK-1 (Leica) to identify optimum Allred cut off to predict DNA content abnormalities.....	138
Table 13: Univariate and multivariate analysis of association between clinicopathological variables and DNA content abnormalities.....	141
Table 14: Sensitivity and specificity analysis to identify optimum Allred cut off to predict DNA content abnormalities. ....	142
Table 15: Comparison of pathologist reported Allred and extent sub scores with percentage immunohistochemical staining with digital image analysis.....	154
Table 16: Comparison of pathologist reported tissue grade with percentage of positive immunohistochemical staining with digital image analysis. ....	155
Table 17: Relationship between pathologist and DIA intensity scores.....	156

Table 18: Relationship between HER2 expression and gene amplification .....	172
Table 19: HER2 expression association with clinicopathological variables .....	174
Table 20: Oesophagogastric cancer survival over time .....	175
Table 21: HER2 diagnostic variables in relation to progression free and overall survival of oesophagogastric cancer.....	177
Table 22: Clinicopathological variables relation to progression free and overall survival of esophagogastric cancer when stratified by HER2 status.....	179
Table 23: Clinicopathological variables influence on PFS and OS of esophagogastric cancer when stratified by HER2 status. ....	180
Table 24: Clinicopathological variables associated with progression free and overall survival and influence on HER2 positive and negative oesophagogastric cancer.....	182
Table 25: Study compliance with REMARK guidelines .....	183
Table 26: Gene Set Enrichment Analysis (GSEA); pathways enriched between normal tissue and OA .....	204
Table 27: Gene Set Enrichment Analysis; pathways enriched between normal tissue and Barrett's oesophagus .....	208



## Figures

Figure 1: Haematoxylin and Eosin stain of Barrett's oesophagus (x10 magnification) .	31
Figure 2: Factors associated with progression from Barrett's to oesophageal cancer.	32
Figure 3: Representation of pathological changes in progression to cancer <sup>41</sup> .	39
Figure 4: Haematoxylin & eosin stain of low grade dysplasia in BE (x10 magnification) .....	41
Figure 5: Haematoxylin & eosin stain of high grade dysplasia in BE (x10 magnification) .....	44
Figure 6: Representation of Prague C & M scoring system showing C2M5 segment. .	45
Figure 7: Paris classification system for visible lesions <sup>60 - 61</sup> .	46
Figure 8: Systems of transnasal endoscopy versus conventional endoscopy to visualise Barrett's epithelium <sup>68</sup> .....	50
Figure 9: Capsule sponge <sup>78</sup> .....	53
Figure 10: UK RFA treatment protocol for Barrett's neoplasia <sup>149</sup> .....	69
Figure 11: Radiofrequency ablation of Barrett's dysplasia with HALO <sup>360</sup> device .....	70
Figure 12: Steps involved in endoscopic resection of Barrett's dysplasia .....	72
Figure 13: The two step method for circumferential EMR for BE to prevent stricture development <sup>161</sup> .....	75
Figure 14: Early Detection Research Network Phases of biomarker discovery <sup>169</sup> .....	79
Figure 15: Epidemiological factors and key biomarkers interplay in the squamous to oesophageal adenocarcinoma sequence <sup>170</sup> .....	80
Figure 16: Genetic model of progression of Barrett's oesophagus to cancer <sup>171</sup> .....	81
Figure 17: p53 immunostaining patterns in Barrett's epithelium .....	85
Figure 18: Representation of Cyclin levels during cell cycle <sup>198</sup> .....	88

Figure 19: Phase specific distribution of cell-cycle biomarkers <sup>201</sup> .....	89
Figure 20: Geminin localisation during human mammary epithelial cell cycle. ....	92
Figure 21: (A) Median overall and (B) progression-free survival in the primary analysis populations (Trastuzumab + chemotherapy vs chemotherapy alone) of Phase III ToGA trial. <Adapted from <sup>229</sup> >.....	95
Figure 22: Structure of MUC1 receptor <sup>246</sup> .....	98
Figure 23: Intensity and extent thresholds for Allred scoring system <sup>261</sup> .....	107
Figure 24: Typical histograms from tissues with normal diploid DNA content (A), and abnormal aneuploid (B) and tetraploid (C) content.....	123
Figure 25: Immunohistochemical expression of antibodies evaluated.....	126
Figure 26: Laser capture microdissection within OA resection specimens <sup>197</sup> .....	128
Figure 27: Scatter plots of biomarker expression across pathological grades. ....	133
Figure 28: Collage of PLK1-M (A) and Geminin (B) immunostaining showing pattern of increasing nuclear positivity in the progression to oesophageal cancer .....	134
Figure 29: ROC curves (A), sensitivity and specificity of significant biomarkers on UV analysis with Allred >3 defining PLK-1 positivity (B). ....	139
Figure 30: ROC curves of biomarkers identified to be predictive of DNA content abnormalities on univariate analysis. ....	143
Figure 31: Field cancerisation influencing biomarker expression in BE next to OA ...	145
Figure 32: PLK-1 expression in BE progressors versus non-progressors .....	147
Figure 33: PLK1 immunostained slide highlighting HGD in selected Region of Interest (ROI) of at low (x2.5) and higher (x10) power .....	149
Figure 34: Bland-Altman plot showing inter-observer agreement of PLK1-M (A) and PLK1-L (B) reporting of pathological grade .....	149

Figure 35: Distribution of pathology in patients found to have DNA CA (A) and in those with normal content (diploid cases) (B). .....	151
Figure 36: Distribution of relationship between DNA CA and incremental pathological grades in the large UCLH cohort of patients referred for image cytometry. ....	151
Figure 37: Examples of digital image analysis mask produced by Ariol software analysis of Barrett's. ....	153
Figure 38: HER2 positive oesophagogastric adenocarcinoma showing characteristic lateral and complete membrane staining (brown) with 3+ intensity. ....	168
Figure 39: Dual-silver in-situ hybridisation (DDISH) schematic showing HER2 and CEP17 gene copy numbers in normal squamous oesophagus (A) and a HER2 amplified oesophageal tumour (B). ....	170
Figure 40: Progression free survival (A) and overall survival (B) of oesophagogastric cancer Kaplan Meir curves stratified by HER2 status.....	176
Figure 41: Scatterplot correlating CEP17 copy number and overall survival. ....	176
Figure 42: Influence of lymphatic infiltration (A & B), tumour stage (C&D) and age (E & F) on overall survival when stratified by HER2 status. ....	181
Figure 43: Heterogeneous HER2 immunohistochemistry in the progression to OA... 201	
Figure 44: Gene set enrichment analysis (GSEA) and microarray analysis of HER2 in the progression to oesophageal cancer (OA).....	202
Figure 45: Binding of TCT to HER2 in a panel of cell lines derived from gastric adenocarcinoma (A), OA (B), squamous oesophagus (C) and BE (D) in vitro.....	212
Figure 46: Ce6 pre-activated to form an anhydride ring between two carboxyl groups. ....	213
Figure 47: Analysis of purity and photo-physical spectral properties of TCT-Ce6.....	214
Figure 48: Selective binding of TCT-Ce6 to HER2 positive OA compared to HER2 negative normal oesophagus in vitro.....	215

Figure 49: Dose and light dependent PDT cytotoxicity of TCT-Ce6 compared to free drug on HER2 positive oesophageal cells (OE19). .....	217
Figure 50: Characterisation of a HER2 positive mouse flank xenograft model of OA. ....	219
Figure 51: Biodistribution of free Ce6 at various timepoints after I.V injection .....	221
Figure 52: IHC distribution of TCT-Ce6 in tumour and overlying skin at 4 hours. ....	224
Figure 53: Optimisation of laser dose after fixed injection of TCT-Ce6 vs saline control .....	225
Figure 54: Effect and tolerability of repeated PDT 10 days apart at 24hour vs 72hour drug light intervals.....	226
Figure 55: Optimisation of drug-laser interval & tolerance to weekly PDT on 3 occasions.....	227
Figure 56: Effect of TCT-Ce6 PDT on OE19 subcutaneous flank tumours in vivo; individual animal data (A) and tumour HER2 characterisation at endpoint (B). .....	228
Figure 57: Tumour growth arrest in vivo after PDT treatment using TCT-Ce6 on OE19 subcutaneous flank tumours. ....	230
Figure 58: Gene set enrichment analysis highlighting pathways during development of Barrett's oesophagus (A) and oesophageal adenocarcinoma (B) from normal squamous oesophagus and the involvement of MUC1 within them.....	244
Figure 59: Gene set enrichment and microarray analysis of MUC1 in the progression to esophageal adenocarcinoma. ....	246
Figure 60: Representation of MUC1 receptor structure in normal and tumour epithelium with binding sites for selected antibodies. ....	248
Figure 61: IHC staining patterns with anti-MUC1 antibodies in high grade dysplasia and HuHMF1 staining in the squamous-metaplasia-dysplasia-carcinoma sequence.....	249
Figure 62: Levels of expression of four MUC1 epitopes in the squamous-metaplasia-dysplasia-carcinoma sequence.....	251

Figure 63: Scatter plot depicting IHC expression of four MUC1 epitopes in the esophageal squamous-metaplasia-dysplasia-carcinoma sequence scored by Allred. .....	252
Figure 64: HuHMFG1 immunostaining optimised to achieve tumour selectivity. ....	253
Figure 65: HuHMFG1 staining MUC1 in invasive esophageal adenocarcinoma and locoregional lymph node metastases. ....	255
Figure 66: MUC-1 expression in oesophageal cell lines of various pathological grades and internalisation into esophageal adenocarcinoma.....	257
Figure 67: Photophysical characterisation of photoactive MUC1 targeting antibody drug conjugates. ....	259
Figure 68: Internalisation and sub-cellular localisation of photoactive MUC1 targeting antibody drug conjugates.....	261
Figure 69: Light dependent cytotoxicity and superior efficacy over equivalent free photosensitiser of a MUC1 specific photoactive antibody drug conjugate. ....	263

# Chapter 1: Barrett's oesophagus

---

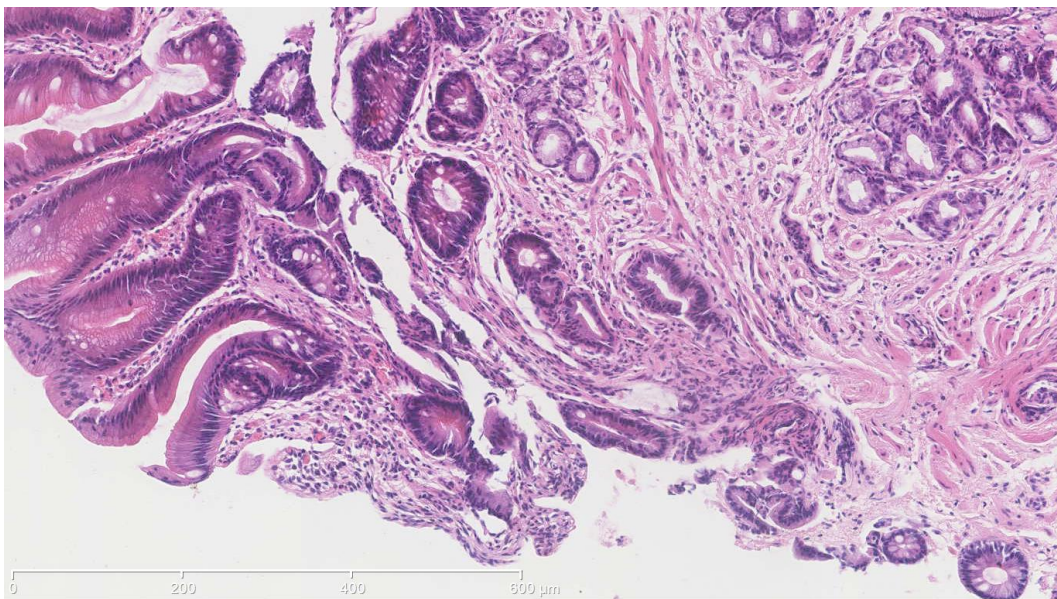
## 1.1. Barrett's oesophagus

Barrett's oesophagus has been given many names over the years reflecting the controversies in its definition including Barrett's epithelium (BE), Barrett's syndrome, columnar lined oesophagus and columnar epithelium lined lower oesophagus (CELLO). The most recent definition taken from the 2013 UK guidelines on the management of Barrett's <sup>1</sup>:

"Barrett's oesophagus is defined as an oesophagus in which any part of the normal distal squamous epithelium lining has been replaced by metaplastic columnar epithelium, which is clearly visible endoscopically above the gastro-oesophageal junction and confirmed histopathologically from oesophageal biopsies".

Established international guidelines from the American Gastroenterological Association have required intestinal metaplasia (IM) for Barrett's diagnosis <sup>2</sup>. IM is not required to define BE in the UK, but it does impact on surveillance <sup>3</sup>.

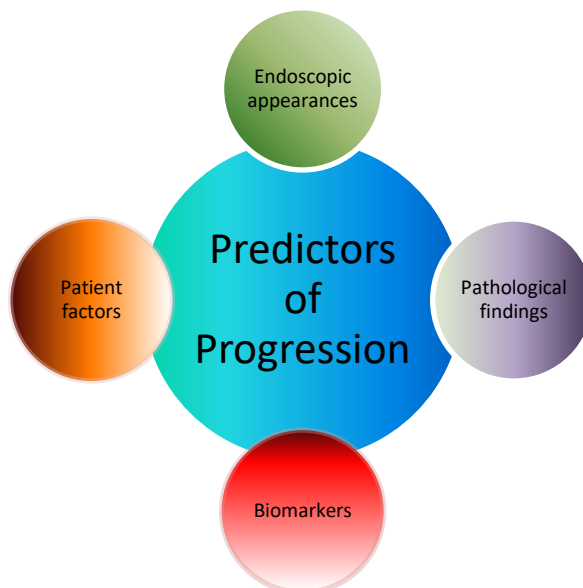
**Figure 1: Haematoxylin and Eosin stain of Barrett's oesophagus (x10 magnification)**



## 1.2 Association of Barrett's with oesophageal adenocarcinoma and importance

BE is a premalignant change in the oesophagus and increases the risk of developing oesophageal adenocarcinoma (OA) 30-100 fold above that for the general population<sup>4,5</sup>. It is thought 64-86% of all OA's arise in BE<sup>6,7</sup> (6,7) and meta-analyses from UK and US data suggest the risk of progression of BE to oesophageal or cardia cancer to be 0.22-0.33% per patient-year<sup>8-10</sup>. Sub-group analysis revealed lower risk in those with short-segment BE (considered to be <3cm length) at 0.19% per year<sup>9</sup>, and in those without IM at index biopsy the risk was only 0.07% per year<sup>10</sup>. OA is the 4<sup>th</sup> leading cause of cancer related mortality in men in the UK and fifth when considering both sexes together<sup>11</sup>. Identifying which patients with BE progress is of vital importance as despite progress in other cancers, the 5-year survival of OA once it develops remains abysmal at under 14%<sup>12</sup>

**Figure 2: Factors associated with progression from Barrett's to oesophageal cancer.**





## **1.3 Epidemiology and risk factors for Barrett's progression**

### **1.3.1 Prevalence**

The prevalence of BE reported in the Swedish population was found to be 2.3% in heartburn sufferers and 1.2% in non-sufferers <sup>13</sup>, however this is likely to be an underestimate of the UK burden of disease as the reported prevalence rates of BE is lower in Northern Europe than it is in the UK .

### **1.3.2 Reflux**

The association between BE and gastroesophageal reflux disease (GORD) has been recognised for many years <sup>14</sup>. The presence of both typical GORD symptoms (heartburn or acid regurgitation) and more frequent symptom episodes, are independent predictors of BE <sup>15</sup>. Reflux of gastric contents is not the only precursor to BE, duodenal reflux is also thought to contribute. This has been shown through the development of BE in individuals post-gastrectomy and through detailed analysis of the refluxate reaching the oesophagus <sup>16</sup>.

BE is found in 5-15% of patients investigated for this symptoms of (GORD), and GORD itself occurs in one fifth of the general population. However, only half of patients with short segment BE have symptoms of GORD <sup>17</sup> again suggesting BE to have a larger population prevalence when added to the unsuspecting asymptomatic population.

### **1.3.3 Age and sex**

BE and OA predominantly affect middle-aged males. In an analysis of 5317 BE patients from the UK Barrett's Oesophagus Registry (UKBOR), the M: F ratio of BE patients was 1.7. BE was also found to present at an earlier age in men (62.0 years) than in women (67.5years), and the incidence peaked at 60–69 years in males and 70–79 years in females. OA rates showed a similar trend with a lower mean ages at diagnosis in men (64.7 years) than in women (74.0 years) <sup>18</sup>.

Men with BE are also twice as likely to progress to OA than women. In a large study of 8522 cases from the Northern Ireland with 16 years' follow-up, the rate of progression to OA in men was 0.28% per year versus 0.13% per year in women. When the age of these patients was examined by category to identify if it too is a risk factor for progression, the highest rate of progression appeared in the 60- to 69-year age range (0.33% per year), and the lowest rate in patients younger < 50 years (0.12% per year)<sup>19</sup>.

### **1.3.4 Ethnicity**

BE is most prevalent in Caucasian males. It is less common in Asian countries and rare in the Caribbean, the Middle East, and much of Africa and South America. The reasons behind this are unclear, but ingestion of a high-fat western diet, and possibly oral and salivary carcinogens that are activated in the region of the gastroesophageal junction, may all play a role<sup>20</sup>.

### **1.3.5 Obesity**

Obesity, defined by body mass index (BMI) >30, is known to be strongly associated with both BE and OA<sup>20,21</sup>. Male pattern of abdominal obesity is a stronger risk factor than total body obesity (as measured by BMI) for both BE and OA<sup>22</sup>. The mechanisms behind this increased risk include the mechanical promotion of GORD in obesity, confounding factors in the behaviour of obese individuals that promote GORD and the carcinogenic properties of pro-inflammatory circulating adipokines. Furthermore, large scale studies support the relationship between increasing BMI and OA risk independently of GORD<sup>23</sup>.

Evidence to support the role of obesity on progression in BE is however limited. A case-controlled study did show a positive correlation<sup>24</sup>, however this was not confirmed by other studies<sup>22</sup>. A cross-sectional study examining association between abdominal fat and biomarkers of progression has shown some association<sup>25</sup>. Current evidence

therefore does not definitively suggest a role of obesity in progression, but the limited data does infer biological plausibility.

### **1.3.6 *Helicobacter Pylori***

*Helicobacter pylori* is known to promote the development of gastritis. The potential role for *H. pylori* in the development of BE and OA however is controversial. It is postulated that individuals with chronic *H. pylori* associated gastritis have reduced gastric acid production. The acidity of BE generating refluxate is subsequently reduced in turn. A recent meta-analysis supported this inverse association in BE when compared with endoscopically normal controls <sup>26</sup>.

### **1.3.7 *Lifestyle factors; smoking, alcohol and diet***

Smoking is known to be associated with OA <sup>27</sup>. The stage at which the smoking plays a critical role, whether in the pathogenesis of BE or conversion from BE to OA, is less certain. Using multivariate analysis, one group conducted a meta-analysis of 5 case-controlled studies comparing 1059 BE patients with 1332 with GORD and 1143 population-based controls. Subjects with BE were found to be significantly more likely to have smoked cigarettes than population controls (odds ratio [OR]=1.67; 95% confidence interval [CI], 1.04–2.67) or GORD controls (OR=1.61; 95% CI, 1.33–1.96) <sup>28</sup>. In a more recent study of 259 BE patients with 2 separate control groups, no significant association was found between BE and various measures of smoke exposure. The group further commented that there was no association between BE and alcohol either. Conversely, moderate alcohol intake (14 – 28 drinks/week) was associated with lower risk <sup>29</sup>.

A review of existing epidemiological studies on dietary factors reported an inverse relationship between intake of vitamin C,  $\beta$ -carotene, fruits and vegetables (particularly raw fruits and dark green, leafy and cruciferous vegetables), carbohydrates, fibre and iron and the risk of OA and BE <sup>30</sup>. It is therefore inferred that people at higher risk for

BE and OA may benefit from increasing consumption of fruits and vegetables and reducing red meat and processed food intake.

### **1.3.8 Endoscopic risk**

#### 1.3.8.1 Length of Barrett's

The association between length of BE segment and progression has been studied extensively. Retrospective studies first inferred a risk of longer BE segments and risk of OA on multivariate analysis; however, studies were biased by inclusion of cases with prevalent high grade dysplasia or OA <sup>31,32</sup>. Prospective studies supported this role reporting risk of development of OA to increase with increasing length of BE <sup>19,33,34</sup>. Opposing views have however been voiced by others when adjusting for histology at study entry <sup>8,35</sup>.

Despite conflicting data in the literature, the consensus of opinion in the UK drawn together in writing the recent UK guidelines for the management of BE favour the positive correlation between BE length and cancer risk, siting length of BE as a grade B recommendation to decide on surveillance regimens <sup>1</sup>.

#### 1.3.8.2 Nodularity and ulceration

It is generally accepted that visible nodules or ulcers at endoscopy within BE segments suggest increased risk. A retrospective study reported that visible lesions, defined as mucosal elevation 1cm or less in diameter (HR 2.6, 95% CI 1.2-5.4), increased risk of progression by x2.5 on multivariate analysis <sup>36</sup>. A cross sectional study meanwhile found that ulcers in HGD had a much higher prevalence of invasive OA than non-ulcerated HGD segments <sup>37</sup>. There is a paucity of data to report the risk of BE progression in patients without HGD or OA in the histology specimens. Therefore, while visible lesions do appear to infer increased risk, this may just reflect the prevalence of higher pathological grades in these regions.

### 1.3.8.3 Hiatus hernias

A large prospective study found HH >6cm in length predicted progression to HGD/OA on multivariate analysis <sup>34</sup>. This finding was supported by another large case-control study where HH was shown to be an independent predictor of HGD/OA on multivariate analysis <sup>32</sup>. HH length therefore does appear to correlate with increased risk of progression and may be explained by the increased severity of GORD in these patients. This is somewhat supported by long term studies in patients undergoing Nissen Fundoplication for GORD with BE, where regression of dysplasia was noted in 44% (7 of 16) <sup>38</sup> and 75% (6 of 8) <sup>39</sup> of patients in whom it was present prior to surgery. However, numbers were small and IM disappeared in only 14% (9 of 63) <sup>38</sup> making definitive conclusions difficult to draw.

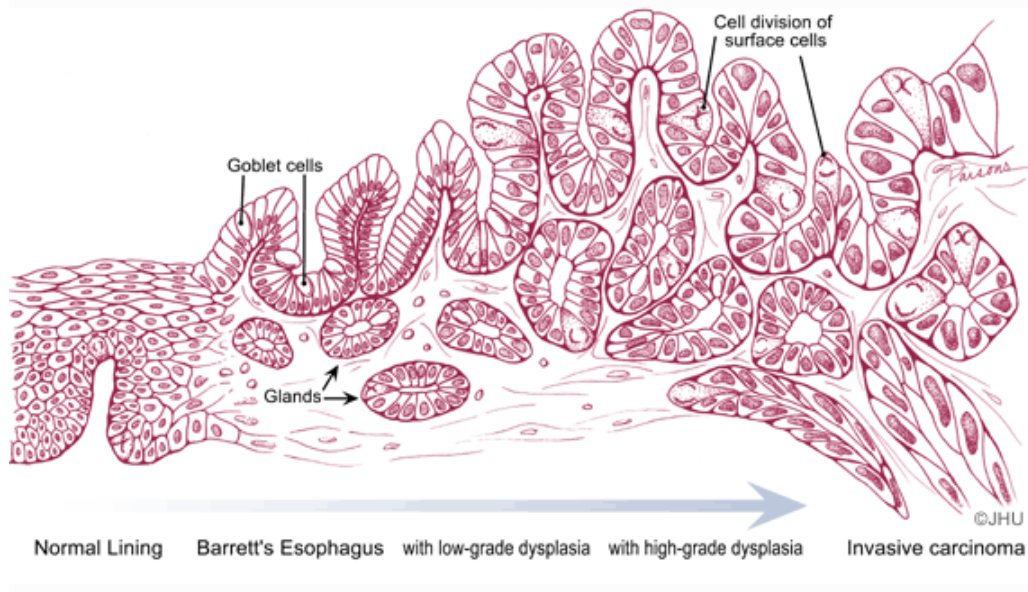
## 1.4 Pathology

Assessing the grade of pathology with BE remains the accepted standard to predict BE risk. Increasing degrees of pathology have been shown to have increasing risks of progression to OA. This is however partially based on the assumption that progression from BE to OA occurs in a regimented fashion via increasing degrees of dysplasia, but this may not always be the case (Table 1).

**Table 1: Modified Vienna classification of oesophageal dysplasia & neoplasia <sup>40</sup>.**

Category 1	No neoplasia
Category 2	Indefinite for neoplasia
Category 3	Low grade dysplasia
Category 4	High-grade neoplasia
4.1	High grade adenoma/dysplasia
4.2	Non-invasive carcinoma (carcinoma in situ)
4.3	Suspicion for invasive carcinoma
4.4	Intramucosal carcinoma
Category 5	Submucosal invasive carcinoma (carcinoma with invasion of the submucosa or deeper)

**Figure 3: Representation of pathological changes in progression to cancer** <sup>41</sup>.



#### **1.4.1 Oesophageal metaplasia**

Metaplasia is the process by which one fully differentiated cell type is replaced by another. In BE, the squamous epithelium that normally lines the oesophagus is replaced by a columnar type epithelium. Three types of metaplasia have been described:

1. Gastric fundic-type: characterised by mucus secreting, parietal and chief cells normally found in the stomach.
2. Cardia type: (also known as junctional type) is composed only of mucus secreting cells.
3. Intestinal type: (also known as specialised intestinal metaplasia and specialised columnar metaplasia) characterised by columnar epithelium that frequently contains goblet cells.

The reported risk of progression to OA from non-dysplastic BE has reduced over the years. Earlier publications over inflated the rates due to publication bias <sup>42</sup> (44). As detailed in section 1.2, more recent studies put the risk of progression between 0.22-0.33% per year <sup>9,10,43,44</sup>.

## **1.4.2 Dysplasia**

Despite decades of searching for a better biomarker, dysplasia remains the platform for risk stratification systems in BE <sup>1,2</sup>. It is defined as “unequivocal neoplastic epithelium strictly confined within the basement membrane of the gland from which it arises” <sup>45</sup>. Although this definition was initially proposed for premalignant changes which can develop in inflammatory bowel disease, it has been progressively extended to the entire gastrointestinal tract, including BE.

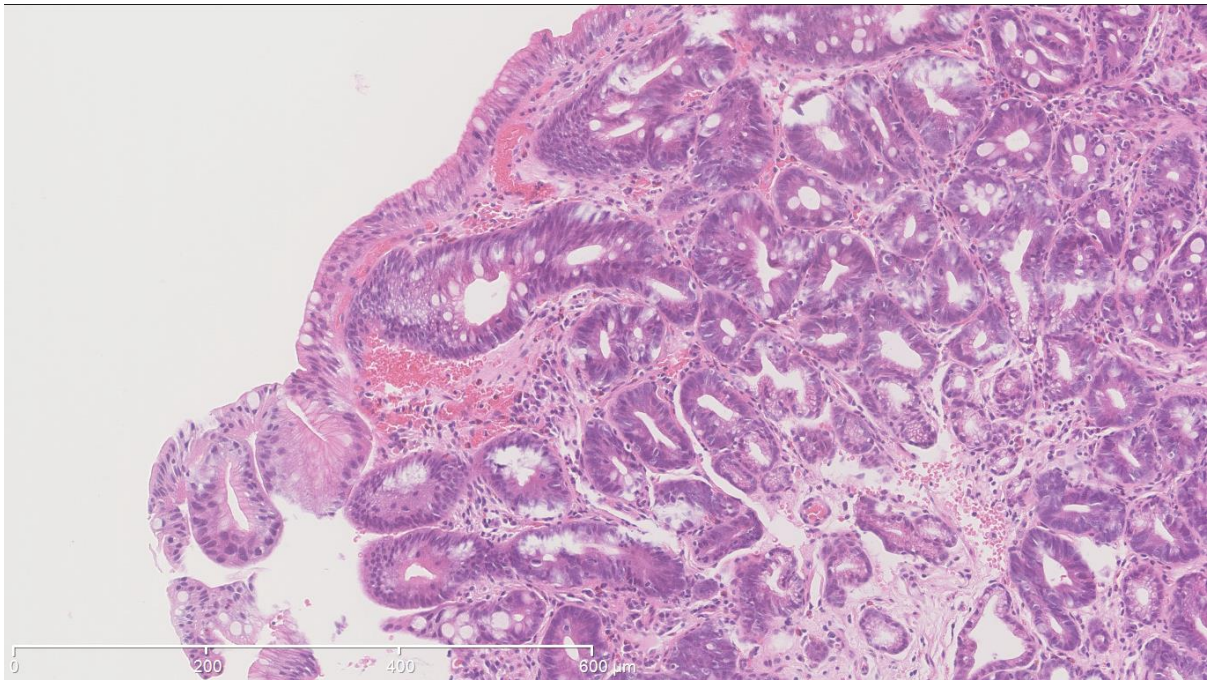
There are two types of classification system for dysplasia; a three tiered system grading dysplasia mild, moderate or severe and the more commonly used modified Vienna classification system, as shown above in Table 1 <sup>40,46</sup>.

### **1.4.2.1 Low grade dysplasia**

In low grade dysplasia, the glandular architecture of BE is preserved or minimally abnormal. Nuclei are typically elongated and crowded at the base cells. They may also be enlarged with mild to moderate hyperchromasia and irregular. Mitotic figures may be present at surface and surface villous transformation may be present.



**Figure 4: Haematoxylin & eosin stain of low grade dysplasia in BE (x10 magnification)**



The natural history of LGD remains unclear with reported risk of progression to cancer varying between 0.6 - 13.4% per patient year in surveillance cohorts <sup>47-52</sup>. One meta-analysis reported that the rate of progression from LGD to OA was 16.98/1000 person-years in comparison to 5.98/1000 person-years in patients with no dysplasia however the authors did comment on heterogeneity between the studies <sup>53</sup>. This compares to 0.3-0.6% for non-dysplastic BE <sup>49,53</sup>.

Uncertainty amongst pathologists around the diagnosis of LGD has led to the requirement in guidelines for at least 2 pathologists to concur when describing dysplasia, one of which who must have experience in gastrointestinal histology <sup>1,2</sup>. It has been shown that as the number of pathologists agreeing on a diagnosis of LGD increases, the cumulative rate of progression also increases in correlation. One study described as these proportions as 28% (1 pathologist only reporting LGD), 41% (2 pathologists in agreement) and 80% (if all 3 pathologists are in agreement) for the diagnosis of LGD <sup>47</sup>.

Uncertainty around cancer risk has led to debate about the advantages and disadvantages of treating low grade dysplasia, particularly with the advent of minimally invasive endoscopic therapies. Some argue that ablation of LGD is more cost effective than surveillance. One group used mathematical modelling to demonstrate that ablation is of significant benefit over surveillance in LGD management if it eradicates at least 28% of the LGD cases<sup>54</sup>. However, these models do not factor in the possibility and proportions of LGD cases that regress to a lower pathological grade.

Outcomes from the SURF (SURveillance vs RadioFrequency ablation for LGD) study in which 136 patients were enrolled across 9 centres found a significant reduction in progression to OA in the RFA group (1.5%, n=68) versus the matched control group (20.6%, n=68). Additionally, 53/54 (98%) treated patients showed no recurrence of BE post ablation. However, the results should be interpreted with caution as entry into the trial required approval and close agreement between a strict panel of specialist gastrointestinal pathologists with respect to the histological diagnosis. This protocol likely sub-selected a higher risk group of LGD cases from those routinely seen in clinical practice. In the trial itself, this led to only 25% of 503 initially referred LGD cases (graded by 2 pathologists; 1 specialised in gastrointestinal pathology) being admitted. This strict entry protocol reflected in the unusually high rate of progression in the LGD surveillance group at 20.6%, much higher than has previously been reported when compared with progressors in the RFA group. This bias skews the reported proportions of progressors in the therapy versus control arms (1.5% vs 20.6%) to increase the apparent magnitude of RFA effect against LGD<sup>55</sup>. This trial was pivotal in amending the UK British Society of Gastroenterology guidelines to recommend endoscopic therapy for LGD if confirmed by a specialist pathologist and on repeat endoscopy after review by the specialist MDT. Surveillance with 6-monthly endoscopy is now recommended if ablation is not undertaken<sup>56</sup>.

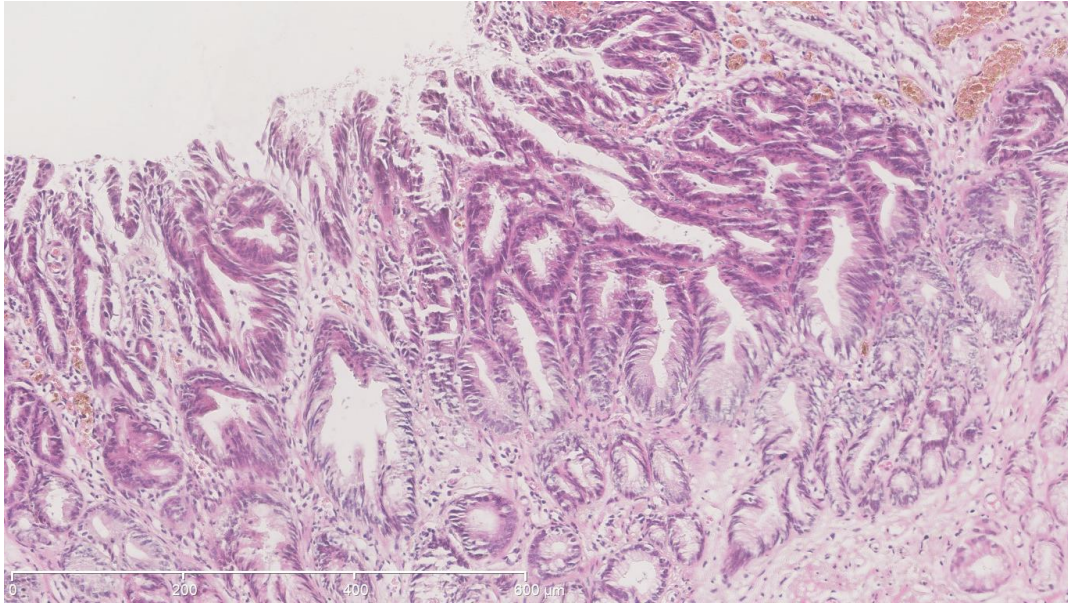
#### 1.4.2.2 High grade dysplasia

High-grade dysplasia (HGD) is characterised by distortion of the glandular BE architecture leaving the mucosal surface in a villiform configuration. Furthermore, dysplastic epithelium on the mucosal surface is required to have loss of nuclear polarity, rounding of the nuclei, and absence of a consistent inter-nuclear relationship of nuclei to each other to meet criteria for HGD.

HGD is the most important marker of cancer progression in BE. Its presence confers a 16-50% risk of progression to OA <sup>36,51,57</sup> within 5 years of the diagnosis. International guidelines therefore accept the presence of HGD as a definitive indication for therapeutic intervention <sup>1,2</sup>. There are several minimally invasive treatment options delivered through the endoscope to treat HGD, however most have now been overtaken by radiofrequency ablation by centres as the therapeutic modality of choice

58

**Figure 5: Haematoxylin & eosin stain of high grade dysplasia in BE (x10 magnification)**



In the UK, guidelines recommend HGD to be managed in the same way as BE related OA confined to the mucosa (intramucosal adenocarcinoma=IMC). It is recommended that <sup>1</sup>:

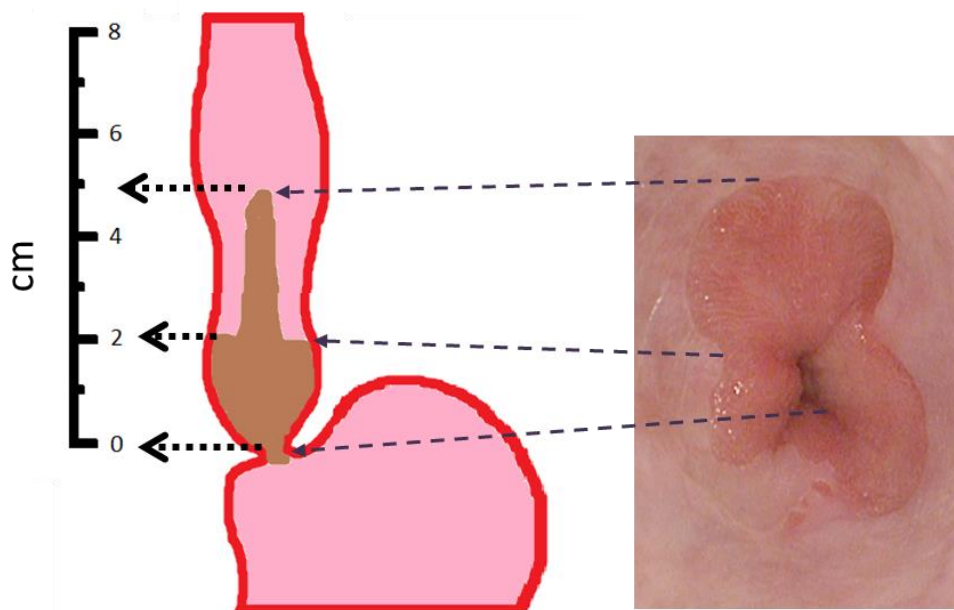
- i. The diagnosis of HGD should be confirmed by 2 expert pathologists.
- ii. Expert high-resolution endoscopy should be carried out in all patients where HGD has been detected.
- iii. Cases should be discussed at a specialist multi-disciplinary team meeting and managed in a specialist centre.
- iv. Endoscopic therapy should be used in preference to oesophagectomy or surveillance.
- v. Endoscopic resection (ER) should be considered as the therapy of choice for nodular disease and used for accurate staging.

## 1.5 Endoscopic classification of Barrett's

### 1.5.1 Prague C & M Criteria

To record the appearance of BE segments at endoscopy, the International Working Group for Classification of Oesophagitis (IWGCO) developed the Prague C&M criteria<sup>59</sup>. This system requires endoscopic measurement of the maximum circumferential (C value, in cm) length of BE above the gastroesophageal junction, and measurement of the extent (M value, in cm) of any BE tongues from their most proximal point to the gastro-oesophageal junction (GOJ).

**Figure 6: Representation of Prague C & M scoring system showing C2M5 segment.**

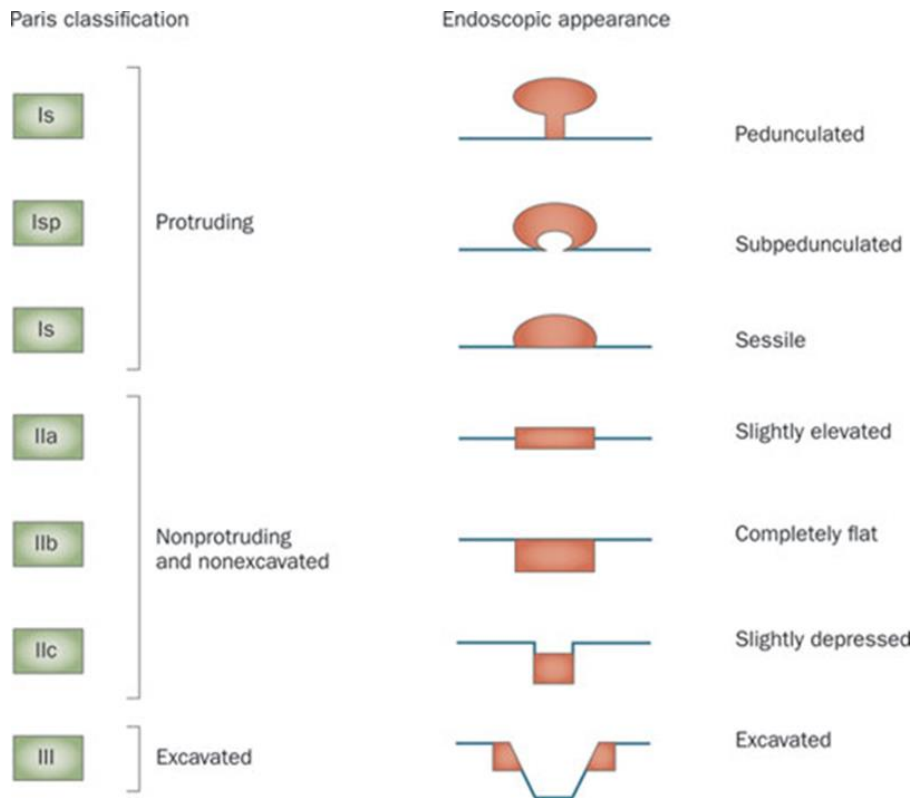


### 1.5.2 Reporting Barrett's segments

Though not strictly part of the Prague classification system, islands of Barrett's separate from the continuous BE segment are recommended to be described separately in terms of length and distance from the incisors. In addition the size and position of any hiatus hernias, a description of any visible lesions in terms of Paris

classification, number and distance from the incisors and biopsy locations and numbers should be provided in endoscopy reports as a minimum dataset <sup>1</sup>.

**Figure 7: Paris classification system for visible lesions** <sup>60 - 61</sup>.



The Paris classification system was proposed as an endoscopic classification system for visible lesions in the digestive tract by an international group of endoscopists, surgeons and pathologists. Lesions are initially broadly divided into protruding (which means a maximum elevation of 3mm above or below the mucosa), non-protruding or excavated followed by subdivisions shown in Figure 7.

## 1.6 Screening

The difficulties of screening for BE include the lack of an easily identifiable patient group, the diagnostic tests available and the prevalence of BE in the wider population.

Despite GORD being considered as essential to the pathogenesis of BE, there is a lack of evidence that symptomatic GORD alone accurately predicts BE<sup>62</sup>. In a study of 102 patients with erosive reflux disease at baseline endoscopy followed up to ascertain

incidence of BE, 9 developed BE<sup>63</sup>. All nine patients had severe oesophagitis at their baseline endoscopy. These patients were referred for dysphagia (n=3) or upper GI bleeding (n=6). None of the patients who were referred for initial endoscopic assessment due to reflux symptoms developed BE after a mean follow up of 25 months.

In another cohort study by the same group looking at 11040 patients who had 2 or more endoscopies 6 or more months apart found 515 GORD patients (412 with no erosive disease on endoscopy, 103 with oesophagitis) and 169 BE patients<sup>64</sup>. None of the 412 GORD patients with non-erosive reflux disease developed BE over a mean follow-up time of  $3.4 \pm 2.2$  years. In the group with oesophagitis (n=103), 5 developed BE. In the BE group no patient had a normal endoscopy at baseline. They concluded that the majority of GORD patients do not appear to develop BE.

These studies suggest severe oesophagitis to be a significant risk factor for the development of BE. This may be because mucosa with this much injury is more likely to heal as BE or that BE is already present but not detectable due to surrounding inflammation. The second study, suggested that in that in the absence of reflux induced erosive disease (non-erosive reflux disease) BE is unlikely to develop. Multivariable analysis was not however carried out in either study to understand if subpopulations within each cohort may have increased risk of BE.

A symptom-based questionnaire study in 517 GORD patients referred for endoscopy looked to understand which subpopulations within those with GORD predicted BE. They found male gender, heartburn, nocturnal pain and odynophagia were associated with the presence of BE in the GORD population<sup>62</sup>. Other confounders such as age, smoking and BMI were not addressed in this study.

A case control study comparing 197 patients with BE with 418 with GORD looked to understand the contribution of other demographic factors in those who had developed

BE. They found male sex, older age, smoking and central obesity to be significant risk factors for the presence BE within the wider GORD population.

Even if high risk groups within the wider GORD population can be identified, the cost of endoscopy-based screening techniques and patient acceptability limit the feasibility of screening. Alternative screening methods such as the capsule sponge are currently under investigation as potentially more suitable in an outpatient setting.

The prevalence of BE in the unselected adult population is difficult to examine due to the need for endoscopy. This was investigated in an Italian<sup>65</sup> and a Swedish<sup>13</sup> study. Endoscopies in 1033 and 1000 adult patients were found to have prevalence of BE of 1.3% and 1.6% respectively. Both studies were however limited by the introduction of selection bias due to the need for endoscopy which may have overestimated the true prevalence.

British Society of Gastroenterology guidelines currently do not advocate screening to be feasible or justified for unselected populations with gastro-oesophageal reflux disease (GORD). It suggests screening to be considered in patients with GORD and multiple risk factors including at least three of age >50, white race, male sex and obesity. The threshold should also be lowered for first degree relatives with Barrett's or OA<sup>1</sup>.

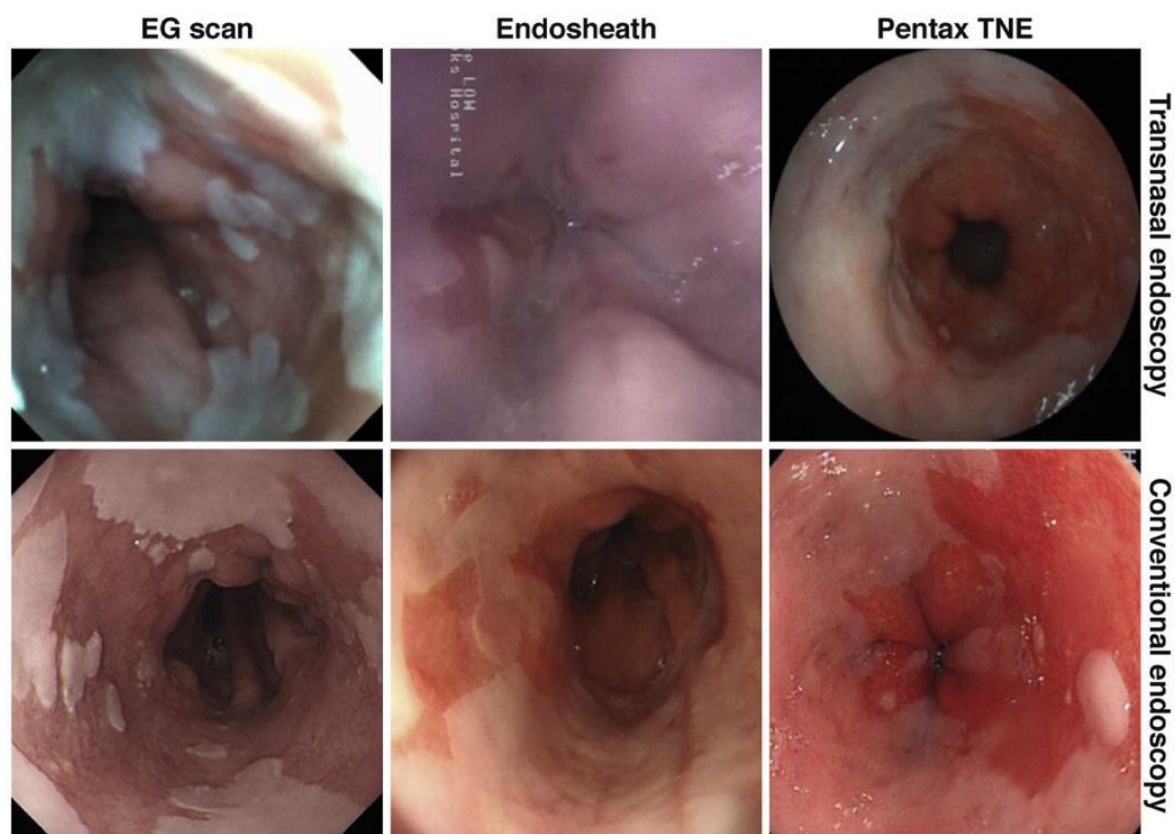
### ***1.6.1 Unsedated transnasal endoscopy***

The development of small-calibre high-quality endoscopes with a diameter under 6 mm, has enabled the use of unsedated gastroscopy as a screening tool to become feasible. This technique is acceptable to patients undergoing surveillance, better tolerated than standard gastroscopy and can be performed in an out-patient setting<sup>66</sup>. Several types of transnasal endoscope are available with either two-way or four-way tip movement. Paediatric biopsy forceps are necessary due to the smaller calibre working channel. Electronic enhancements such as narrow band imaging is available with certain manufacturers though magnification endoscopy is not.



In a comparative study of 32 patients undergoing transnasal and standard gastroscopy, there was no significant difference between the histological diagnosis of IM or dysplasia between the two endoscopic modalities <sup>67</sup>.

**Figure 8: Systems of transnasal endoscopy versus conventional endoscopy to visualise Barrett's epithelium<sup>68</sup>**



Despite the increased feasibility and tolerability of transnasal unsedated endoscopy, this in itself does not lead to a large increase in the number of referrals for BE screening<sup>69</sup>. Other factors that influence referral patterns need to be addressed before this promising technique can have more of a role in BE screening in clinical practice.

### **1.6.2 Wireless capsule endoscopy**

The first company to introduce and commercialise capsule endoscopy were Given Imaging in 2001. Their flagship product the PillCam® capsule revolutionised the study of the small bowel. In 2004 the PillCam® ESO was developed and given approval by the United States Food a Drugs Administration. This new capsule differed from the small bowel capsule having the ability to obtain 7 frames per second versus 4 frames per second. The second generation ESO2 capsule was released in 2007 and enables 9 frames per second to be captured. The oesophageal capsules additionally have dual versus a single camera allowing the capture of 14 (ESO) and 18 (ESO2) images per

second. To minimise the oesophageal transit time, the capsule is suggested to be swallowed in the lateral position. This technology allows oesophageal visualisation without the need for sedation and the accompanying discomforts and risks of conventional endoscopy <sup>70</sup>.

Studies on the utility of WCE as a screening tool for BE have followed. The initial multicentre study of 106 patients found positive oesophageal findings in 66 patients. PillCam ESO identified matching abnormalities in 61 with sensitivity of 92% and specificity of 95%. The ability to detect Barrett's within this cohort found PillCam ESO to have a sensitivity 97% and specificity 99%<sup>71</sup>. The study was however criticised due to its post-hoc adjudication process. Subsequent studies have not shown this same degree of success. In a prospective blinded study of 66 screening patients with GORD and 24 surveillance patients with BE comparing gastroscopy findings with histology as the standard with those seen with the PillCam ESO capsule. This study demonstrated only a moderate sensitivity (67%) and specificity (84%) for the identifying BE. Inadequate visualisation of the gastroesophageal junction was mentioned as one the key reasons behind the suboptimal accuracy of the WCE <sup>72</sup>. In another study, 94 patients with GORD or BE under surveillance had WCE and standard gastroscopy. BE was found in 45 of the 53 patients suspected of having BE with PillCam ESO equating to a sensitivity 79% and specificity 78%. A meta-analysis that pooled nine studies, including 618 patients in total, demonstrated a pooled sensitivity and specificity of PillCam ESO for the diagnosis of BE were 77% and 86 % respectively <sup>73</sup>. Though PillCam was found to be safe, it is not yet accurate enough to replace gastroscopy as the modality of choice for suspected BE. It may have role for those who cannot tolerate standard gastroscopy due to its excellent safety profile and high rate of patient tolerance.

One major drawback for the use of WCE is the rapid transit time through the oesophagus causing inadequate visualisation of the oesophageal mucosa and GOJ. A new approach of string-capsule endoscopy (SCE) was piloted in a feasibility study of

50 patients with BE. Strings were attached to the WCE to allow its controlled movement up and down the oesophagus. The mean recording time was 7.9 minutes with all patients having BE correctly identified. A single capsule was used in 24 studies and the high-level disinfection protocol used rendered negative microbial cultures. Patient preference comparing WCE to gastroscopy found WCE was safer and better tolerated by patients <sup>74</sup>.

A subsequent prospective blinded comparative study from the same in 100 consecutive patients with GORD symptoms undergoing for screening gastroscopy for BE. SCE preceded gastroscopy for all patients in the study protocol. The sensitivity and specificity of SCE for the visualisation of BE was 78% and 83%, and for the histological diagnosis of BE were 94% and 79% respectively. 4 capsules were used in the study and 80% of patients preferred SLE to standard gastroscopy <sup>75</sup>.

Another major disadvantage of WCE, is the inability to collect tissue. In the future, when technological advances in power sources permit, capsules have been theorised to facilitate the integration of sensors to make diagnostic and therapeutic tasks feasible such as biopsy and drug delivery<sup>76</sup>.

WCE have many inherent advantages over standard endoscopy as screening tools. Their minimally invasive design, safety profile and tolerance facilitate its use in both primary care settings and in clinics led by allied health professionals. However, despite these advantages, it is not yet accurate enough to hold its own as a primary screening tool. The inability to collect tissue also precludes it from having a role in Barrett's surveillance. Technological advances in the design, power and propulsion of WCE's may in future overcome these limitations.

### **1.6.3 Capsule sponge**

Originally referred to as the oesophageal brush biopsy capsule, the capsule sponge was first developed and used in the Transkei region of Southern Africa in 1987 to screen 1000 residents postulated as having low-, intermediate- and high risk of

developing oesophageal cancer <sup>77</sup>. The gelatine capsule contains a reticulated polyurethane sponge attached to a string. After ingestion, the capsule is digested in the stomach over 3–5 min after which time the sponge can be retrieved via the string. During retrieval cells are scraped from the entire length of the oesophagus. Tissue captured within the capsule can then be retrieved, embedded and sent for cytological analysis.

**Figure 9: Capsule sponge** <sup>78</sup>



*Capsule in gelatine capsule (right) and expanded (left).*

In a feasibility study of 504 patients with GORD in a primary care setting, cytopathological analysis of cells collected with the capsule sponge detected BE with a sensitivity of 73% for BE  $\geq 1$ cm, and 90% for BE  $\geq 2$ cm <sup>78</sup>. Though 82% of patients had only low levels of anxiety before the procedure and the sponge was swallowed by 99% of patients with no serious adverse events. Due to the low prevalence of BE in this cohort of 3% ( $\geq 1$ cm of BE with IM), the feasibility study could not determine diagnostic accuracy.

In the subsequent follow up case-controlled study by the same group, 11 UK centres recruited 1110 patients including 647 patients with BE, and 463 controls with dyspepsia

and GORD symptoms. The capsule sponge (referred to Cytosponge) was coupled with immunostaining for the biomarker Trefoil Factor 3 for the diagnosis of BE. The sponge was swallowed successfully in 94% and no serious adverse events were attributed to the device. The Cytosponge rated favourable with endoscopy when assessed with a visual analogue scale ( $p < 0.001$ ) and patients who were not sedated, rated the Cytosponge higher than endoscopy ( $p < 0.001$ ). The sensitivity of the test to detect BE overall was 79.9% ( $\geq 1$ cm BE length), increasing to 87.2% for BE segments  $\geq 3$ cm which is known to infer greater risk. The sensitivity increased to 89.7% in the subgroup of 107 patients who swallowed the capsule twice. Overall specificity for diagnosing BE was 92.4%. Though the Cytosponge-TFF3 test was safe, acceptable and had a comparable accuracy to other screening tests, its case-control design cannot be applied to the wider primary care population. Despite this, the Cytosponge-TFF3 test provides an inexpensive method to detect which patients with GORD would warrant further endoscopic assessment <sup>79</sup>.

The accuracy of the Cytosponge to risk stratify patients with BE was more recently found to be enhanced through coupling clinical and molecular biomarkers in a multicentre cohort study of 468 patients with BE. Patients had their Cytosponge test before their surveillance endoscopy where samples were collected for p53, c-Myc and Aurora Kinase A proteins, MYOD1 and RUNX3 methylation markers, glandular atypia and TP53 mutation status. These molecular markers were combined with clinical and demographic data and then using multivariable logistic regression, a more simplified risk stratification tool was created. The simplified model which retained high classification accuracy consisted of glandular atypia, P53 protein abnormality and Aurora Kinase A positivity with the interaction of age, waist-to-hip ratio and BE length. In the discovery cohort, of the 162 (35%) patients classified into the low risk category, the probability of being truly non-dysplastic was 100%, and the probability of having HGD or IMC was 0%. In the 58 (12%) patients classified as high risk, the probability of having NDBE was 13% and HGD/IMC 87%. These results were substantiated in the

validation cohort where of the 25 (38%) of 65 patients were classified as low-risk. Of these the probability of NDBE was 96% (99% CI 73-80-99-99). In the high-risk group, no NDBE cases were found. The authors infer this combined biomarker risk stratification tool could be applied to determine patients at low risk of cancer progression, negating the need for endoscopy<sup>80</sup>.

## 1.7 Surveillance

The rationale of surveillance in BE is the detection of OA at an early stage, receipt of potentially curative therapy reducing cancer related mortality. For BE, a four quadrant biopsy protocol (the 'Seattle' protocol) consisting of jumbo forceps biopsies from every 2cm of columnar mucosa (BE), was first proposed for surveillance in 1993<sup>81</sup>. This is now accepted as the standard technique for sampling segments of BE.

Data from observational studies suggest patients enrolled in surveillance programmes have OA detected at an earlier stage than non-surveillance detected cancers, with subsequent improved survival<sup>82,83</sup>. A study of 817 patients in the UKBOR cohort, demonstrated that despite wide variation in surveillance practice across the UK, a large proportion of dysplastic disease is detected on specific surveillance endoscopies. Shorter endoscopic intervals for surveillance of LGD were also found to be associated with an increased detection of HGD/OA<sup>84</sup>. The largest and probably most influential study today examined 29536 patients diagnosed with BE during 2004-2009 excluding those with condition affecting overall survival. 424 patients developed OA during a mean follow up of 5 years. Of those developing OA, 209 (49.3%) were diagnosed from within BE surveillance programmes. These patients were more likely to have OA at an earlier stage (stage 0/1 in 74.7% vs 56.2%,  $p < 0.001$ ), survived longer (median 3.2 vs 2.3 years,  $p < 0.001$ ) and have lower cancer related mortality (34% vs 54%,  $p < 0.001$ ) compared to OA diagnosed outside of such programmes ( $n=215$ ). Surveillance among patients with BE was associated with significantly better OA outcomes including cancer related mortality compared with those diagnosed outside of surveillance programmes.

Analytical models suggest two yearly BE surveillance costs less than £25,000/ life-year saved<sup>85,86</sup>. In contrast, another study modelled surveillance strategies in the UK using the PenTAG cost-utility model with 3 yearly surveillance for NDBE, annual surveillance for LGD and 3 monthly for HGD. They found with this strategy, surveillance was not cost-effective and was found to do more harm than good<sup>87</sup>. These studies however do not model current surveillance strategies for BE in BSG guidelines, so their conclusions may not be directly inferred to current clinical practice. Cost effectiveness analysis of surveillance programmes depend upon the prevalence of BE, increment detection rate of dysplasia by endoscopic surveillance and the risk of progression to cancer. As the studies examining progression are predominantly retrospective, this makes cost effective models difficult to interpret. This led to the design and approval of the largest UK based multi-centre randomised controlled trial, entitled the Barrett's Oesophagus surveillance study or BOSS<sup>88</sup>. In it, 2 yearly BE surveillance was compared with endoscopy at need dictated by symptoms. The trial has completed its recruitment of 3400patients and results are awaited.

## **1.8 Registries**

Several Barrett's registries have been set up to answer questions into the epidemiology and pathogenesis of BE (Table 2). These include identifying changes in the trends in the diagnosis of BE, their relationship to OA, mapping the evolution of Barrett's metaplasia and identifying variables associated with future cancer risk. Current registries are either institution-based or population-based pooling data from links between histological databases and institutions. Both types of registry provide infrastructure for pathological confirmation of BE and facilitate coordination and recruitment into clinical studies. Follow-up from registered patients allows the study of important clinical outcomes<sup>89</sup>.



**Table 2: Institution and population-based Barrett's registries**

Population-based	Institution-based
Northern Ireland Barrett's Registry	Mayo Clinic Barrett's Registry
Danish Barrett's Oesophagus Registry	Cleveland Clinic Barrett's Registry
Dutch Nationwide Cohort Registry	Venice Region Barrett's Registry
	UK Barrett's Oesophagus Registry

Databases recruiting from pathological samples provide a relevant population denominator while institutional registries enable the identification and potential recruitment of large numbers of BE patients into studies and access to other potentially important clinical data. Population databases can further facilitate the study of potential geographic variation in the natural history of BE. Both types of registry can further facilitate studies considering the cost-benefit of BE diagnosis, surveillance and therapy. This will in future refine surveillance strategies into smaller sub-populations at higher risk of progression to OA and within those, potentially select out the highest risk to early endoscopic therapy before dysplasia has even developed.

## **1.9 Medical Management**

### **1.9.1 *The role of GORD***

GORD is postulated to be essential for the development of BE and may have a role in promoting tumour development. Refluxate contains numerous toxic substances such as acid, bile and ingested substances which individually or in concert may trigger acute and chronic inflammation of the oesophageal mucosal surface. Treatments have therefore been suggested to prevent reflux induced mucosal injury, and the secondary inflammatory response that subsequently occurs.

### 1.9.2 Proton pump inhibitor therapy

The inference that proton pump inhibitor therapy should preclude the development or progression of BE, when GORD plays such a crucial role in the pathogenesis of BE seem intuitive. Studies have however been conflicting.

The role of proton pump inhibitors as chemopreventative agents for BE is postulated to be strong particularly for those with BE and symptomatic GORD which in itself is a known risk factor for OA<sup>90</sup>. In asymptomatic BE patients, PPI therapy is generally accepted in primary care to reduce the risk of progression to OA<sup>91</sup>.

Most of clinical studies investigating the relationship between PPIs and BE have a retrospective design and lack randomisation. A study of 502 with BE found that in patients not on PPIs when diagnosed high-risk endoscopic features such as nodularity or ulcers, or LGD were 3.4 x more likely than patients who were on a PPI<sup>92</sup>. The group also reported patients who delay starting PPIs by  $\geq 2$  years after confirmation of BE had a subsequent x5 to x20 fold increased risk for developing HGD or OA respectively when compared with patients who started PPIs shortly after their diagnosis<sup>93</sup>. In a prospective study of 236 patients followed up for 1170-person years, the cumulative incidence for the development of dysplasia was significantly lower in patients who received PPI compared with those who did not ( $p < 0.001$ ). Furthermore, longer PPI use was further associated with risk a reduced frequency of dysplasia occurrence<sup>94</sup>.

The risks and benefits of long term PPI use has recently been expertly reviewed in a best practice paper from the American Gastroenterological Association<sup>95</sup>. Several potential side effects have been linked with PPI usage. These include chronic kidney disease<sup>96</sup>, dementia<sup>97</sup>, bone fractures<sup>98</sup> myocardial infarction<sup>99</sup>, small intestinal bacterial overgrowth<sup>100,101</sup>, gastrointestinal infection with the pathogens *Campylobacter*<sup>102,103</sup>, *Salmonella*<sup>102,103</sup> and *Clostridium difficile*<sup>104</sup>, spontaneous bacterial peritonitis<sup>105</sup>, pneumonia<sup>106</sup>, micronutrient deficiencies<sup>107,108</sup> and gastrointestinal malignancies<sup>109</sup>. Evidence to support these claims have been consistently low to very low and are

summarised in Table 3. The absolute risk of increase for patients are modest at best at once daily dosing.

The best practice paper recommends patient groups where the benefits of PPI outweigh risks include those with complicated GORD, uncomplicated GORD with objective evidence of excess acid, BE with GERD symptoms, and NSAID bleeding prophylaxis if high-risk. In patients who do not fall within these categories the risk-benefit equation is less clear. Nonetheless, the advice given for asymptomatic BE patients remains that long-term PPI therapy should be considered. The best strategy to mitigate the potential risks of long-term PPIs are to avoid their prescription in the absence of a strong indication, and where indicated, long-term dosing should be monitored and the lowest effective dose prescribed <sup>95</sup>.

**Table 3: Summary of evidence for potential PPI-associated adverse effects<sup>95</sup>**

Potential adverse effect	Types of studies	Threats to validity	Overall quality of evidence
<b>Kidney disease</b>	Observational only	Modest effect size  Residual confounding would bias towards harm Absence of dose-response effect	Very low
<b>Dementia</b>	Observational only	Modest effect size  Residual confounding would bias towards harm	Very low
<b>Bone fracture</b>	Observational only	Inconsistent results  Modest effect size Residual confounding would bias towards harm	Low or very low
<b>Myocardial infarction</b>	Observational  RCT	Results differ between RCTs and observational studies Secondary analysis of RCT data Modest effect size Residual confounding would bias towards harm	Very low
<b>Small intestinal bacterial overgrowth</b>	Observational  Crossover	Sparse data  Residual confounding would bias towards harm	Low

<b>Spontaneous bacterial peritonitis</b>	Observational only	Protopathic bias Modest effect size	Very low
		Residual confounding would bias towards harm	
<b>Clostridium difficile infection</b>	Observational only	Modest effect size	Low
		Residual confounding would bias towards harm	
<b>Pneumonia</b>	Observational	Results differ between RCTs and observational studies	Very low
	RCT	Secondary analysis of RCT data Modest effect size Absence of dose-response effect Residual confounding would bias towards harm Protopathic bias	
<b>Micronutrient deficiencies</b>	Observational only	Inconsistent results	Low or very low
		Modest effect size Absence of dose-response effect Residual confounding would bias towards harm	
<b>Gastrointestinal malignancies</b>	Observational	Results differ between RCTs and observational studies	Very low
	RCT	RCTs use surrogate outcomes Modest effect size Residual confounding would bias towards harm Confounding by indication and protopathic bias	

### 1.9.3 *Bile acids*

It is traditionally inferred that mucosal injury from GORD is secondary to caustic injury from gastric contents which contain both acid and pepsin. Therapeutic strategies therefore focus on targeting caustic injury in BE. However, the refluxate produced in patients with GORD is frequently mixed with duodenal bile. Studies have found that in those given PPI therapy, reflux of bile salts can be seen in up to a third of patients<sup>110,111</sup>. In 2009, Souza et al published an alternative concept to the pathogenesis of

reflux induced oesophagitis where injury was caused by cytokine-mediated rather than caustic acid injury<sup>112</sup>.

Bile salt injury is dependent upon the acid dissociation properties of bile salt can produce injury over a wide range of pH conditions. In acidic refluxate environments (pH 4), Taurine-conjugated bile salts can cause chronic mucosal injury<sup>113</sup>. In pH neutral or alkaline refluxate unconjugated bile salts cause mucosal injury<sup>114</sup>.

Bile salts such as deoxycholic acid have been shown to cause DNA damage while simultaneously inducing NF- $\kappa$ B pathway activation<sup>115,116</sup>. The damage caused was found to be mediated by reactive oxygen and nitrogen species (ROS/RNS). Pre-treatment with the ROS scavenger, N-acetyl-L-cysteine prevented DNA damage after exposure to deoxycholic acid. Activation of the NF- $\kappa$ B pathway was detected by the examination of biopsy specimens before and after exposure to deoxycholic acid. It is hypothesised that these are the mechanisms by which bile refluxate cause carcinogenesis in BE.

Treating biliary reflux in BE may have chemopreventative role. In a five-year prospective open randomised study, 62 patients were enrolled and randomised to receive 40mg omeprazole or combination 40mg omeprazole with 10mg/kg of ursodeoxycholic acid (UDCA) daily. In the combination therapy group, the diagnosis of erosive oesophagitis reduced from 86.7% to 16.6% ( $p < 0.001$ ) compared with 80.6% to 51.6% in the PPI only group. A lack of intestinal metaplasia at follow up endoscopy was found more frequently with combination therapy rather than PPI monotherapy (32.3% vs 6.5%,  $p = 0.01$ )<sup>117</sup>. However, these findings were not supported in a separate study of 9 BE patients where high dose twice daily PPI therapy for 6 months was compared with high dose PPI with 600mg UDCA daily for 6 months in the same patients. UDCA was not found to influence significant histological or immunohistochemical changes in BE<sup>118</sup>. More recently a pilot clinical study of 13 to 15 mg/kg/day UDCA treatment for 6 months was evaluated in 29 patients with BE supported the lack of efficacy of UDCA.

Clinical activity of UDCA was assessed by evaluating changes in gastric bile acid composition and tissue markers of oxidative DNA damage (8-hydroxydeoxyguanosine), cell proliferation (Ki67), and apoptosis (cleaved caspase-3) in BE biopsy material. The proportion of UDCA in gastric bile acids increased following treatment 18.2% at baseline to 93.4% ( $p < 0.0001$ ). The selected tissue biomarkers remained unchanged after 6 months UDCA treatment. The study concluded that while UDCA increased caused favourably changes in the composition of gastric bile acids it did not influence selected markers of oxidative DNA damage, cell proliferation, and apoptosis in BE <sup>119</sup>.

#### **1.9.4 Pepsin**

Gastric pepsin is one of the main constituents of refluxate in patients with GORD. Non-acid pepsin reflux has been shown to be directly contributory to the development of laryngeal carcinoma<sup>120</sup>. As the development of OA has not been prevented by PPI therapy, a potential role for pepsin in OA carcinogenesis has been postulated. This is supported by a study in 8 patients with BE in treated with pepsin (0.01-1mg/ml; 1-20hours) and acid (pH4) +/- pepsin (5minutes). The authors identified how pepsin can be synthesised by metaplastic BE, and how it promotes PTSG2 (COX-2) and IL1 $\beta$  expression and cell migration in vitro inferring its potential role in OA carcinogenesis <sup>121</sup>.

#### **1.9.5 COX-2**

Cylooxygenase-2 (COX-2) is a membrane bound glycoprotein that is postulated to play a role in the development of a number of cancers including OA<sup>122</sup>. It catalyses the rate limiting step in the production of prostaglandins from arachidonic acid and is induced through cytokines and other inflammatory mediators<sup>123</sup>.

COX-2 expression levels increase during progression through metaplastic-dysplasia-adenocarcinoma sequence in patients with BE <sup>124</sup>. This finding is supported by a population-based case-control study, where the associations of the COX-2 8473 T>C polymorphisms were evaluated from genomic DNA extracted from blood samples.

Subjects OA (n=230), BE (n=212) and reflux oesophagitis (n=230) were compared with age and sex matched normal population controls (n=248). COX-2 8473 C alleles (1 or more) were associated with increasing risk of OA (adjusted OR, 1.58; 95% CI, 1.04-2.40). The study suggests COX-2 8473 C alleles have potential as genetic marker for OA susceptibility.

Blocking the action of COX-2 has therefore been considered as a therapeutic strategy to prevent progression to BE and OA. Studies on COX-2 inhibitors have reported conflicting results. Agents that can block COX-2 include selective COX-2 inhibitors such as celecoxib, aspirin, non-steroidal anti-inflammatory drugs (NSAIDs) and steroids.

The chemoprevention for Barrett's oesophagus trial, studies the effect of 48-weeks treatment with Celecoxib in a multicentre, randomised placebo-controlled study of 222 participants. No differences in the rate of progression of BE, LGD or HGD to OA was identified compared with placebo<sup>125</sup>. Meanwhile, a multi-centre, randomised study of 45 BE patients treated with 10 days of Celecoxib found it reduced COX-2 expression and cell proliferation in patients with BE<sup>126</sup>.

Studies investigating non-selective COX-2 inhibition with NSAIDs have additionally revealed conflicting results. A case-controlled study on 230 reflux esophagitis, 224 BE, and 227 OA and 260 population controls found BE and OA patients were less likely than controls to have used NSAIDs, indicating it to have a protective effect. This was supported by a separate case-control study of 434 patients with BE where aspirin appeared to reduce the risk of developing BE<sup>127</sup>. The protective effect of NSAIDs and aspirin for OA was evaluated in a meta-analysis of 9 studies including 1813 cancer cases to conclude protective association between both agents and OA and suggest evidence for a dose effect<sup>128</sup>. On the other hand, a large population based study of 1350 patients with BE (n=285), dysplastic BE (n=108), oesophageal inflammation at endoscopy (n=313) and populations controls (n=644) did not find any association

between aspirin to be associated with non-dysplastic BE and population (OR=1.01, 95% CI 0.71-1.43) or inflammation controls (OR=1.16, 95% CI 0.8 – 1.68).

Furthermore, no association between aspirin or NSAID use and risk reductions for dysplastic BE was found. The study was not however designed to detect if aspirin plays a role in the development of BE or progression of dysplasia to OA<sup>129</sup>.

Though it appears promising, currently there is insufficient data to suggest COX-2 inhibition with aspirin or NSAIDs in patients to prevent the development of BE or reduce the incidence of OA progression in patients with established BE. Results of the multi-centre randomised Aspirin Esomeprazole Chemoprevention Trial (AspECT trial) are eagerly awaited to shed further light on this issue. The open, randomised 2x2 factorial design has completed recruitment of 2513 patients. It is due to complete in May 2017 to report on the primary outcome measure, the conversion of BE to HGD or OA<sup>130</sup>.

## **1.10 Endoscopic management**

Endoscopic therapy is now increasingly being considered in the UK as first line therapy for LGD, HGD and intramucosal cancer in centres with access to them. Several minimally invasive treatments for BE have been studied and have shown effective eradication of HGD, reducing the risk of progression to cancer.

### **1.10.1 Photodynamic therapy**

Photodynamic therapy (PDT) is a unique medical technology in which a drug known as a photosensitiser (PS) becomes active when it is illuminated with light of a specific wavelength. The light triggers a photochemical reaction to convert molecular oxygen into highly cytotoxic reactive oxygen species (ROS)<sup>131</sup>. The PS can then either kill the cell or fluoresce to highlight it for imaging.

PDT is attractive as it causes little damage to connective tissue components such as collagen and elastin, preserving the mechanical integrity of hollow organs such the



gastrointestinal tract<sup>132</sup>. Furthermore, once a PDT-treated area has healed, it can be treated repeatedly without cumulative toxicity, and it may be safely given to treat areas of recurrent cancer even if they have received maximal radiotherapy, making it ideal as an adjunct to current therapy.

#### 1.10.1.1 Porfimer sodium (Photofrin)

The effectiveness of Photofrin PDT vs omeprazole treated controls was confirmed in a multicentre, international randomised controlled trial of 200 patients with high grade dysplasia in BE<sup>133</sup>. Complete reversal of HGD (CR-HGD) at 1 year was achieved in 71% of Photofrin treated patients vs. 30% controls ( $p<0.001$ ). In the subsequent follow up study at 5 years, CR-HGD was 77% for Photofrin vs 39% ( $p<0.001$ ) in omeprazole controls<sup>134</sup>. The secondary endpoint looking at progression to OA, also found significant benefit in those treated with Photofrin (15% progression rate) vs controls (29% progression rate;  $p=0.027$ ). Photofrin treated patients also took significantly longer to progress to OA ( $p=0.004$ ). This finding was supported by a more recent study examining long term outcomes (median 62months; range 36-114 months) of 21 BE patients with HGD treated in a single centre. Photofrin successfully achieved CR-HGD in 84% of patients, and a similar rate of progression to OA of 15% was seen in this study<sup>135</sup>.

Two common side effects of PDT using porfimer sodium are photosensitivity reactions and oesophageal strictures. Photosensitivity can occur up to 3 months after treatment and is reported in more than 60% of patients<sup>133</sup>. It necessitates strict light precautions and cause severe burns if not adhered to. As the drug and light penetrate down to the submucosa, the stricture rate is significant and is reported at 18% with one PDT session and 50% after two sessions<sup>136</sup>. Other adverse events include nausea and vomiting, dysphagia, odynophagia and chest pain lasting up to 1 week<sup>137</sup> and more rarely atrial fibrillation pleural effusions<sup>138</sup>.

Following on from these studies, PDT with Photofrin was given National Institute for Health and Clinical Excellence approval for the treatment of HGD in BE<sup>139</sup>, early OA<sup>140</sup> and for OA palliation<sup>141</sup>. However, despite these approvals it is now rarely used due to the poor side effect profile of Photofrin and has been superseded by other ablative therapies for the treatment of BE HGD and early neoplasia.

#### 1.10.1.2 5-aminolaevulinic acid

To overcome this, alternative photosensitisers have been evaluated in BE. A single centre randomised controlled trial carried out by our group in UCL evaluated the more superficially penetrating photosensitiser 5-aminolaevulinic acid (ALA) in comparison to Photofrin in 64 patients. Strictures and skin photosensitivity were significantly more common in the Photofrin vs ALA treated patients (33% vs 9% and 43% vs 6% respectively;  $p < 0.05$ ) giving ALA a better risk profile than Photofrin PDT. After median follow up of 24 months, CR-HGD did not differ significantly between ALA (47%) and Photofrin (40%) PDT. However, CR-HGD was significantly higher for shorter segments of BE ( $\leq 6$ cm) with ALA PDT ( $p = 0.02$ ). Adverse events to ALA are rare and when occurring photosensitivity last only 36 hours. More commonly, patients have nausea, vomiting and transiently raised transaminases<sup>142</sup>.

#### 1.10.1.3 Second generation photosensitisers for oesophageal PDT

More recently, second generation photosensitisers have been developed for PDT such as Verteporfin and Talaporfin sodium.

Verteporfin is attractive as it is activated by light further into the infrared than that used to activate Porfimer sodium (689nm vs 630nm). This would infer deeper tissue penetration of the light and theoretically enable Verteporfin to treat deeper into tissues than Porfimer sodium. Data of its use in OA is limited to one study in canines. In this phase 1 dose escalation study, 0.75mg/kg administered intravenously achieved similar degrees of mucosal ablation with 630nm laser fluence of 60, 80, 145 and 200 J/cm when delivered at 15, 30, 60 and 120 minutes after the drug injection, respectively<sup>143</sup>.

Being activated at 664nm (the near infrared spectral region), Talaporfin sodium can penetrate more deeply into tissue than ALA or Photofrin PDT. In the initial phase 1, laser dose escalation study, 9 patients who failed chemoradiotherapy for oesophageal cancer were enrolled. A fixed dose of drug was administered 4-6hours before irradiation. The fluence of the 664nm diode laser was evaluated in groups of 3 patients at 50J/cm<sup>2</sup>, 75J/cm<sup>2</sup> and 100J/cm<sup>2</sup>. No dose limiting toxicity was observed in any patient and 5 of 9 (55.6%) achieved complete local response<sup>144</sup>. Following on from these results, the fluence was set at 100J/cm<sup>2</sup>. In the subsequent multi-institutional phase II study, 26 patients who failed chemoradiotherapy for oesophageal cancer were administered Talaporfin sodium. 23 of 25 (88.5%) of patients followed up achieved local complete response (L-CR). No skin photosensitivity and no grade 3 or worse non-haematological toxicity related to PDT were observed<sup>145</sup>. Talaporfin was therefore shown to be a safe and effective salvage therapy in oesophageal cancer patients who have failed chemoradiotherapy. Further studies on the efficacy of this photosensitiser in treatment naïve oesophageal cancer, or after failure of other ablative therapies are warranted.

### ***1.10.2 Radiofrequency ablation***

Due to the low success rates of PDT to reverse dysplasia, and more importantly to eradicate the Barrett's mucosa, the use of HALO radiofrequency ablation (RFA) has superseded PDT for the minimally invasive treatment of HGD<sup>1</sup> and more recently LGD<sup>146</sup> arising from BE. Through delivery of a short pulse of radiofrequency energy at a power of 40W, a uniform ablation depth of between 0.5-1mm is achieved. RFA has been shown to successfully eradicate BE dysplasia in the context of both rigorously conducted US clinical trials<sup>147</sup> and in follow up data from RFA outcome registries<sup>58,148</sup>, of whom we are the custodians in the UK.

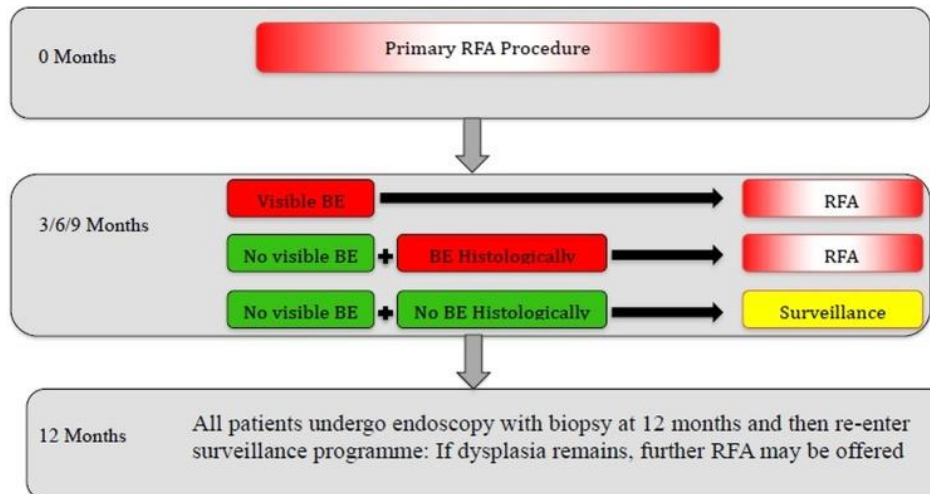
Initial data on the efficacy of RFA for HGD was reported in a 16 centre US Registry<sup>148</sup>. In total 142 patients with HGD in BE underwent RFA. No serious adverse events were

reported, and 1 asymptomatic stricture was reported. Ninety-two patients had at least 1 follow-up biopsy session (median follow-up 12 months, IQR 8-15 months). CR-HGD was achieved in 90.2% of patients, CR-Dysplasia (CR-D) in 80.4%, and CR-intestinal metaplasia (CR-IM; eradication of BE) in 54.3%.

We reported outcomes from the UK National HALO registry in 2013. Of 335 patients with BE and early neoplasia (72% HGD, 24% intramucosal carcinoma, 4% low grade dysplasia) HGD was cleared from 86% of patients, all dysplasia from 81%, and BE from 62% at the 12-month time point. Complete reversal dysplasia (CR-D) was 15% less likely for every 1-cm increment in BE length (odds ratio = 1.156; 95% CI: 1.07-1.26; P < .001). Endoscopic mucosal resection prior to RFA did not provide benefit. 3% (n=10) of patients subsequently developed invasive cancer developed in 10 patients (3%) by 12-months, and disease progressed in 5.1% (n=17) after a median follow-up of 19 months. Symptomatic strictures developed in 9% of patients and were treated by endoscopic dilatation. 94% of patients remained clear of dysplasia nineteen months after therapy<sup>58</sup>.

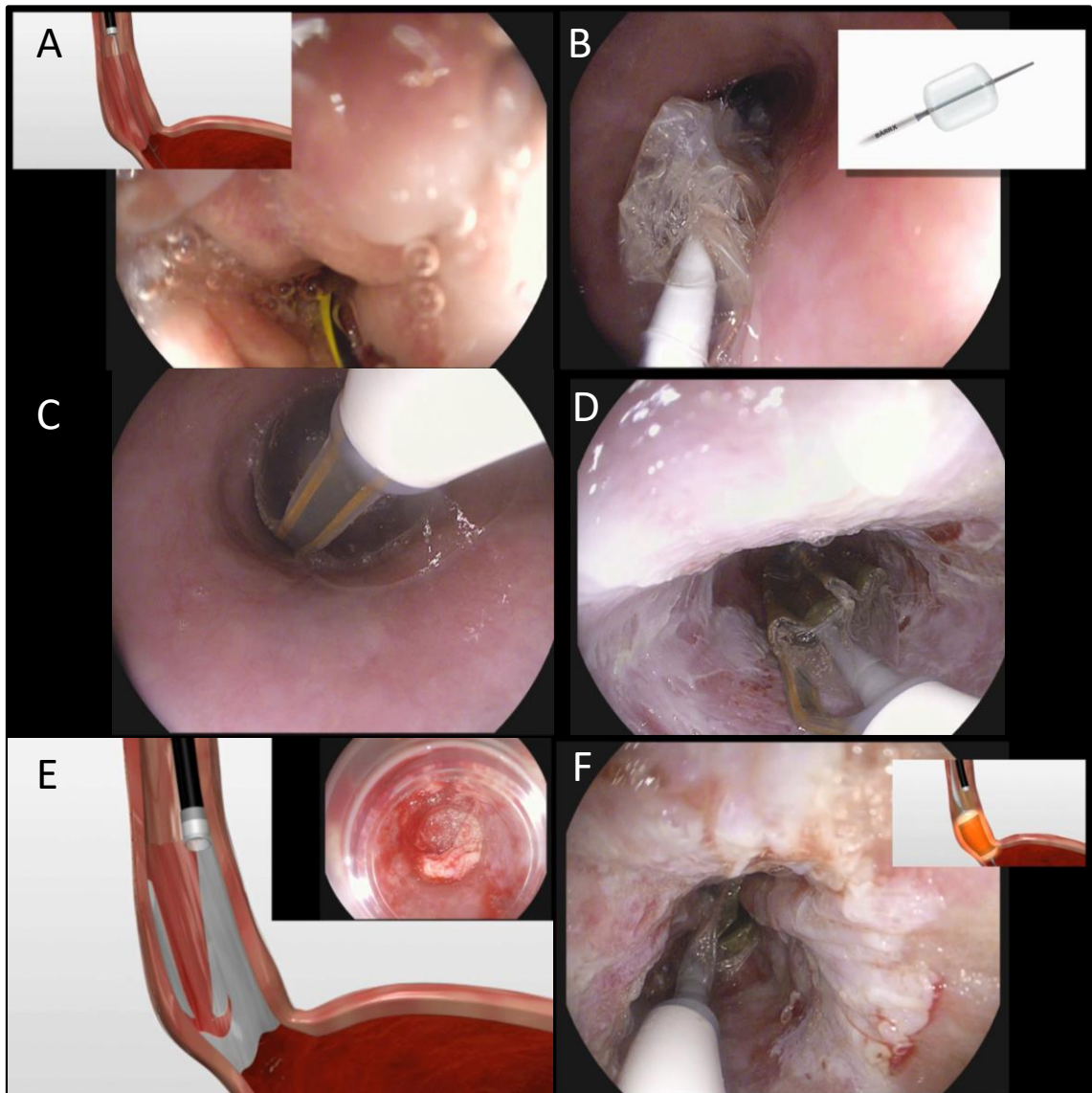
RFA for BE is well tolerated in most patients. Mild transient symptoms occur in some which usually resolve within 4 days. Adverse events include gastrointestinal bleeding (1%), chest pain necessitating admission (2%) and stricture formation (6%)<sup>147</sup>.

**Figure 10: UK RFA treatment protocol for Barrett's neoplasia <sup>149</sup>**



In a follow-up study we evaluated whether outcomes have progressively improved over time. Prospective data from the UK HALO RFA registry evaluated RFA treated patients with BE and early neoplasia during 2-time periods, 2008-2010 and 2011-2013. Efficacy of RFA and durability of successful treatment and progression to OA were evaluated. In 508 patients who completed treatment, CR-D and CR-IM improved significantly between the former and later time periods, from 77% to 92% and 56% to 83%, respectively ( $p < 0.0001$ ). The number of patients undergoing EMR for visible lesions prior to RFA also increased (48% to 60%;  $p = 0.013$ ). Rescue EMR after RFA decreased from 13% to 2% ( $p < 0.0001$ ) and progression to OA at 12 months did not differ between the time periods (3.6% vs 2.1%,  $p = 0.51$ ) <sup>149</sup>. We concluded that due to improved lesion detection and more aggressive resection strategies for visible lesions, outcomes have improved significantly over time.

**Figure 11: Radiofrequency ablation of Barrett's dysplasia with HALO<sup>360</sup> device**



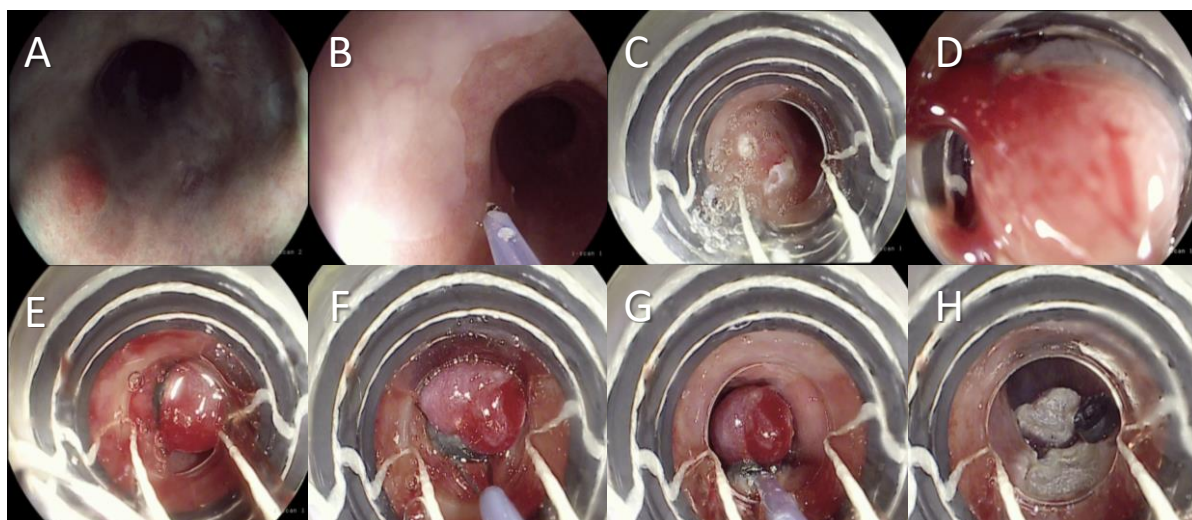
*A) The JAG wire is first passed under direct vision into the stomach to guide instrumentation. B) Sizing balloon measures oesophageal calibre under direct vision. C) HALO 360 balloon inflated and circumferential RFA delivered to 3cm segments. D) For long segment BE, overlapping RFA delivered. E) Ablated coagulum scraped into stomach to improve contact for repeat ablation. F) HALO 360 reapplied to previously treated BE segment.*

### **1.10.3 Endoscopic Resection**

Endoscopic resection, also referred to as endoscopic mucosal resection (EMR) is a technique developed to remove sessile or flat neoplasms from the gastrointestinal tract. EMR is a misnomer as the resected specimen can contain tissue down to the

submucosa as typically can measure 10-30mm in size. In contrast to ablative treatments such as PDT and RFA, EMR allows histological assessment of the treated specimen to assess tissue characteristics, depth of invasion and infiltration into the lateral or basal margins<sup>150</sup>. UK guidelines for the diagnosis and management of oesophagogastric cancers advocate its use as a diagnostic and therapeutic option in T1a tumours, and select T1b tumours where the depth of invasion is limited to the superficial 1/3 of the submucosa<sup>151</sup>. This is important as accurate staging of T1 cancer is essential to guide subsequent management toward endoscopic or surgical therapy. Tumours limited to the mucosa have very low rate of lymph node metastases of between 0-0.03% vs. submucosal cancers (T1b) which infer a 18-41% risk of lymph node metastases<sup>152-154</sup>. In addition, two studies demonstrate that there is less interobserver variability among pathologists analysing EMR samples vs biopsy specimens for the diagnosis of dysplasia<sup>155,156</sup>.

**Figure 12: Steps involved in endoscopic resection of Barrett's dysplasia**



*A) Mucosal target in segment of BE highlighted with iScan 2 imaging. B) The lesion is demarcated on either side. C) Duette applied and lesion identified. D) Target suctioned into cap. E) Mucosectomy band deployed post suction at base of target. F) Snare applied to base of Duette band. G) Base coagulated and snare slowly closed. H) Resected target post EMR.*

The efficacy of EMR in the treatment of BE with HGD was seen on a large scale in a prospective study of 100 EMR's in patients with low-risk oesophageal lesions. Patients were treated with either cap-assisted or ligation-assisted EMR. The study reported local remission was achieved in 97% (60/62) patients and at mean follow up of 20.7 months (median 20months, range 17-24 months) metachronous lesions were observed in 9.7% (6/62)<sup>157</sup>. There were several limitations in this study, the authors report durable success in 91.3% of patients. However, they only report on a subset of those originally treated. The reasons for exclusion of 10 other cases include presence of deeper submucosal or lymphatic invasion in the original specimen or subsequent specimens in 2, the need for further thermal ablative therapy in 1, and extensive carcinomas based on proven or suspected deep submucosal or lymph node involvement in 7 who subsequently needed palliative stenting. The authors report in the 58 cases who had successful EMR for adenocarcinoma, only 1 patients had deep submucosal invasion. However, by their own admission, several of these original



histology reports when re-reviewed suspected of definitively found deeper submucosal invasion in a further 9 of the 58 original patients. CR-D should rather have been referred to as 82% (48/58 successful resections) based on this rather than the success rate reported in the earlier discussion. Furthermore, the authors report their R0 resection rate to have been 98% (57/58) for OA EMR. However, lateral infiltration of tumour was found in 32/77 of index resection specimens and in a further 11/77, lateral resection margins couldn't be evaluated due to thermal resection artefact. The true R0 resection rate should therefore have been reports as 43% as only 33/77 original specimens had true deep and lateral. This was supported by the finding by the group that in 36/58 original patients, biopsies taken from the margin of the malignancy had tumour.

A subsequent follow up study by the same group in 349 patients treated with EMR +/- ablation therapy (PDT) for HGD or IMC with mean 5 year follow up<sup>158</sup>. Complete response was now reported to be 96%, though subsequent endoscopy found metachronous lesions in 21.5% (n=74) of patients. The 5-year survival rate to 84%.

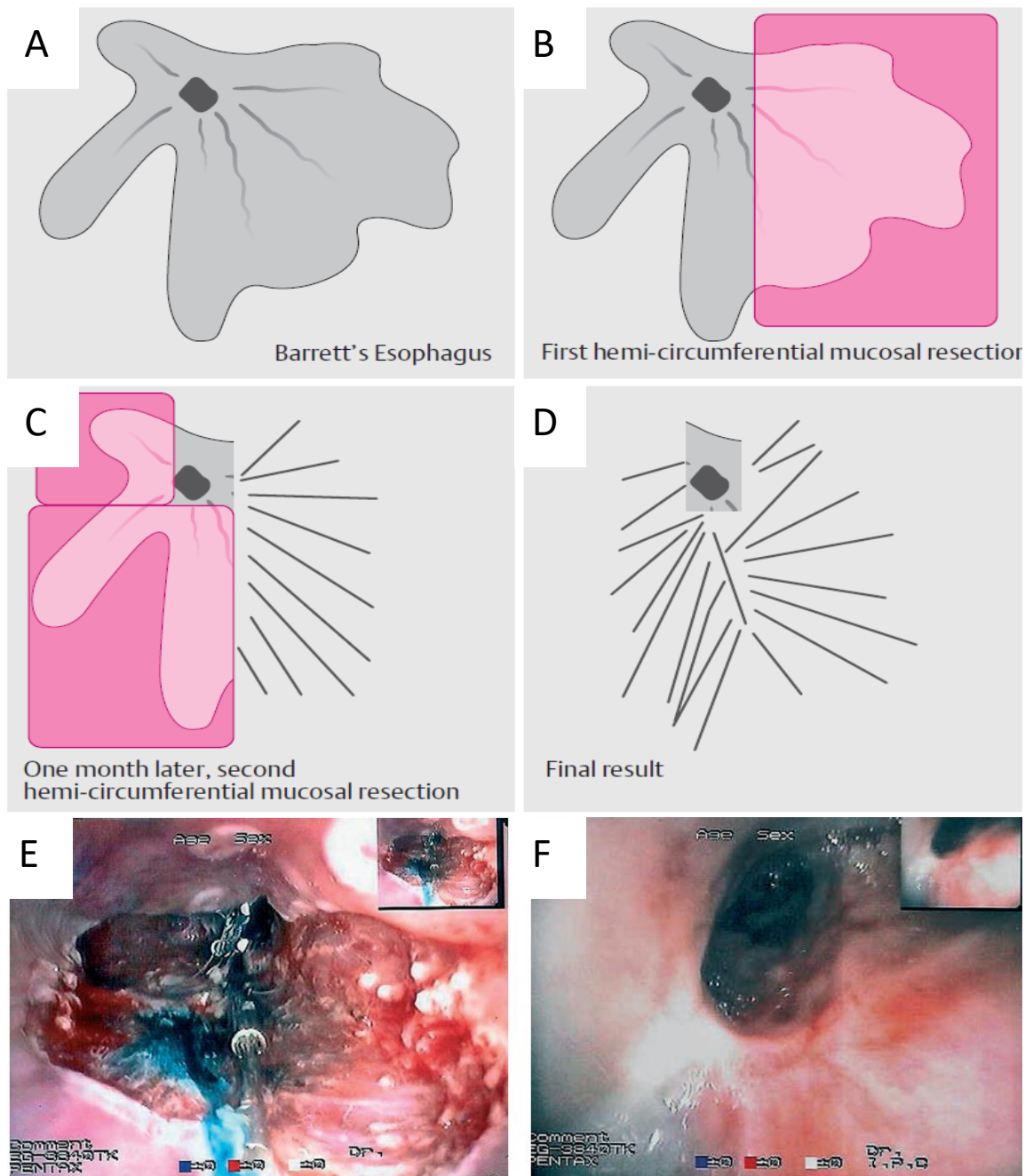
Complication rates of EMR are low from published series. When assessing 12 trials published on EMR alone in 805 patients the overall acute minor bleeding (treated with single modality, no drop Hb>2g/dl or need for transfusion) was in the range 0.6% to 6%. Strictures occurred in 4% and increased in frequency when greater than 50% of the oesophageal lumen was resected. Perforations are rare in the oesophagus (0.12% of all patients) when compared to the stomach (4.9%)<sup>159</sup>.

Complete Barrett's excision (CBE), also referred to as stepwise EMR, is as the name suggests, the removal of the entire visible BE segment with sequential overlapping EMR's with the curative intent of removing all early neoplasia and reducing the risk of metachronous lesion development. The approach also allows the accurate assessment of pathological stage from the entire BE segment. The potential of the technique was first shown in a study of 12 patients with BE and HGD/IMC. Segments were

sequentially removed with a median of 5 EMRs per patient over median 2.5 sessions. The median length of BE treated was 5cm. 2/12 (17%) developed stricture and 4/31 (13%) of EMRs were complicated by minor bleeds. After median follow up of 9 months, no recurrence of BE or malignancy was observed <sup>160</sup>. Two further small studies on the short term efficacy of CBE showed equivalent levels of efficacy of 86% (18/21 patients)<sup>161</sup> and 89% (33/37 patients)<sup>162</sup> for CR-BE and symptomatic stenosis occurred in 0% and 26% of patients in the studies. The prevention of stricture development in the former study was likely due to the 2 step methods of circumferential EMR employed in this study (Figure 12). These initial studies were small, showed the technique had promise but lack data regarding the consequent rate of metachronous lesions due to lack of control group and short follow. This information was first reported in a single centre study of 49 patients with HGD/IMC. All patients first had endoscopic ultrasonography (EUS) to exclude deeper infiltration. CBE was completed in 32/49 patients and subsequent surveillance confirmed CR-BE in 97% of those (31/32) over a median of 17 months (IQR 11-38). EMR upstaged pathology in 14% and down staged in 31%. 37% (18/49) developed symptomatic stenosis after a median of 13 days (standard deviation 27.8), all of whom were effectively treated with endoscopic dilatation.

Comparing this study to data on the effectiveness of focal EMR followed by RFA in BE from the landmark AIM dysplasia trial <sup>147</sup>, CBE seemed much more effective at CR-IM (CR-BE) than RFA (97% vs 77.4% respectively). However, it is difficult to draw direct comparisons. This was made in a tertiary multi-centre randomised clinical trial comparing CBE with focal EMR followed by RFA for 47 patients with BE neoplasia (HGD/IMC)  $\leq$ 5cm. The study reported CR-IM to be 100% vs 96% for CBE vs EMR/RFA respectively. However, the stricture rate with CBE was far greater (88% vs 14%,  $p < 0.001$ ). The study concluded EMR/RFA may be preferable to CBE due to the significantly lower complication rate with near equivalent efficacy<sup>163</sup>.

**Figure 13: The two step method for circumferential EMR for BE to prevent stricture development<sup>161</sup>**



### 1.11 Surgery

Up until relatively recently oesophagectomy was the mainstay of therapy for BE with HGD. The advantage purported by surgery is the ability to harvest nodes for regional disease, and treat tumours infiltrating into and through the submucosa (T1b and beyond). This changed significantly due to advances in endoscopy in recent years which now show similar survival outcomes can be achieved whilst avoiding the

mortality and morbidity associated with major surgery. Morbidity are seen in up to 50% of patients and include perforations, fistulas, strictures, dumping syndrome, regurgitation and diarrhoea <sup>164,165</sup>. The introduction of minimally invasive surgical techniques have reduced length of stay, improved quality of life and reduced pulmonary complications compares to open surgery<sup>166</sup>.

Despite these advances, endoscopic therapy is now recommended as the first line treatment for HGD and intramucosal carcinoma by the British Society of Gastroenterology in preference over surgery or surveillance<sup>1</sup>. At the time of the recent 2016 National Oesophagogastric Cancer re-audit which collected data from 1331 patients with HGD, only 65.7% received endoscopic treatment. Of the remainder 72 patients (5.4%) had surgical resection and 363 (28.9%) had surveillance. The large proportion of patients in the UK still undergoing surveillance for HGD is a concern. Of those receiving endoscopic therapy, the 69% underwent EMR and 24.4% RFA. In those who receive surgical resection, nationwide survival rates are now 96.8% at 3 months, a considerable improvement from the previously.

Endoscopic therapy is recommended for patients with T1a cancer (limited to the mucosal layer. Tumour infiltration into the submucosal layer (T1b), the presence of lymphovascular or perineural invasion and poorly differentiated histology all increase the probability of lymph node involvement and are considered to support role for surgery for early OA <sup>167</sup>. For a select few patients with significant co-morbidities that preclude surgery, T1b disease limited to the 1<sup>st</sup> third of submucosa are recommended to be considered for EMR <sup>151</sup>.

Overall of all oesophagogastric cancers studied in the audit, 37.6% were managed with curative intent. The mainstay of treatment remains surgery, but suitability to this may be affected by frailty, nutritional status, other co-morbidities and patient preference. Most patients are managed with palliative intent. Options for treatment include

endoscopic stenting, palliative chemoradiotherapy, palliative surgery and best supportive care.

At present, studies comparing outcomes between minimally invasive endoscopic and surgical therapy for HGD and early cancer are misleading due to selection bias (157, 158). Endoscopic therapy was predominantly used in older individuals with smaller segments of BE and earlier tumours. The SEER database of the National Cancer Institute (USA) was the first population-based study to look at survival in early tumours (Tis and T1 disease without node or metastatic spread) treated endoscopically or with radical surgery. It found equivalent long-term survival in both treatment groups, supporting the effectiveness for managing these patients with endoscopic therapy (158).

There has recently been a paradigm shift in the use of minimally invasive endoscopic therapies for HGD, and the question of whether they should be offered to all patients with HGD, as a first line treatment, is the subject of great debate. Up until 2013, UK guidelines on the management of oesophageal cancer still presented surgery as the first line treatment option for early oesophageal cancer, recommending further research into minimally invasive endoscopic therapies for HGD and early mucosal cancer despite a growing body of evidence in its favour. In contrast, American College of Gastroenterology guidelines report that 70-80% of HGD can be successfully treated with endoscopic therapy with PDT, RFA or EMR, and recommend surgery be reserved for disease infiltrating the submucosa (T1b disease) after evaluation by surgical centres that specialise in the treatment of foregut cancers and high-grade dysplasia. In 2013, the British Society of Gastroenterology revised its guidelines on the management of BE. It recognised the efficacy of endoscopic therapy in HGD and T1a adenocarcinoma and recommending it to be used over oesophagectomy or surveillance in these patients<sup>1</sup>.

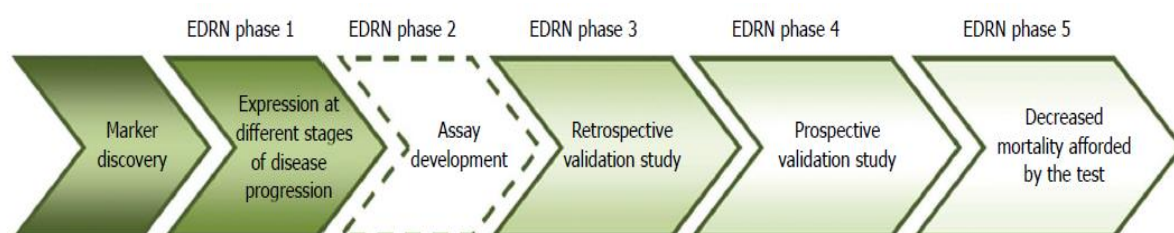
## **Chapter 2: Tissue biomarkers for the risk stratification and therapy of Barrett's neoplasia**

---

## 2.1. Tissue biomarkers for progression in Barrett's oesophagus

The Biomarkers Definitions Workgroup stated in 2001 that 'a biological marker – biomarker – is a characteristic that is objectively measured and evaluated as an indicator of normal biological processes, pathogenic processes, or pharmacologic responses to a therapeutic intervention <sup>168</sup>. The different phases of biomarker are highlighted in Figure 14 below.

**Figure 14: Early Detection Research Network Phases of biomarker discovery <sup>169</sup>.**

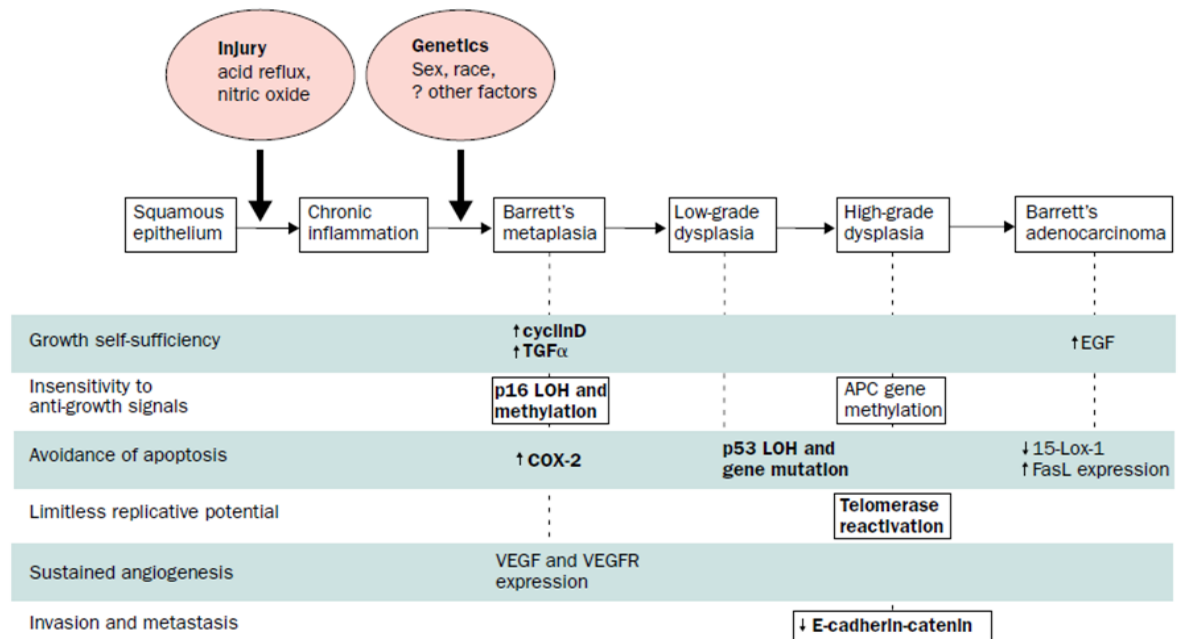


Biomarkers may indicate a change in expression or characteristics of a molecular entity that correlates with a certain diagnosis (for early detection of disease), risk (for progression of disease or prognostic), or susceptibility to a certain treatment.

Biomarkers therefore once validated, aim to inform or alter clinical management.

Figure 15 displays the relationship of when biomarkers develop in the progression to OA, and where the influence of inflammation and epidemiological factors is thought to prominently affect this sequence.

**Figure 15: Epidemiological factors and key biomarkers interplay in the squamous to oesophageal adenocarcinoma sequence** <sup>170</sup>.



Despite decades of research and discovery, the only established and accepted biomarker in widespread clinical use in BE management is dysplasia. This is usually identified from endoscopic surveillance biopsies taken according to the Seattle protocol. This requires quadratic biopsies to be taken at 2cm-intervals in non-dysplastic BE (NDBE) and 1 cm if dysplastic with additional targeted biopsy of mucosal irregularities <sup>2</sup>.

The following sections describe the current literature on tissue biomarkers investigated in BE to give a background to the work carried out in this thesis.



Figure 16: Genetic model of progression of Barrett's oesophagus to cancer <sup>171</sup>.

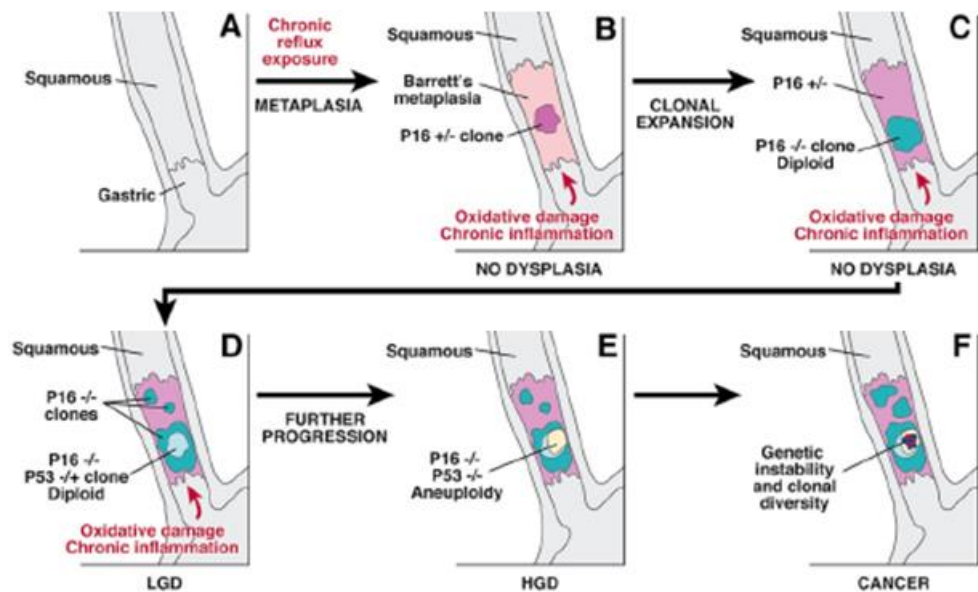


Figure 16 illustrates the potential sequential somatic genetic changes during progression from normal squamous oesophagus to Barrett's oesophagus and then adenocarcinoma. Squamous oesophageal epithelium undergoes metaplastic transformation in response to chronic inflammation caused by long standing gastroesophageal reflux. The initial change is followed by the loss of one p16 allele (B); and later the 2nd p16 allele (C) with the formation of p16 null clones (blue area). Mutations of TP53 then develop with subsequent loss of p53 proteins in parallel with the development of dysplasia (D). Genetic instability from increasing numbers of mutations can lead to abnormalities in DNA content known as aneuploidy. This is often seen with high grade dysplasia (HGD) (E). As mutations multiply, numerous clones can develop, causing variables degrees of genetic instability that may eventually progress to invasive adenocarcinoma (F)

<sup>171</sup>.

## 2.2. DNA content abnormalities (aneuploidy and tetraploidy)

DNA content abnormalities (DNA-CA) reflect genomic instability and confer an increased risk of cancer progression. They are one of the most frequent characteristics

of cancer cells and were originally described 121 years ago leading to Boveri's hypothesis in 1902 and 1914 that aneuploid cells are the progenitors of tumours <sup>172</sup>. Normal cells have 2 copies, also referred to as 2n or a diploid number, of each chromosome. Aneuploidy is an abnormal gain or loss of DNA content in these chromosomes. There are two ways in which aneuploidy can develop; the first is due to alterations in the number of intact chromosomes from errors in mitosis and is also known as whole-chromosome aneuploidy. Tetraploidy is a subtype of this category of aneuploidy and describes cells with 4 chromosome copies, twice the normal chromosome number. The alternative method of aneuploid development is due to structural rearrangements such as insertions, deletions or translocations that disrupt the DNA content. In BE, aneuploidy in chromosomes 4, 7, 8 and 17 have been shown to be early events in carcinogenesis <sup>173,174</sup>.

The early landmark experiments were carried out by Reid et al in a prospective study of BE patients with GORD. Using flow cytometry, a significantly increased risk of progression to OA was found in those individuals with tetraploidy (RR 11.7, 95% CI: 6.3-22) and aneuploidy (RR 9.5 CI: 4.9- 18) <sup>175-177</sup> compared with controls <sup>176</sup>. Furthermore, when combined with HGD, the five-year risk of cancer with DNA-CA equated to 66%, compared with 42% (HGD only) and 28% (DNA-CA only).

The method of flow-cytometry used to detect DNA-CA in these early studies was however cumbersome and could not be applied to archived formalin-fixed paraffin embedded (FFPE) material; the standard method for storing tissue in clinical biobanks. This limitation was overcome by the development of image cytometry (IC) which has been shown by our group to have equivalent accuracy to flow cytometry in the detection of DNA-CA <sup>178</sup>. The efficacy of DNA-CA measured with IC as an independent predictor of cancer progression was highlighted in our recently published population-based study on the Northern Ireland Barrett's Registry. In the study, the adjusted Odd Ratio (OR) of LGD alone was 3.74 (95% confidence interval, 2.43-5.79), for each additional biomarker,

Aspergillus oryzae lectin (AOL) and DNA-CA, the risk increased by 2.99 highlighting the benefit of a biomarker panel to predict progression more accurately <sup>179</sup>.

Based on this and more recent work DNA-CA is now considered to be a phase 4 biomarker but are yet to be included in clinical guidelines due to the difficulties in implementing them into routine clinical practice. We recently published the first abstract of our clinical experience with DNA-CA testing in a tertiary centre. We analysed 682 FFPE specimens from 189 patients who had matching H&E specimens taken at the time of IC analysis <sup>180</sup>. DNA-CA was found to directly correlate with increasing pathological grade (Pearsons R=0.96; p=0.039). Similar findings of a direct correlation between pathological grade and DNA-CA's have been shown in older smaller studies <sup>181,182</sup>. In our centre, IC was requested for the reasons described in Table 4:

**Table 4: Indications for clinical evaluation of DNA content abnormalities.**

	Indication for image cytometry (IC)	Outcome
1	Persistent or recurrent low-grade/indefinite for dysplasia	Increased surveillance/ endoscopic therapy
2	Clinical suspicion of progression. For example, long BE segment and family history of OA	
3	Suspicion of having relapsed after prior endoscopic treatment of HGD/IMC	

*DNA-CA is presently a phase 4 biomarker but follow up prognostic studies from this research are anticipated to propagate this to phase 5 biomarker status.*

### **2.3. Loss of tumour suppressor loci – p16 and p53**

Loss of heterozygosity (LOH) refers to the loss of a chromosome segment after a faulty cell division, and hence the loss of the functioning genes in that segment.

LOH of the tumour suppressor genes (TSG) p16 (9p) and p53 (p17) have been extensively studied in BE. Both genes have also been shown to be silenced by DNA

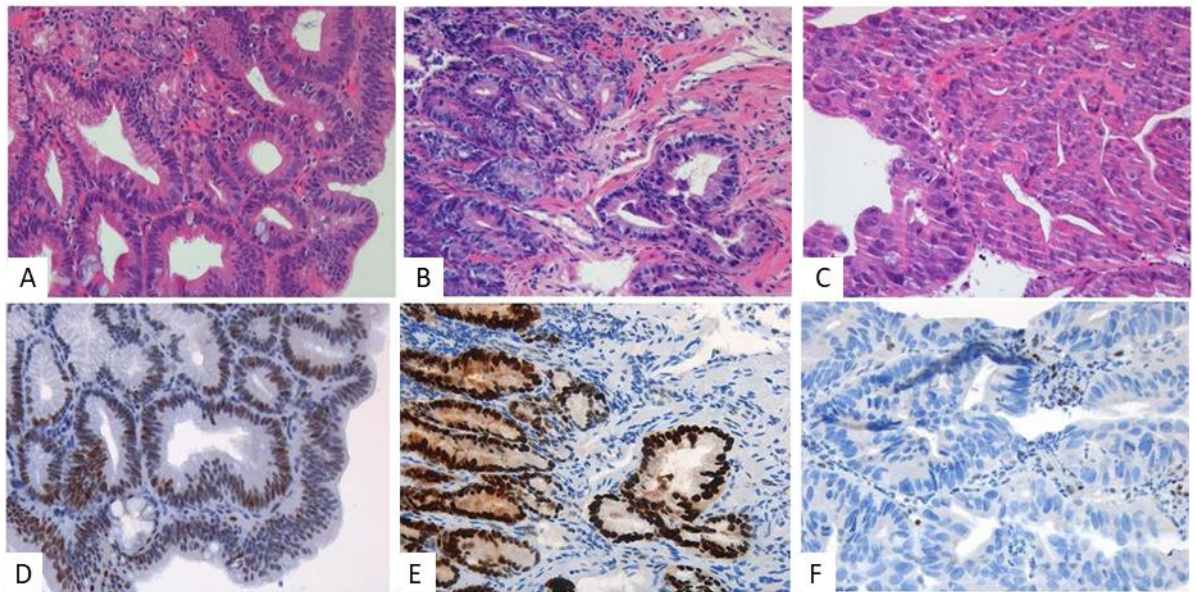
methylation and mutations <sup>169</sup>. It is known that p16 silencing occurs early on in BE pathogenesis, however on its own this is not clinically useful as shown in one study where no correlation between p16 silencing and oesophageal dysplastic grade was found <sup>183</sup>. The importance of p53 LOH however has been shown in a prospectively studied cohort of 325 BE patients. Those who showed p53 LOH had 16x increased risk of progression to OA (95% CI: 6.2-39) <sup>184</sup>. The p53 tumour suppressor protein is responsible for the integrity of the genetic sequence. DNA damage normally results in increased expression of p53, subsequent cell arrest in the G1 phase followed by DNA repair or apoptosis. In LOH, or when mutated, silencing of p53 occurs making this self-repair mechanism redundant. Extending from this work, the Reid group demonstrated in a landmark study how a biomarker panel of p53 LOH, 9p LOH and DNA-CA can predict OA progression risk much more effectively than each individual biomarker <sup>177</sup>.

UK guidelines recommend p53 immunohistochemistry (IHC) to be used as an adjunct in the diagnosis of dysplasia and indefinite for dysplasia <sup>1</sup>. This national guideline is the first to recommend the routine use of a biomarker other than dysplasia to assist in the diagnosis and hence risk stratifications of patients. Due to the specialised nature of p53 IHC, cases should be reviewed by 2 expert pathologists to decide on the outcome. Three patterns of staining p53 staining have been identified, normal, overexpression and absence of expression (Figure 17). For simplicity in reporting, overexpression and absence of p53 expression are grouped together into an “aberrant p53 expression” category as both patterns are abnormal for research and clinical use.

Although there was 90% agreement amongst the BSG guideline panel recommending p53 IHC, data around the efficacy of correlation between p53 LOH and IHC shows that it at best performs reasonably <sup>1</sup>. In a nested case controlled study of a large population of BE patients, p53 IHC predicted only 32% of those cases who progressed to OA <sup>185</sup>. When considering progression from dysplasia to HGD/OA, p53 performed considerably better with 88% sensitivity and 75% specificity quoted in one study <sup>186</sup>. Other studies have also shown p53 to increase risk of neoplastic progression when present in BE,

however when combined with dysplasia the risk was noted to be even greater <sup>179,187</sup>. These studies therefore support the use of p53 in the UK guidelines to decide on the presence of dysplasia, but the guidelines do not factor in the independent predictive value of p53 which would translate it into wider clinical use than recommended at present <sup>1</sup>.

**Figure 17: p53 immunostaining patterns in Barrett's epithelium**



H&E staining (A-C) and corresponding p53 protein immunohistochemistry (D-F) highlighting distinct oesophageal p53 staining patterns: (A+D) BE with low-grade dysplasia (LGD) and normal p53 expression; (B+E) BE with LGD and p53 overexpression and (C+F) oesophageal adenocarcinoma with loss of p53 expression (adapted from 187).

#### **2.4. Epigenetic changes**

Epigenetics refers to post-transcriptional silencing of specific genes by a variety of mechanisms such as hyper- or hypomethylation or acetylation. Methylation of DNA cytosine residues in the promoter CpG island is a common gene silencing mechanism that has been shown to occur early in BE associated OA tumour genesis of genes such as APC, CDH1, CDKN2A (p16) and ESR1 (estrogen receptor alpha) <sup>188</sup>. Similarly,

promoter methylation of BNC 2 and CDKN2A has been shown to occur in large areas of contiguous Barrett's epithelium suggesting clonal expansion of hypermethylated cells or field methylation of metaplastic BE (86,87). The early stage of methylation changes in the BE-OA sequence, highlights the potential for these biomarkers to be used to predict which patients with BE are likely to progress.

Methylation induced inactivation of the p16 TSG is one of the most common genetic abnormalities in BE and regulates cell cycle progression. In patients with BE, p16 methylation is highly prevalent (34 – 66 % )<sup>189</sup>. Furthermore, p16 (OR 1.74; CI 1.3-2.2), RUNX3 (OR 1.8; CI 1.1-2.8) and HPP1 (OR 1.8; CI 1.1-2.8) methylation<sup>190</sup>, and p16 with APC hypermethylation (OR 14.97; CI 1.73-inf)<sup>191</sup> have been shown to be independent risk factors for progression in patients with NDBE and LGD.

Though these findings are promising, the complex biochemical methods required to assess methylation status has hampered translation to the clinic as they are very demanding and time consuming.

## **2.5. Cell cycle biomarkers**

This encompassing category of biomarkers broadly includes previous sub-divisions of biomarkers involved in the cell cycle named cell cycle predictors, proliferative markers and DNA replication licencing factors. Cell cycle biomarkers are thought to be useful for predicting progression to OA as they are intimately involved in all aspects of the cell duplication machinery. As the cell machinery dysregulates in the progression to cancer, it is thought that certain cell cycle biomarkers may also alter their profile in correlation with these changes and may be used as surrogates for abnormalities of DNA content.

### ***2.5.1 Initiation of DNA replication (G1 phase): Pre-replication complex***

The pre-replication complex (pre-RC) is a complex that forms at the origin of DNA replication. Formation of the pre-RC is essential for initiation of cell division and in mammalian cells is composed of 6 ORC proteins, Cdc6, CDT1 and a heterohexamer of

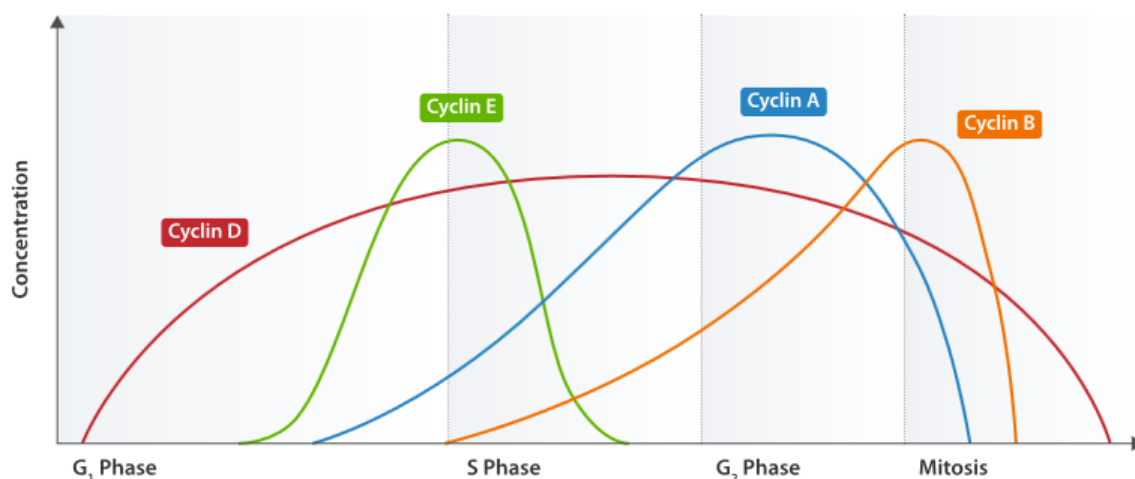
6 mini chromosome maintenance proteins (MCM 2-7)<sup>192</sup>. These pre-RC proteins have been categorised by some authors as 'proliferative abnormalities' of risk in BE<sup>169,193</sup>.

Controversy continues as to the utility of whether proliferation markers accompany development of dysplasia. In BE, Mcm2 and Mcm5 surface positivity were found to correlate with the severity of dysplasia<sup>194</sup>. A subsequent study using the same immunostain for Mcm2, demonstrated that aberrant surface expression increases along the metaplasia-dysplasia-carcinoma sequence. Interestingly, in the study mcm2 was more sensitive than Ki67 for detection of dysplasia<sup>195</sup>. This finding was supported in a phase-3 study which showed that BE biopsies in patients who progressed to OA had Mcm2 expression in 28.4 % of the luminal cells as compared with 3.4 % of non-progressors<sup>196</sup>. Studies into other potential proliferation markers, particularly Ki-67, to predict progression to OA in BE have shown promising results but again need validation in larger cohorts<sup>197</sup>.

### **2.5.2 Cyclins**

Cyclins were originally named after cycling as their concentration in the cell varied in a cyclical fashion during cell division. When bound to the dependent kinases such as cdk1, cyclins form maturation-promoting factors (MPF). MPF are in turn then responsible for key cell cycle events including microtubule formation and chromatin remodelling. Cyclins are subdivided into 4 categories based on their behaviour during the cell cycle.

**Figure 18: Representation of Cyclin levels during cell cycle** <sup>198</sup>.



In BE and OA, cyclins A and D particularly have been investigated. Cyclin D1 is proto-oncogene protein and antagonist of p16 and together they regulate cell cycle progression. It has been shown that BE patients positive for cyclin D1 detected with IHC were more likely to develop OA (OR 6.85; CI 1.6-29.9) <sup>199</sup>. These findings were not repeated by others in a larger population based study, who instead commented on the usefulness of p53 in the prediction of progression <sup>185</sup>. This however may have been due to an older cohort of patients with shorter follow-up being studied.

Cyclin A is a key checkpoint protein in the G<sub>1</sub>-S transition phase of the cell cycle. In one study conducted by our group, biopsies expressing Cyclin A were found to correlate with increasing pathological grades, and biopsies expressing cyclin A were far more likely to progress (OR 7.5; CI 1.8-30.1) to OA than those without <sup>200</sup>.

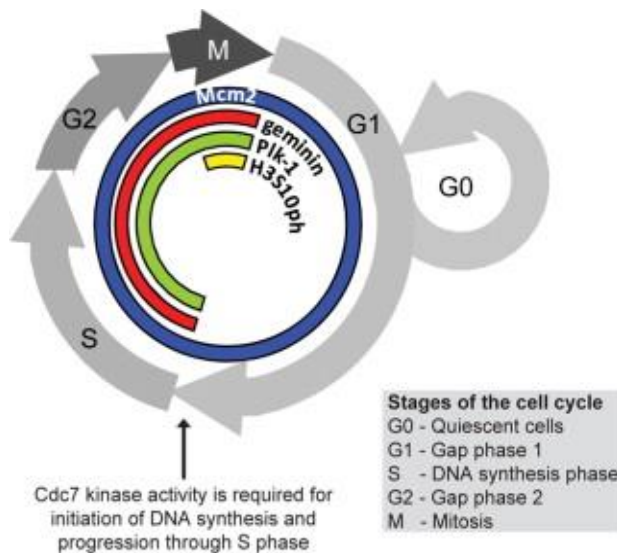
### **2.5.3 Cell cycle biomarkers as a surrogate for DNA content abnormalities**

It has previously been hypothesised that cell cycle markers may be utilised as surrogate markers for aneuploidy. The first pilot study suggesting this link in BE and OA was performed by our group. It examined various grades of pathology extracted from 10 oesophagectomy specimens from patients with established BE related OA. The different pathological grades were obtained via laser capture microdissection (LCM) and matched



samples examined using IC and IHC. The cell cycle markers Polo-like Kinase-1 (PLK-1), Geminin and Cdc-7 Kinase were found to correlate best with DNA-CA, most notably, PLK-1 ( $P < 0.01$ , Pearson's coefficient  $R^2 = 0.776$ ). With a cut off value of 30%, PLK-1 exhibited a sensitivity of 86% and specificity of 100% for aneuploidy detection <sup>197</sup>.

**Figure 19: Phase specific distribution of cell-cycle biomarkers** <sup>201</sup>.



Though promising, this early work was limited as all pathological grades were obtained from OA specimens making field cancerisation a potential confounder of the studies outcomes. Furthermore, the small number of cases meant the study was not powered highly enough to definitively make the conclusions suggested. These two issues will be investigated in further detail through this thesis.

### 2.5.3.1. Polo-like kinase 1

Polo-like kinases are a family of serine-threonine kinases among which, PLK1 has been the best characterised. PLK1 is overexpressed in a variety of human cancers <sup>202</sup>. For oesophageal cancer, PLK1 overexpression has been reported in 80-97% of tumours, but it is not overexpressed in the normal oesophagus <sup>202,203</sup>. Proportion of PLK1 positive cells have been shown to correlate with histological grade in other cancers <sup>204</sup> and so it is postulated that in the progression to OA, PLK1 is progressively upregulated. Whether this occurs early or late in the progression to cancer requires access to longitudinal population-based tissue from BO progressors and matched controls. This information is

essential for understanding PLK1 as a biomarker for risk.

PLK1 is a key regulator of cell division and is also a central player in maintaining genome stability during DNA replication and in modulating the DNA damage response<sup>205</sup>. PLK1 is required in most of the mitotic steps, but when overexpressed PLK1 overrides mitotic checkpoints and leads to immature cell division without proper chromosome alignment and segregation<sup>206</sup>. Defects in mitotic checkpoints are known to cause DNA content abnormalities such as aneuploidy<sup>207</sup>.

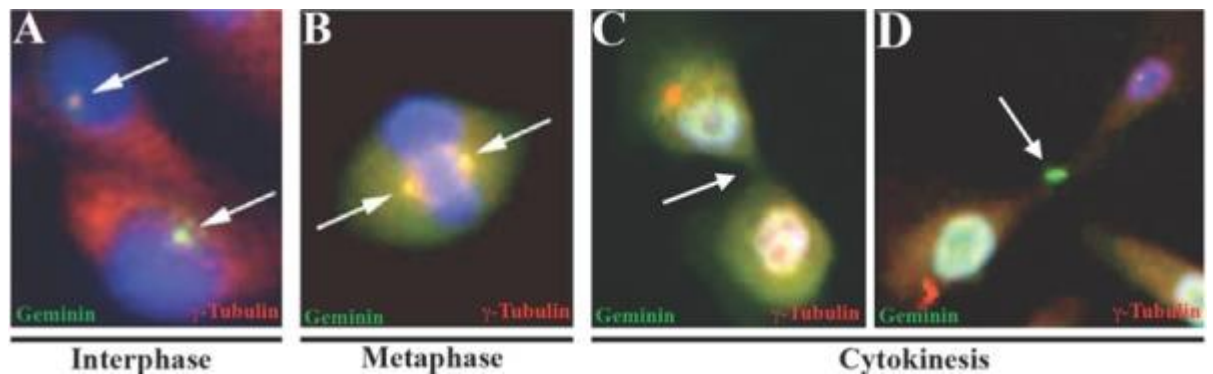
#### 2.5.3.2. Geminin

Geminin is a multifunctional protein with several roles to play in cytokinesis summarised in Table 5. A direct relationship between Geminin and aneuploidy has been reported in human tumours<sup>208,209</sup>. In Geminin overexpressing cells, completion of topoisomerase II $\alpha$  chromosome decatenation was seen to be prevented leading to aneuploidy in human mammary epithelial cells<sup>210</sup>. Geminin upregulation has also been shown to correlate with poor clinical outcome using IHC in other glandular carcinomas supporting its potential role as a potential predictor of pathological grade independent of aneuploidy.

**Table 5: Functions of Geminin in cytokinesis** <sup>208</sup>.

	Function
1	Binds Cdt1 at the origin of replication preventing recruitment of MCM2-7 complex, and hence inhibiting DNA replication
2	Antagonises transcriptional activity of Six3 and HoxB9
3	Co-ordinates proliferation and differentiation in nervous system by assisting transcriptional modulators like polycomb and SWI/SNF in control of cell cycle progression, chromatin organisation and transcription
4	Modulates T-cell proliferation and expansion in the immune response.
5	Supresses large scale chromosome de-condensation induced by Cdt1 and MSM in G1 phase
6	Regulates pluripotent cells self-renewal by silencing expression of self-maintenance proteins, Oct4, Sox2 and Nanog.

**Figure 20: Geminin localisation during human mammary epithelial cell cycle.**



*Geminin (green) is localised with  $\gamma$ -tubulin (red) to centrosome in late interphase (A), spindle in metaphase (B) and cleavage furrow and mid-body in cytokinesis (C and D) (Adapted from <sup>208</sup>).*

## **2.6. Therapeutic biomarkers**

Research on the molecular biology of cancer has identified numerous novel receptors that may be targeted via multiple approaches for cancer therapy. Targeted therapy focuses on individual aspects of the malignant cells machinery, including fundamental molecules involved in cell invasion, apoptosis, metastasis, cell-cycle control, and tumour-related angiogenesis <sup>209</sup>. These fundamental molecules, or tumour related antigens (TRAs) may arise as products of oncogenes, loss of function of tumour suppressor genes through insertions, deletions or translocations, or they may be normal proteins with abnormal expression patterns.

### **2.6.1. Targeting and classification of Tumour Related Antigens**

TRAs may be extracellular, leaving them open to direct targeting via antibodies, or intracellular which may indirectly be targeted by T cells, or more specifically T cell receptors (TCR). TCRs found on the surface of T cells, look into cells via the endogenous pathway involving major histocompatibility complex (MHC) class I molecules. In this pathway, MHC class I molecules present peptides from intracellular proteins, such as TRAs, to the cell surface.

TRA's may be sub-classified further into tumour specific antigens and tumour associated antigens. Tumour specific antigens (TSA), as the name suggests, are located on tumours only such as the extracellular epidermal growth factor receptor. Tumour associated antigens (TAA) meanwhile are expressed on but are not specific to tumour tissue. Well known extracellular TAAs include carcinoma-embryonic antigen (CEA), prostate specific antigen (PSA), and the oestrogen receptor (ER). Antibodies raised against extracellular tumour associated antigens are therefore inherently non-specific and potentially cross react with more normal cells when compared with antibodies to tumour specific antigens.

Most intracellular TRA's are identified via transfection of genomic DNA or cDNA libraries into the appropriate MHC molecule followed by detection of transfectants with human T cells or cytokine release <sup>211</sup>. To target these intracellular TRA's however requires an additional level of complexity to extracellular TRAs. Potential targeting strategies include viral mediated gene transfer <sup>212</sup>, immunoliposomes <sup>213</sup>, TCRs engineered to cytotoxic payloads <sup>214</sup> and photochemical internalisation (PCI) <sup>215</sup>.

### ***2.6.2. Diagnostic and prognostic role for TRA in abdominal malignancy***

TRA's have a role in clinical practice for certain cancers. Common TRA's include CEA, Ca-125,  $\alpha$ FP, Ca 15-3 and Ca 19-9. The latter two evaluate serum MUC1 glycoepitopes. The role of such TRA's in screening for luminal gastrointestinal malignancy is however limited. For colorectal cancer, a large retrospective Finish study of TRA screening reported the specificity and sensitivity for CEA and Ca 19-9, were 91% and 64%, and 74% and 73% respectively <sup>216</sup>. For breast, ovarian, lung or pancreatic cancers, a comprehensive study on the potential role of MUC1 glycoepitopes found they could not be used as a screening test for these either <sup>217</sup>. UK guidelines for the diagnosis of pancreatic cancer however include a recommendation for CEA to be measured when evaluating cystic lesions in the pancreas in addition to cytology to improve diagnostic accuracy <sup>218</sup>. TRA's such as CEA and Ca 19-9 in pancreatic malignancy <sup>219</sup> and CEA for colorectal malignancy have a further role in disease follow up where levels were raised

at outset. For, CEA they form part of established guidelines for follow up post-treatment of colorectal cancer <sup>220</sup>.

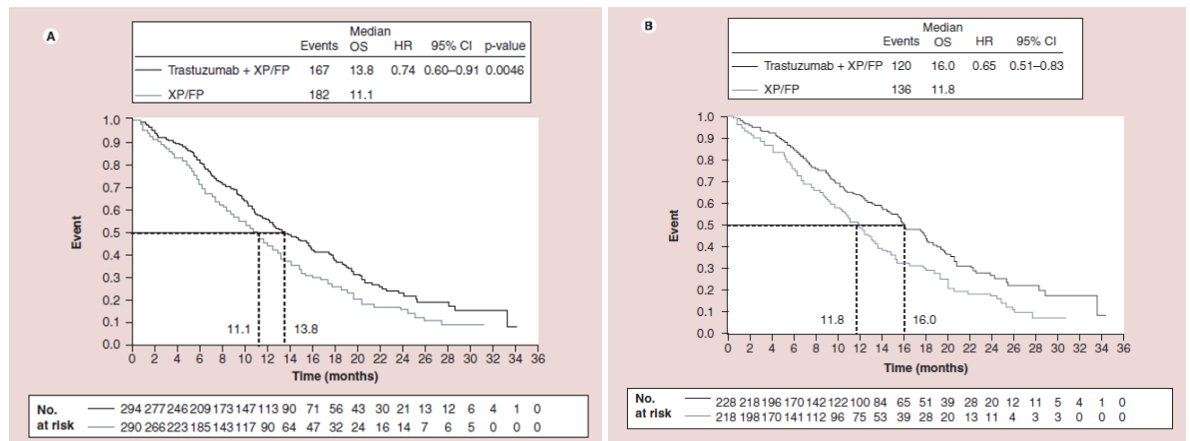
### **2.6.3. Human Epidermal growth factor Receptor 2**

Among potential therapeutic targets for OA, human epidermal growth factor receptor 2 (HER2) targeted therapy has had the most significant impact into widespread clinical practice. Also referred to as Her2/neu, ErbB-2, p185 or CD34, HER2 is a membrane bound receptor tyrosine kinase encoded by the ERBB2 proto-oncogene located on chromosome 17q21. It is normally involved in signal transduction pathways leading to cell growth and differentiation<sup>221</sup>.

HER2 overexpression by IHC has been shown to occur in ~20% of resected breast cancers <sup>222,223</sup>, 9.4% - 20% of gastric cancers <sup>224</sup>(118), and 15-16% OA <sup>225,226</sup>. When present, HER2 expression in gastric cancer is associated with disease progression <sup>227</sup>. Furthermore, a systematic review of 49 reported studies relating to gastric HER2, totalling 11,337 patients, identified overexpression to also be associated with poor survival and intestinal type tumours <sup>228</sup>.

The potential of the HER2-targeting agent Trastuzumab was shown in the Phase III ToGA study in patients with gastric and junctional oesophagogastric cancers. In patients expressing this marker, statistically significant improvement in response rate, progression-free and overall survival was seen in addition to standard therapy <sup>229</sup>. This led to the approval of Trastuzumab for the treatment of HER2 positive oesophagogastric cancers by both the European Commission <sup>230</sup>, National Institute for Health and Care Excellence in the UK <sup>221</sup> and Food and Drugs Administration in the USA <sup>231</sup>.

**Figure 21: (A) Median overall and (B) progression-free survival in the primary analysis populations (Trastuzumab + chemotherapy vs chemotherapy alone) of Phase III ToGA trial. <Adapted from <sup>229</sup>>.**



Although expression profiles of HER2 have been examined in oesophagogastric cancers, the pathological stage at which HER2 expression begins in the BE to OA sequence warrants further clarification and will be examined in this thesis.

#### **2.6.4. Epidermal Growth Factor Receptor**

Epidermal Growth Factor Receptor (EGFR) (also known as ErbB-1), is a member of the ErbB receptor tyrosine kinase family that includes like HER2 (ErbB-2) <sup>232</sup>. The natural ligands of EGFR, EGF and transforming growth factor-alpha (TGF- $\alpha$ ), both activate EGFR by binding the extracellular domain. This then induces the formation of receptor homodimers or heterodimers, followed by activation of the receptors' intrinsic tyrosine kinase. HER2 plays a significant role in this signal network, because activated heterodimer complexes containing HER2 and EGFR are more stable at the cell surface than complexes with the other EGFR family members <sup>233,234</sup>.

EGFR mutations have been found in 11-30% OA tumours. EGFR assessment could therefore select patients for targeted EGFR therapies <sup>235-237</sup>. There are 2 methods to

target EGFR, mAbs to the EGFR and small-molecule tyrosine kinase inhibitors. Many clinical studies have recently been published with both classes of agent.

Preliminary data with ABX-EGF, a high affinity human IgG2 EGFR monoclonal antibody (mAb) reported cessation of progression in one OA patient. However the phase 3 open-label REAL 3 study evaluating chemotherapy with or without ABX-EGF across 63 UK centres was halted early by the independent clinical trial committee as it was found not to increase overall survival <sup>238</sup>. Similarly, the results of SCOPE1 (Chemoradiotherapy with or without cetuximab in patients with oesophageal cancer) and EXPAND (Erbix in Combination with Xeloda and Cisplatin in Advanced Esophago-gastric Cancer) open labelled clinical studies investigating the role of cetuximab, a chimeric (mouse/human) mAb were also recently published with disappointing results. In EXPAND, 904 patients were enrolled across 164 sites in 25 countries but the investigators found the addition of cetuximab to standard chemotherapy in gastric and gastro-oesophageal junction cancers provided no benefit to chemotherapy alone <sup>239</sup>.

Erlotinib and Gefitinib are small molecules that inhibit ATP binding within the tyrosine kinase domain, completely blocking EGFR autophosphorylation and signal transduction <sup>240</sup>. Both have been evaluated in phase 2 studies that have recently been published. For Gefitinib, the study was undertaken over 7 years and enrolled 58 patients in which only 7% had partial response and 17% stable disease <sup>241</sup>. The addition of Erlotinib to radiotherapy in elderly patients with oesophageal cancer showed more promising results in a phase 2 trial of 17 patients, 16 of which had adenocarcinoma. Sub-group analysis found that overall survival was longest in patients expressing the EGFR receptor and non-smokers at 22.3 and 16.6 months respectively <sup>242</sup>.

In summary, studies evaluating both classes of EGFR targeting agents have had relatively poor results in the clinic to date and therefore do not support the use of this biomarker in the management of BE or OA.

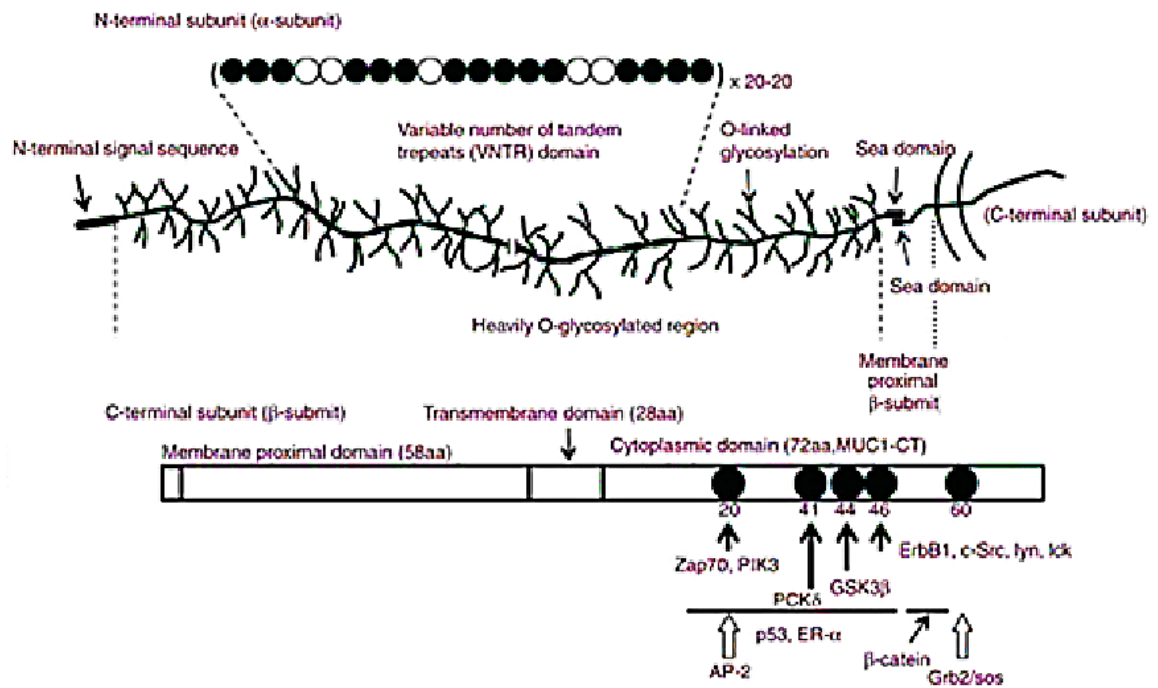


### **2.6.5. The glycoprotein Mucin 1**

Molecular patterns on the epithelial cell-surface have recently been used to detect risk of progression to OA such dysplasia <sup>243</sup>. Biochemical alterations in glycans and carbohydrates are particularly promising due to their abundance on the cell surface and the historical wealth of data around them. These surface targets have the potential of being translated into therapeutic benefit.

Mucin 1 (MUC1) is densely glycosylated type 1 transmembrane protein anchored to the apical surface of many epithelia including the breast, ovary, pancreas, airway and gastrointestinal tract <sup>244</sup>. The structure of MUC1 is composed of carbohydrates O-linked to serines and threonines within the variable number of tandem repeats (VNTR) of 20 amino acids (GVTSAPDTRPAPGSTAPPAH) region of the extracellular domain, (N-terminal  $\alpha$ -subunit), and C-Terminal subunit. The number of VNTR's in epithelial tissues is allele dependent, and varies between 20-125 in MUC1 <sup>245</sup>. The C-terminal subunit is divided further into the 58-amino acid (aa) membrane proximal domain, a 28-aa transmembrane domain, and a 72-aa intracellular cytoplasmic tail domain (MUC1-CT). Extracellular MUC1 domains is divided post translation at the SEA (sea urchin sperm protein, enterokinase and agrin) domain into 2 subunits, the much larger heavily glycosylated  $\alpha$ -subunit and membrane proximal portion of the  $\beta$ -subunit.

Figure 22: Structure of MUC1 receptor <sup>246</sup>.



MUC1 expression is known to strongly increase during progression through increasing grades of pathology towards cancer. This is aberrantly glycosylated during the development of cancer, by down regulation of glycosyltransferases and upregulation of sialyltransferases. This results in premature termination of glycosylation exposing distinct carbohydrates, proteins or glycoprotein motifs that may be utilised as tumour specific or associated antigens. These exposed carbohydrate antigens on MUC1 include Tn, sialyl-Tn, monosialyl TF, disialyl-TF <sup>247</sup>, sialyl Lewis A, sialyl Lewis C, Lewis X and sialyl Lewis X <sup>248</sup> hidden in normal cells. The exposed extracellular amino acid sequences are described further in Table 6 below.

**Table 6: Methods for tumour associated antigen creation in MUC1 and antibodies to detect them adapted from <sup>247,248</sup>.**

<b>Epitope regions</b>	<b>Unique carbohydrate antigens, VNTR amino acid sequences or combinations of both bound by antibodies</b>	<b>Antibody</b>
<b>O-linked carbohydrate structures</b>	T (Gal $\beta$ 1-3GalNAc-O-S/T)	3C9
	Tn (GalNAc-O-S/T)	5F4
	Sialyl-Tn (Neu5Ac $\alpha$ 2-6GalNAc-O-S/T)	TKH2
	Sialyl Lewis A	NS19.9
	Sialyl Lewis C	DuPan2
	Lewis X	P12
	Sialyl Lewis X	CSLEX
<b>Sialylated amino acids</b>	Neu5Ac $\alpha$ 2-3Gal $\beta$ 1-3GalNAc linked to VTS	MY.1E12
	Unknown carbohydrate linked to PDTRPAP	NCL-MUC-1
<b>Core amino acids</b>	TRPAPG	NCL-MUC1-CORE
	TRPAPGS	DF3
<b>Glycosylated amino acids on VNTR region</b>	Fully glycosylated MUC1 linked to core peptide PDTR	HuHMFG1
<b>Cytoplasmic tail amino acids*</b>	RYVPPSSTDRSPYEKVSAG	MUC1-014E
	SSLSYTNPAVAATSANL	CT2

\* cytoplasmic antibodies are not tumour associated and have been added for comparison

Studies on the expression of MUC1 in BE and OA have shown conflicting data. This may be due to the multitude of antibodies and targets on MUC1 and the variety of antibodies raised against them (Table 6). Histological data from 52 patients in one study with BE associated OA, confirmed that 100% of tumours expressed MUC1

strongly using IHC. Furthermore, in the Barrett's, dysplasia-carcinoma sequence, whilst most mucin genes were downregulated, in severely dysplastic and neoplastic oesophageal tissues MUC1 was upregulated, but expression was not specific for dysplasia or OA <sup>249</sup>. Upregulation of MUC1 in the progression to OA from normal squamous patients was also reported in a study of 46 cases using mRNA detection with in-situ hybridisation (ISH) and immunohistochemistry (IHC) <sup>250</sup>. Conversely, Guillem et al examined expression of MUC1 at the RNA level using ISH in normal squamous oesophagus and patients with BE and BE with LGD, HGD and OA. MUC1 was detected in 100% of the normal squamous oesophagus cases but in none of the BE, BE with LGD, HGD or OA patients <sup>251</sup>.

#### 2.6.5.1. Humanised milk-fat globule-1

Humanised human milk-fat globule-1 (HuHMFG1, formerly known as AS1402 and R1550) is a fully human monoclonal antibody directed against the PDTR amino acid sequence of MUC1, located in the VNTR of the  $\alpha$ -subunit. This sequence is thought to be hidden by glycosylation patterns in normal epithelium offering discrimination between normal and tumour tissue and therefore a window to develop targeted therapies against it <sup>252</sup>.

AS1402 has been evaluated in clinical trials, initially relying on its ability to generate antibody dependent cellular cytotoxicity. In phase 1 and 2 studies against advanced breast cancers, however, no therapeutic benefit was observed but treatment was tolerated with manageable toxicity <sup>252</sup>. Another study used yttrium-90-AS1402 in ovarian cancers post de-bulking surgery. The passive labelled AS1402 infusion provoked endogenous production of anti-MUC1 IgG, and in those cases where this was noted, there was survival benefit <sup>253</sup>.

#### 2.6.5.2. CT2

CT2 is an Armenian monoclonal antibody directed against the last 17 amino acids (SSLSYTNPAVAATSANL) of the MUC1 cytoplasmic tail. It reacts well to both human

and mouse MUC1 in immunoprecipitation , immunoblot and IHC <sup>254,255</sup>. It is like CT1 polyclonal antiserum and recognises the same antigen. The epitope bound by CT2 is protected from epigenetic changes in the progression to cancer, and so it functions as a useful control to evaluate presence of MUC1 in tissues IHC.

#### 2.6.5.3. NCL-MUC-1

Produced by Novocastra, Leica Biosystems, NCL-MUC-1 is one of the main MUC1 antibodies available commercially and detects the presence of a carbohydrate epitope of the human MUC1 glycoprotein. Specifically, this carbohydrate is bound to the PDTRP peptide sequence on the VNTR backbone of MUC1. It has been shown to work well on gastric tissue using IHC in a number of studies and was therefore hypothesised to have similar efficacy on BE and OA tissues <sup>256–259</sup>.

### 2.7. Summary

Biomarkers offer great potential at multiple points in the clinical pathway of BE patients; from early disease diagnosis, to assessing progression to personalised therapy. Studies suggest that panels of currently available biomarkers are likely to be required to achieve the sensitivities and specificities required in clinical practice. Although many candidate biomarkers have been proposed, few have progressed to large population-based studies however the recent implementation of p53 into UK guidelines holds promise for future work. Translation of biomarkers into clinical practice remains challenging but could be facilitated by consortium approaches and shared biobank resources for validation studies.

## Chapter 3: Research aims and hypothesis

---

### 3.1. Overview of research aims and hypothesis

This thesis aims to translate molecular biomarkers for the risk stratification and targeted therapy of patients with Barrett's epithelium (BE) and oesophageal adenocarcinoma. The null hypothesis is that selective biomarkers for more advanced stages of BE and OA may not be used to:

- a. identify those patients with BE that may progress to cancer sooner.
- b. treat these higher-grade pathologies with superior efficacy and selectivity than previously possible with traditional photodynamic therapy, by combining tumour specific antibodies to second generation photosensitisers.

Cases at various pathological grades through the metaplasia-dysplasia-cancer sequence from normal squamous oesophagus to OA will initially be selected to make the case for these objectives. Cases will be screened to ensure they have never previously had higher pathological grades. For example, a squamous case cannot have had previous BE, and a LGD case can only have had non-dysplastic BE in the past, not HGD or cancer. The utility of a range of biomarkers to predict advanced pathological grades will then be examined.

Surface exposed biomarkers with potential for future targeted therapies will then be assessed. The expression of HER2 will first be examined from the population of metastatic oesophagogastric cancer tissue specimens referred to UCLH advanced diagnostics laboratory. The relationships between HER2, clinicopathological factors and prognosis will be investigated.

The stage at which HER2 is expressed in the squamous to OA sequence will first be examined using gene set enrichment analysis. Tissue expression will then be evaluated in from each pathological stage during cancer progression. An attempt to digitally evaluate tissue expression will be made and compared with pathologists scores to see if the utility of this approach. Finally, binding of a HER2 targeting

antibody fragment will be assessed in oesophageal lines of various pathological grades.

The HER2 targeting antibody fragment will be conjugated to a manufactured photosensitiser to create a photoactive antibody drug conjugate. The development and characterisation of this compound will be carried followed by evaluation of its therapeutic efficacy in vitro and vivo.

As HER2 is known to target only up to a quarter of OA patients, the next phase of work will focus on the characterisation of the glycoprotein Mucin 1 in oesophageal tissue. Gene set enrichment analysis will first detect expression in published datasets. IHC will then examine MUC1 expression with a range of antibodies targeting different epitopes of the MUC1 receptor. Flow cytometry will again be used to detect MUC1 expression levels in living cell lines matching the stages of OA progression. Finally binding and internalisation of an antibody targeting MUC1 will be examined with confocal microscopy.

A first in class photoactive antibody drug conjugate (ADC) targeting the MUC1 receptor will then be developed and characterised. The mechanism by which this ADC may destroy oesophageal cells will be evaluated through the manufacture of a second ADC attached to an imaging agent. The internalisation kinetics of both drugs will then be evaluated with confocal microscopy. Finally, the therapeutic efficacy over PDT and selectivity to cells only expressing the MUC1 epitope will be evaluated in vitro.

### **3.2. Risk stratification of Barrett's oesophagus**

#### ***3.2.1. Is abnormal p53 the most accurate biomarker for dysplasia in BE?***

When examining patients with BE, the most important diagnostic question for endoscopists is whether the BE segment has progressed to dysplasia or neoplasia. Making a diagnosis of dysplasia, particularly low-grade can be challenging even for experts. However once established, LGD directly impacts subsequent management



with a strategy of endoscopic eradication rather than ongoing surveillance recommended.

Abnormalities of Tumour protein 53 (TP53) oncogene detected by over or under expression of p53 protein in tissue specimens is presently the only tissue biomarker advocated for use in British Society of Gastroenterology guidelines to assist with the diagnosis of dysplasia<sup>1</sup>. Whether this is the most effective biomarker to answer this diagnostic dilemma is questionable. DNA content abnormalities (DNA-CA) such as aneuploidy and tetraploidy are one of the only Early Detection Research Network (EDRN) stage 4 biomarkers currently available for the risk stratification of patients with BE. Our group has previously shown how DNA-CA are more powerful predictors of progression to OA than abnormal p53 expression<sup>179</sup>. We have also shown in a small pilot study of patients with OA how replication licencing factors (RLF's) expression correlates with DNA-CA<sup>197</sup>. In the current work, the proliferative marker Ki67 will be evaluated in parallel with DNA-CA. All biomarkers will be evaluated in a panel of tissue specimens from squamous to high grade dysplasia to identify which biomarker predicts dysplasia most accurately to assist pathologists where there is diagnostic doubt.

### ***3.2.2. Replication licencing factors as surrogates for DNA-CA***

Leading on from this analysis, this thesis will examine if the RLF's, PLK1 and Geminin, may be used as a surrogate for DNA-CA. Field cancerisation in GI tissue<sup>260</sup> and the small numbers of cases in this pilot work make definitive conclusions difficult to draw from the promising RLFs identified. A previous pilot study identified PLK1 to be the most accurate RLF for predicting DNA-CA<sup>197</sup>. PLK1 will be examined with antibodies from 2 companies (Millipore and Leica), and compared with expression of the proliferative marker Ki67 using antibodies from two different companies (Dako and Leica) and p53 expression. Panels of cases from pathological grades of oesophageal disease, from normal to OA, will be examined to confirm the promising correlation seen

in the OA specimens is preserved. RLF's will be optimised for high-throughput IHC on the Leica BOND-MAX automated immunostaining platform for consistency.

### ***3.2.3. Biomarkers to predict neoplastic progression***

RLF IHC will then be separately analysed to see if it may be used, independently, as a predictor for cancer progression. IHC expression profiles will be scored by expert 2 gastrointestinal pathologists using the semi-quantified Allred scoring system (Figure 23), which is normally applied to score biomarker positivity in breast cancer <sup>261</sup>.

Pathologist scores will then be compared with digital image analysis algorithms created to duplicate pathologist reporting of the slides.

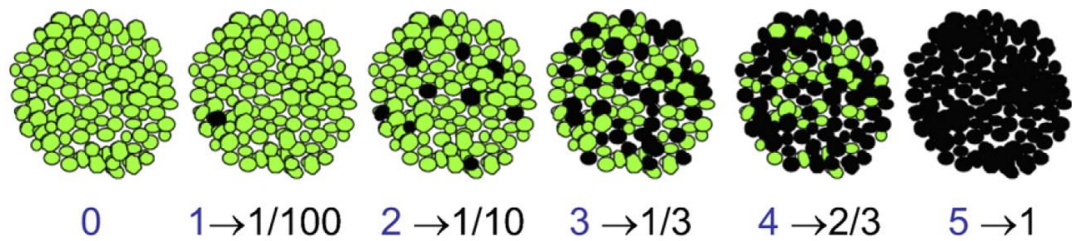
### ***3.2.4. Field cancerisation of BE surrounding OA***

The initial pilot study examining RLF expression in OA and the tissue surround it used a method known as the labelling index to quantify tissue expression. This method has inherent bias and relies upon the reporting technician to subjectively select the highest expressing areas within any degree of tissue pathology and quantify that sub-segment only. Within these selected areas, only 3-5 fields at x400 magnification were then sub-selected subjectively again for counting. Within these sub-selected areas, the 500 cells counted were again not counted randomly.

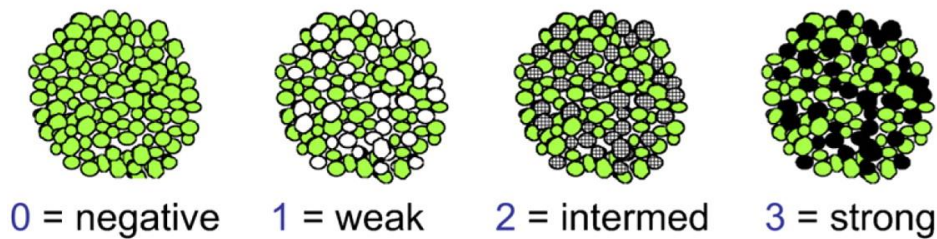
Due to this inherent bias in the reporting of this pilot study, these slides were retrieved and reported objectively using the Allred scoring system (Figure 23), to score both the intensity of staining and extent within the regions of interest examined.

Figure 23: Intensity and extent thresholds for Allred scoring system <sup>261</sup>.

A Proportion Score (PS)



B Intensity Score (IS)



$$\text{Allred Score} = \text{PS} + \text{IS} \text{ (range 0-8)}$$

### 3.3. HER2 and clinicopathological prognostic relationships in oesophagogastric cancer

HER2 is the most established biomarker target in gastric and oesophagogastric junction cancers, driven by the success of the Phase III ToGA study in which patients expressing this marker had statistically significant improvement in response rate, progression-free and overall survival in addition to standard therapy <sup>229</sup>. It is hypothesised that expression patterns of HER2 will be similar in BE, which is anatomically adjacent and biologically similar to junctional cancers assessed in ToGA. It is further postulated that HER2 expression is upregulated late in the progression to oesophageal adenocarcinoma.

HER2 expression will be examined in an audit of oesophagogastric cancer specimens sent to our reference HER2 pathology service in UCL. The relation between two modalities of measuring HER2 status will first be compared. Specific relationships between HER2 expression and clinicopathological factors, will be investigated.

Individual prognostic relationships between HER2 and clinicopathological features will then be highlighted. A multivariate analysis of these individual relationships with backward logistic regression will finally be examined to exclude confounders and select independent predictors of prognosis in oesophagogastric cancer.

### **3.3. HER2 expression in the squamous-metaplasia-dysplasia-adenocarcinoma sequence**

Expression of HER2 as distinct pathological stages will first be compared using gene set enrichment analysis. Quantified mRNA expression levels will be compared between oesophageal squamous epithelium and BE or OA. Tissue expression of HER2 in patients in the progression from normal squamous epithelium to OA will then be assessed using accepted automated IHC techniques for consistency. Live binding of the HER2 targeting single chain antibody fragment C6.5 to oesophageal and HER2 negative cell lines will be confirmed with FACS. It is hypothesised that oesophageal cell lines expressing HER2 will bind to C6.5 on FACS.

### **3.4. Development of HER2 targeting Antibody Directed Phototherapy (ADP) for OA**

Molecular targeted therapies are rapidly becoming widespread in cancer therapeutics. Targets may be expressed on the cell membrane, within the cells compartments or in the nucleus. Externally expressed surface targets are particularly attractive as they may be relatively easily bound by several vehicles. It is hypothesised that with targeting, the efficacy, potency and side-effect profile of non-selective therapies such as photodynamic therapy (PDT) may be improved.

The most widely researched vehicles to carry therapeutic agents in the clinic are antibodies and this emerging market has therefore been aptly named “Antibody-Drug Conjugates” (ADC). The ultimate next aim of this thesis is to develop a novel platform technology in oesophageal cancer therapeutics previously referred to as targeted

photodynamic therapy, that I recently renamed “Antibody Directed Phototherapy” (ADP)<sup>262</sup>.

To facilitate ADP for OA, targets are required to be tumour selective and expressed on the external epithelial surface to allow access via the gastrointestinal tract (for activation by laser light at a precise wavelength) and vasculature (for drug administration). Receptors should also be internalised to allow potential carriage of a photosensitiser (PS) payload which can then be activated by light to impart cell death. Earlier work is hypothesised to show how HER2 possesses these essential attributes.

The single-chain fragment variable (scFv) C6.5 will first be re-engineered into a new fragment. ScFv's are the smallest unit of immunoglobulins whose main function is binding to the target antigen. They consist of variable regions of heavy and light chains bound by a flexible peptide linker<sup>263</sup>.

C6.5 will be conjugated with a derivative of the photosensitiser Chlorine-e6 activated in the near infrared spectral region. Binding of the manufactured HER2 targeting ADC will then be examined in oesophagogastric cancer cell lines and their cytotoxic efficacy examined in vitro.

An in-vivo tumour model bearing oesophageal cancers in the flanks of mice will be created with optimised growth characteristics to enable drug evaluation. Upon reaching the target tumour size, pharmacokinetic studies of intravenously injected manufactured HER2 ADC will be conducted to identify the optimum parameters for subsequent therapeutic studies. The HER2 ADC will then be evaluated in vivo after laser activation and compared with controls to identify its therapeutic efficacy against the tumours.

### **3.5. MUC1 as a therapeutic target for antibody directed therapy**

During progression to cancer, glycosylation of peptide-repeats that form the backbone of the MUC1 receptor vary significantly. In breast tissue, aberrant glycosylation reveals sequences hidden on this peptide backbone hidden in normal cells that may be bound

extracellularly by antibodies. This offers aberrantly glycosylated MUC1 targets a degree of cancer selectivity. Studies in breast cancer confirm that when bound by the antibody HuHMFG1, the antibody-MUC1 receptor complex is rapidly internalised <sup>264</sup>. If a similar pattern of expression and internalisation is present in dysplastic BE and OA, this could make MUC1 an excellent therapeutic target for these conditions. However, reports of MUC1 expression in oesophageal tissue vary widely, with 0-100% expression in OA reported in the literature <sup>249,251</sup>.

MUC1 expression in pathways during progression to BE and OA will first be examined using gene set enrichment analysis. MUC1 tissue expression in panels of cases with histology reflecting different stages of disease in the progression from normal to OA will be assessed. Expression will be characterised with the antibodies binding 4 distinct epitopes of the MUC1 receptor.

To see if expression characteristics are similar in epithelium and nodes infiltrated with metastatic disease, a separate group of cases with local node infiltration (N1) who underwent oesophagectomy and had clear margins will be evaluated. Three matched sets of samples from primary tumour, infiltrated lymph nodes and disease-free resection margins will be examined.

Occasionally patients presenting to hospital with abdominal symptoms and initially inaccessible growths suspicious for cancer are screened by clinicians for cancer with a blood test known as “tumour markers”. The evidence to support tumour marker screening is poor.

Live binding of the antibody HuHMFG1 to known MUC1 positive and negative cell lines, and cells reflecting the metaplasia-dysplasia-carcinoma sequence, will be examined with Fluorescence-activated cell sorting (FACS). Flow cytometry will then be used to examine binding of the most relevant MUC1 targeting antibody in panel of cell lines mimicking the distinct stages of pathology from normal squamous to OA. Finally

binding and internalisation of the selected MUC1 antibody will be examined with confocal microscopy.

### **3.6. Development and characterisation of MUC1 targeting photoactive ADC**

As has been discussed, to realise the potential of MUC1 in oesophageal targeted therapeutics, a photoactive MUC1 targeting ADC will be created. The antibody HuHMFG1 will be conjugated to the photosensitiser PS1. PS1 is a hydrophilic photosensitiser derived from the photosensitiser pyropheophorbide alpha (PPa) that has the potential to form bioconjugates to antibodies for PDT targeting. PPa doesn't itself have a track record of clinical use, but its related compound hexyl methyl PPa known as Photoclor, is in clinical trials for bronchial cancers<sup>265</sup>. The photophysical properties of PS1 are favourable compared to PPa with enhanced absorption in the red spectral range and substantial oxygen quantum yield. Translated into clinical practice this should allow deeper tissue penetration and enhanced cytotoxic efficacy respectively<sup>266</sup>.

The conjugate of HuHMFG1 and PS1 (HhHMFG1:PS1) will undergo photophysical characterisation, and its binding will be evaluated in range of MUC1 expressing and a MUC1 negative cell line. The mechanism and subcellular localisation of HuHMFG1:PS1 will be examined with confocal microscopy. Due to activation of the HuHMFG1:PS1 ADC with lasers used in confocal microscopy, a second MUC1 ADC will be created conjugating HuHMFG1 to the dye Cy5.5. The HuHMFG1: Cy5.5 conjugate will then be examined with and without a marker of endosomal localisation to postulate on the subcellular localisation of the ADCs post internalisation. The therapeutic HuHMFG1:PS1 ADC will then be compared to equivalent free PS1 photosensitiser against an OA cell line to evaluate which is superior. The therapeutic HuHMFG1:PS1 ADC will finally be evaluated in MUC1 positive and negative cell lines to determine the specificity of the new drug.

**Chapter 4: Biomarkers associated with Barrett's  
risk of progression to oesophageal  
adenocarcinoma**

---



## 4.1 Introduction

Gastroesophageal reflux can lead to Barrett's epithelium (BE), in which the squamous mucosa of the distal oesophagus is replaced by columnar epithelium. The importance of BE lies in its potential to progress, via a metaplasia-dysplasia-adenocarcinoma sequence, to oesophageal adenocarcinoma (OA). It is thought 64-86% of all OA's arise in BE <sup>6,7</sup>. As the five-year survival rate following diagnosis of OA remains abysmal at less than 15% <sup>12</sup>, identifying which patients with BE are at risk of progression remains of paramount importance. Despite systematic reviews with economic modelling suggesting surveillance programmes for BE are likely to do more harm than good, costing more and conferring lower quality of life than no surveillance <sup>267</sup>, expert guidelines still advocate surveillance for patients with BE in certain populations <sup>1,268</sup>(5,6). A large cohort study of 29536 with BE identified 424 patients who developed OA during a mean follow-up of 5 years confirmed the clinical case for surveillance recently. Those identified from BE surveillance programmes were more likely to be diagnosed at an earlier stage, survive longer and had a lower cancer-related mortality <sup>269</sup>.

The reported risk of progression from non-dysplastic BE (NDBE, also referred to as Barrett's metaplasia) to OA has been shown to be lower than previously thought. Meta-analyses suggest the risk of progression of BE to oesophageal or cardia cancer to now be 0.22-0.33% per patient-year <sup>8-10</sup>and is even lower at 0.07% in patients with BE segments less than 3 cm in the absence of intestinal metaplasia <sup>10</sup>. Despite decades of searching for a better biomarker, progression is unpredictable, and dysplasia remains the standard for risk stratification systems in BE. The presence of either low- or high grade dysplasia are now accepted as indications for endoscopic therapy due to the significant risk of progression in LGD and superiority of ablation over surveillance for this indication <sup>1,146</sup>.

The diagnosis of dysplasia is sometimes difficult to reach, requiring repeat sampling and consensus opinion. Uncertainty amongst pathologists, particularly around the diagnosis of LGD has led to the requirement in guidelines for at least 2 pathologists to concur when describing dysplasia, one of whom must have specialist experience in gastrointestinal histopathology. It has been shown that as the number of pathologists agreeing on a diagnosis of LGD increases, the progression rate also increases. In one study, individual pathologists' diagnosis did not correlate with progression, but when 2 pathologists agreed on LGD, there was a significant association with progression (41%,  $p=0.04$ ), increasing to 80% ( $p=0.012$ ) if 3 pathologists were in agreement<sup>48</sup>. To assist in the histopathological assessment of dysplasia, the British Society Guidelines advocate the use of p53 immunostaining as an adjunct to routine clinical diagnosis<sup>1</sup> based on evidence that p53 stained LGD positively in 88% (7/8) of patients who progressed to HGD or OA versus only 25% (2/8) of nonprogressors<sup>186</sup>. Our group previously evaluated a panel of biomarkers including p53 and DNA content abnormalities in a large population-based nested case-controlled study using the Northern-Ireland BE Register, comparing 89 patients who progressed to HGD or OA with 291 nonprogressor controls, matched for age, sex and year of diagnosis. In backward selection, a panel of LGD (OR=11.78,  $<0.001$ ), abnormal DNA ploidy (OR=3.22,  $p<0.001$ ) and Aspergillus Oryzae lectin (OR=3.17,  $p0.002$ ) most accurately identified progressors from those who did not. Interestingly correlation between p53 immunostain and progression did not reach statistical significance ( $p=0.08$ )<sup>179</sup>.

Identifying better biomarkers predictive for cancer progression as well as adjuncts for a diagnosis of dysplasia, may help focus limited resources on targeted surveillance or therapy. One of the most promising are DNA ploidy abnormalities (aneuploidy / tetraploidy). Normal cells have 2 copies, also referred to as 2n or a diploid number, of each chromosome. Aneuploidy is an abnormal gain or loss of DNA content in these chromosomes and has consistently been shown as a marker of risk of progression in

NDBE in phase 3 biomarker trials<sup>175,177,179</sup>. A correlation between pathological grade and DNA ploidy abnormalities has previously been shown<sup>51</sup>.

DNA ploidy abnormalities are markers of genomic instability and can be measured in formalin fixed paraffin embedded (FFPE) tissue allowing analysis of archival material, as well as ease of set up and potential for automation. Despite these advantages, adoption of this technique for risk stratification of NDBE outside of research centres and into district general hospital pathology departments is unlikely. One potential solution would be a central hub and spoke model whereby regional pathology departments (where the majority of Barrett's surveillance takes place) would send their samples to designated centres. This may result in a huge number of samples and work for a very small reward, as most patients with NDBE would be diploid.

A simple test that allows screening of the patient for DNA content abnormalities would be beneficial. Once screened as high risk, this could be confirmed by formal image cytometry analysis. As this is a screening tool, the test would need to be highly sensitive for aneuploidy, to maximise the negative predictive value of the test. To be suitable for widespread clinical use this candidate surrogate biomarker would need to be quantified from samples that are easy to obtain (serum, tissue biopsy) and the assay method simple, accurate, highly reproducible and cheap using facilities used routinely in clinical diagnostics. Reporting of these immunostained specimens may also be automated using digital image analysis techniques to improve efficiency and reduce workload in busy histology departments.

DNA replication licensing factors (RLFs) ensure precise duplication of the genome and contribute to genomic stability by ensuring DNA is replicated only once per cell cycle<sup>270</sup>. Dysregulation of replication licencing can cause under- or over-replication of chromosomal DNA and could explain genomic instability<sup>271</sup>. PLK-1 expression changes during cell cycle progression peaking in the M-phase and is required at most mitotic steps<sup>272</sup>. Overexpression overrides mitotic checkpoints causing immature cell

division resulting in chromosomal instability, the hallmark of DNA ploidy abnormalities<sup>204</sup>. The RLF geminin has also been found to be associated with the formation of aneuploidy in breast cancer cells when overexpressed. In this state, geminin promotes cytokinesis failure to produce aggressive aneuploidy breast tumours<sup>208</sup>.

The aims of this study were to determine whether immunohistochemical expression of the RLFs PLK-1 and geminin could be used as surrogate markers of dysplasia and aneuploidy. In addition, the standard proliferation marker Ki-67 and p53 protein expression were assessed to identify if p53 is the best predictor for dysplasia.

## **4.2 Materials and methods**

### **4.2.1 Tissue specimens**

Tissue samples were obtained from formalin fixed paraffin embedded (FFPE) blocks held in the UCL biobank for studying health and disease. Anonymised details from three retrospective cohorts of patients were selected from the pathological archives of University College London. FFPE tissue specimens were retrieved and where available, data on age, sex, date of diagnosis were collected. Where data was retrieved, local guidelines were followed for the use of blinded clinical information for research purposes. Appropriate consent and ethical approval to conduct this research was obtained from studies detailed in Table 7. All patients had endoscopic evidence of Barrett's epithelium. All specimens were reviewed blindly by two independent expert gastrointestinal pathologists (MN & MRJ). The histological grade of each was the highest achieved by the patient during active follow up until the time of tissue collection. To ensure consistency of reporting, a Bland-Altman plot of the first batch of 36 immunostained PLK1 cases between pathologist's cases was conducted (Figure 34).

**Table 7: Clinical projects providing tissue for biomarker research**

Project title	Research Ethics Committee (REC) reference
Retrospective biological samples collection for patients with Barrett's oesophagus, oesophageal and gastric cancer	EC13.13
Barrett's oesophagus surveillance with optical biopsy using elastic scattering spectroscopy to target high risk lesions	08/H808/8
A National Patient Registry for HALO 360 and HALO 90 radiofrequency ablation of Barrett's columnar oesophagus	08/H0714/27
Randomised control trial of ALA and Photofrin PDT for HGD in Barrett's Oesophagus	05/Q1602/193

Three patient cohorts were evaluated in this chapter. Cohort 1 evaluated the relationship between pathological grade and clinicopathological factors. This cohort included 18 non-dysplastic Barrett's epithelium (NDBE), 12 low grade dysplasia (LGD), 19 high grade dysplasia (HGD) and 13 oesophageal adenocarcinoma's (OA). The median age was 68 (range 40-85) and the majority were men (74%). Cohort 2 evaluated the influence of field cancerisation and included 26 patients with NDBE. 8 patients had NDBE adjacent to OA in tumour resection specimens and were isolated using laser capture microdissection (LCM). These were compared with 18 patients with NDBE who had never progressed to dysplasia or cancer from cohort 1. Matched areas were examined for Ki-67, PLK-1 and geminin expression with immunohistochemistry and DNA content with image cytometry. The median age was 64 (range 49-81) and

56% were men. Cohort 3 was a case control cohort of 6 patients with NDBE but were known to have progressed to dysplasia or cancer later, with 1 or 2 controls matched for age ( $\pm 5$  years) and sex who did not progress beyond NDBE with a median follow up of 36.5 months (range 12-62months). A total of 10 controls were identified. Only PLK1 was assessed with pathological grade in this cohort due to a lack of patient material (Table 8).

**Table 8: Patient cohorts and characteristics**

			Frequency (%)
Cohort 1	Age	Median	68
		Range	40 - 85
	Sex	Male	46 (74)
		Female	13 (21)
		Unknown	3 (5)
	Grade	Non-dysplastic Barrett's epithelium	18 (29)
		Low-grade dysplasia	12 (19.4)
		High-grade dysplasia	19 (30.6)
		Oesophageal adenocarcinoma	13 (21)
	Cohort 2	Age	Median
Range			49 - 81
Sex		Male	9 (56)
		Female	7 (44)
Phenotype		Never-dysplastic Barrett's epithelium	18 (69)
		Non-dysplastic Barrett's adjacent to cancer	8 (31)
Cohort 3	Phenotype	Never-dysplastic Barrett's epithelium	10 (63)
		Non-dysplastic Barrett's who later progressed	6 (37)
	Follow up (months)	Median	36.5
		Range	12-62

**4.2.2. Microtome sequence**

For cohort 1 biomarker studies including DNA-CA and RLF IHC, tissue sections were initially cooled on an ice block and the cut with a microtome (Leica RM2235 or Leica SM2400) in the following sequence:

4-micron section for haematoxylin and eosin (H&E)

40-micron section for image cytometry

4-micron section for H&E

4-micron section for PLK1-M

4-micron section for PLK1-L

4-micron section for Geminin

4-micron section for p53

4-micron section for Ki-67-L

4-micron section for Ki-67-D

Cut sections for H&E and biomarker IHC were laid into a water bath and then lifted onto electrostatically charged (VWR Superfrost® Plus) slides. The 40-micron sections for IC were allowed to curl into a swiss roll and captured into an Eppendorf.

For Cohort 2, 40-micron sections were mounted onto UV excited P.A.L.M. membrane slides (Positioning and Ablation with Laser Microbeams (P.A.L.M.) Microlaser Technologies, Germany).

For cohort 3 tissue were sectioned and mounted onto superfrost slides in Cambridge University and kindly gifted by Professor Rebecca Fitzgerald and her group.

#### ***4.2.3. Haematoxylin and Eosin staining***

Sections were initially deparaffinised in xylene (10 minutes) and then rehydrated through 3 reducing concentrations of ethanol (100%, 90%, 50%) (5 minutes each) prior to water. Slides were then stained with Mayers haematoxylin (Leica, 3801582E) for 15 minutes and rinsed in running tap water for 15 minutes or longer to bring out the blue colouration. Counterstaining with Eosin was then performed for <2minutes until appropriate counter colouration. Slides were then dehydrated in graded ethanol (50%, 95% and 100%) before cleaning with xylene bath, drying in a fume hood, and mounting under coverslips secured with DPX.

Regions of interest (ROI) were marked on the slides and scanned images from these sections and correlated with the subsequent cut slides. These findings were confirmed by repeat analysis of the final H&E slide to confirm the morphology had not changed.



#### **4.2.4. Image cytometry**

##### **4.2.4.1. Liberation of nuclei for image cytometry**

This method for image cytometry has been adapted from the European Society of Analytical Cellular Pathology (ESACP) guidelines<sup>273</sup>.

A Leica SM 2400 microtome was used to cut a 40 $\mu$ M section from a paraffin block of interest. Sections were then de-waxed by emersion in Xylene for 10 minutes and then centrifuged for 1 minute at 13,000 rpm and the supernatant removed. The pellet was then resuspended in 1.5ml of the following solutions with a Vortex (Vortex Genie 2) for 5 seconds, centrifuged at 13,000rpm and then the supernatant removed in this sequence:

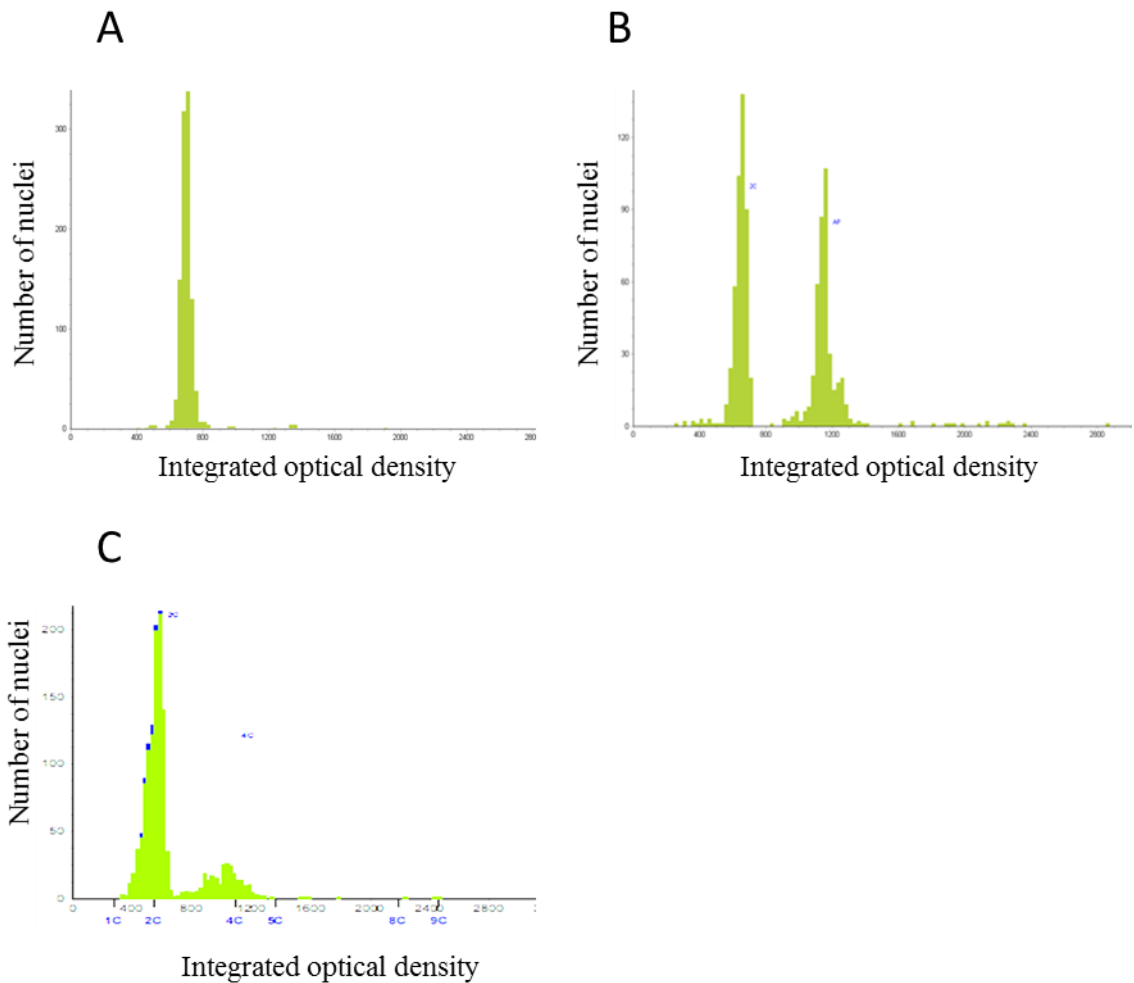
1. 100% ethanol (Fisher)
2. Distilled water
3. Phosphate buffered saline (PBS, pH 7.4, Phosphate buffer 0.01M, 0.0027M KCl, 0.137M NaCl)

200 $\mu$ L of proteinase XXIV (Sigma-Aldrich) at concentration of 5mg/ml in PBS (0.05g in 10mls PBS) was then added at 37°C, for 1-3hours until it solubilised. 1.4mls further PBS was then added and the sample chilled to 4°C. The mixture was then filtered through a 40 $\mu$ M nylon mesh cell strainer (BD Biosciences) and the supernatant centrifuged for 10minutes at 1600rpm. The supernatant was then removed, and the pellet resuspended in 200 $\mu$ L PBS with a 10second vortex. Suspensions were then attached to electrostatically charged Superfrost Plus slides (VWR) by injecting the suspension into a single use cytofunnel (Thermo Scientific) attached to a Cytospin (Shandon Cytospin 4). This was then set at 1500rpm for 5minutes and the attached nuclei air dried at room temperature for 1 hour.

#### 4.2.4.2. Measurement of DNA ploidy

The Fairfield DNA Ploidy system (Fairfield Imaging, Kent, UK) is an automated image cytometric analyser that consists of a Zeiss Axioplan microscope (Zeiss, Jena, Germany), a 546-nm green filter, and a black-and-white, high-resolution digital camera (Hamamatsu Photonics, Japan). Optical density and nuclear area were measured, and integrated optical density of each nucleus calculated. Background optical density was corrected for each nucleus. Segmentation software (a range of pre-defined criteria relating to the physical properties of the nuclei) automatically selects whole nuclei. At least 1000 nuclei were scanned automatically and sorted into 4 separate galleries for each cell type: nuclei of interest for measurement, lymphocytes, plasma cells and fibroblasts. The lymphocytes were used as reference cells to determine the position of the diploid peak (2c). All galleries were then edited manually to discard any cut or overlapping nuclei. The integrated optical density of each nucleus of interest was calculated and a histogram of DNA content produced. Ploidy-related parameters such as DNA index (DI) and percentages of cells exceeding 5c (5c ER) and 9c (9c ER) were also noted when computed by the software.

**Figure 24: Typical histograms from tissues with normal diploid DNA content (A), and abnormal aneuploid (B) and tetraploid (C) content.**



#### 4.2.4.3. Histogram interpretation

Histograms were analysed according to European Society for Analytical Cellular Pathology (ESACP) guidelines<sup>273</sup> as follows -

- i. A specimen was defined as diploid when there was only one peak (which was 2c, or DI 0.9-1.1) during the G0 or G1 phase, or when there was a second 4c peak (DI 1.9-2.1) representing less than 6% of the total, and when the number of nuclei with a DNA content of more than 5c did not exceed 1% of the total.
- ii. A specimen was defined as DNA tetraploid when there was a population of 4c nuclei (DI 1.9-2.1) more than 6% of the total, representing stage G2 of the cell cycle.

iii. A specimen was defined as aneuploid when there was a population of nuclei with abnormal DNA content, separated from the diploid peak ( $DI > 1.1$ ), and representing more than 2.5% of the total or when the number of nuclei with a DNA content of more than 5c or 9c exceeded 1% of the total.

All specimens were given unique coded identifiers and the histograms were first reported by the computer and later the results confirmed by independent trained observers.

#### 4.2.4.4. Audit of specialist clinical image cytometry service to identify relationship between of predicted DNA CA and pathological grade

In our specialist referral centre for BE, assessment for DNA CA is requested for cases with persistent or recurrent low-grade/indefinite for dysplasia (LGD/IFD), clinical suspicion of progression due to, for example, a strong family history of OA in long segment BE, or cases suspected to relapse after prior treatment for high-grade dysplasia/intramucosal cancer (HGD/IMC).

#### 4.2.5. *Immunohistochemistry*

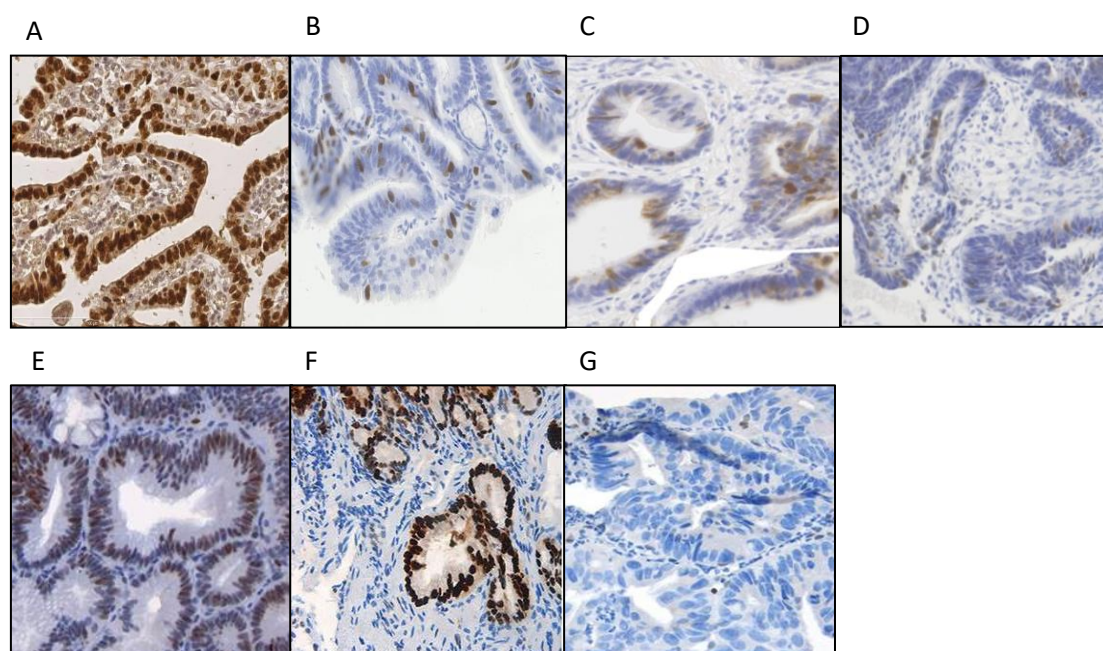
IHC slides were split into three sets and carried out partly in Newcastle by Mr Colin Tristram (Leica) and predominantly in UCL. Protocols, consumables and hardware used were identical. Sections underwent automated dewaxing and endogenous peroxidase blocking using 4% hydrogen peroxide. Antibodies were then re-optimised for use on the BOND-Max using heat induced epitope retrieval in 0.1 M citrate-based (pH6.0) retrieval solution for 20 minutes, using the BOND autostainer (Leica) following the manufacturer's instructions. Dilution curves for antibodies were carried out with 15-minute incubation at ambient temperature, and signal visualised using Bond Polymer Refine Detection kit (DS9800) and haematoxylin counterstain on 4µm-thick sections of reactive tonsils. Slides were then reviewed (MAB, DO, MG, MRJ, MN) and optimal conditions chosen based upon the criterion of background-free selective cellular labelling. Optimum dilution was at 1/50 for p53 (Leica), 1/300 for Ki67 (Dako), 1/100 for

Ki67 (Leica), 1/20 for geminin, 1/1000 for PLK-1 (Millipore) and 1/5 for PLK-1 (Leica) (Table 9). Examples of tissue immunostains are shown in Figure 25.

**Table 9: Summary of immunohistochemical antibodies evaluated**

Antibody	Abbreviation	Clone
<b>Polo-like kinase 1 (Millipore)</b>	PLK1-M	Clone 35-206
<b>Polo-like kinase 1 (Leica)</b>	PLK1-L	Clone MJS1
<b>Geminin</b>	Geminin	Clone EM6
<b>p53 (Leica)</b>	p53	Clone DO-7
<b>Ki-67 (Leica)</b>	Ki67-L	Clone MM1
<b>Ki-67 (Dako)</b>	Ki67-D	Clone MIB-1

**Figure 25: Immunohistochemical expression of antibodies evaluated**



*Immunohistochemical expression of Ki-67 (Dako) (A), geminin (B), PLK-1 (Millipore) (C) and PLK-1 (Leica) (D) in high-grade dysplasia (x400). Examples of normal p53 (E), and abnormal p53 overexpression (F) and p53 under-expression (G). Histograms*

*produced from image cytometry in diploid (H) and aneuploid (I) Barrett's cell populations.*

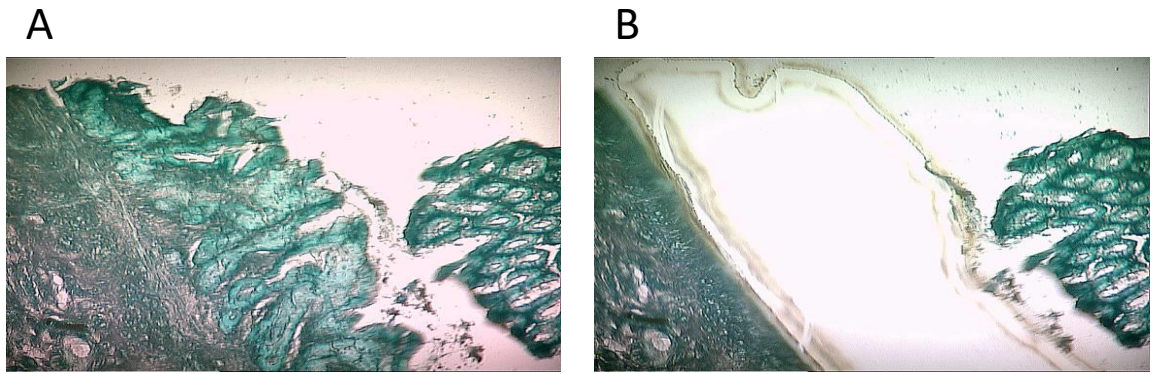
#### **4.2.6. Protein expression profile analysis**

All slides were blinded for nuclear Ki67 and RLF staining intensity (0 – 3) and extent (0 – 5) were independently scored by 2 expert gastrointestinal pathologists (MN and MRJ) using the Allred scoring system as previously described<sup>261</sup>. To define tissue positivity, a cut of Allred score of >5 for Ki67, and >3 for PLK-1 and geminin were applied. For p53, staining was reported as normal, over or under expressed independently by expert 2 gastrointestinal pathologists (MRJ or AW) (Figure 17 E, F and G). The latter two p53 phenotypes were both considered abnormal and consensus of expression was reached in all cases.

#### **4.2.7. Laser capture microdissection**

The P.A.L.M UV Laser Microdissection system (P.A.L.M. Microlaser Technologies, Germany) was used to isolate the NDBE adjacent to OA in cohort 2 from 8 patients first identified and marked on the H&E slides. These areas were correlated with the LCM methylene green stained slides, marked with a pen and cut out from the laser capture slides and catapulted into the adhesive caps of eppendorf tubes, before immersion in UV pre-treated PBS (Figure 26 5 A, B). Forty-micron sections were used, which are quite thick for LCM (routine use is 6-20 microns) but this minimised cutting error that can potentially lead to underestimation of DNA tetraploidy.

**Figure 26: Laser capture microdissection within OA resection specimens**<sup>197</sup>



#### **4.2.8. Digital Image Analysis**

An increasing number of digital image analysis platforms such as Aperio® and Ventana have been clinically validated and FDA (US Food and Drugs Administration) for the diagnosis and quantification of brightfield IHC in breast tissue using biomarkers such as ER, PR, HER2 and Ki67 in laboratories under defined conditions<sup>274</sup>. This section aimed to compare pathologist extent scores with designed digital algorithms for the quantification of nuclear biomarkers and correlate digital outputs with DNA CA.

34 IHC cases stained with the RLF's PLK1-M, PLK1-L and Geminin and scored by 2 specialist pathologists with Allred were compared with digital outputs of mean intensity and extent scores using Ariol® software (Leica Biosystems). Analysis protocols were trained using Ariol® to identify mask limits of positively and negatively immunostained nuclei in the regions of interest (ROI). ROI's were the highest grades of pathology in the progression to cancer within the specimen examined. To illustrate the analysis performed,



Figure 37 shows the extrapolated images post DIA that the program then quantifies. Background tissue was initially manually excluded through the selection of ROI's and later digitally excluded. Mean intensity and mean counts for analysed positive (red) and negative (green) nuclei were then quantified to calculate percentage positivity and compared with constituents of pathologist Allred scores.

Expression of RLFs measured with DIA was finally evaluated with DNA CA and pathologist's estimations of Allred pathology scores.

Immunostained slides for PLK1 and Geminin after pathology reporting with Allred score, were catalogued and scanned with a Leica SCN400 automated slide scanner. Scanned slides were then uploaded into the software program Ariol ® for digital quantification of the slide image.

Briefly the following protocol was followed to obtain scores:

#### Nuclear stains (PLK1/Geminin)

1. A region of interest was selected from a control slide highlighting positive and negative areas of immunostaining.
2. Colour masks were the set, selecting maximum colour (brightness/intensity thresholds for positivity and negativity) for positive (brown) and negative (blue) nuclei.
3. Size and shape masks were then set for the nuclei to be scanned and the protocols saved.
4. All slides from the same biomarker were then uploaded into the software.
5. Regions of interest were then selected from each slide in turn. For example, in a slide showing 4 biopsy specimens, only one of which had HGD, this region of HGD would be selected for further analysis.
6. Slides were then analysed consecutively using the image algorithms developed in 2 and 3.

Ariol scores for nuclear and membranous immunostains were then tabulated and compared with pathologist Allred scores using GraphPad Prism and IBM SPSS statistic programmes using Spearman's Rank, ROC curves and logistic regression.

#### **4.2.9. Statistical analysis**

Relationships between biomarkers and progression through pathological grades in cohort 1 were assessed with Jonckheere-trend test. Relationships between groups were then analysed with Tukey's multiple comparison test. Biomarker expression was summarised with the mean, 95% confidence interval and standard deviation.

Multivariable analysis for the prediction of dysplasia and aneuploidy were carried out in two steps using binary logistic regression. All factors were initially assessed separately and those with  $p < 0.05$  retained. Remaining factors were then collectively added into a single model and backward elimination applied with  $p = 0.05$  to identify significant independent predictors. Odds Ratio, p-values and standard error on initial univariate and subsequent multivariate analysis were recorded. Receiver operator curves were then constructed for remaining factors after defining cut-offs for significant biomarkers. The area under curve, sensitivity, specificity, negative predictive value and positive predictive value of the biomarkers to predict dysplasia or DNA ploidy abnormalities was then computed. The distribution of biomarker expression between NDBE phenotypes in cohorts 2 and 3 were summarised with mean and standard deviation and compared with Mann-Whitney U or Fisher's exact tests. All tests were two-sided and used a significance level of 0.05. Analysis was performed using IBM® SPSS® statistics version 22 and GraphPad Prism version 5.

## 4.3. Results

### 4.3.1. Relationship between biomarkers and pathological grade

#### 4.3.1.1. Background

This section will examine the relationship between several biomarkers hypothesised to be predictive of malignant progression in oesophageal epithelium in a range of pathologies from normal to cancer. These biomarkers include the replication licensing factors Ki67, PLK-1 and geminin, the oncoprotein p53 and DNA-content abnormalities (aneuploidy and tetraploidy). To identify if expression is influenced by antibody clones, two biomarkers Ki-67 and PLK-1 will be examined with antibodies manufactured by different companies.

#### 4.3.1.2. Results

The expression of biomarkers in the metaplasia-dysplasia-carcinoma sequence are summarised in Table 10 and the respective distributions displayed in Figure 27. The mosaic in Figure 28 shows examples of RLF expression patterns across pathological grades. All biomarkers were found to be associated with progressive tissue differentiation when evaluated collectively (Jonckheere-trend test  $<0.05$ ). Ki67 (Leica) appeared upregulated in all grades of dysplasia, but Ki67 (Dako) was down regulated during progression to LGD ( $p=0.022$ ) before being upregulated again in HGD ( $p<0.001$ ) and OA. There was little difference in the staining pattern of RLFs geminin and PLK-1 (Leica) and p53, with all three showing relatively low expression levels in NBDE and LGD, followed by progressively increased expression in HGD and OA. Interestingly, expression of PLK-1 (Millipore) and DNA ploidy status appeared marginally down regulated from HGD to OA. There is little difference for most biomarkers between normal and LGD, and between HGD and cancer.

**Table 10: Relationship between biomarker expression and pathological grades**

	Non-dysplastic Barrett's epithelium (n=18)	Low-grade Dysplasia (n=12)	High-grade Dysplasia (n=19)	Oesophageal adenocarcinoma (n=13)	p-value †
Ki-67 (Dako) *	5.09 (4.2-5.9) <sup>#</sup> 1.65 <sup>§</sup>	4.22 (3.45-4.99) 1	6.16 (5.66-6.66) 1.0415	6.5 (5.82-7.18) 1.118	<b>0.002</b>
Ki-67 (Leica) *	5.68 (4.93-6.42) 1.446	6.06 (5.65-6.46) 0.527	6.05 (5.6-6.51) 0.941	6.54 (6.18-6.9) 0.594	<b>0.028</b>
Geminin *	3.088 (2.33-3.85) 1.4709	3.44 (2.51-4.38) 1.2105	4.711 (3.74-5.67) 2.016	5.12 (3.93-6.31) 1.9701	<b>&lt;0.001</b>
PLK-1 (Millipore) *	2.09 (1.05-3.13) 2.0251	3 (1.93-4.07) 1.3919	4.53 (3.51-5.54) 2.1113	3.81 (2.76-4.89) 1.7385	<b>0.003</b>
PLK-1 (Leica) *	2.09 (1.36-2.82) 1.417	2.17 (0.94-3.4) 1.601	4 (3.14-4.86) 1.787	4.46 (3.61-5.31) 1.406	<b>&lt;0.001</b>
p53 ^	0.176 (-0.03-0.38) 0.393	0.444 (0.04-0.85) 0.527	0.789 (0.59-0.99) 0.4189	0.92 (0.78-1.09) 0.2774	<b>&lt;0.001</b>
Ploidy <sup>  </sup>	0.059 (-0.07-0.18) 0.2425	0.22 (-0.12-0.56) 0.441	0.84 (0.66-1.02) 0.3746	0.462 (0.15-0.78) 0.5189	<b>0.002</b>

\* Quantified with Allred score

^ Abnormal p53 (over or under expression) defined in binary

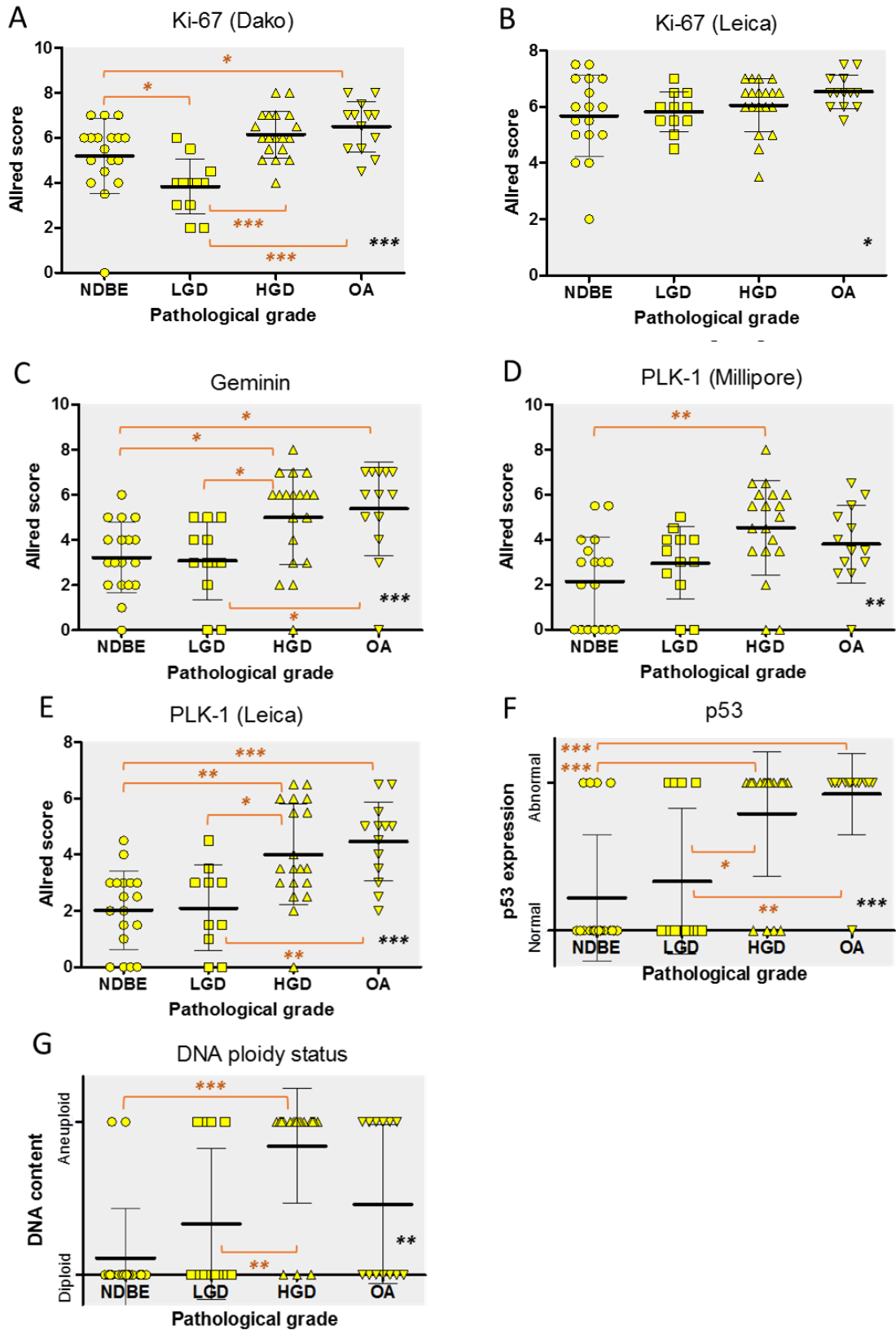
|| Abnormal DNA content (aneuploidy of tetraploidy) defined in binary

# Mean (95% confidence interval)

§ Standard deviation

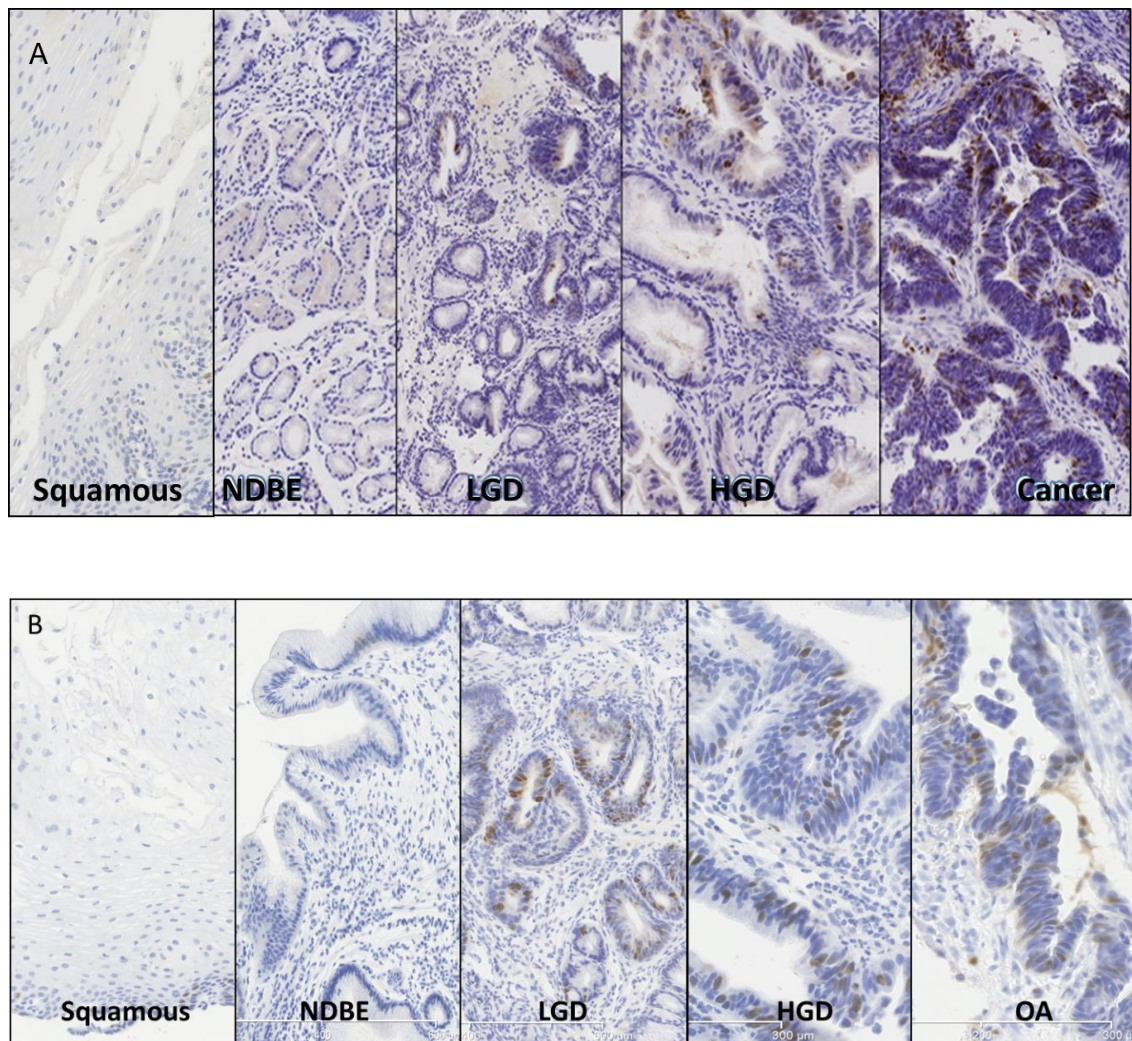
† Jonckheere-trend test

**Figure 27: Scatter plots of biomarker expression across pathological grades.**



\* Level of significance of Jonckheere-trend test across tissue grades. \* Significance of post-test analysis with Tukey multiple comparison test between groups. Plots (mean and SD).

**Figure 28: Collage of PLK1-M (A) and Geminin (B) immunostaining showing pattern of increasing nuclear positivity in the progression to oesophageal cancer**



*During progression through pathological grades of oesophageal tissue from squamous, non-dysplastic Barrett's epithelium (NDBE), low grade dysplasia (LGD), high grade dysplasia (HGD) and cancer (oesophageal adenocarcinoma; OA), the extent of positive immunostaining (brown nuclear staining) for polo-like kinase-1 (A) and geminin (B) increases sequentially. Haematoxylin (blue) used for background staining.*

#### 4.3.1.3. Summary

RLF's were generally upregulated during progression of oesophageal epithelium through incremental pathological grades. Abnormalities in p53 protein expression and DNA content were similarly seen with increasing frequency during progression of oesophageal epithelium when compared to normal epithelium. The transition for most

biomarkers from normal to increased expression (for RLFs) or abnormal (p53 and DNA-CA) is seen to occur most often between low- and high-grade dysplasia. There is variation in the expression of Ki67 and PLK-1 depending on which antibody is used to evaluate them.

#### ***4.3.2. Association between clinicopathological variables and dysplasia***

##### **4.3.2.1. Background**

When oesophageal adenocarcinoma has developed, the morphological changes noted in the tissue on H&E staining are normally so significant that further biomarkers are not required to assist in the diagnosis. There remains much debate on the presence of dysplasia however, particularly low grade dysplasia, and so p53 immunostaining is currently advocated as an adjunct to assist pathologists in making this diagnosis<sup>1</sup>. The distinction between normal epithelium and LGD is crucial as the latter puts the patient in a much higher risk category for subsequent progression to cancer and qualifies them to receive endoscopic therapy to eradicate the dysplasia<sup>1,146</sup>. Whether p53 immunohistochemistry is as good if not better than other biomarkers we are evaluating at making this distinction will be examined in this section.

##### **4.3.2.2. Results**

For comparison, patients with any degree of dysplasia in cohort 1 were grouped and compared with NDBE. Baseline demographics confirmed there were no differences in age or sex between both groups. Expression of Ki67 and geminin did not differ significantly between groups. On univariate analysis, both PLK-1, p53 and DNA-CA had a significant association with dysplasia, with ploidy being the strongest association with an OR of 14.5. To ascertain which if any of these variables were independently associated with dysplasia, multivariate analysis of significant variables identified on initial univariate filtering (PLK1-M, PLK1-L, p53 and DNA-CA) was carried out. This identified DNA-CA to be independently predictive for dysplasia ( $p=0.001$ ,  $OR=15.2$ ) (Table 11).

To ascertain the optimum cut off Allred score for the prediction of dysplasia for PLK-1 (Millipore) and PLK-1 (Leica), the Youden's index was calculated (Table 12). This established the optimum cut off mean Allred score for both antibodies to be 3.25. An Allred score of >3 was therefore selected to define PLK-1 positivity.

Using a cut off for PLK-1 of >3, all ROC curves remained significant for the prediction of dysplasia (Figure 29). DNA-CA were most closely predictive of any dysplasia (AUC: 0.772,  $p=0.002$ ) with a high specificity (88.9%) and positive predictive value (90.9%).

Assessment of DNA-CA with image cytometry is difficult to obtain in clinical practice, while immunohistochemistry is routinely available. To ascertain which immunohistochemical biomarkers best predict dysplasia, multivariable analysis was repeated excluding DNA ploidy. Abnormal p53 protein ( $p=0.015$ , OR: 6.42) and PLK-1 (Millipore) ( $p=0.012$ , OR: 1.6) were found to be independently associated with dysplasia.

To ascertain whether the independently predictive biomarkers for dysplasia can be combined in a 2 or 3 biomarker panels to become more predictive for dysplasia, DNA-CA, p53 protein and PLK-1 (Millipore) were combined in various ways. All combinations were predictive of dysplasia but the combination of DNA-CA and p53 was most predictive ( $p=0.001$ , OR: 8.914). However, this was still less predictive for dysplasia than DNA-CA alone (OR: 14.5 vs 8.9).

When the presence of abnormal PLK1-M or p53 were combined to predict dysplasia, the combination was found to be more predictive ( $p=0.006$ , OR=6.5) than when each marker is assessed alone.

#### 4.3.2.3. Summary

The RLF's geminin and Ki-67 were not predictive of dysplasia. When assessed individually, DNA-CA was most predictive of dysplasia, and stood out as the main



independently predictive variable for dysplasia on multivariate analysis. Identifying abnormal PLK1-M and p53 predicted dysplasia better than either biomarker alone.

**Table 11: Relationship between biomarker expression and dysplasia**

	n	NDBE	Dysplasia	SE	p-value*	OR*	p-value†	OR†
Age	42	63.3 (56.3-70.3)‡	69.6 (65.7-73.6)	0.03	0.06	1.059		
Sex	Male	35	28.6%	71.4%	0.71	0.302	2.083	
	Female	11	45.5%	54.5%				
Ki-67 (Dako)	49	4.9 (4-5.8)	5.5 (5-6.1)	0.19	0.892	1.026		
Ki-67 (Leica)	49	5.4 (4.6-6.3)	6.1 (5.7-6.4)	0.28	0.387	1.272		
Geminin	49	3 (2.1-3.9)	4.3 (3.6-5)	0.17	0.097	1.319		
PLK-1 (Millipore)	49	2.2 (0.9-3.4)	4 (3.3-4.8)	0.16	<b>0.009</b>	<b>1.525</b>		
PLK-1 (Leica)	49	2 (1.1-2.9)	3.4 (2.7-4.2)	0.20	<b>0.023</b>	<b>1.586</b>		
p53 expression	Normal	26	53.8%	46.2%	0.68	<b>0.011</b>	<b>5.542</b>	
	Over / under	23	17.4%	82.6%				
DNA content	Diploid	27	59.3%	40.7%	0.84	<b>0.001</b>	<b>14.545</b>	<b>0.001</b> <b>15.2</b>
	Aneuploid	22	9.1%	90.9%				
<b>Combined biomarker abnormalities</b>								
DNA ploidy or p53 protein	49	17.2%	82.8%	0.30	<b>0.001</b>	<b>8.914</b>	<b>0.001</b>	<b>8.914</b>
PLK-1 (Millipore) <sup>§</sup> or p53 protein	49	23.5%	76.5%	0.68	<b>0.006</b>	<b>6.5</b>		
PLK-1 (Millipore) <sup>§</sup> or DNA ploidy	49	23.3%	76.7%	0.63	<b>0.017</b>	<b>4.518</b>		
PLK-1 (Millipore) <sup>§</sup> , DNA ploidy or p53 protein	49	25.7%	74.3%	0.68	<b>0.015</b>	<b>5.2</b>		

Abbreviations: NDBE (non-dysplastic Barrett's epithelium), SE (standard error), Odds Ratio

‡ Mean (95% confidence interval)

\* Univariate logistic regression for prediction of dysplasia

† Multivariate logistic regression post univariate filtering (p<0.05) for prediction of dysplasia

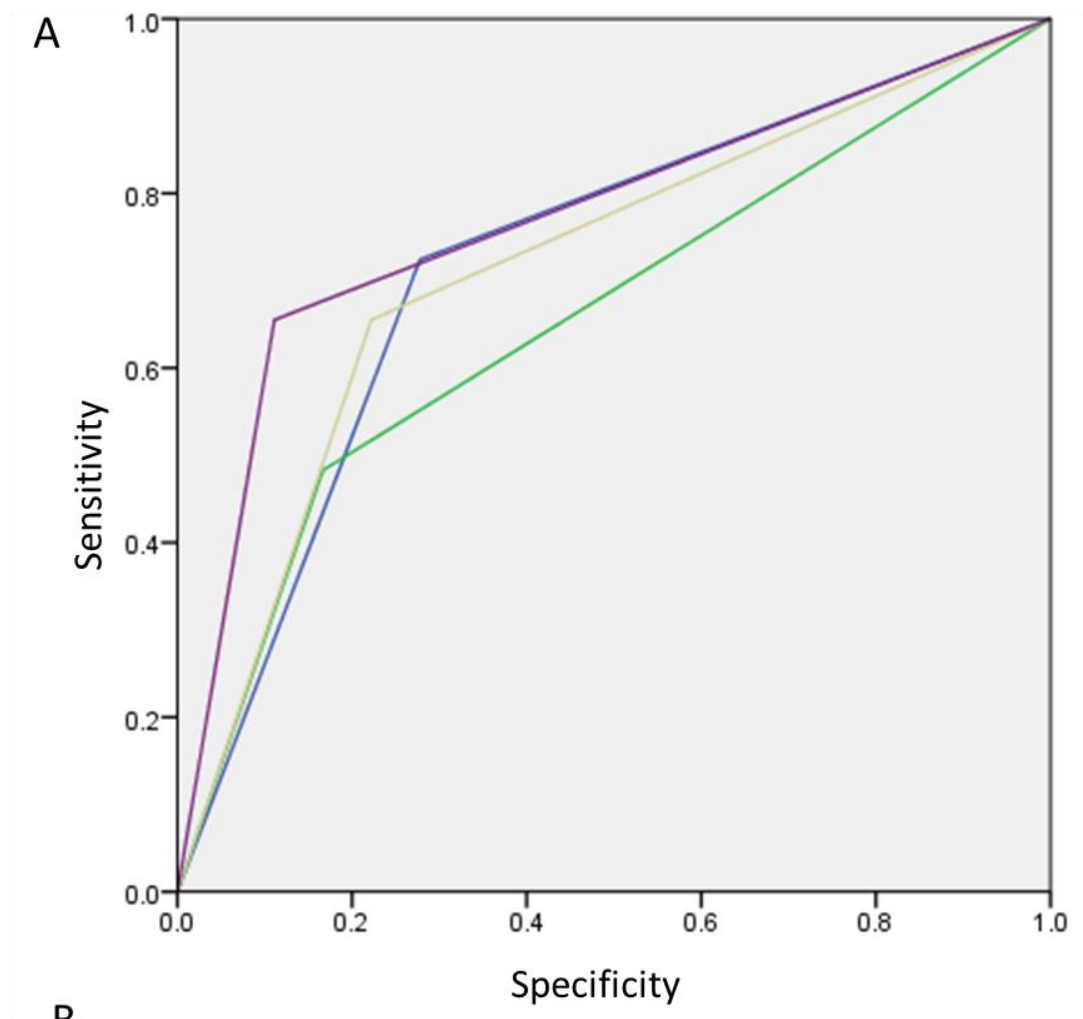
**Table 12: Sensitivity and specificity analysis of PLK-1 (Millipore) and PLK-1 (Leica) to identify optimum Allred cut off to predict DNA content abnormalities.**

	^Mean Allred score	Sensitivity	Specificity	Youden's index
PLK-1 (Milipore)	1	0.902	0.412	0.314
	2.25	0.854	0.529	0.383
	2.75	0.78	0.529	0.309
	<b>3.25</b>	<b>0.683</b>	<b>0.706</b>	<b>*0.389</b>
	3.75	0.561	0.765	0.326
	4.25	0.439	0.882	0.321
	4.75	0.341	0.882	0.223
	5.25	0.293	0.882	0.175
	5.75	0.195	1	0.195
	6.25	0.098	1	0.098
PLK-1 (Leica)	0.5	0.927	0.235	0.162
	1.25	0.902	0.235	0.137
	1.75	0.878	0.353	0.231
	2.25	0.829	0.471	0.3
	2.75	0.756	0.588	0.344
	<b>3.25</b>	<b>0.585</b>	<b>0.882</b>	<b>*0.467</b>
	3.75	0.439	0.882	0.321
	4.25	0.39	0.941	0.331
	4.75	0.341	1	0.341
	5.25	0.244	1	0.244
5.75	0.171	1	0.171	
6.25	0.098	1	0.098	
7.5	0	1	0	

\*Optimum Youden's index

^Mean Allred score from 2 pathologists

Figure 29: ROC curves (A), sensitivity and specificity of significant biomarkers on UV analysis with Allred >3 defining PLK-1 positivity (B).



	AUC	p-value	Sensitivity	Specificity	PPV	NPV
— PLK-1 (Millipore) <sup>§</sup>	0.723	<b>0.011</b>	0.71	0.722	0.815	0.591
— PLK-1 (Leica) <sup>§</sup>	0.658	0.071	0.483	0.833	0.823	0.5
— p53	0.716	<b>0.013</b>	0.612	0.778	0.826	0.539
— Aneuploidy	0.772	<b>0.002</b>	0.645	0.889	0.909	0.593

AUC: Area under curve, PPV: Positive Predictive Value, NPV: Negative Predictive Value

<sup>§</sup> Allred >3 defines positivity

### **4.3.3. Association between clinicopathological variables and DNA content**

#### **1.1.1.1. Background**

The previous sections demonstrated DNA-CA to be the most predictive for the presence of dysplasia (LGD or HGD). Case-control studies support this finding and have shown how DNA-CA in NDBE can predict progression to HGD or OA irrespective of dysplasia and abnormal p53 immunohistochemistry<sup>19,179</sup>. In the NI registry nested case-controlled study, p53 immunohistochemistry was not shown to be predictive of progression from NDBE to HGD or OA ( $p=0.08$ ), while DNA-CA was independently associated with progression to HGD or OA in the absence of LGD (OR: 3.81, CI 1.43-9.48). If further studies support the finding that DNA-CA predicts progression in NDBE, DNA-CA may in future be considered as an indication for endoscopic therapy in NDBE. The ability of clinical laboratories to analyse for DNA-CA using image cytometry is however limited to certain specialist centres. This next section evaluates whether DNA-CA can itself be predicted by the RLFs Ki67, PLK-1 or Geminin, or abnormal p53 protein expression.

#### **1.1.1.2. Results**

Cases of aneuploidy and tetraploidy in cohort 1 were grouped and compared with diploid cases. Baseline demographics confirmed there were no differences in age or sex between groups. Expression of Ki67 (Leica) and geminin did not differ significantly. On univariate analysis Ki-67 (Dako), PLK-1 and abnormal p53 expression were associated, with p53 having the strongest association (OR: 4.3,  $p=0.009$ ).

To assess which of the significant biomarkers on univariate analysis were independently predictive, multivariate analysis was conducted. PLK1-M (OR: 1.99,  $p=0.001$ ) and abnormal p53 expression (OR: 4.03,  $p=0.037$ ) were found to be independently predictive for DNA-CA. The combination of seeing abnormalities in either PLK1-M or p53 was most strongly associated with DNA-CA (OR: 9.1,  $p=0.007$ ) (Table 13).

**Table 13: Univariate and multivariate analysis of association between clinicopathological variables and DNA content abnormalities.**

	n	Diploid	Aneuploid	SE	p-value*	OR	p-value	OR	
Age	59	66.17 (61.94-70.39)‡	69.72 (66.04-73.4)	0.025	0.507	1.017			
Sex	Male	46	47.8%	52.2%	0.67	0.18	2.46		
	Female	13	69.2%	30.8%					
Ki-67 (Dako)	62	5.1 (4.52-5.68)	6.2 (5.73-6.67)	0.2	<b>0.03</b>	<b>1.53</b>			
Ki-67 (Leica)	60	5.83 (5.42-6.24)	6.22 (5.83-6.61)	0.67	0.35	1.28			
Geminin	62	3.62 (2.95-4.29)	4.8 (3.99-5.61)	0.14	0.07	1.29			
PLK-1 (Millipore)	62	2.52 (1.75-3.29)	4.7 (4.09-5.31)	0.2	<b>&lt;0.001</b>	<b>2.05</b>	<b>0.001</b>	<b>1.99</b>	
PLK-1 (Leica)	60	2.65 (1.98-3.32)	4.1 (3.39-4.81)	0.16	<b>0.012</b>	<b>1.51</b>			
p53 expression	Normal	27	74.1%	25.9%	0.558	<b>0.009</b>	<b>4.3</b>	<b>0.037</b>	<b>4.03</b>
	Over / under	35	40%	60%					
<b>Combined abnormalities</b>									
PLK-1 (Millipore) <sup>§</sup> or p53	62	43.5%	56.5%	0.681	<b>0.007</b>	<b>9.1</b>			

Abbreviations: NDBE (non-dysplastic Barrett's epithelium), SE (standard error), UV (univariate), MV (multivariate)

‡ Mean (95% confidence interval)

\* Univariate logistic regression for prediction of dysplasia

† Multivariate logistic regression post univariate filtering (p<0.05) for prediction of dysplasia

To ascertain the optimum cut off Allred score for the prediction of DNA-CA, the Youden's index was calculated for biomarkers found to be predictive for DNA-CA on univariate analysis (Table 14). This established the optimum cut off Allred score for both PLK-1 antibodies to be 3.25, and for Ki67 (Dako) to be 5.25. Allred score cut-offs of >3 for PLK-1 antibodies and >5 for Ki67 (Dako) were therefore selected to define biomarker positivity to predict DNA-CA.

**Table 14: Sensitivity and specificity analysis to identify optimum Allred cut off to predict DNA content abnormalities.**

^Mean Allred Score	PLK-1 (Millipore)			PLK-1 (Leica)			Ki67 (Dako)		
	Sensitivity	Specificity	Youden's index	Sensitivity	Specificity	Youden's index	Sensitivity	Specificity	Youden's index
0.5.	.	.	.	0.96	0.182	0.142.	.	.	.
1	1	0.333	0.333.	.	.	.	.	.	.
1.25.	.	.	.	0.96	0.212	0.172.	.	.	.
1.5.	.	.	.	.	.	.	1	0.03	0.03
1.75.	.	.	.	0.92	0.273	0.193.	.	.	.
2.25	0.96	0.424	0.384	0.88	0.364	0.244.	.	.	.
2.75	0.92	0.485	0.405	0.84	0.485	0.325.	.	.	.
3.25	<b>0.84</b>	<b>0.636</b>	<b>*0.476</b>	<b>0.68</b>	<b>0.727</b>	<b>*0.407</b>	1	0.091	0.091
3.75	0.68	0.697	0.377	0.48	0.758	0.238	1	0.121	0.121
4.25	0.6	0.848	0.448	0.44	0.818	0.258	0.92	0.273	0.193
4.75	0.44	0.848	0.288	0.4	0.879	0.279	0.92	0.364	0.284
5.25	0.4	0.879	0.279	0.32	0.939	0.259	<b>0.84</b>	<b>0.515</b>	<b>*0.355</b>
5.75	0.28	0.97	0.25	0.24	0.97	0.21	0.64	0.545	0.185
6.25	0.16	1	0.16	0.12	0.97	0.09	0.4	0.758	0.158
6.75.	.	.	.	.	.	.	0.36	0.818	0.178
7.25	0.04	1	0.04	0	1	0	0.16	0.97	0.13
7.75.	.	.	.	.	.	.	0.16	1	0.16
8.5.	.	.	.	.	.	.	.	.	.
9	0	1	0.	.	.	.	0	1	0

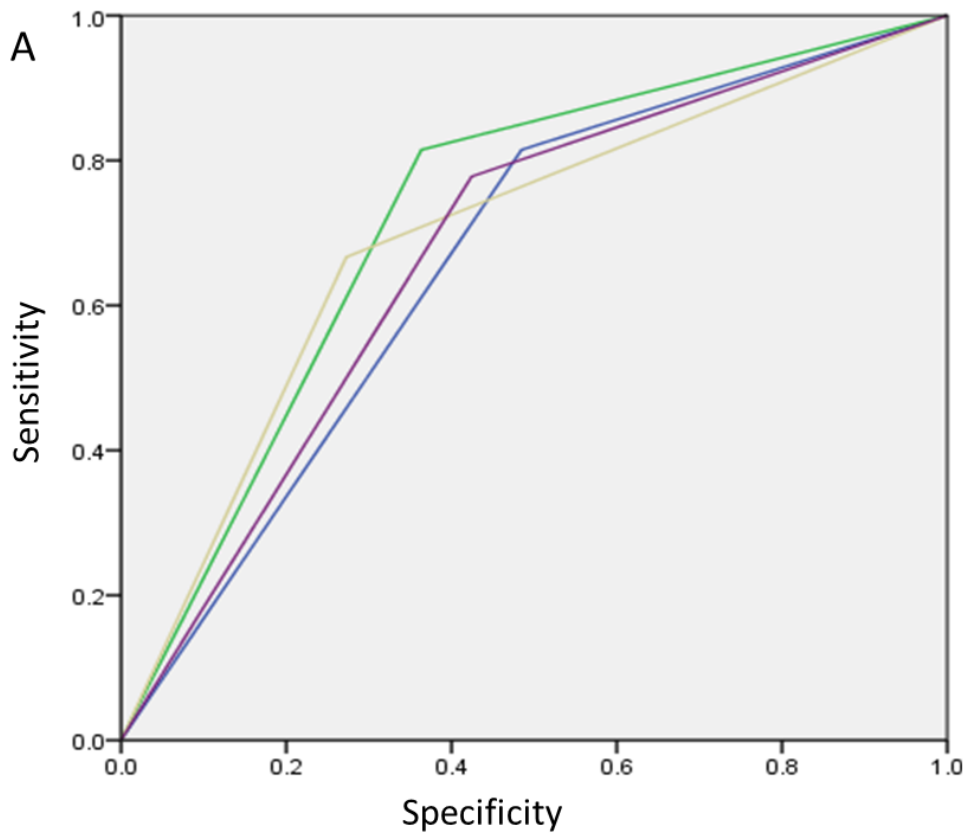
\*Optimum Youden's index

^Mean Allred score from 2 pathologists





Using the defined cut off scores, ROC curves for immunohistochemical biomarkers were designed to predict DNA-CA (Figure 30). All variables remained significant. PLK-1 (Millipore) overexpression most closely predicted abnormal DNA content (AUC: 0.73, p=0.003), over p53 and Ki67 and with a high sensitivity (82.1%) and negative predictive value (81.5%).

**Figure 30: ROC curves of biomarkers identified to be predictive of DNA content abnormalities on univariate analysis.**

**A**



**B**

	AUC	p-value	Sensitivity	Specificity	PPV	NPV
 Ki-67 (Dako) <sup>‡</sup>	0.665	<b>0.029</b>	0.786	0.529	0.579	0.75
 PLK-1 (Millipore) <sup>§</sup>	0.726	<b>0.003</b>	0.821	0.647	0.657	0.815
 PLK-1 (Leica) <sup>§</sup>	0.697	<b>0.009</b>	0.667	0.727	0.667	0.727
 p53	0.677	<b>0.019</b>	0.75	0.588	0.6	0.74

AUC: Area under curve, PPV: Positive Predictive Value, NPV: Negative Predictive Value

<sup>§</sup> Allred >3 defines positivity; <sup>‡</sup> Allred >5 defines positivity

### 1.1.1.3. Summary

Several tissue biomarkers were found to be predictive for DNA-CA. On univariate analysis, Ki67 (Dako), both PLK-1 antibodies, and abnormal p53 predicted DNA-CA.

Multivariate analysis subsequently found only PLK-1 (Millipore) and abnormal p53 protein to be predictive of DNA-CA, and the combination of abnormalities in either PLK1-M or p53 was superior to them individually. Youden's index identified the optimum cut off to predict DNA-CA for PLK-1 to be >3 and for Ki67 (Dako) to be >5. ROC curves using these cut offs for tissue markers with abnormal p53 protein identified PLK-1 (Millipore) predicted DNA-CA best.

#### ***4.3.4. Are replications licensing factors overexpressed prior to dysplasia or cancer?***

##### **4.3.4.1. Background**

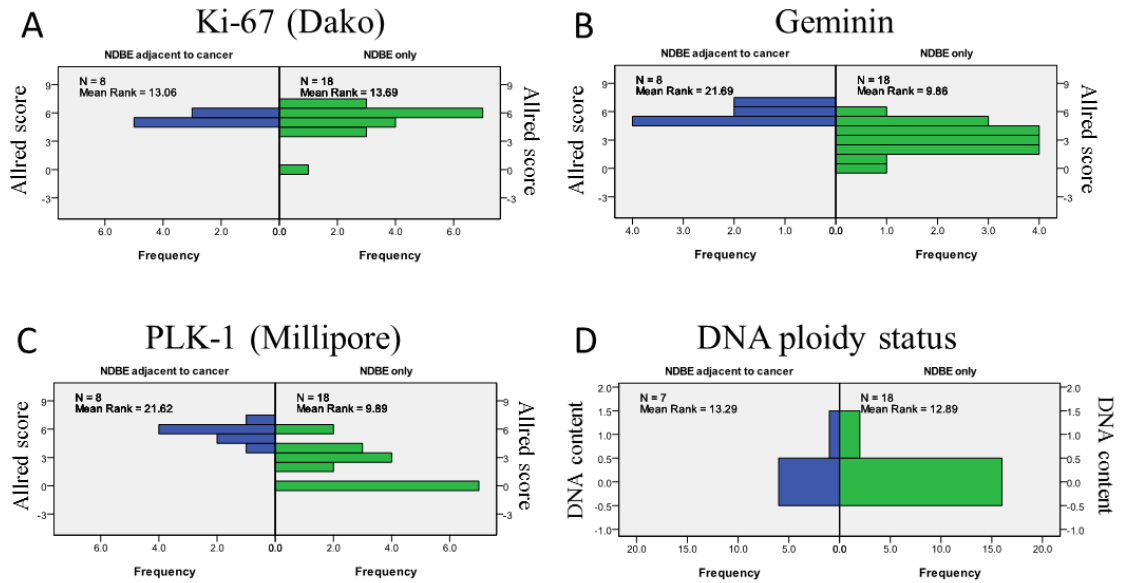
Earlier experiments found overexpression of RLF's can predict dysplasia and DNA-CA. If RLF overexpression is an early event in the progression to cancer, it can be postulated that this could be used to select those patients with NDBE who would warrant surveillance, or perhaps early endoscopic therapy. It is inferred that RLF expression patterns in NDBE influenced by field cancerisation would have a biomarker profile like that seen in patients with NDBE who are at risk of progressing. Comparing expression of RLFs and DNA-CA in NDBE tissue adjacent to cancer, to that seen in NDBE in patients who never progressed to dysplasia or OA will be used to test this hypothesis.

##### **4.3.4.2. Results**

8 NDBE areas adjacent to OA from tumour resection specimens were laser captured, 1/8 failed analysis. The distribution plots and subsequent analysis show that DNA content and Ki67 (Dako) expression was similar in NDBE only (patients with NDBE who did not progress) and NDBE adjacent to OA. PLK-1 (5.56 vs 3.03;  $p < 0.001$ ) and Geminin (5.56 vs 2.14;  $p < 0.001$ ) were however upregulated in NDBE adjacent to OA when compared to NDBE only.



**Figure 31: Field cancerisation influencing biomarker expression in BE next to OA**



**E**

	NDBE adjacent to OA	NDBE only	p-value	
Ki-67 (Dako)	5.38 (0.42)	5.19 (1.66) <sup>#</sup>	0.85 <sup>*</sup>	
Geminin	5.56 (0.68)	3.03 (1.45)	<0.001 <sup>*</sup>	
PLK-1 (Millipore)	5.56 (0.82)	2.14 (1.98)	<0.001 <sup>*</sup>	
DNA content				
	Diploid	27.3%	72.7%	1 <sup>†</sup>
	Aneuploid	33.3%	66.7%	

Abbreviations: NDBE (non-dysplastic Barrett’s epithelium), OA (oesophageal adenocarcinoma)  
<sup>#</sup> Mean (standard deviation); <sup>\*</sup> Mann-Whitney U test; <sup>†</sup> Fisher’s exact test

*Analysis of field cancerisation comparing Ki-67 (A), Geminin (B), PLK-1 (C) expression and DNA content (D) in laser capture microdissected non-dysplastic Barrett’s epithelium (NDBE) adjacent to cancer versus NDBE expression in those who did not progress. Distribution of expression between groups is displayed (A-D) and analysed in Table (E).*

**4.3.4.3. Summary**

Using tissue expression of RLFs in NDBE influenced by field cancerisation as a surrogate for patients with NDBE yet to progress, in comparison to NDBE who never

progressed, it was shown that PLK-1 and Geminin overexpression may be early events in cancer progression. The small sample size and surrogate for actual patients with NDBE who progressed however limit any conclusions that can be drawn.

#### **4.3.5. *Is polo-like kinase 1 upregulated in Barrett's progressors?***

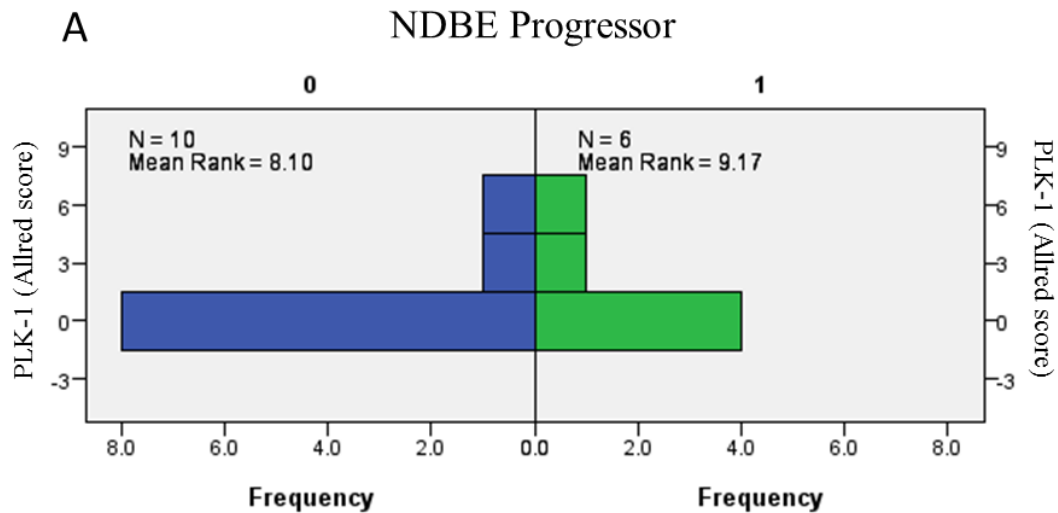
##### **4.3.5.1. Background**

The experiments so far have shown that out of all the RLFs examined, PLK-1 (Millipore) was the most predictive for dysplasia and DNA-CA. It was also shown to be upregulated in NDBE adjacent to OA. To establish whether PLK-1 is upregulated in patients who are known to have progressed to HGD or OA (BE progressors), this section will evaluate the expression of PLK-1 (Millipore) in archival sections taken from patients with NDBE before it progressed in comparison to patients with NDBE who never progressed to dysplasia or malignancy (BE non-progressor).

##### **4.3.5.2. Results**

PLK-1 expression was examined in BE progressors and non-progressors. The median length of time between presentation and disease progression was shorter for progressors (26 months) than the time between endoscopies for the BE non-progressors (39 months). This was not significant ( $p=0.368$ ). Mean expression scores for PLK-1 (Millipore) were marginally higher in NDBE who later progressed to cancer versus non-progressors (1.5 vs 0.9) but this was not significant ( $p=0.71$ ) (Figure 32).

**Figure 32: PLK-1 expression in BE progressors versus non-progressors**



**B**

	NDBE nonprogressor	NDBE progressor	p-value*
n	10	6	
PLK-1 expression	0.9 (2.03) <sup>#</sup>	1.5 (2.51)	0.713
Follow up (months)	38.96 (24.35-48.17) <sup>□</sup>	25.57 (12.05-48.37)	0.368

Abbreviations: NDBE (non-dysplastic Barrett's epithelium)

<sup>#</sup> Mean (standard deviation) Allred score

<sup>□</sup> Median (interquartile range)

\* Mann-Whitney U test

*Distribution plot of PLK-1 expression evaluated with Allred scoring in progressors versus non-progressors is displayed (A) and analysed further in Table (B).*

#### 4.3.5.3. Summary

These experiments did not find PLK-1 overexpression to be an early event in the progression of NDBE to OA. Whilst the levels of PLK-1 expression were higher in BE progressors versus non progressors, they did not differ significantly. It may be that PLK1-M overexpression occurs closer to the time of progression to dysplasia or cancer.

### **4.3.6. Inter-observer agreement between pathologists reporting IHC biomarkers**

#### 4.3.6.1. Background

There remains controversy about the reporting of dysplasia, particularly LGD between pathologists. For this reason that UK guidelines on the diagnosis of LGD or HGD recommend a second pathologist review specimens to confirm the diagnosis due to the implications for subsequent treatment<sup>1,146</sup>. Controversy in the diagnosis of Barrett's dysplasia is not limited to general pathologists however. Skacel et al examined the interobserver variability between 3 specialists GI pathologists for a previously established diagnosis of LGD in 43 cases. Pathologists classified the specimens as either NDBE, indefinite for dysplasia, LGD or HGD. Individual pathologist agreed with the original diagnosis in 70%, 56% and 16% of cases. The study concluded that there is a high level of interobserver variability in the diagnosis of LGD<sup>48</sup>. If biomarkers require defined cut-off values to define positivity, such as is proposed for RLF staining in Barrett's, it should be ascertained if there is significant interobserver variability exists between pathologists reporting these cases. In this experiment, two expert GI pathologists (Professor Marco Novelli and Dr Manuel Rodriguez-Justo) were asked to report slides immunostained with PLK-1 antibodies, scoring selected regions of interest (Figure 33) containing the highest grade of pathology in the specimen.

#### 4.3.6.2. Results

Interobserver agreement was calculated for the 2 immunohistochemical stains, PLK1-M and PLK1-L. Linear Kappa scores were calculated as a statistical measure of agreement. This found better inter-observer agreement between pathologists with PLK1-M scores ( $\kappa=0.72$ ; 95% CI 0.6-0.83) than PLK1-L ( $\kappa=0.53$ ; 95% CI 0.38-0.68). It was noted that pathologist 2 had a trend to score PLK-L more highly but overall agreement was good as most scores can be seen to lie within 2 SD of each other.

**Figure 33: PLK1 immunostained slide highlighting HGD in selected Region of Interest (ROI) of at low (x2.5) and higher (x10) power**

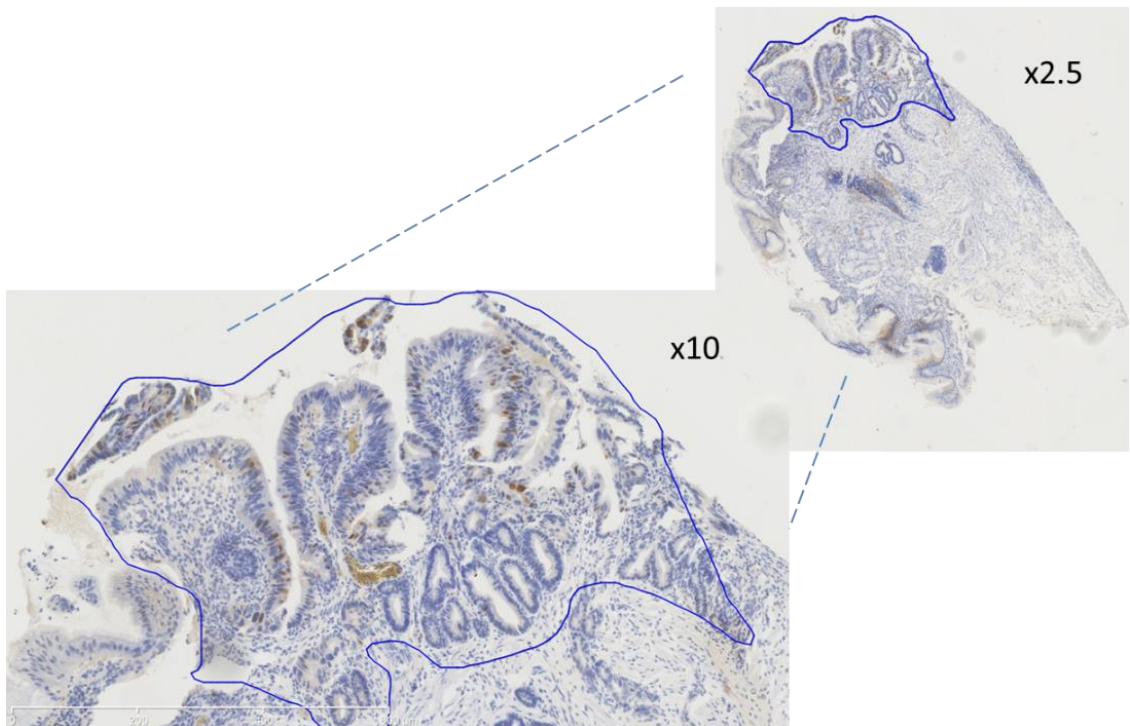
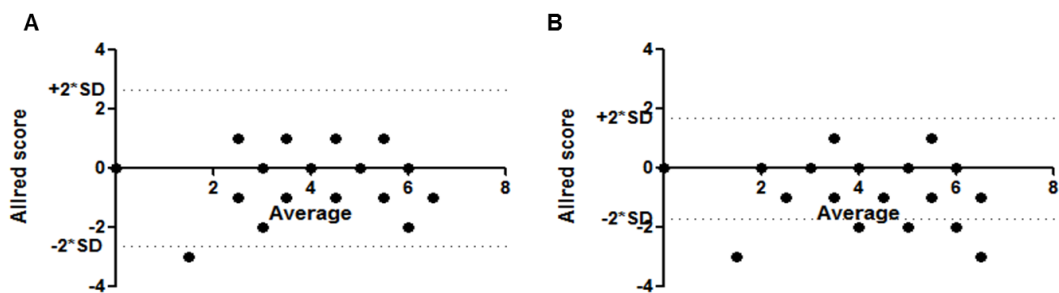


**Figure 34: Bland-Altman plot showing inter-observer agreement of PLK1-M (A) and PLK1-L (B) reporting of pathological grade**



#### 4.3.6.3. Summary

Immunohistochemical staining can be reported in a reproducible way using the Allred scoring system. Although 1 pathologist tended to score one antibody more generously, the majority of reports were within 2 SD with good agreement. Unlike a diagnosis of LGD, biomarker reporting with Allred score seems consistent between specialist GI

pathologists and may not require a second pathologist to corroborate the level of IHC positivity if this system is subsequently applied into clinical practice.

#### ***4.3.7. Audit of specialist clinical image cytometry service to identify relationship between predicted DNA CA and pathological grade***

##### **4.3.7.1. Background**

To assist in the risk stratification of BE, patients in University College Hospital are occasionally referred for image cytometry in addition to histology to identify those at increased risk of progression. Whether DNA-CA themselves can assist in the diagnosis of dysplasia, and the prevalence of DNA-CA within different pathological grades will be examined in this audit of the image cytometry service.

##### **4.3.7.2. Results**

189 cases were referred for assessment of DNA CA in our specialist referral centre from 4 institutions up until 2014. The male to female ratio of referred cases was ~4:1 (n=151:38).

**Figure 35: Distribution of pathology in patients found to have DNA CA (A) and in those with normal content (diploid cases) (B).**

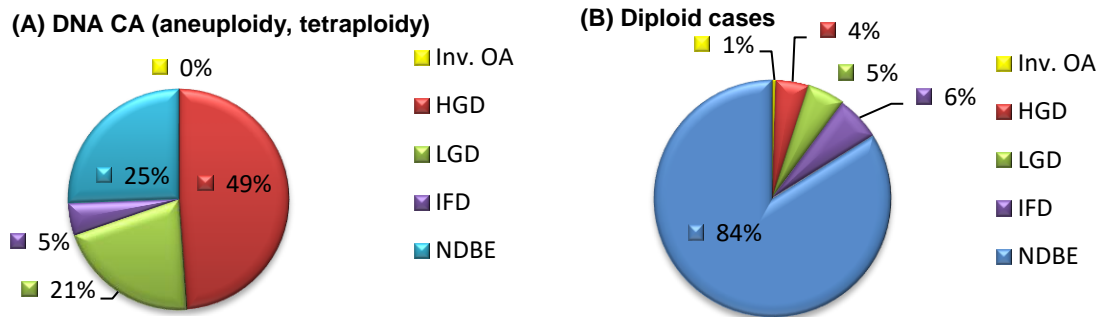
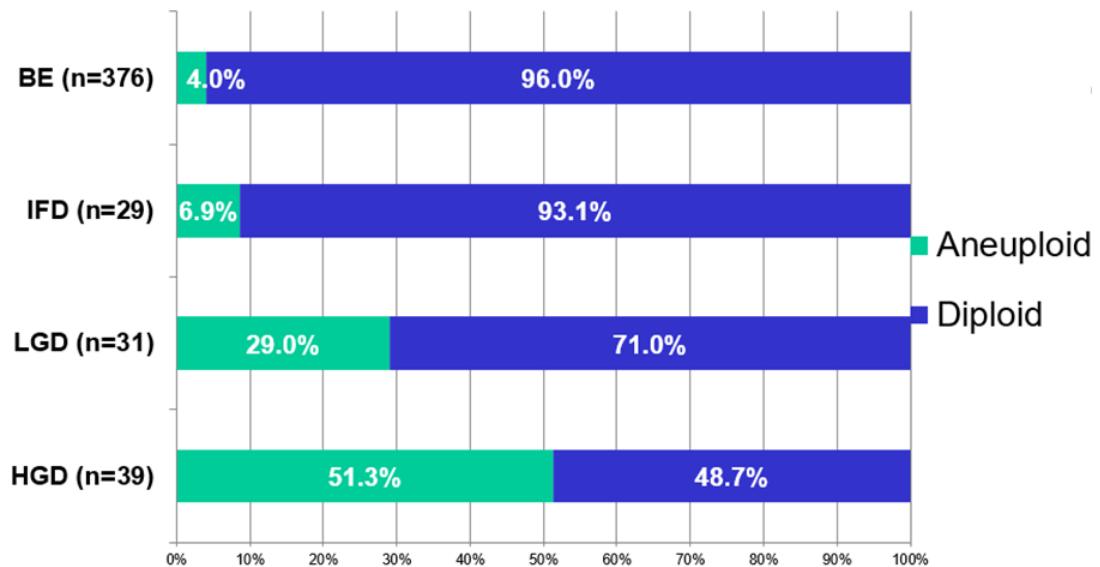


**Figure 36: Distribution of relationship between DNA CA and incremental pathological grades in the large UCLH cohort of patients referred for image cytometry.**



Pearson product-moment correlation coefficient comparing % ploidy in pathological grades progressing to cancer was  $r=0.96$  ( $p=0.039$ ), confirming significant correlation between increasing degree of dysplasia and DNA-CA. DNA-CA was found in 29% of LGD cases and 51.3% of HGD.

#### 4.3.7.3. Summary

The proportion of patients with DNA-CA increases sequentially during progression through incremental pathologies to HGD. We have shown in section 3 how DNA-CA are superior to p53 protein expression in the prediction of dysplasia and the data from

this audit supports this finding. In future if DNA-CA becomes established as an adjunct to assist pathologists in the diagnosis of dysplasia, its presence in indefinite for dysplasia may give pathologists the confidence to make the diagnosis of LGD if appropriate.

#### **4.3.8. Digital Image Analysis of immunostained slides**

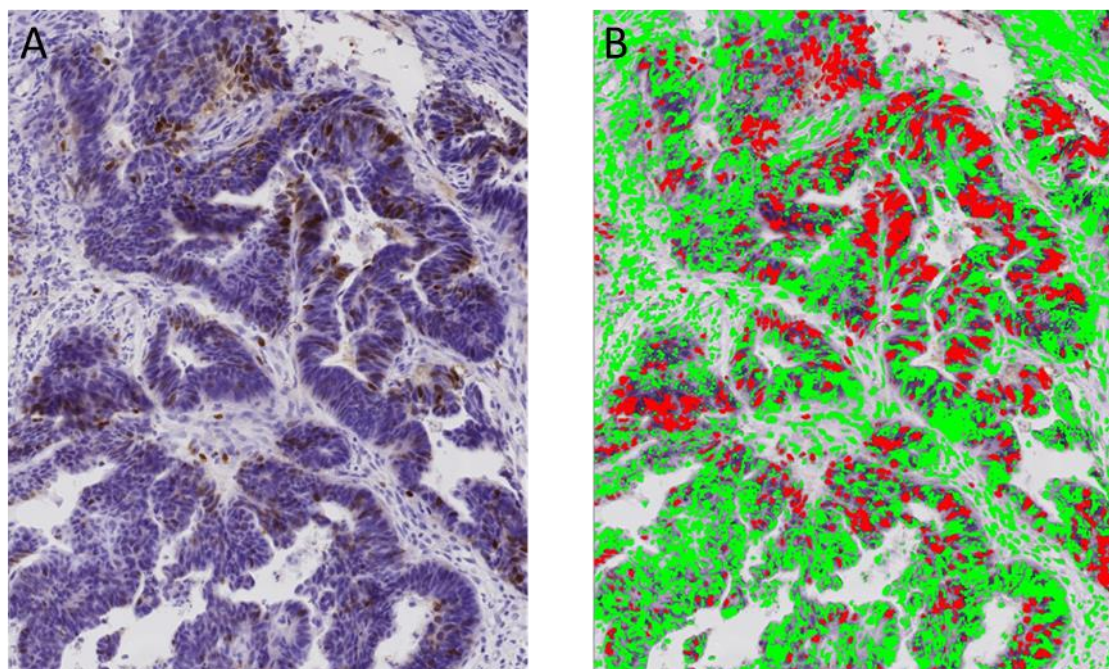
##### **4.3.8.1. Background**

When scoring using the Allred score, pathologists are asked to estimate the approximate percentage of positively stained nuclei in the selected ROI with a score between 0-5 (0=0%, 1=0-1%; 2=1-10%, 3=10-33%, 4=33-66%; 5=>66%). If this process could be automated, it would save pathologist time, the precision of this scoring system and its reproducibility. This next set of experiments will evaluate if image analysis software can be programmed to undertake this task, and if so, what's its correlation to pathologist reporting using Persons r will be. At first extent of staining will be analysed, and later intensity of staining as well in comparison to Allred scores for these parameters.

Regions of interest (ROI) within scanned slides of a particular pathology were physically highlighted by pathologists by drawing onto the slide under the microscope. These same areas were then traced digitally to establish the ROI to be examined (Figure 33). Within these ROI, Ariol ® image analysis software was used to create digital mask to recognise nuclei stained with haematoxylin (blue) and antibody (brown), converting them into green and red digital images respectively. Figure 37 shows a typical output from the digital analysis within a targeted ROI. The output of % tissue staining red and green were totalled, and the % of tissue calculated to be positively stained with antibody produced.



**Figure 37: Examples of digital image analysis mask produced by Ariol software analysis of Barrett's.**



*Immunostaining of oesophageal adenocarcinoma (A) showing PLK-1 positive nuclei (brown) on background haematoxylin stained tissue (blue). (B) Same area analysed with Ariol® image analysis software with masks trained to quantify positive PLK-1 stained tissue (red) and negative background haematoxylin staining (green).*

#### 4.3.8.2. Results

##### 4.3.8.2.1. Comparison between DIA percentage positivity with Allred and extent sub scores

Only extent scores for PLK1-L ( $R=0.95$ ,  $p<0.001$ ) and Geminin ( $R=0.99$ ,  $p=0.0001$ ) stained slides correlated with DIA (Table 15). This was perhaps influenced by the quality of the immunostaining. Both Geminin and PLK1-L had excellent immunostaining with minimal if any background tissue stained. PLK1-M immunostaining had significant background tissue staining. DIA could not easily distinguish between actual and background tissue staining without further processing. Pathologists exclude background staining inherently.

When intensity was factored in with extent sub scores to establish the final Allred score, a significant correlation was seen between all pathologist scores and DIA percentage positivity irrespective of antibody used.

**Table 15: Comparison of pathologist reported Allred and extent sub scores with percentage immunohistochemical staining with digital image analysis.**

		Correlation with percentage positivity with DIA		
		PLK1-M	PLK1-L	Geminin
Allred score	R	<b>0.763</b>	<b>0.7249</b>	<b>0.9444</b>
	p	<b>0.006</b>	<b>0.008</b>	<b>0.004</b>
	95% CI	0.301-0.935	<b>0.259-0.917</b>	<b>0.716-0.990</b>
Allred Extent Sub score	R	0.337	<b>0.950</b>	<b>0.992</b>
	p	0.415	<b>&lt;0.001</b>	<b>0.0008</b>
	95% CI	0.882-0.999	<b>0.778-0.990</b>	<b>0.882-0.999</b>

#### 4.3.8.2.2. Comparison between DIA percentage positivity and pathology grade

To examine whether RLF quantification using DIA may be used as a surrogate to predict pathological grade of the tissue being examined, the relationship between DIA percentage positivity and pathological grade was examined. Table 16 summarises this relationship. Only Geminin was found to show a correlation with pathological tissue grade (R=0.97; p=0.033; CI: 0.083-0.999).

**Table 16: Comparison of pathologist reported tissue grade with percentage of positive immunohistochemical staining with digital image analysis.**

		Correlation with percentage positivity with DIA		
		PLK1-M	PLK1-L	Geminin
Pathology grade	R	0.914	0.797	<b>0.967</b>
	p	0.086	0.203	<b>0.033</b>
95% CI		-0.388-0.998	-0.701-0.996	<b>0.083-0.999</b>

*Oesophageal tissue grade was compared with the DIA output of Ariol® software programmed to quantify percentage immunohistochemical tissue positivity for the biomarkers PLK1-M, PLK1-L and Geminin. This was to assess if DIA positivity of these biomarkers could be used to predict the corresponding pathological tissue grade.*

*Pearsons R was used to assess the relationship between variables. Pathological grade was considered as ordinal data with grades of increasing severity following the Barrett's metaplasia, low grade dysplasia, high grade dysplasia, carcinoma sequence.*

#### 4.3.8.2.3. Comparison between DIA computed intensity and pathologist intensity scores

During programming of the DIA algorithm, Ariol® required initial optimisation of the thresholds of colour and intensity that the software subsequently considered as positively stained nuclei. During training, the operator sets the threshold of minimal colour, this would equate to a pathologist's score of 1+. The algorithm also requires the upper limit of colour and intensity to be set. Based on these thresholds the Ariol® produces a mean intensity of all nuclei registered within the selected ROI. These mean intensity score for positively masked nuclei were compared with pathologist intensity scores between 0-3 (0=negative, 1=mild, 2=moderate, 3=strong). Each RLF antibody required individual algorithm optimisation as subtle differences in antibodies and immunostaining protocols have profound effects on DIA output. During training it was apparent that background brown staining of blood and artefact surrounding the surface

of biopsy specimens can be considered as positively stained nuclei on occasion. This was difficult to exclude using DIA.

Only PLK1-L pathologist intensity sub score and DIA intensity scores were seen to correlate in this analysis (R=0.985; p=0.02; CI: 0.435 – 0.999) (Table 17). PLK1-L antibody also had the least background staining and was considered the cleanest antibody out of those examined.

**Table 17: Relationship between pathologist and DIA intensity scores**

		Correlation with DIA intensity		
		PLK1-M	<b>PLK1-L</b>	Geminin
Allred Intensity Sub score	R	0.1473	<b>0.9845</b>	0.7142
	p	0.8527	<b>0.02</b>	0.2858
	95% CI	-0.948-0.971	<b>0.435-0.999</b>	-0.993-0.788

#### 4.3.8.3. Summary

Digital image analysis with the software Ariol® can allow rapid processing of multiple scanned slides to quantify biomarker positivity when the biomarker is stained with a different colour to background. We found DIA to correlate well with pathology reported Allred scores in both PLK-1 antibodies and Geminin.

DIA provides individual outputs for percentage of tissue staining positively, and the intensity of tissue staining. These sub scores were therefore compared to Allred sub scores. Comparison of extent found both PLK1-L and Geminin correlated, while for intensity, only PLK1-L was seen to correlate. It was further examined if pathological grade would correlate with DIA percentage positivity. Only Geminin was seen to have this pattern.

During training of the DIA algorithm and analysis itself, it became rapidly apparent that clean antibodies with minimal background tissue staining performed much better than

those slides where background staining was more apparent. This seemed to have had a particularly negative effect on PLK1-M DIA scores where the masks made it apparent that background tissue staining was not being excluded. Other image analysis platforms such as Definiens ® allow selection of nuclei by both colour and shape which can overcome this limitation.

#### **4.4. Discussion**

This chapter examined the relationships between DNA-CA, RLFs, p53 protein expression and pathological grade of Barrett's epithelium. It further evaluated if RLFs can be quantified as effectively as pathologist reporting using digital image analysis. Our results indicate that while abnormal p53 protein expression was associated with dysplasia, PLK-1 and DNA ploidy abnormalities were also predictive. When compared using multivariate analysis, DNA ploidy abnormalities were seen to be most strongly and independently predictive of dysplasia. PLK-1 (Millipore) was found to have potential as a surrogate for DNA content abnormalities. Using a cut off Allred score of >3 to define positivity, PLK-1 (Millipore) had the highest area under curve, sensitivity and negative predictive value for aneuploidy prediction suggesting it may have clinical utility when evaluation of DNA ploidy abnormalities is not easily accessed or affordable.

The improving efficacy and tolerability of ablative therapies for BE <sup>275</sup>, coupled with the superiority of a therapy over surveillance for BE with LGD <sup>55</sup> has led to societal guidance to be amended. Both low and high-grade dysplasia in BE are now considered as indications for endoscopic therapy. This makes confirmation of dysplasia when the diagnosis is in doubt a priority <sup>268</sup>. Evaluation of p53 expression is currently recommended in guidelines as an adjunct to help make the diagnosis of dysplasia <sup>1</sup>. This recommendation is supported by the observation that TP53 mutations are one of the earliest events in the evolution of BE towards cancer <sup>276</sup>, however whether the same can be said for p53 protein expression is uncertain as abnormal p53 expression is only a surrogate for TP53 mutations. False negatives can occur due to deletion mutations

while false positives may also be present from mutations causing p53 stabilisation. Discordance between the presence of TP53 mutations and p53 expression has previously been noted in 73 patients with ovarian cancer. TP53 mutations were noted in 34% of cases, however abnormal p53 staining only had a sensitivity of 58% and specificity of 71% at predicting TP53 mutations <sup>277</sup>. We evaluated the relationship between TP53 mutations and p53 protein expression in a pilot study of 37 patients with BE and varying degrees of dysplasia using next generation sequencing (NGS) on archival FFPE tissue. Of the 15 cases with TP53 mutations, only 40 % had concordant abnormal p53 protein expression, leaving the majority (60%) undetected with this approach <sup>278</sup>. NGS for all TP53 mutations however is both expensive and time consuming so better surrogates for this milestone in neoplastic progression are needed. The poor sensitivity of p53 protein expression as a marker of malignant progression has been suggested in case control studies. In a population based case control study of 35 BE patients with tissue taken before the development of HGD or OA, abnormal p53 staining was only seen in 32.4% of initial biopsies prior to disease progression <sup>185</sup>. Although expression did correlate with malignant progression, it's utility to inform surveillance strategies could not be advocated. Our finding of the superiority of DNA ploidy abnormalities to predict dysplasia is supported by our previously reported nested case-controlled study of BE progressors in the Northern Ireland Barrett's Registry. After excluding progressor cases with LGD in the index biopsies, DNA ploidy abnormalities were the strongest predictors of neoplastic progression to HGD or OA of all biomarkers examined whether evaluated with a panel of 7 biomarkers (adjusted OR=3.81) or a reduced biomarker panel of only 2 biomarkers (adjusted OR=3.43). Our findings therefore advocate the evaluation of DNA ploidy abnormalities over p53 protein expression when there is diagnostic uncertainty regarding the diagnosis of dysplasia. Our audit of the image cytometry service confirmed there is a demand for this biomarker in clinical practice.

RLFs such as PLK-1 and p53 protein expression assessed with immunohistochemistry have great potential for clinical use as they can be easily performed and are amenable to high throughput screening using automated immunostaining platforms. Although we found PLK-1 predicted DNA-ploidy abnormalities and dysplasia marginally better than abnormal p53 expression, this will not currently influence clinical decision making as both DNA ploidy abnormalities and abnormal p53 were more associated with the presence of dysplasia. When association of immunohistochemical biomarkers with dysplasia in the absence of DNA content were evaluated, abnormal p53 expression and PLK-1 (Millipore) were independently associated on multivariable analysis. A 2-biomarker panel of abnormalities in either biomarker was found to be more predictive of dysplasia than p53 or PLK-1 (Millipore) alone. PLK-1 protein expression may therefore be considered helpful clinically if evaluating DNA content cannot be performed, due to lack of available expertise or cost. We have shown how image cytometry can be effectively performed on FFPE specimens previously so access to archival tissue should not preclude assessment<sup>178</sup>. PLK-1 may be useful either in combination with p53, or in the presence of normal p53 protein expression where the diagnosis of dysplasia remains uncertain. Abnormalities in PLK-1 may however be more crucial for dysplasia and cancer development than we have identified. We found 62% (8/13) of oesophageal cancers in our cohort overexpressed PLK-1 protein. Tokumitsu et al used PLK-1 gene expression to determine the significance of PLK-1 in 49 oesophageal and 75 gastric carcinomas. PLK-1 over expression was noted in 97% (47/49) of oesophageal tumours and PLK-1 mRNA expression status was an independent prognostic factor for patients with oesophageal carcinoma. The degree of PLK-1 overexpression was also noteworthy. Patients with high-grade PLK-1 overexpression had significantly worse 3-year survival than those with low-grade expression (54.9% vs 24.8%,  $p < 0.05$ )<sup>203</sup>. Determining abnormal PLK-1 status with protein expression alone may therefore be insufficient. PLK-1 gene overexpression may be more accurate at determining its neoplastic potential, however this would be at the expense of a more

complex and less available technique, overcoming the main benefit of PLK-1 immunohistochemistry.

We found all evaluated biomarkers in our study to be upregulated when considering progression to cancer collectively (Table 10). When observed individually some interesting patterns can be speculated (Figure 27). Ki67 is upregulated early, with high expression levels in NDBE. Expression of PLK-1 (Millipore), p53 and DNA content abnormalities seems to be the next events at the time of development of LGD. These continue to be upregulated further in HGD when geminin also becomes upregulated. At the time of cancer progression, geminin, p53, Ki67 (Leica) and PLK-1 (Leica) are mildly upregulated again but PLK-1 (Millipore) and DNA content abnormalities are both down regulated. Understanding the order of events may provide an insight into the sequence of molecular machinery during cancer progression. This is of relevance when considering surveillance strategies in BE and predictors for dysplasia.

Using laser capture microdissection to remove areas of interest, the precise co-registration of aneuploid cell populations with histological staining and RLF expression was achieved. This meticulous technique was necessary to unequivocally examine the relationship between these markers. Laser capture also abrogates the risk of stromal cell analysis at the expense of analysing much smaller cell populations. Using image cytometry, accurate histogram interpretation was still achieved with fewer nuclei. It is unlikely that this experiment could be repeated on archival material using flow cytometry, as this requires cells to have been taken prospectively and frozen. This is not the standard for tissue processing and storage in the UK national health service for Barrett's epithelium.

We found both replication licensing factors in our study, geminin and PLK-1, to be upregulated in microdissected NDBE adjacent to OA. It can be hypothesised that the same clones that had driven development in the adjacent OA are exerting some influence on the microdissected NDBE tissue due to a field cancerisation<sup>279</sup>. These



RLFs represent the S-G2-M phases of the cell cycle and play a key role in DNA synthesis, centrosome maturation and formation of the mitotic spindle, regulation of chromosome segregation and prevention of reduplication. Interestingly, the increased expression of our RLFs was not matched in this NDBE phenotype by concordant DNA ploidy abnormalities. This suggests RLF upregulation to be an earlier event, preceding the development of aneuploidy during cancer progression. Others have similarly noted aneuploidy to be later event in clonal evolution and not the initial trigger <sup>276</sup>. The presence of diploid clones harbouring significant genetic abnormalities such as 9p21 allelic losses and CDKN2 mutations may explain this phenomena <sup>280</sup>. These mutated diploid clones may have the effect of upregulating RLF. These data support the hypothesis that aneuploidy may occur because of cell cycle dysregulation, and that the RLFs are intricately linked to the development of genomic instability.

Our data support PLK-1 as an early event in BE evolution. This finding is supported by another study looking at how mRNA expression levels of PLK-1 are upregulated between BM and OA using quantitative RT-PCR <sup>281</sup>. The role of PLK-1 in OA development was further reported in a study based on metadata analysis of microarray data. Upregulation of PLK1 was found to be a common event in OA along with FOXM1 with whom it functions in a positive feedback loop to control periodic gene expression during G2 and M phases of the cell cycle <sup>282</sup>. The strongest evidence supporting an early role of PLK-1 overexpression in neoplasia development may be explained by its direct interaction with TP53 where it suppresses its transcriptional as well as pro-apoptotic activity <sup>283,284</sup>. The intimate and significant association between PLK-1 and TP53 ( $p=0.0063$ ) was further noted in a study of 215 breast cancer patients. Patients with both TP53 mutations and PLK-1 overexpression were found to have significantly worse survival than those with either biomarker alone <sup>285</sup>. This led to a more recent study which found that TP53 mutations are most accurately detected in breast cancer when evaluated by a panel including p53, PLK-1 and p21 immunohistochemistry. The

utility of and prognostic implications of such a panel combined with evaluation of DNA content in BE would be an interesting area for future research.

In our study the proliferation marker Ki67 was upregulated during progression to OA and correlated well with DNA ploidy status when positivity was defined by a cut off Allred score >5. Ki67 could not predict dysplasia and its expression levels did not differ between NDBE tissue hypothesised to be influenced by field cancerisation. These findings are in agreement with a recent cohort study by the Reid group, which demonstrated high Ki67-positive proliferative fractions were not associated with future development of cancer <sup>286</sup>. In that study there was also no correlation with p16 or p53 mutations, although aneuploidy was not evaluated.

To evaluate a potential prognostic role for PLK-1 in surveillance for BE, we examined PLK-1 expression in a small panel of 6 BE patients known to have progressed to dysplasia or OA in comparison to NDBE only (cohort 3). Although no significant difference in PLK-1 expression was seen between groups, the study was not powered to evaluate for such an effect and so its utility here cannot yet be discounted.

We have shown that DIA with the Ariol® software analysis platform can be trained to develop DIA algorithms to predict and duplicate specialist GI pathologist scores for nuclear biomarker positivity. Certain antibodies perform better for image analysis likely due to cleaner staining seen with them. More powerful DIA platforms such as Definiens however can overcome this limitation of DIA by training slides for nuclear shape as well as intensity. Utilising this robust tool in the era of automated immunostaining offers DIA great potential for high-throughput application in busy clinical services. The close correlation with pathologist scoring seen in these experiments makes a clear case as to how DIA software can improve the efficiency of tissue reporting systems. However, work is still required to improve DIA to show consistent correlation with a range of clinical antibodies.

To our knowledge, this is the first study to explicitly highlight the value of DNA ploidy abnormalities over aberrant p53 expression in the prediction of dysplasia in BE. There are some limitations however, as has been alluded to above. The relatively small numbers of patients, retrospective design and paucity of BE progressors in our study population mean conclusions from cohorts 2 and 3 warrant further studies to answer the question as to whether RLFs have a role in BE surveillance.

In summary, this work definitively demonstrates DNA ploidy abnormalities as a more powerful surrogate for dysplasia in BE than abnormal p53 expression which has currently established this role in clinical practice. PLK-1 in combination with p53 immunohistochemistry may have utility when the diagnosis of dysplasia is in question and evaluation of DNA ploidy unavailable. PLK-1 overexpression appears to precede development of aneuploidy and dysplasia and may have a role as a prognostic marker for BE progression in the surveillance population subject to further study.

**Chapter 5: Evaluation of the therapeutic  
biomarker HER2 and relationships with  
prognosis in oesophagogastric adenocarcinoma**

---

## 5.1. Introduction

Oesophagogastric cancers are the 3rd commonest cancers worldwide<sup>287</sup>, and the 2nd commonest cause of cancer death. In the United Kingdom, an estimated 16,000 new cases are diagnosed annually with majority being adenocarcinomas<sup>288</sup>. Despite advances, five-year survival of oesophageal and gastric cancer remains poor at 15% and 19% respectively<sup>289,290</sup>. The mortality rate for esophageal cancer is the highest in Europe for both males and females<sup>289</sup>. The high death rates seen are due to most patients presenting at an advanced, inoperable stage.

Tumour histology, site and pathological stage are used to select the most appropriate treatment modalities, with curative treatment pathways limited to only around 30% of patients<sup>291</sup>. As a result, interest has been drawn to molecular therapeutic targets. Profiling of multiple signalling pathways led to the development of several monoclonal antibodies against the molecular machinery of foregut cancers. Of these, only human epidermal growth factor receptor 2 (HER2) targeted therapy has been incorporated into widespread clinical practice in the European Union and United States for gastric and gastroesophageal junction (GOJ) adenocarcinomas with HER2 overexpression. This was based on the landmark Trastuzumab for gastric cancer (ToGA) study where Trastuzumab in combination with chemotherapy improved both progression free survival (PFS) and mortality rates (MR) for HER2 over-expressing gastric and GOJ adenocarcinomas when compared with chemotherapy alone<sup>229</sup>.

Many studies have evaluated associations between clinicopathological features of foregut tumours, HER2 expression and prognosis. Most focus on GC with<sup>7-11</sup>, or without<sup>298-305</sup> GOJ cancers with relatively few looking at expression in OA<sup>223,306,307</sup>. They have reported HER2 overexpression as a negative prognostic factor<sup>298</sup>, a positive prognostic factor<sup>296</sup> or having no influence at all<sup>293,297,301</sup>. A few have noted negative association between HER2 expression and poor prognosis in specific subgroups such as those with expansive tumours<sup>300</sup> intestinal type<sup>302</sup> or homogenous overexpression<sup>303</sup>

. Most studies follow international guidance on testing for gastric HER2 with immunohistochemistry (IHC) and confirmatory in-situ hybridization (ISH) for IHC scores of 2+<sup>293–295,299,301,303,304,306</sup>. However some use different thresholds to define HER2 positivity such as an IHC score of 2+ without confirmatory ISH<sup>300 305</sup> or the same score to define negativity<sup>296</sup>. These variations as well as the ethnicity of populations evaluated may explain the conflicting prognostic implications of HER2.

During the ToGA trial, both gastric and GOJ tumours were considered and anatomically classified as gastric carcinoma using TNM guidelines. Approvals subsequently followed in many countries sanctioning the use of Trastuzumab for these HER2 overexpressing foregut tumours<sup>221,231</sup>. The latest TNM staging guidelines (TNM7) have undergone major revisions since then. The most fundamental change with relevance to Trastuzumab has been the reclassification of many GOJ cancers as esophageal rather than gastric<sup>308</sup>. This anatomical reclassification has had the effect of expanding the remit of Trastuzumab therapy into what is now considered to be distal OA<sup>309</sup>.

The purpose of this chapter is to evaluate the relationship between HER2 expression patterns and clinicopathological features of oesophagogastric adenocarcinomas (OGA) in a tertiary reference diagnostic laboratory. In addition, the prognostic impact of variables measured in HER2 diagnostics and clinicopathological variables stratified by HER2 expression were evaluated.

## **5.2. Materials and methods**

### ***5.2.1. Tissue specimens and patient cohorts***

Clinicopathological details from 1029 anonymised cases of OGA's, referred for HER2 testing to University College London's Advanced Diagnosis laboratory between 2003 and 2015 were retrospectively reviewed (parent cohort). 59 centres from across the UK sent in cases for evaluation. HER2 positivity was defined according to current guidelines as an IHC score of 3+, or an IHC score of 2+ with confirmatory HER2 gene

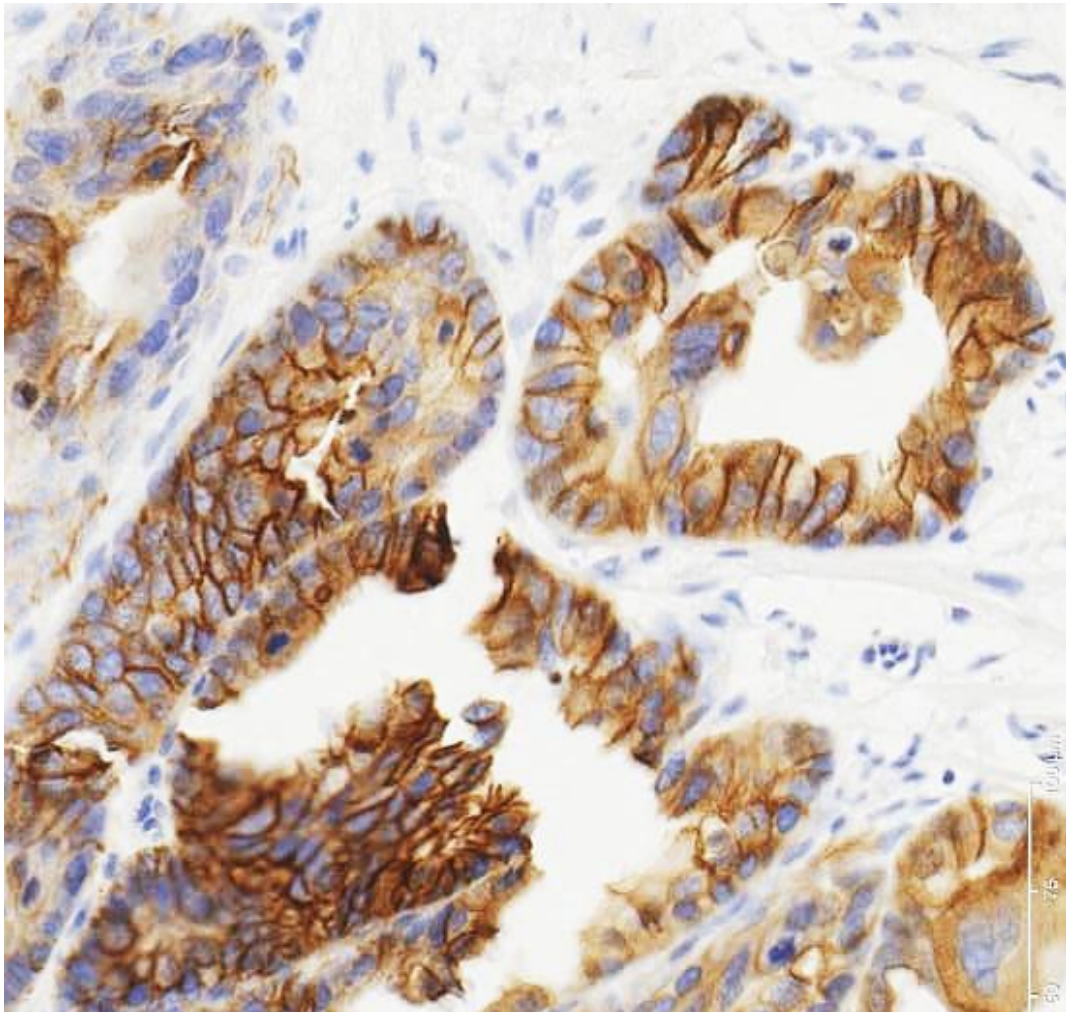
amplification identified using ISH<sup>310</sup>. HER2 gene amplification is measured using probes that label the HER2 gene and chromosome enumeration probe 17 (CEP17) which labels an epitope on chromosome 17. If the ratio of HER2 gene probes to CEP17 is  $\geq 2$  gene amplification is present. Prior to establishment of current guidelines in 2012, confirmatory ISH was performed alongside IHC. ISH was subsequently performed only in cases scoring equivocally (2+) on IHC. Overall 287 cases had both IHC and ISH performed. Within the parent cohort, 199 cases were referred from the laboratory's affiliated institution, University College Hospital. Further clinicopathological and prognostic information were available from local cases. Ethical approval was obtained for use of clinical samples and information for research purposes (Reference: EC13.13).

### **5.2.2. Immunohistochemistry**

Formalin fixed paraffin-embedded (FFPE) tissue sections mounted on slides were received, or 3-4 $\mu$ m sections prepared from FFPE tissue blocks for evaluation. HER2 expression was assessed on a Bond-III instrument (Leica, Biosystems), using the Bond Oracle HER2 IHC System (TA9145 lot 10288) and Roche Benchmark Ultra staining platform. The primary antibodies used were CB11 (mouse monoclonal, Leica Biosystems), and 4B5 (Rabbit monoclonal, Ventana/Roche Diagnostics) using pre-programmed protocols. Parallel IHC were conducted with local graded FFPE positive controls and manufacturer provided HER negative control in a ready to use format containing IgG at equivalent concentrations on each run of the protocol.

All cases were scored by specialist gastrointestinal pathologists (MRJ and MN) at University College London Hospital adhering to published guidelines<sup>310</sup>. Representative IHC samples required complete, basolateral or lateral membrane staining in >10% of the tumour for resection specimens, or  $\geq 5$  cells with the same pattern in at least one tumour cell cluster (TCC) for biopsy samples (Figure 38). IHC appearances were then scored as 0, 1+, 2+ or 3+.

**Figure 38: HER2 positive oesophagogastric adenocarcinoma showing characteristic lateral and complete membrane staining (brown) with 3+ intensity.**



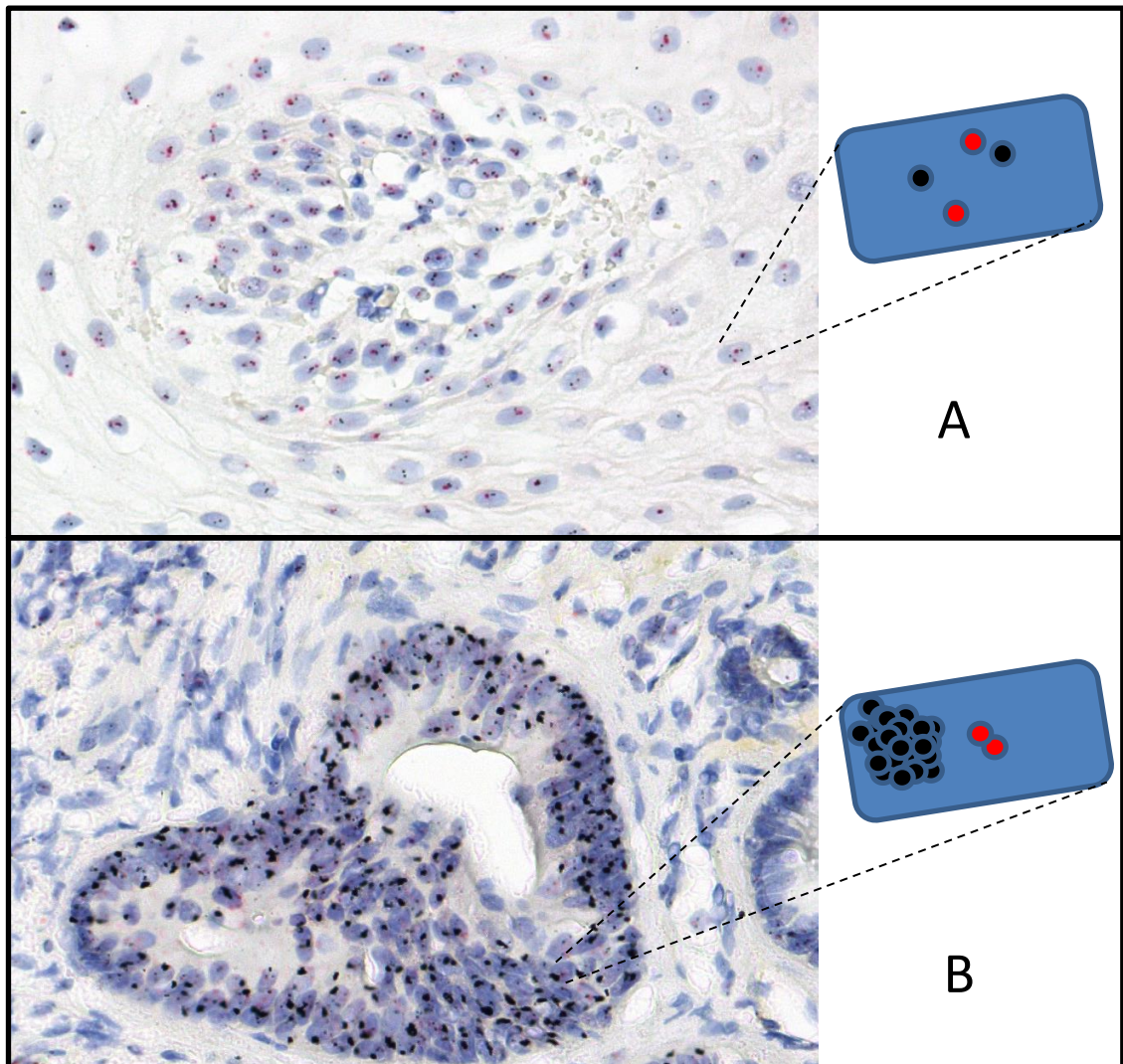
### **5.2.3. *In situ hybridisation***

HER2 gene amplification status was evaluated in comparison to chromosome enumeration probe 17 (CEP17) using either fluorescent- (PathVysion, Abbott Molecular) or dual-colour, dual-hapten (DDISH, Ventana HER2 Dual ISH DNA probe cocktail) in situ hybridization. For each probe, 20-40 cells were microscopically evaluated and the HER2:CEP17 gene ratio calculated. Cases were reported as non-amplified ( $\leq 1.80$ ), borderline non-amplified (1.81-1.99), borderline amplified positive (2.00-2.19) or amplified positive ( $\geq 2.20$ ). For borderline cases, a second review with 20-40 additional cells was performed. The final report was then compiled with a



definitive HER2:CEP17 ratio defined as  $\geq 2.00$ <sup>311</sup>. The updated 2013 College of American Pathologists / American Society of Clinical Oncology (CAP/ASCO) guidelines for HER FISH testing lowered the HER2/CEP17 ratio cut off for HER2 amplification to  $\geq 2.0$  and introduced HER copy number criterion where high mean HER2 gene count ( $\geq 6$ /cell) also defined HER2 gene amplification<sup>312</sup>. HER2 gene counts of  $\geq 4$  but  $< 6$  were categorised as equivocal. Tumours with  $\geq 3$  CEP17 signals (chromosome 17 polysomy) were likely to be impacted by this ratio driven criteria, making it more likely for them to be classified as HER2 equivocal. The frequency of high HER2 gene count ( $\geq 6$ /cell) and CEP17 polysomy ( $\geq 3$  gene signals) and its impact on clinicopathological variables and outcomes will be evaluated.

**Figure 39: Dual-silver in-situ hybridisation (DDISH) schematic showing HER2 and CEP17 gene copy numbers in normal squamous oesophagus (A) and a HER2 amplified oesophageal tumour (B).**



*Dual-silver in-situ hybridisation (DDISH) schematic showing (A) comparative HER2 (black dots) and chromosome enumeration probe 17 (CEP17) (red dots) gene copy numbers in normal squamous oesophageal tissue. (B) An abnormal ratio of HER2/CEP17 in a HER2 amplified oesophageal tumour defined as having borderline (2+ immunohistochemical) HER2 protein expression.*

#### **5.2.4. Clinicopathological detail**

For the full patient cohort, where available, anonymised data for age (grouped as <40, 40-59, 60-79, ≥80), sex, Lauren tumour type (intestinal, diffuse or mixed)<sup>313</sup>, tumour

grade and anatomical tumour location were collected. For the 199 local cases, additional information was collected including vascular invasion, perineural invasion, lymphatic infiltration, associated Krukenburg tumour and any evidence of linitis plastica on imaging or at the time of resection. Background pathology was recorded if present including evidence of dysplasia, Barrett's oesophagus, gastric intestinal metaplasia, atrophic gastritis, chronic active gastritis or background inflammation inferred by the presence of lymphocytes, plasma cells, histiocytes, and granulocytes within the lamina propria.

Endpoints for survival analysis included overall survival (OS) and PFS. OS was defined as the time between pathological confirmation of OA or GC and death from any cause and censored at the date of last recorded clinical contact. PFS was defined as the time between initiation of treatment and cancer progression or death from any cause.

#### **5.2.5. Statistics**

The Student's t-test was used to compare mean age between groups.

Clinicopathological relationships were evaluated with  $\chi^2$  and Fisher exact tests.

Multivariate analysis was then performed following binary logistic regression to assign an odds ratio (OR) to predict HER2 positivity.

PFS and OS are expressed as medians, standard error (SE) and confidence intervals (CI). Survival rates were analysed with Kaplan-Meier curves and differences compared using the log rank (Mantel-Cox) test. A multivariate analysis for variables reaching significance was performed with Cox proportional hazard model. A scatterplot of the association between CEP17 copy number and survival was examined and  $R^2$  correlation coefficient of the line of best fit assigned.

All p values were 2-sided and  $<0.1$  was taken as evidence of potential predictive value as has previously been reported<sup>314</sup>. All statistical analyses were performed using IBM® SPSS® statistics Version 22 (IBM Corporation) and the study was carried out in accordance with REMARK (REporting recoMmendAtions for tumour maRKer)

guidelines. The REMARK guidelines for reporting tumour marker studies was a major recommendation of the National Cancer Institute-European Organisation for Research and Treatment of Cancer (NCI-EORTC) First International Meeting on Cancer Diagnostics in 2000. They suggest studies on tumour markers should provide relevant information about study design, hypotheses, patient and specimen characteristics, assay methods and statistical analysis methods. The goal was to encourage transparent reporting so relevant material is available for others to judge the usefulness of the data and understand the context of any conclusions drawn<sup>315</sup>.

### 5.3. Results

#### 5.3.1. Analysis of HER2 protein expression and amplification

Of the 1029 patients in the parent cohort, 232 (22.5%) were HER2 positive and would subsequently have been eligible for HER2 therapy in Europe. 663 (64.4%) patients scored negative (0 or 1+), 134 (15.8%) were equivocal (2+) and 203 (19.7%) positive (3+). 29 (17.8%) of the equivocal IHC cases were subsequently shown to be HER2 positive.

Concordance between non-equivocal IHC and ISH results in the 287 cases evaluated with both methods was 97.6%, 2 were negative with IHC but displayed HER2 amplification, while 1 showed HER2 overexpression (IHC 3+) but no HER2 gene amplification. 41 (14.3%) cases were HER2 gene amplified and 246 (85.7%) were considered gene amplification negative. HER2 protein overexpression was demonstrated in 40 cases (13.9%) (Table 18).

**Table 18: Relationship between HER2 expression and gene amplification**

IHC status	HER2 negative		HER2 positive		Total		ISH negative		ISH positive		Total	
	n	%	n	%	n	%	n	%	n	%	n	%
Negative (0/1+)	663		0		663	64.4%	111		2		113	39.4%
Equivocal (2+)	134		29		163	15.8%	134		29		163	56.8%
Overexpression (3+)	0		203		203	19.7%	1		10		11	3.8%
<b>Total</b>	<b>797</b>	<b>77.5%</b>	<b>232</b>	<b>22.5%</b>	<b>1029</b>		<b>246</b>	<b>85.7%</b>	<b>41</b>	<b>14.3%</b>	<b>287</b>	

High HER2 gene copy number ( $\geq 6$  /cell), which would define the case as HER2 gene amplified irrespective of IHC status, [32] was noted in 29 cases (10.6% total group). When high HER2 gene copy number was stratified by IHC status, 1 case (0.01%) scored negative, 18 cases were equivocal (IHC 2+) (11.04%) and 10 scored positive (IHC 3+) (90.9%). When compared with final HER2 status, 5 cases were subsequently classified as HER2 negative, 80% (4/5) of which were due to CEP17 polysomy (mean CEP17 copy number  $\geq 3$ ). CEP17 polysomy [32] was noted in 39 cases (14.3% group tested with IHC and ISH). Of these, 13 cases (33.3%) showed high HER2 amplification, 4 of which (30.8%) were subsequently classified as HER2 negative (1.5% of cases tested with IHC and ISH).

### ***5.3.2. Clinicopathological relationships with HER2 expression***

There was no difference in the age at which HER2 positive and HER2 negative tumours ( $64.9 \pm 13.7$  years' vs  $62.3 \pm 13.2$  years) present ( $p=0.66$ ). Patients age, gender and tumour location were not associated with HER2 status. Tumours of intestinal type and well/moderate grade were both associated with HER2 positivity ( $p < 0.001$ ). These variables remained significant on multivariate analysis with tumours of intestinal and mixed type being 3.7 ( $p < 0.001$ ) and 2.1-fold ( $p=0.076$ ) more associated with HER2 positivity than those of diffuse type. Moderately differentiated tumours were more frequently associated with HER2 positivity (1.7-fold,  $p=0.048$ ) than those with poor differentiation (Table 19).

**Table 19: HER2 expression association with clinicopathological variables**

		n	% group	HER2 -ve %	HER2 +ve %	UV p	MV -p	OR
<b><u>Parent cohort</u></b>		1029		77.5%	22.5%			
Age		516	64.6±13.4	62.3±13.2	64.9±13.7	*0.66		
	<40	23	4.5%	78.3%	21.7%	^0.776		
	40-60	142	27.5%	82.4%	17.6%			
	60-80	301	58.3%	79.4%	20.6%			
	>80	50	9.7%	76.0%	24.0%			
Gender	Female	133	28.2%	79.7%	20.3%	"0.795		
	Male	339	71.8%	81.1%	18.9%			
Tumour type	Intestinal	383	57.2%	71.3%	28.7%	^<0.001	<0.001	3.741
	Mixed	100	14.9%	87.0%	13.0%		0.076	2.117
	Diffuse	186	27.8%	90.9%	9.1%			
Tumour grade	Moderate	186	25.2%	67.7%	32.3%	"<0.001	0.048	1.652
	Poor	553	74.8%	83.7%	16.3%			
Tumour origin	Oesophagus	83	32.8%	78.3%	21.7%	"0.385		
	Stomach	170	67.2%	83.5%	16.5%			
Tumour stage	T1	28	18.1%	96.4%	3.6%	^0.165		
	T2	27	17.4%	85.2%	14.8%			
	T3	74	47.7%	83.8%	16.2%			
	T4	26	16.8%	96.2%	3.8%			
Nodal stage	N0	39	26.5%	84.6%	15.4%	^0.124		
	N1	41	27.9%	87.8%	12.2%			
	N2	33	22.4%	90.9%	9.1%			
	N3a	24	16.3%	100.0%	0.0%			
	N3b	10	6.8%	70.0%	30.0%			
Metastatic stage	M0	81	61.4%	88.9%	11.1%	"0.785		
	M1	51	38.6%	86.3%	13.7%			
Vascular stage	No	35	43.8%	91.4%	8.6%	"0.724		
	Yes	45	56.3%	86.7%	13.3%			
Lymphatic infiltration	No	33	29.7%	84.8%	15.2%	"0.336		
	Yes	78	70.3%	91.0%	9.0%			
Perineural invasion	No	46	66.7%	84.8%	15.2%	"0.707		
	Yes	23	33.3%	91.3%	8.7%			
Dysplasia	No	65	61.3%	92.3%	7.7%	"0.07	0.006	4.966
	Yes	41	38.7%	70.7%	29.3%			
Inflammation	No	44	35.8%	89.6%	11.4%	"0.582		
	Yes	66	53.7%	87.9%	12.1%			
<b><u>Organ specific variables</u></b>								
Barrett's epithelium	No	73	81.1%	90.4%	9.6%	"0.209		
	Yes	17	18.9%	76.5%	23.5%			
Linitis plastica	No	153	94.4%	87.6%	12.4%	"1.0		
	Yes	9	5.6%	88.9%	11.1%			
Gastric intestinal metaplasia	No	43	41.0%	88.4%	11.6%	"0.737		
	Yes	62	59.0%	91.9%	8.1%			
Atrophic gastritis	No	103	92.8%	88.3%	11.7%	"0.595		
	Yes	8	7.2%	100.0%	0.0%			
Chronic active gastritis	No	52	44.1%	90.4%	9.6%	"1.0		
	Yes	66	55.9%	89.4%	10.6%			

\*Student's t test; ^χ2 test; "Fishers exact; ∩ logistic regression; UV: univariate; MV: multivariate; OR: Odds ratio.

Further analysis of clinicopathological relationships in local cases did not identify a relationship between HER2 status and TNM stage, linitis plastica, lymphatic infiltration, vascular infiltration, perineural invasion, gastric intestinal metaplasia, atrophic gastritis, chronic active gastritis or background inflammation ( $p>0.1$ ). Background dysplasia ( $p=0.07$ ) was associated with HER2 status. Staining in background dysplasia and tumour was concordant and its presence was independently associated with an increased likelihood of HER2 positivity on multivariate logistic regression ( $p=0.006$ ; OR=4.966).

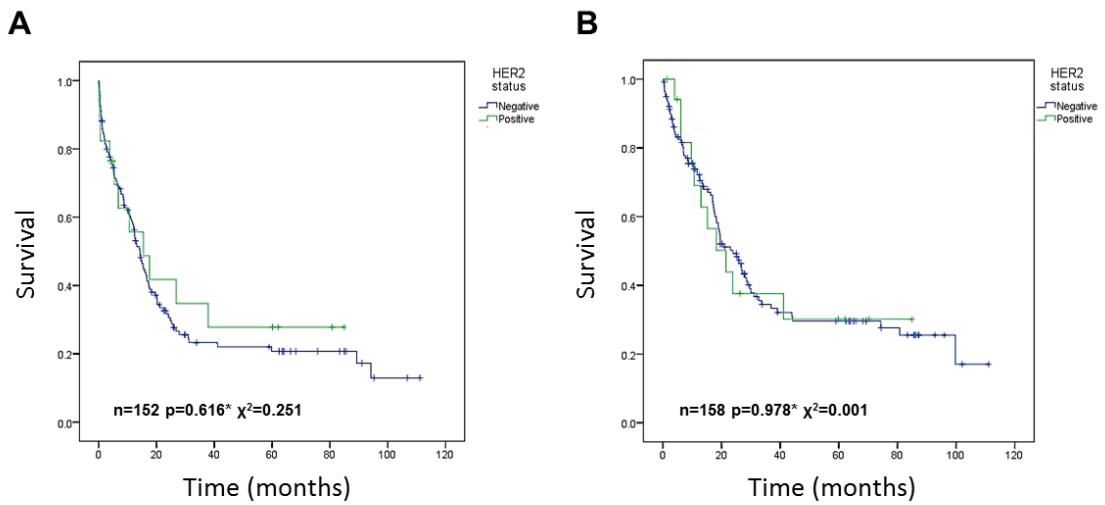
### **5.3.3. HER2 diagnostics and HER2 status relationships with survival**

PFS data was available from 166 patients and OS data from 172 patients. The median time from initiation of treatment to progression was 14.1 months (range: 0.07 – 111.1) and to death 21.5 months (range 0.03 – 111.1). At 1, 5 and 9 years, PFS was 56%, 21.9% and 13.7%, while OS was 70.9%, 28.9% and 16.8% (Table 20). HER2 status did not influence PFS ( $p=0.616$ ) or OS ( $p=0.978$ ) (Figure 40).

**Table 20: Oesophagogastric cancer survival over time**

<b>Years</b>	<b>1</b>	<b>5</b>	<b>9</b>
<b>Progression free survival</b>	56.0%	21.9%	13.7%
<b>Overall survival</b>	70.9%	28.9%	16.8%

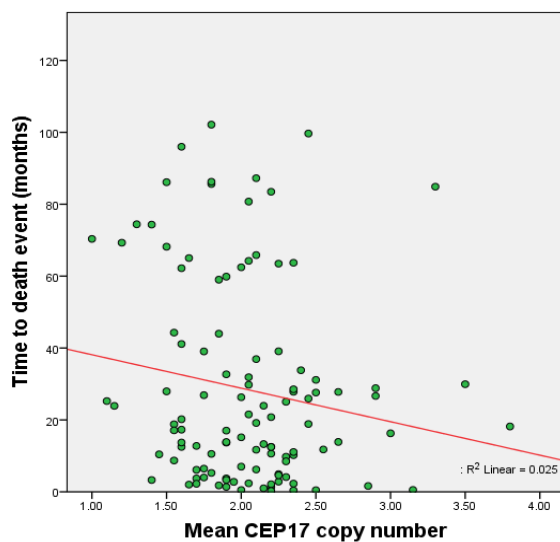
**Figure 40: Progression free survival (A) and overall survival (B) of oesophagogastric cancer Kaplan Meir curves stratified by HER2 status.**



\* Log rank .Mantel Cox.

When evaluating HER2 diagnostic parameters, CEP17 mean copy number was found to influence OS ( $p=0.088$ ; HR=1.492) but not PFS ( $p=0.502$ ). Increasing mean CEP17 copy number negatively correlated with OS ( $R^2=0.025$ ) (Figure 41).

**Figure 41: Scatterplot correlating CEP17 copy number and overall survival.**





No association between PFS or OS was seen with IHC score, ISH status, HER2:CEP17 ratio stratified by borderline ranges, CEP 17 polysomy ( $\geq 3$ ), high HER2 copy number ( $\geq 6$ ), actual HER2:CEP17 ratio or mean HER2 copy number (Table 21).

**Table 21: HER2 diagnostic variables in relation to progression free and overall survival of oesophagogastric cancer.**

		Progression free survival					Overall survival					
		n	Median	SE	CI	*p	n	Median	SE	CI	*p	HR
Cases with IHC and ISH		166	14.10	1.22	11.71 - 16.49		172	21.53	2.81	16.02 - 27.04		
HER2 status	Negative	135	14.23	1.26	11.77 - 16.69	0.616	140	23.93	3.15	17.76 - 30.11	0.978	
	Positive	17	15.45	6.51	2.69 - 28.21		18	21.53	6.31	9.17 - 33.89		
IHC status	negative (0/1+)	133	14.23	1.24	11.79 - 16.67	0.582	138	25.08	3.19	18.83 - 31.33	0.947	
	equivocal (2+)	8	17.62	7.59	2.74 - 32.50		8	18.18	6.69	5.06 - 31.30		
	overexpression (3+)	11	15.45	11.84	0.00 - 38.65		12	21.53	.	.	- .	
ISH status	Negative	92	15.45	2.32	10.90 - 20.00	0.34	97	27.94	3.97	20.16 - 35.73	0.867	
	Positive	15	26.86	17.62	0.00 - 61.40		16	41.12	19.93	2.07 - 80.18		
ISH HER2:CEP17 ratio	$\leq 1.80$	90	15.45	2.29	10.96 - 19.94	0.348	95	28.53	2.83	22.99 - 34.08	0.891	
	1.81-1.99	1	0.46	.	.	- .	1	0.46	.	.	- .	
	2.0-2.19	1	1.15	.	.	- .	1	1.61	.	.	- .	
	$>2.20$	14	37.97	17.02	4.61 - 71.33		15	41.12	19.46	2.97 - 79.27		
CEP17 polysomy	No	100	15.94	2.48	11.08 - 20.80	0.639	106	28.53	3.80	21.08 - 35.98	0.502	
	Yes	5	17.62	5.65	6.54 - 28.70		5	18.18	2.09	14.09 - 22.27		
HER2 amplification $\geq 6$	No	96	15.42	2.26	10.98 - 19.86	0.224	101	26.89	2.87	21.26 - 32.52	0.412	
	Yes	10	26.86	16.09	0.00 - 58.39		11	41.12	.	.	- .	
ISH counts	Mean CEP17 copy number	105				-	0.502	111			-	<b>0.089 1.492</b>
	Mean HER2 copy number	105				-	0.935	111			-	0.556

\* Log rank Mantel Cox; Abbreviations: SE: standard error; HR: hazard ratio; ISH: In situ hybridisation; IHC: Immunohistochemistry; CEP17: Chromosome enumeration probe

#### **5.3.4. Clinicopathological relationships with survival**

On univariate analysis PFS was significantly associated with age ( $p < 0.001$ ), gender ( $p = 0.095$ ), tumour type ( $p = 0.015$ ), tumour grade ( $p = 0.012$ ), T stage ( $p < 0.001$ ), M stage ( $p < 0.001$ ), linitis plastica ( $p = 0.006$ ), lymphatic ( $p < 0.001$ ), vascular ( $p < 0.001$ ) and perineural infiltration ( $p = 0.045$ ), background Barrett's epithelium ( $p = 0.027$ ), chronic active gastritis ( $p = 0.017$ ) and inflammation ( $p = 0.004$ ). Tumour origin, background dysplasia and gastric intestinal metaplasia did not influence PFS. Multivariable analysis of the significant associations on univariate analysis, found T stage ( $p < 0.001$ ; HR=3.238) and lymphatic infiltration ( $p = 0.012$ ; HR=5.108) have a detrimental effect on PFS, while perineural invasion ( $p = 0.009$ ; HR=0.192) and inflammation ( $p = 0.006$ ; HR=0.185) appeared protective.

OS was significantly associated with age ( $p = 0.001$ ), tumour grade ( $p = 0.041$ ), T stage ( $p < 0.001$ ), M stage ( $p < 0.001$ ), linitis plastica ( $p = 0.002$ ), lymphatic ( $p < 0.001$ ), vascular ( $p < 0.001$ ) and perineural invasion (0.059) and background Barrett's epithelium (0.023) on univariate analysis. Gender, tumour type, tumour origin, background dysplasia, inflammation, gastric intestinal metaplasia and chronic active gastritis did not influence OS. Multivariable analysis of the significant associations found increasing age ( $p = 0.002$ ; HR=2.737), advancing T stage ( $p < 0.001$ ; HR=3.278) and lymphatic invasion ( $p = 0.015$ ; HR=3.918) to independently influence OS (Table 22).

**Table 22: Clinicopathological variables relation to progression free and overall survival of esophagogastric cancer when stratified by HER2 status.**

Variable	Progression free survival						Overall survival					
	n	UV χ <sup>2</sup>	*p	HR	MV CI	^p	n	UV χ <sup>2</sup>	*p	HR	MV CI	^p
<i>Common variables</i>												
Age: <40 vs 40-60 vs 60-80 vs >80	152	18.701	<0.001				158	15.804	0.001	2.787 (1.452 - 5.351)		0.002
Gender: male vs female	152	2.788	0.095				158	.	0.808			
Tumour type: intestinal vs mixed vs diffuse	146	8.416	0.015				152	.	0.11			
Tumour grade: moderate vs poor	151	6.293	0.012				157	4.156	0.041			
Tumour origin: esophagus vs stomach	152	.	0.674				158	.	0.973			
Tumour stage: T1 vs T2 vs T3 vs T4	151	42.681	<0.001	3.238 (1.704 - 6.15)		<0.001	155	36.673	<0.001	3.185 (1.6 - 6.339)		0.001
Metastatic stage: M0 vs M1	129	71.599	<0.001				147	50.034	<0.001			
Vascular invasion: yes vs none	78	12.289	<0.001				80	12.576	<0.001			
Lymphatic invasion: yes vs none	109	22.189	<0.001	5.108 (1.434 - 18.197)		0.012	111	16.736	<0.001	4.847 (1.435 - 16.375)		0.011
Perineural invasion: yes vs none	68	4.013	0.045	0.192 (0.056 - 0.66)		0.009	69	3.556	0.059			
Background dysplasia: yes vs none	78	.	0.906				89	.	0.69			
Inflammation: yes vs none	118	8.327	0.004	0.185 (0.056 - 0.611)		0.006	123	.	0.14			
<i>Organ specific variables</i>												
Barrett's epithelium	86	4.877	0.027				88	5.17	0.023			
Linitis plastica	152	7.437	0.006				158	9.802	0.002			
Gastric intestinal metaplasia	100	.	0.787				105	.	0.948			
Chronic active gastritis	113	5.688	0.017				118	.	0.247			

\* Log rank Mantel Cox, ^ Cox proportional hazards regression. Abbreviations: UV: univariate analysis; MV: multivariate analysis; HR: hazard ratio.

### 5.3.5. Clinicopathological relationships with survival when stratified by HER2 status

Relationships between clinicopathological variables and survival when stratified by HER2 status were analysed to identify significant individual associations. Multivariable analysis of these individual significant relationships with survival when stratified by HER2 status found tumour stage (p<0.001), lymphatic infiltration (p=0.012), perineural invasion (p=0.009) and inflammation (p=0.006) remained significantly associated with PFS, while tumour stage (p=0.001), lymphatic infiltration (p=0.011) and age (p=0.002) remained associated with OS (Table 23).

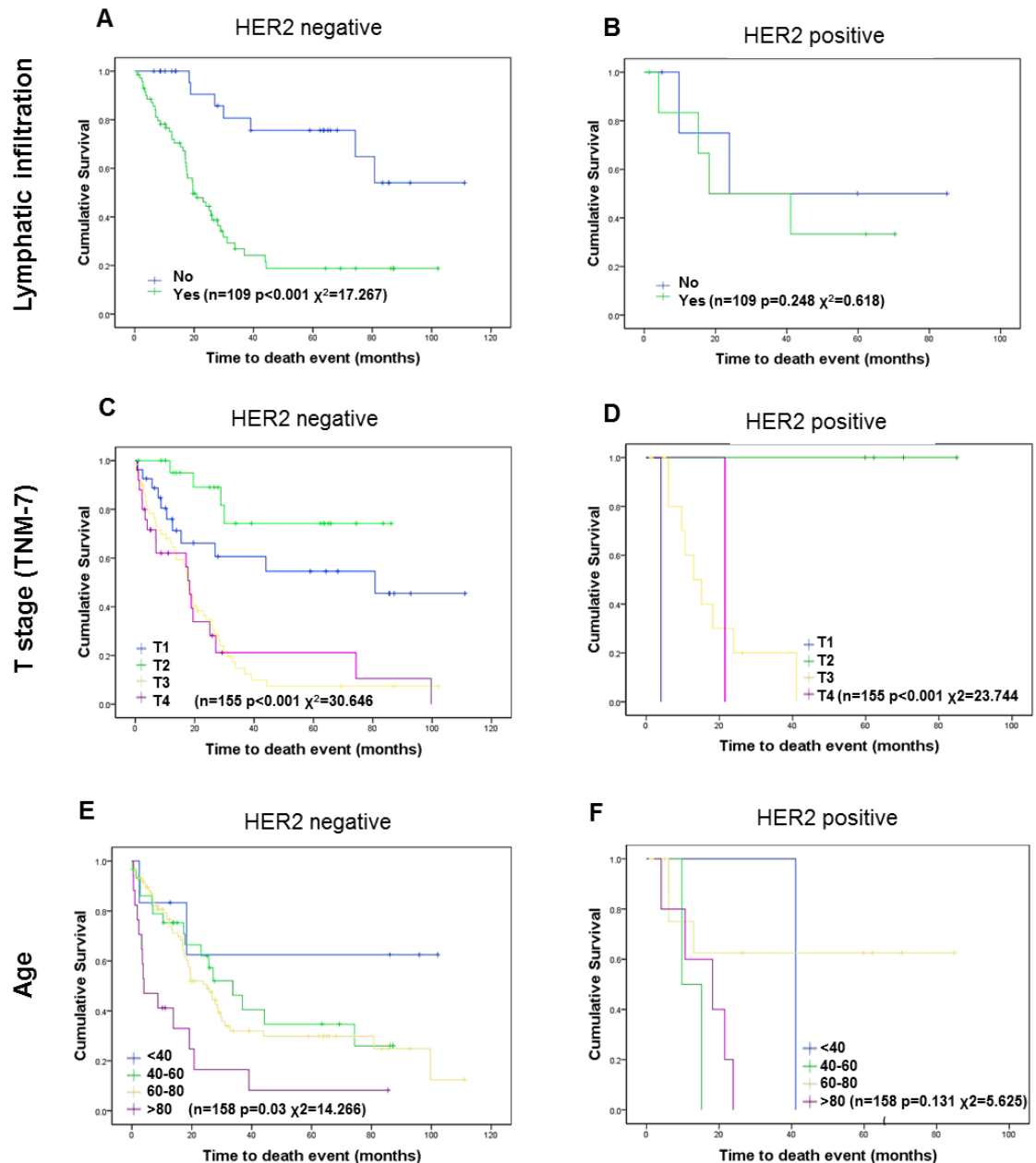
**Table 23: Clinicopathological variables influence on PFS and OS of esophagogastric cancer when stratified by HER2 status.**

	Progression free survival											Overall survival																		
	HER2 negative			HER2 positive			UV		MV			HER2 negative			HER2 positive			UV		MV										
	Mean	SE	CI	Mean	SE	CI	$\chi^2$	p	HR	p	SE	CI	Mean	SE	CI	Mean	SE	CI	Upper	$\chi^2$	p	HR	p	SE	CI					
<b>Esophagogastric variables</b>																														
<b>Age</b>																														
<40	28.158	17.576	0	62.606	37.97	0	37.97	37.97	18.701	<0.001			68.057	19.293	248105.866	41.124	0.41	1.244	1.2415	8.04	0.001	2.787	0.002	0.333	1.452	5.351				
40-60	28.096	6.757	14.852	41.341	11.125	4.325	2.648	19.602					42.112	6.924	28.541	55.683	12.459	2.695	7.176	17.742										
60-80	36.379	5.111	26.362	46.395	48.623	13.184	22.782	74.464					42.289	5.044	32.402	52.176	56.196	13.11	30.581	8.892										
>80	7.493	2.48	2.633	12.353	7.884	4.159	0	16.036					16.413	6.244	4.175	28.651	15.647	3.673	8.448	22.846										
<b>Gender</b>																														
Female	21.29	5.456	10.596	31.984	19.564	7.765	4.344	34.785	2.788	0.095			41.82	7.377	27.36	56.279	23.706	7.024	9.939	37.473			0.808							
Male	33.456	4.397	24.837	42.075	40.293	13.096	14.625	65.961					41.686	4.732	32.41	50.961	44.766	12.053	21.142	68.389										
<b>Tumour type</b>																														
Intestinal	40.167	5.605	29.182	51.153	34.806	11.169	12.915	56.697	8.416	0.015			48.422	5.821	37.013	59.832	40.434	10.234	20.374	60.493			0.11							
Mixed	19.635	7.712	4.52	34.751	19.165	18.805	0	56.023					30.451	9.112	6.16	48.286	22.567	18.557		0.58	9.38									
Diffuse	18.889	3.959	11.129	26.648	36.395	18.247	0.631	72.159					38.202	7.125	24.238	52.167	37.591	17.399		3.488	71.691									
<b>Tumour grade</b>																														
Moderate	46.073	8.12	30.159	61.988	36.429	15.113	6.808	66.051	6.293	0.012			49.981	7.004	36.253	63.709	48.674	14.902	19.466	77.881			4.156	0.041						
Poor	26.177	3.935	18.465	33.889	24.57	7.633	9.61	39.53					38.252	4.545	29.343	47.161	25.644	6.571	12.766	38.522										
<b>Tumour origin</b>																														
Oesophagus	24.338	5.584	13.393	35.282	19.593	9.639	0.701	38.486	0.178	0.674			44.945	7.949	29.366	60.524	21.564	7.466	6.932	36.197			0.973							
Stomach	33.853	4.531	24.973	42.733	33.853	10.63	13.018	54.687					41.887	4.707	32.662	51.112	42.299	10.467	21.785	62.813										
<b>Tumour stage</b>																														
T1										42.681	<0.001	3.238	<0.001	0.327	1.704	6.15								36.673	<0.0001	3.185	0.001	0.351	1.6	6.339
T2																														
T3																														
T4																														
<b>Nodal stage</b>																														
N0	75.488	9.558	56.754	94.223	40.627	16.824	7.651	73.603					75.685	8.436	59.15	92.22	41.06	16.02	9.66	72.46										
N1	31.004	6.396	18.468	43.54	29.002	9.246	10.881	47.123					39.797	7.123	25.836	53.758	35.43	10.15	15.54	55.32										
N2	20.564	5.107	10.553	30.574	54.087	21.811	11.336	96.837					31.719	7.251	17.507	45.931	33.45	15.64	2.81	64.10										
N3a	8.654	1.579	5.558	11.749									14.448	2.098	10.337	18.56														
N3b	7.109	3.193	0.851	13.367	7.975	2.615	2.85	13.1					9.946	3.49	3.106	16.786	9.53	3.45	2.77	16.30										
<b>Metastatic stage</b>																														
M0	50.752	6.089	38.817	62.687	49.085	14.675	20.321	77.849	71.599	<0.001			58.072	5.896	46.515	69.629	10.978	1.716	7.615	14.342	50.034	<0.0001								
M1	6.084	1	4.123	8.045	12.221	5.506	1.43	23.013					45.947	12.827	20.807	71.087	17.437	6.31	5.069	29.804										
<b>Vascular invasion</b>																														
No										12.289	<0.001													12.576	<0.0001					
Yes																														
<b>Lymphatic invasion</b>																														
No	83.575	9.57	64.818	102.333	58.853	21.251	17.202	100.505	212.189	<0.001	5.108	0.012	0.648	1.434	18.2	83.282	8.354	66.907	99.657	50.854	17.194	17.153	84.555	16.736	<0.0001	4.847	0.011	0.621	1.435	16.375
Yes	25.146	4.007	17.293	33.388	33.33	12.91	13.53	64.137					34.455	4.775	25.096	43.814	36.527	10.749	15.459	57.596										
<b>Perineural invasion</b>																														
No	63.05	8.027	47.316	78.784	53.364	15.105	23.758	82.97	4.013	0.045	0.192	0.009	0.629	0.056	0.66	70.323	7.588	55.451	85.195	47.797	12.409	23.476	72.118	3.556	0.059					
Yes	28.28	5.112	18.26	38.299	61.425	16.585	28.918	93.932					37.664	8.474	21.054	54.274	63.001	15.469	32.681	93.321										
<b>Dysplasia</b>																														
No	42.334	6.618	29.363	55.305	37.358	10.115	17.532	57.184	0.014	0.906			51.021	6.645	37.996	64.046	38.691	9.733	19.614	57.768			0.69							
Yes	31.974	7.171	17.919	46.029	21.155	5.705	9.973	32.337					39.311	8.884	21.898	56.723	21.783	2.765	16.364	27.203										
<b>Inflammation</b>																														
No	17.056	3.475	10.245	23.866	68.654	14.513	40.209	97.099	8.327	0.004	0.185	0.006	0.61	0.056	0.611	37.735	7.122	23.777	51.694	51.068	17.067	17.616	84.52	0.14						
Yes	46.816	6.43	34.213	59.419	32.729	7.822	17.397	48.06					52.159	6.084	40.235	64.083	37.683	8.351	21.315	54.051										
<b>Organ specific variables</b>																														
<b>Esophageal</b>																														
<b>Barrett's epithelium</b>																														
No	45.237	6.124	33.235	57.239	35.608	8.579	18.793	52.424	4.877	0.027			52.684	6.071	40.786	64.582	41.438	8.858	24.075	58.8	5.17	0.023								
Yes	13.02	3.96	5.259	20.782	15.45	0	15.45	15.45					24.672	8.238	8.526	40.818	19.526	4.372	10.957	28.095										
<b>Gastric</b>																														
<b>Limtis plastica</b>																														
No	32.608	3.892	24.981	40.235	34.021	9.303	15.787	52.255	7.437	0.006			43.715	4.218	35.448	51.983	38.293	8.704	21.234	55.353	9.802	0.002								
Yes	6.691	2.373	2.041	11.341	10.59	0	10.59	10.59					9.895	3.106	3.807	15.984	12.984		0.12	9.84	12.984									
<b>Gastric intestinal metaplasia</b>																														
No	38.777	8.039	23.021	54.533	36.055	15.352	5.965	66.145	0.073	0.787			52.218	8.303	35.943	68.492	38.714	46.610	34.767	67.052			0.948							
Yes	39.628	6.288	27.303	51.953	39.515	11.884	16.223	62.807					41.715	5.494	30.947	52.483	44.049	10.138	24.179	63.919										
<b>Atrophic gastritis</b>																														
No	32.276	4.179	24.085	40.467	41.175	10.91	19.791	62.559					44.08	4.831	34.61	53.549	67.653	15.62	37.037	98.269										
Yes	81.616	17.625	47.07	116.161	41.175	10.91	19.791	62.559					44.731	10.445	24.259	65.203	44.731	10.445	24.259	65.203										
<b>Chronic active gastritis</b>																														
No	20.555	4.205	12.313	28.798	61.737	18.896	24.7	98.774	5.688	0.017			40.772	6.825	27.394	54.15	52.202	16.411	20.037	84.367			0.247							
Yes	46.67	6.675	33.587	59.752	35.608	8.579	18.793	52.424					52.272	6.478	39.574	64.969	41.438	8.858	24.075	58.8										

Abbreviations: SE: standard error; CI: confidence interval; UV: univariate analysis with log rank (Mantel Cox); MV: multivariate analysis with Cox proportional hazards regression; HR: hazard ratio.

To identify how HER2 status influenced these independent relationships, Kaplan Meir survival curves were plotted to examine their association in HER2 negative and positive patients separately (Figure 42).

**Figure 42: Influence of lymphatic infiltration (A & B), tumour stage (C&D) and age (E & F) on overall survival when stratified by HER2 status.**



Compared with Log-rank Mantel Cox.

In HER2 negative patients, survival curves found PFS was detrimentally associated with increasing T stage ( $p<0.001$ ;  $\chi^2=35.894$ ), lymphatic infiltration ( $p<0.001$ ;  $\chi^2=21.815$ ) and perineural invasion ( $p=0.035$ ;  $\chi^2=4.455$ ). While OS was worse with increasing age ( $p=0.003$ ;  $\chi^2=14.27$ ), T stage ( $p<0.001$ ;  $\chi^2=30.646$ ) and lymphatic infiltration ( $p<0.001$ ;  $\chi^2=17.267$ ). Inflammation was associated with improved PFS ( $p=0.001$ ;  $\chi^2=10.458$ ). In HER2 positive patients, only increasing T stage significantly influenced PFS ( $p<0.001$ ;  $\chi^2=31.59$ ) and OS ( $p<0.001$ ;  $\chi^2=23.744$ ). Lymphatic infiltration, perineural invasion and inflammation were not associated with PFS. Age and lymphatic infiltration did not influence OS (Figure 42, Table 24).

**Table 24: Clinicopathological variables associated with progression free and overall survival and influence on HER2 positive and negative oesophagogastric cancer.**

	Clinicopathological variables	n	HER2 -ve		HER2 +ve	
			$\chi^2$	$\wedge p$	$\chi^2$	$\wedge p$
	influencing survival on MV analysis*					
PFS	Tumour stage: advanced vs local	151	<b>35.894</b>	<b>&lt;0.001</b>	<b>31.587</b>	<b>&lt;0.001</b>
	Lymphatic invasion: yes vs none	109	<b>21.815</b>	<b>&lt;0.001</b>	0.627	0.428
	Perineural invasion: yes vs none	68	<b>4.455</b>	<b>0.035</b>	0.001	0.981
	Inflammation: yes vs none	118	<b>10.458</b>	<b>0.001</b>	0.649	0.42
OS	Tumour stage: advanced vs local	155	<b>30.646</b>	<b>&lt;0.001</b>	<b>23.744</b>	<b>&lt;0.001</b>
	Lymphatic invasion: yes vs none	111	<b>17.267</b>	<b>&lt;0.001</b>	0.248	0.618
	Age: older vs younger	158	<b>14.266</b>	<b>0.003</b>	5.625	0.131

$\wedge$  Log rank Mantel Cox analysis of HER2 subgroups influenced by clinicopathological variables. \* Cox proportional hazards regression analysis of independently predictive

*clinicopathological variables affecting OS (overall survival) or PFS (progression free survival) from Table 23. MV: multivariate analysis.*

**Table 25: Study compliance with REMARK guidelines**

Introduction and objectives`	HER2 was the biomarker evaluated. To determine if HER2 is associated with clinicopathological variables and survival and how clinicopathological variables influence prognosis when stratified by HER2 receptor status Hypotheses; HER2 positivity is associated with a negative prognosis in subgroups of esophagogastric patients
Patients	All patients with esophagogastric adenocarcinoma referred for HER2 testing to a reference laboratory in UCL.
Specimen characteristics	Formalin fixed paraffin-embedded tissue from biopsies or resection specimens
Assay method	Standard IHC and FISH/DDISH scored according to gastric cancer guidelines <sup>28</sup> . Standard positive/amplified and negative/non-amplified controls were used with each run.
Study design	Retrospective analysis of clinicopathological variables and outcomes from patients evaluated prospectively for HER2 expression in a clinical diagnostics unit. Clinical end-points of progression free survival (PFS) and overall survival (OS) used Sample size determined by the availability of tissue from 1029 patients; with the observed number of deaths power to detect interaction effects (ratio of treatment HRs) was ~80% for 0.5 and ~70% for 0.5 as has been previously reported.
Statistical methods	Associations between clinicopathological variables and HER2 expression were assessed according to published guidelines Association with age was evaluated with Students t test. Age sub-groups, tumor type, tumor stage and nodal stage were analyzed with Chi squared. Gender, tumor grade, origin, metastatic stage, vascular, lymphatic and perineural involvement, background dysplasia, inflammation, Barrett's, gastric intestinal metaplasia, atrophic gastritis, chronic active gastritis and linitis plastica were assessed using Fisher's exact test. Prognostic value of HER2 diagnostic and clinicopathological variables on PFS and OS directly and when stratified by HER2 status were separately using Kaplan–Meier survival curves compared with the log-rank (Mantel Cox) test. Multivariate Cox proportional hazards regression analysis was undertaken after univariate filtering. The relationship between CEP17 copy number and OS is displayed in a scatterplot and assigned a line of best fit evaluated with R <sup>2</sup> correlation coefficient.
Results Data	1029 patients were evaluated for HER2 status according to published guidelines. Of this cohort, details for age, sex, tumour type, grade and origin were extrapolated where reported. 199 local cases were examined within the main cohort. Additional details for TNM stage, vascular, lymphatic, perineural invasion and background dysplasia, inflammation, Barrett's epithelium, linitis plastica, gastric intestinal metaplasia, atrophic gastritis and chronic active gastritis was recorded where reported. Baseline demographic characteristics and prognostic variables are detailed in Table 2.
Analysis and presentation	Relationship of HER2 with standard prognostic variables is reported in Table 2. Univariate and multivariate analyses results are reported. Kaplan Meier survival curves for effect of HER2 on survival are shown in Figures 1, and the prognostic influence of clinicopathological variables HER2 positive and negative tumors is shown in Figure 3.
Discussion	HER2 infers no prognostic effect in keeping with the majority of studies in the West. When HER2 positive and negative tumors are assessed separately, certain clinicopathological variables were noted to influence survival in each group and are described in Table 4 and have been reported previously. This study is the first to report an association between CEP17 copy number and worse OS. Study limited by sample size, low HER2 positivity rate and the retrospective design.

## 5.4. Discussion

Meta-analyses report wide variations in the rates of HER2 overexpression between 4 - 53% for GC<sup>228</sup> and 7 - 49% for OA<sup>316</sup>. Variation is partly explained by geographical location and sample size, but the most crucial factor is the differing criteria used to define HER2 positivity. Gu *et al* attempted to address this discrepancy in their meta-analysis on studies reporting HER2 expression in GC, filtering only those who used ToGA criteria, and reported expression rates between 9.4% and 20%<sup>224</sup>. Overall, we found the rate of HER2 overexpression in esophagogastric adenocarcinoma in our UK population to be 22.5%, similar to the 23.6% HER2 positivity rate reported in the European population of ToGA<sup>292</sup>.

In the US, 3+ tumours with HER2 IHC or those showing HER2 gene amplification (HER2:CEP17 ratio  $\geq 2$ ) were defined as positive following the ToGA trial criteria. The definition for gastric HER2 positivity however altered during submission to the European Medicines Agency (EMA) to appreciate heterogeneous expression patterns seen in GC<sup>230</sup>. A primary role for IHC was suggested with confirmatory gene amplification reserved for tumours staining 2+, reducing the original population of ToGA approved for therapy by 25% (594 to 446 people)<sup>311</sup>. In our patients where ISH had been performed, an additional 5% of cases (42/487 vs 40/287) would have been offered HER2 therapy if US (ToGA) criteria had been followed<sup>317</sup>.

Studies examining HER2 status using both IHC and ISH report high concordance rates between 87.5% - 95.1%<sup>229,293,318,319</sup>. We found concordance in 89.8% (258/287) of cases. Discordance in many cases is due to CEP17 polysomy or co-amplification masking HER2 amplification. Whether CEP17 polysomy is due to amplification of the entire chromosome 17 or just the centromere detected by CEP17 probes remains uncertain, but it is thought that in breast cancer altering CEP17 probe to a different position may change the CEP17 status due to the region specific nature of probes<sup>320</sup>. If the latter, alternative chromosome 17 probes may clarify expression in borderline



HER2 ISH cases (ratio 1.81-2.19). In all, 2.8% (39/1029) of our parent cohort had CEP17 polysomy compared with 4.1% in the ToGA study<sup>292,311</sup>. Other studies have reported markedly varying CEP17 polysomy rates between 1.1% in a Chinese regional study on 726 patients<sup>297</sup> and 73% in a cohort of 726 patients from the Mayo clinic<sup>321</sup>. When factoring in only those cases in our study where both IHC and ISH was performed, the rate of CEP17 polysomy increased to 13.6% (39/287) which is still well below that seen in the Mayo clinic study. In the presence of CEP17 polysomy, mean HER2 gene copy number  $\geq 6$  has been recommended HER2 positivity is inferred<sup>311</sup>. Prior to these revised criteria, 0.01% (3/287) of patients in our study were reported as HER2 negative (HER2:CEP17 ratio  $< 2.0$ ) despite the HER2 gene being amplified ( $\geq 6$ ). Our rate of discordance is similar Kunz *et al* in their US population who identified 2/122 (0.016%) cases in which this was a diagnostic issue<sup>293</sup>.

We found patients with intestinal tumour type (intestinal and mixed type), moderately differentiated tumours and in our local population background dysplasia to be associated with HER2 overexpression. These relationships with HER2 and intestinal type<sup>293,294,296,297,300,322</sup> and tumour grade have been previously<sup>224,314,318</sup> reported but not the association with background dysplasia.

We did not find PFS or OS to be influenced by HER2 status as has been reported by others. Chua *et al* in their meta-analysis reviewed 6 studies reporting PFS and 35 studies reporting OS with HER2 status. 3 studies reported no difference while 3 studies found PFS to be worse with HER2 overexpression. The synthesised median data identified poorer PFS in patients with HER2 overexpression at 3 years (58% vs 86%)<sup>228</sup>. Of those reporting OS rates, 20 (57%) found HER2 expression to have no influence on OS, 2 (6%) studies reported significantly longer survival and 13 (37%) studies reported OS to be significantly worse with HER2 overexpression. The synthesised median data again illustrated a negative association of HER2 positivity and OS (median survival 21 vs 33 months; 5-year survival 42% vs 52%) in the report.

All laboratories involved in HER2 diagnostics with dual ISH probes compute mean CEP17 counts. This is the first study to analyse the prognostic value of this biological variable to highlight an independent prognostic correlation of increasing CEP17 copy number with worse overall survival in patients with esophagogastric cancers. To understand the role of CEP17 copy number, one must first appreciate the relationships between terms used to describe chromosomal and DNA content abnormalities. Quantitative changes, whether caused by duplication or deletion of either whole chromosomes or parts of chromosomes are referred to as chromosomal instability (CIN). Abnormalities causing a variable number of chromosomes in an organism are a subtype of CIN defined as aneuploidy. Polysomy is a subtype of aneuploidy that defines circumstances where there is at least one additional chromosome copy above the normal two copies. Abnormal chromosomal events whether defined as polysomy, aneuploidy or CIN cause modifications of DNA content in tandem. Changes in the content of DNA are defined as aneuploidy. Authors have used these terms interchangeably in the literature with respect to chromosomal abnormalities where they refer to the same clinical scenario. Chromosome 17 polysomy in HER2 diagnostics may be referred to as chromosome 17 aneuploidy, instability or aneuploidy. Strictly speaking, the latter 2 definitions mirror the clinical scenario most accurately. In HER2 diagnostics, CEP17 amplification precisely defines increased numbers of the centromeric region detected by the ISH probe in use. It is therefore used as a surrogate in clinical practice for chromosome 17 polysomy.

A potential role for CEP17 copy number in the pathogenesis of foregut cancers may be postulated. Studies looking at the evolution of OA identified an accelerating landscape of background losses and gains of whole chromosomes and chromosome arms starting over 2 years prior to the development of cancer<sup>323</sup>. These aberrations cause abnormalities of DNA content (aneuploidy). We examined the relationship between aneuploidy and incremental grades of Barrett's epithelium during progression to OA confirming it to be more prevalent<sup>324</sup> and predictive<sup>179</sup> for cancer progression. The role

of CIN in GC is also clearly recognised<sup>325</sup>. Abnormalities of chromosome 17 such as chromosome 17 aneusomy, HER2 amplification and TP53 loss are reported as co-existing common events in GC<sup>326</sup>. Our identification of a relationship between increasing CEP17 copy number and worse OS is supported by Yoon *et al* who examined HER2 heterogeneity and chromosome 17 copy number aberrations in 676 OA's<sup>321</sup>. CEP17 polysomy was associated with reduced disease-specific survival rates ( $p=0.012$ ) on univariate analysis. This effect did not remain significant on multivariate analysis, but when stratified by HER2 status, CEP17 polysomy was found to independently be associated with worse disease-specific ( $p=0.012$ ) and OS ( $p=0.023$ ) among HER2 non-amplified (negative) cancers. A similar pattern of CEP17 polysomy conferring a more aggressive phenotype in HER2 non-amplified tumours is seen breast cancer. Krishnamurti *et al* found CEP17 polysomy ( $CEP17\geq 3$ ) ( $n=44$ ) in non-amplified tumours to be associated with higher nuclear grade, mitotic activity, Nottingham score, histologic grade, tumour stage, and greater oestrogen receptor negativity when compared to those without amplification or polysomy<sup>327</sup>. Vanden Bempt *et al* did not see a direct association between CEP17 polysomy and aggressive pathological features in primary invasive breast carcinoma patients ( $n=226$ ), however when stratified by HER2 amplification, a trend to worse disease-free survival was observed with CEP17 polysomy in HER2 non-amplified tumours ( $p=0.056$ )<sup>328</sup>.

We found T stage, lymphatic infiltration, perineural invasion and absence of background inflammation to be associated with a worse PFS, while older age, increasing T stage and lymphatic infiltration were associated with better OS on MV analysis. These negative associations continued in the subgroup of patients without HER2 expression, but only advancing T stage independently predicted PFS and OS in HER2 positive patients. He *et al* similarly stratified the prognostic impact of clinicopathological variables on OS according to HER2 expression in their Chinese cohort of 197 patients, but only found tumours with better differentiation to possess significant disadvantage with HER2 overexpression<sup>318</sup>.

The association between background inflammation and improved PFS is of note. Several studies have reported a negative association between systemic inflammation and cancer prognosis when measured on indices such as the Glasgow Prognostic Score (a combination of CRP and albumin)<sup>329,330</sup>. However, inflammation in the tumour containing tissue has been associated with better prognosis. Schumacher *et al* evaluated CD8(+) T cell infiltration in OA specimens to highlight their presence to be associated with better OS in both squamous cell and OA's<sup>331</sup>. More recently Teng *et al* evaluated tumour infiltrating lymphocytes (TILs) before and after neoadjuvant chemoradiotherapy for rectal cancer. CD3(+) and CD8(+) TILs were shown to be associated with favourable therapeutic response to chemoradiotherapy (p=0.033 and p=0.021), better disease free survival (p=0.010 and p=0.022) and OS (p= 0.019 and p=0.003)<sup>332</sup>.

Strengths of our study include a large patient population, with tumours originating from across the country and one of the largest examinations of HER2 expression in OGC in the west to date. We used clinically validated assays and consensus definitions to define HER2 status, minimizing bias and measurement error making the results applicable to other patients in Western countries. The long follow-up time for our local cohort was an additional strength. Limitations include our retrospective design and the variable numbers of patients with each clinicopathological detail recorded. This may have contributed to the loss of significance on multivariate analysis of many variables shown to be predictive on univariate analysis. Our survival data was also extrapolated from a single centre only. External validation in prospective large scale multicentre studies will be needed to confirm our results.

In summary, we report clinicopathological variables of prognostic importance in HER2 positive and negative OGA in the West. We further examined how variables used routinely in gastric HER2 diagnostics may influence prognosis to highlight the negative association between increasing CEP17 copy number and OS of OGA.

**Chapter 6: Development of a HER2 targeting  
photoactive antibody drug conjugate against  
oesophageal adenocarcinoma**

---

## 6.1. Introduction

An estimated 9,000 new cases of oesophageal adenocarcinoma (OA) are diagnosed each year in the UK and the 5-year survival is 15% <sup>289</sup>. The most important precursor for the development of OA is Barrett's epithelium (BE), with the risk increasing as it develops dysplasia <sup>1</sup>. Current treatments for early stage OA and BE that is localised to the mucosal layer include endoscopic resection (EMR) and ablation. These therapies are gastroenterologist directed and despite high quality imaging, small tumours are still hard to detect and can have indistinct edges, this can lead to incomplete removal of the cancer and subsequent recurrence. Over-zealous treatment to reach deeper or suspicious but negative tumour margins can lead to normal tissue damage and oesophageal strictures or perforations <sup>58,333</sup>.

Photodynamic therapy (PDT) is a non-invasive therapeutic treatment ideal for OA and is used, alongside EMR, to treat BE with high grade dysplasia as well as advanced OA to help improve swallowing <sup>139-141</sup>. PDT drugs, known as photosensitisers (PS), accumulate passively in the tumour. Activation occurs via the targeted application of laser light to the tumour area. Cellular destruction occurs *via* multiple reactive oxygen species (ROS) and/or free radical pathways so consequentially resistance is rare <sup>334-336</sup>. PDT can also activate an immune response to cancer, a key step in establishing a prolonged remission <sup>337,338</sup>. The wider acceptance of PDT has been limited by a sub-optimal pharmacokinetic profile and poor tumour selectivity. This leads to low potency and off-target photosensitivity that can cause scarring and stricture formation within the oesophagus as well as sensitivity to natural light, leading to severe 'sunburn' in light exposed areas <sup>134,140</sup>. Antibody directed phototherapy aims to overcome this by reducing both PS clearance time and non-specific uptake <sup>262,339,340</sup>. Antibody fragments are generally taken up into the tumour more rapidly, exhibit quicker serum and tumour clearance times and generally lead to a higher tumour: normal tissue ratio than whole monoclonal antibodies <sup>341,342</sup>.

HER2 is an established biomarker for cancers of the digestive system<sup>343</sup>. The HER2-targeting antibody Trastuzumab in combination with chemotherapy is licensed for oesophagogastric cancer patients where it was shown to improve progression-free and overall survival in those overexpressing HER2<sup>229,344</sup>. However, the link between patient prognosis and HER2 overexpression remains controversial and HER2 positivity levels in the literature range from 5 to 30% in gastroesophageal junction and OA cancer patients<sup>227,345–347</sup>. This is likely due to heterogeneous expression, study bias for cancer position or grade and the previous variation in HER2 scoring across the field<sup>348,349</sup>.

A novel HER2 targeted phototherapeutic for PDT could be combined with existing surgical therapy to allow minimally invasive destruction of tumour tissue beyond localised disease and beyond that visible down the endoscope. Ideally this agent would also be available to patients with borderline or heterogenic HER2 expression who may not have previously been offered therapies targeting HER2. C6.5 is well characterised single-chain variable fragment (ScFv) against HER2<sup>350,351</sup>. It was selected to produce a novel phototherapy agent targeted against HER2. C6.5 was re-engineered in a form optimal for bioconjugation and then reacted with a pre-activated form of the water-soluble photosensitiser chlorin e6. The final phototherapy agent was tested both *in vitro* and in an *in vivo* tumour model with clinically relevant heterogeneous HER2 expression.

The experiments in this chapter were designed, co-ordinated and supervised by me as part of a Technology Strategy Board, Biomedical Catalyst – Early Stage Award to develop “Antibody Directed Phototherapy for Oesophageal Adenocarcinoma.” The lead for the project from Antikor was Dr Mahendra Deonarain, and principal investigator in UCL was Professor Laurence Lovat. This was a collaborative effort with a small team of scientists who had various roles in the data presented in this chapter.

## **6.2. Materials and methods**

### **6.2.1. Patient cohort**

A panel of formalin fixed paraffin embedded (FFPE) oesophageal specimens was identified from the upper gastrointestinal service at University College London Hospital. Each sample was the highest grade of dysplasia or cancer the patient had at the time of sampling. Ethical approval was obtained from the UK Research Ethics Committee (EC13.13; 08/H808/8; 08/H0714/27). Samples were selected from 111 patients containing; normal squamous tissue (n=8; Sq), Barrett's epithelium (n=32, BE), low grade dysplasia (n=21; LGD), high grade dysplasia (n=26; HGD) and OA (n=24; OA). Sections were stained with haematoxylin and eosin (H and E) and the reported pathological grade confirmed by a specialist gastrointestinal pathologist (MRJ or MN).

### **6.2.2. HER2 immunohistochemistry, and scoring**

Immunohistochemical (IHC) staining was performed on 4µm slices of paraffin-embedded tissue using the automated Bond-Max system (Leica) and a citrate-based epitope retrieval solution at pH 6.0 (30 min). Endogenous peroxidase activity was blocked using 0.3% hydrogen peroxide (5 min). The primary antibody against HER2 (NCL-L-CBE-356, Leica), was diluted 1:100. Slides were incubated at room temperature with primary antibody for 15 minutes followed by secondary rabbit anti-mouse for 8 minutes and finally a tertiary goat anti-rabbit polymer reagent for 8 min. This was developed using a bond polymer refine detection kit using 3,3'-diaminobenzidine tetrahydrochloride as a chromogen over 10 min.

Samples were reported for HER2 staining intensity and extent by a pathologist (MRJ or MN) according to the Allred scoring system and established clinical guidelines. Both systems score intensity as negative (0), weak (1), moderate (2+) or strong (3+). Extent was scored in Allred as 0% (0), <1% (1), 1-<10% (2), 10-<33% (3), 33-<66% (4) or ≥66% (5). HER2 positivity requires complete, basolateral or lateral membrane staining of 3+ intensity, or 2+ intensity with confirmatory positive in-situ hybridisation in ≥10% of



tumour resections specimens, or  $\geq 5$  cells with the same pattern in at least one tumour cell cluster (TCC) for biopsy samples. This is in line with NICE guidelines for oesophagogastric cancer.

### **6.2.3. HER2 gene set enrichment analysis**

Microarray data was obtained from Gene Expression Omnibus studies <sup>352–356</sup>. The data sets included 19 normal squamous epithelia, 20 Barrett's epithelium (BE) and 21 OA samples. Gene set enrichment analysis was carried out according to a previously described method on around 4000 cellular pathways by Dr Rifat Hamoudi <sup>357</sup>. The HER2 gene probe 216836\_s\_at was used to mine the original gene expression microarray data for raw mRNA expression levels.

### **6.2.4. Chemical synthesis of the photosensitiser Chlorin e6-anhydride (Ce6-Anhydride)**

Photochemistry studies were planned with Dr Gokhan Yahioglu, chief chemist, Antikor, UK and conducted by Dr Hayley Pye. The methods used was modified from Chen et al. 2015 [8] and Xu et al 2008 [9].

To a stirred solution of chlorin e6 (100 mg, 0.17 mmol) and N,N-diisopropylethylamine (58  $\mu$ L, 0.15 mmol) in anhydrous dimethylformamide (2 mL) at room temperature was added HATU (1-[Bis(dimethylamino)methylene]-1H-1,2,3-triazolo[4,5-b]pyridinium 3-oxid hexafluorophosphate, N-[(Dimethylamino)-1H-1,2,3-triazolo-[4,5-b]pyridin-1-ylmethylene]-N-methylmethanaminium hexafluorophosphate N-oxide) (57 mg, 0.15 mmol) and stirred protected from light for 1 h. The crude reaction mixture was then concentrated under reduced pressure and purified by preparative thin-layer chromatography eluting with anhydrous acetone and the residue recrystallised from dichloromethane with n-hexane.

### **6.2.5. Production and characterisation of anti-HER2 antibody drug conjugate**

Conditions for optimum conjugation and characterisation studies were established with Dr Hayley Pye, our photochemist and conducted by Ms Halla Reinert, our laboratory technician. C6.5, a fully human anti-HER2 single-chain Fv was first described by Schier et al., 1995 was the antibody selected to develop the ADC<sup>351</sup>. The original clone from Prof J. Marks (University of California, San Francisco), was re-engineered with a T7 tag added to the C terminus. The surface exposed lysine residues were re-engineered for improved affinity and retention of function with aqueous solubility after lysine residue bioconjugation (Optilink™ technology Antikor). The new fragment, now referred to as TCT, was expressed and purified by Antikor Biopharma (sequence proprietary information) and stored at -20°C at 12mg/ml in sodium acetate buffer with NaCl at pH5.0, MW 28160 Da.

Prior to use, TCT was filter sterilised through a 0.22 µm Polyvinylidene difluoride (PVDF) membrane and diluted into PBS pH7.4 as required. For chemical synthesis of the photosensitiser Chlorin e6-anhydride (Ce6-Anhydride) see supplementary data. Ce6-Anhydride (Antikor Biopharma) MW 579 was stored as a solid at 4 °C in the dark under vacuum in a desiccator. Inactivated Ce6 (Medkoo Biosciences Cat. 500410) was stored in the dark at -20 °C. Handling of the photosensitive drugs and subsequent conjugates was carried out under dim light conditions. At least 24 hours prior to reaction the Ce6-anhydride was diluted to 20 mg/mL in anhydrous dimethyl sulphoxide (DMSO), snap frozen and stored at -20 C. Frozen aliquots were used within 3 days. Conjugation reaction; for a 700 µL reaction volume; TCT was diluted to 35.5µM in PBS (pH 7.4). To this the Ce6-anhydride was added (final concentration 350 µM) with 10 volumes of DMSO to give a 20% solution. Reaction mixture was incubated in a closed eppendorf in the dark on a flatbed shaker (125 rpm) at 37 °C for 2 hours centrifuging to remove any precipitated material (10,000 g, 2 minutes) and filtered through a 0.22 µm filter. Excess reagents were removed by desalting (7kDa MWCO Zeba) into fresh buffer (PBS, pH 7.4). The average antibody recovery between batches was ~70%. The product was stable for up to a month at 4°C in PBS pH7.4. In addition, snap frozen

TCT-Ce6 stored at -20°C demonstrated equivalent cell binding and spectroscopic properties once thawed.

Samples diluted into pH6.8 Tris-HCl loading buffer with final concentration of 2% SDS and 10% glycerol without reducing agents or tracking dyes and boiled for 5 minutes at 70-100 °C. Gels were hand cast 1 mm gels with a discontinuous buffer system containing 0.1% Ammonium persulphate (APS) and 0.1% Tetramethylethylenediamine (TEMED) to polymerise; Resolving gel: 12% acrylamide/bis 0.1% Sodium dodecyl sulfate–polyacrylamide (SDS), in 0.37 M Tris-HCl pH8.8. Stacking gel: 4% acrylamide/bis 0.1% SDS, in 0.12 M Tris-HCl pH6.8. Samples were loaded at 2 µg protein alongside a marker (Thermo 26619). Gels ran at 30 mA per gel until bands well resolved in 1X running buffer (0.25M Tris base + 2.5 M glycine + 0.1% SDS). Unstained gels were imaged for fluorescence using a CCD camera flatbed imager using a Blue light LED transilluminator (Ex450-485nm Em>500nm) (G: BOX CHEMI HR1.4, Syngene). Gels were then fixed and stained with 0.1% Coomassie Brilliant Blue G in a 10% acetic acid 40% methanol buffer.

UV-Vis spectroscopy was used to analyse the fluorescence spectra of samples using a Lambda 25 (Perkin Elmer) spectrophotometer. Samples were placed in a micro volume 1cm path length quartz cuvette and diluted 1:20 into PBS (pH7.4). Spectra were normalised to 900 nm and the fluorescence from solvent background digitally removed. Concentrations were calculated using the following equation  $A = \epsilon lc$  where A is absorbance of the sample,  $\epsilon$  = molar absorptivity, l = path length in cm and c = concentration in molar. Molar extinction coefficient (M<sup>-1</sup> cm<sup>-1</sup>) were calculated in PBS pH 7.4 as follows; TCT 280 nm  $\epsilon$  = 65235, Ce6-anhydride 280 nm  $\epsilon$  = 9816, 402 nm  $\epsilon$  = 81020, 654 nm  $\epsilon$  = 17353.

#### **6.2.6. Cell culture**

The HER2 positive oesophageal columnar epithelial adenocarcinoma cell line OE19 and the HER2 negative immortalised normal squamous epithelial oesophageal cell line

Het1A were obtained from the European collection of authenticated cell cultures (ECACC) and cultured according to their recommendations. NCI-N87 a known HER2 positive gastric cancer cell line was obtained from the American Type Culture Collection (ATCC) Nov 2013 and cultured according to ATCC guidelines. Cells were confirmed mycoplasma free and kept within a 20-passage range. BART was gifted by Prof Rhonda Souza (UT Southwestern, USA) and is a human cell line established from an area of non-neoplastic Barrett's columnar epithelium that has been telomerase-immortalised<sup>358</sup>.

#### **6.2.7. Flow cytometry**

Experiments were conducted under the supervision and with the assistance of Dr Hayley Pye. Cells were detached with Accutase (Millipore SCR005), and 200,000 cells per sample were washed and incubated on ice with various concentrations of TCT. After 1-hour cells were washed and incubated with 300nM rabbit  $\alpha$ -T7 Tag IgG DyLight488 conjugate (Abcam ab117486) on ice for 30 minutes before two final washes. All steps carried out in Foetal calf buffer (PBS + 2% FCS (Foetal calf serum) + 1 mM EDTA). Flow cytometry was carried out on a Beckman-Coulter Cyan ADP, FITC detection channel; (Ex 488 nm Em 510–550 nm), PS detection channel; (Ex 635 nm Em655–675). Data from 10,000 cells was gated to exclude, doublets, aggregates and debris. Single colour controls were used to ensure there was no bleed-through between the detection wavelengths. Data was analysed and quantified using the geometric mean of the curve using Flowing Software Version 2.5.1 (Perttu Terho, Turku Centre for Biotechnology, Finland). For analysis of the ADCs TCT antibodies were incubated at 30 nM, a concentration shown to be less than the cell surface saturation of OE19 cells.

#### **6.2.8. In vitro Photodynamic therapy (PDT)**

Experiments were conducted under the supervision of Dr Mahendra Deonarain with Dr Hayley Pye. 25,000 OE19 cells were plated in clear bottomed black walled 96 well

plates. The following day media was replaced with media containing experimental compound at varying concentrations. Plates were protected from light and incubated at 37 °C and 5% CO<sub>2</sub> for one hour. Cells were washed twice with PBS and returned to warm media before being exposed to a 670 nm Laser (Hamamatsu LD670C) at a dose of 5 J/cm<sup>2</sup> delivered at 80 mW/cm<sup>2</sup>. Non-irradiated control cells were protected from light and returned to the incubator. Light was delivered via fibre optic/frontal light distributor (model FD-1 Medlight S.A SN FD1-1345) and pre-calibrated for exact energy delivery (Gentec TDM-300 / PSV-3103). To assess remaining cell viability 24 h later, media was replaced with MTT reagent (Sigma-Aldrich M5655) at 0.5 mg/mL in FCS free cell culture media, more specifically the MTT assay measures the reducing ability of cells, i.e. cells with metabolic activity. Plates were protected from light and incubated at 37 °C and 5% CO<sub>2</sub> for two hours, MTT media was replaced with 100 µL DMSO and shaken until all crystals had dissolved. A490nm was measured on a ELx800 Absorbance Microplate reader (BioTek). To calculate IC<sub>50</sub> data was fitted using SigmaPlot (Systat Software Inc.) with a Four Parameter Logistic Curve according to the equation  $(f1 = \min + (\max - \min) / (1 + (x/IC_{50})^{-Hillslope}))$ . Statistical difference between curves was tested with area under the curve analysis according to Cleves et al,<sup>359</sup>.

#### **6.2.9. *In vivo* mouse tumour model protocol**

In vivo experiments were primary conducted by Dr Laura Funnel under my supervision and with my assistance. Female SCID (CB17/lcr-PrkdcSCID/lcrIcoCrI) mice were purchased from Charles River Laboratories (Margate, UK). Mice (7-10 weeks) were inoculated with 7 million OE19 cells subcutaneously (s.c.) into the depilated right dorsal flank in a volume of 0.2ml PBS. Tumour growth was monitored at least 3 times a week using digital vernier callipers (volume = (length x width x depth)/2). Mice were sacrificed when tumour measurements exceeded 2cm x 1.5cm in two dimensions, if tumour volume was calculated to be higher than 2000mm<sup>3</sup> or if the animals were exhibiting any adverse effects that affected their welfare as defined in our license.

Tissues were fixed immediately in 10% neutral buffered formalin and processed to formalin fixed paraffin embedded (FFPE) blocks for analysis.

#### **6.2.10. Pharmacokinetics and biodistribution of TCT-Ce6 and Ce6**

Once tumours reached a suitable size (approximately 120mm<sup>3</sup> in 2 weeks), 30 SCID mice were treated with 0.1ml of either TCT-Ce6 (1mg/ml) or the equivalent amount of free Ce6 intravenously (i.v.) into the tail vein. Mice were sacrificed at 2, 4, 8, 24 and 72 hours after injection (n= 3 per time point) and their tissues harvested for analysis.

Control tissue was harvested from 3 tumour bearing SCID mice following i.v. injection of PBS to control for tissue specific autofluorescence and quenching. Tumours failed to grow in 3 mice, thus n=2 for Ce6 treated mice sacrificed at 4, 8 and 24 hours. Tissues and serum were collected and snap frozen immediately. Thawed tissue was individually weighed and dissolved into Solvable™ (Perkin Elmer) at 37.5mg/ml and standards made of known amounts of either TCT-Ce6 or Ce6 dissolved in control tissues at 37.5mg/ml in Solvable™. Fluorescence of all samples was measured in black walled 96 well plates with excitation at 400nm and emission at 660nm. Standard curves were fitted with  $Y=mX+C$  where  $Y=RFU$ ,  $X= ng\ Ce6$  (either free or within the conjugate),  $M = gradient\ or\ quenching\ power$  and  $C = Y-axis\ intercept\ or\ autofluorescence$ . Standard curves were used to calculate the concentration of Ce6/mg tissue.

#### **6.2.11. HER2 immunohistochemistry, and scoring**

Eleven days after tumour implantation 24 SCID mice were assigned to treatment groups: Saline (n=8), TCT-Ce6 plus laser (n=8) and TCT-Ce6 minus laser (n=8). Mice were treated with 0.2ml of either saline or TCT-Ce6 (0.5 mg/ml) injections (i.v.). Four hours following treatment a 2cm diameter spot covering the tumour was illuminated using a 200J/cm<sup>2</sup> laser dose (150mW/cm<sup>2</sup> over 22min 11sec). Laser power was kept at or below 150mW/cm<sup>2</sup> to prevent tissue heating. The rest of the mouse was covered with a black cloth to limit illumination of normal tissue, and the room was maintained in

dim light. TCT-Ce6 plus laser and saline treatment groups received laser illumination, while TCT-Ce6 minus laser mice received the equivalent duration of anaesthesia only. Mice were treated twice a week for 2 weeks (days 11, 14, 18, 21 following tumour inoculation) and kept under slightly subdued-lighting conditions throughout treatment and the following day. Animals were observed, and tumours measured 3 times a week until the experimental end point, up to 40 days after tumour inoculation. One-way ANOVA followed by Bonferroni's multiple comparison tests were used to determine significant differences in tumour volume between groups using the SPSS program (IBM Corp. Armonk, NY). Kaplan-Meier survival curves were plotted and tested with Cox's proportional hazards model (Log-rank Mantel-Cox Test) (GraphPad PRISM Software, San Diego, CA)<sup>360</sup>.

#### **6.2.12. T7 Immunohistochemistry**

IHC analysis was carried out on 4µm slices of paraffin-embedded tissue. Protocols were optimised by our laboratory technician Mr Ignacio Puccio. The primary antibody against T7 (ab9115, Abcam) was diluted 1:1000. Immunostaining was carried out using the automated Bond-Max system (Leica) using on board heat-induced antigen retrieval and a citrate-based epitope retrieval solution at pH 6.0 (30 min). Endogenous peroxidase activity was blocked using 0.3% hydrogen peroxide (5 min). The histological specimens were incubated at room temperature with primary antibody for 30 minutes, followed by secondary rabbit anti-mouse for 16 minutes and finally a tertiary goat anti-rabbit polymer reagent for 8 min. This was developed using a bond polymer refine detection kit using 3,3'-diaminobenzidine tetrahydrochloride as a chromogen over 10 min. Samples were reported by an expert GI pathologist (MN).

### **6.3. Results**

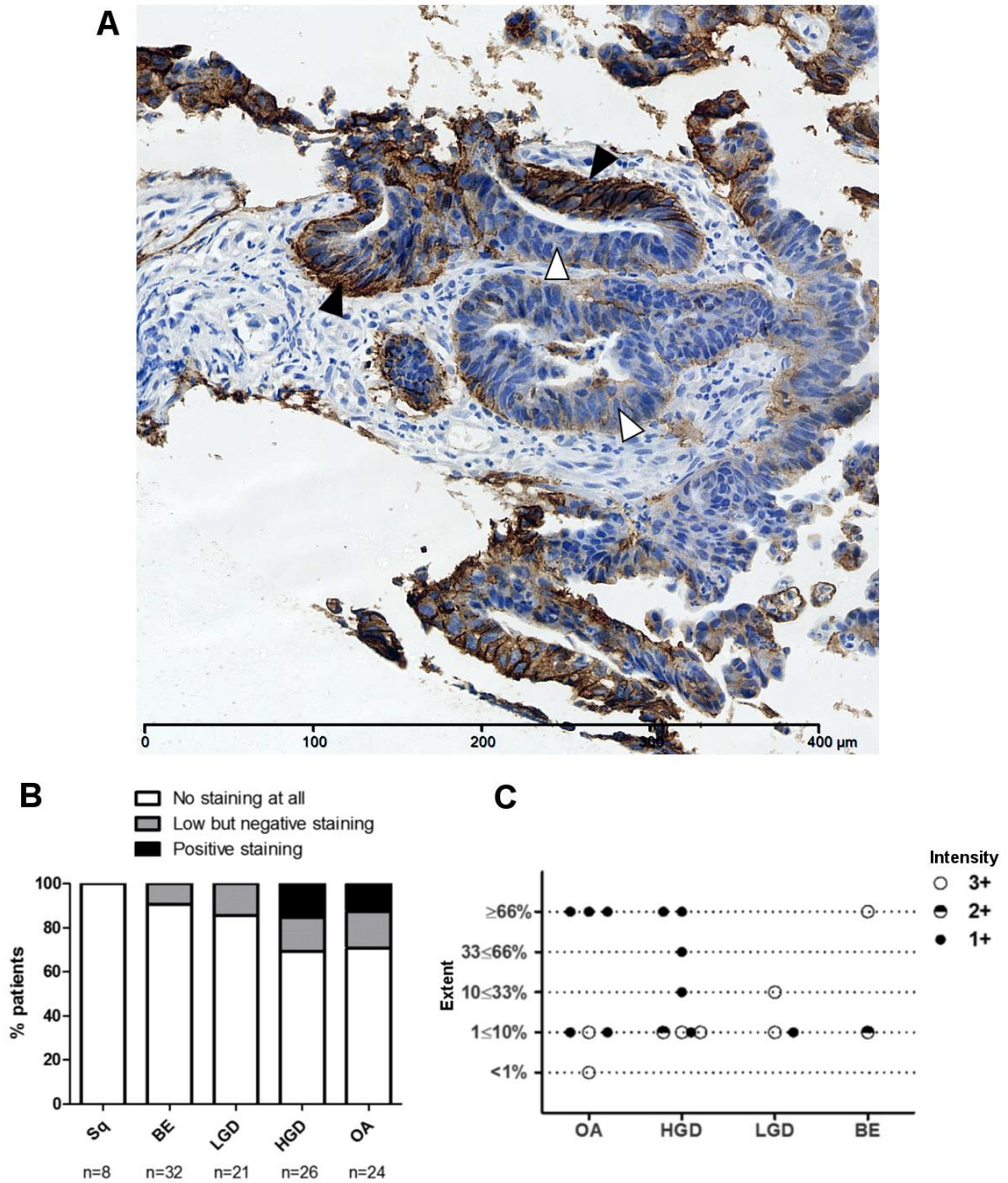
#### **6.3.1. HER2 protein expression as a biomarker in oesophageal adenocarcinoma.**

To confirm HER2 as a biomarker for OA, a panel of oesophageal tissue specimens taken from 111 patients of varying pathological grades underwent HER2 IHC. Positivity

was defined according to the NICE guidelines for gastric cancer<sup>344</sup>. HER2 staining was negative in all Sq, BE and LGD tissue, and despite heterogeneity stained positive in 15.4% and 12.5% of patients with either high grade dysplasia (HDG) or oesophageal adenocarcinoma (OA) respectively. A further 16.7% of OA, 15.4% of HGD, 14.3% of LGD and 9.4% of BE samples stained weakly or to a lower level and so did not reach the criteria for positivity (Figure 43).



**Figure 43: Heterogeneous HER2 immunohistochemistry in the progression to OA**

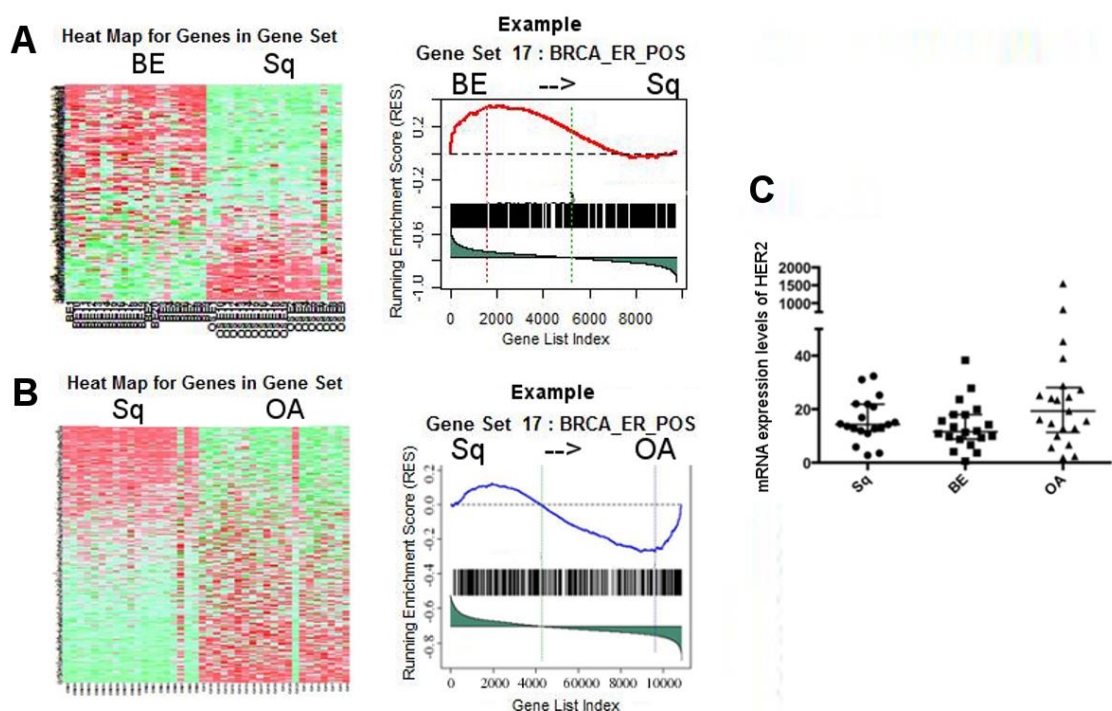


(A) Example of heterogeneous HER2 staining in invasive OA, areas of HER2 positivity (black arrows) and negativity (white arrows). (B) HER2 expression is squamous (Sq), Barrett's epithelium (BE), low-grade dysplasia (LGD), high grade dysplasia (HGD) and oesophageal adenocarcinoma (OA). (C) Representation of Allred score for each patient (5).

### 6.3.2. HER2 mRNA expression as a biomarker in oesophageal adenocarcinoma.

HER2 mRNA expression during cancer progression was investigated in published datasets. Results show a small subgroup (~10%) of the OA samples with high HER2 mRNA levels that are 60-100-fold above the median value for squamous tissue (Figure 44). However, there were no significant differences in HER2 expression between the groups (Mann-Whitney test) supporting previous data from Kim et al <sup>361</sup>.

**Figure 44: Gene set enrichment analysis (GSEA) and microarray analysis of HER2 in the progression to oesophageal cancer (OA).**



(A) Heat map and example probability plot of the gene set enrichment analysis for Barrett's oesophagus (BE) vs normal oesophageal squamous epithelium (Sq) and (B) oesophageal adenocarcinoma (OA) vs normal oesophageal squamous epithelium (Sq). (C) Microarray analysis, raw expression values of HER2 mRNA in Squamous, BE and OA tissue.

Using gene set enrichment analysis (GSEA), performed by Dr Rifat Hamoudi, HER2 expression was linked to progression to OA. Comparison of OA to Sq gave 27 significantly enriched pathways in OA including 19 (70%) involving HER2 (Table 26).

Comparison of BE to normal oesophageal squamous epithelium gave 28 significantly enriched pathways in BE and of these 23 (82%) included HER (Table 27). This recurrent appearance of HER2 in significant pathways implies its involvement in neoplastic transformation of the oesophagus.

**Table 26: Gene Set Enrichment Analysis (GSEA); pathways enriched between normal tissue and OA**

Gene Set	Contains HER2?	SIZE	Enrichment Score (ES)	Normalised ES	Nominal p-value	False Discovery Rate (FDR) q-val	FWER p-val	Tag %	Gene %	Signal	FDR (median)	glob. p.val
BRCA_ER_POS	NO	377	0.37525	1.7535	0	0.013113	0.04905	0.366	0.302	0.265	0	0.001
ENZYME_LINKED_RECEPTOR_PROTEIN_SIGNALING_PATHWAY	YES	87	0.43756	1.8645	0	0.0084891	0.01502	0.356	0.227	0.278	0	0.001
FERNANDEZ_MYC_TARGETS	NO	109	0.39083	1.7664	0	0.015905	0.04404	0.44	0.347	0.291	0	0.002
POST_TRANSLATIONAL_PROTEIN_MODIFICATION	YES	294	0.29568	1.4925	0	0.042743	0.3073	0.306	0.293	0.222	0	0.001
PROTEIN_MODIFICATION_PROCESS	YES	388	0.30516	1.5859	0	0.045142	0.1702	0.309	0.293	0.227	0	0.003
TPA_RESIST_EARLY_DN	NO	52	0.42742	1.6617	0	0.031003	0.1041	0.269	0.169	0.225	0	0.003
TRANSMEMBRANE_RECEPTOR_PROTEIN_TYROSINE_KINASE_SIGNALING_PATHWAY	YES	48	0.49821	1.9249	0	0.0038311	0.005005	0.458	0.287	0.328	0	0.001

REGULATION_OF_MAP_KINASE_ACTIVITY	YES	44	0.46894	1.7623	0.00190 5	0.013432	0.04505	0.477	0.287	0.341	0	0.001
LEI_MYB_REGULATED_GENES	NO	240	0.43097	1.7861	0.00214 1	0.015645	0.03403	0.454	0.315	0.318	0	0.004
REGULATION_OF_PROTEIN_KINASE_ACTIVIT Y	YES	101	0.37146	1.5852	0.00571 4	0.041711	0.1722	0.426	0.322	0.291	0	0.003
HSC_HSCANDPROGENITORS_FETAL	NO	397	0.30164	1.521	0.00585 9	0.040204	0.2613	0.338	0.336	0.233	0	0
HSC_HSCANDPROGENITORS_ADULT	NO	408	0.30283	1.5266	0.00587 1	0.040631	0.2502	0.336	0.333	0.233	0	0.001
REGULATION_OF_CELL_PROLIFERATION	YES	184	0.37611	1.6016	0.00595 2	0.045447	0.1612	0.413	0.329	0.282	0	0.005
REGULATION_OF_KINASE_ACTIVITY	YES	102	0.36812	1.5612	0.00767 8	0.042096	0.1972	0.422	0.322	0.289	0	0.002
REGULATION_OF_KINASE_ACTIVITY	YES	102	0.36812	1.5612	0.00767 8	0.042096	0.1972	0.422	0.322	0.289	0	0.002

REGULATION_OF_CATALYTIC_ACTIVITY	YES	165	0.32708	1.5335	0.00988 1	0.042522	0.2402	0.388	0.345	0.258	0	0.001
REGULATION_OF_TRANSFERASE_ACTIVITY	YES	103	0.36712	1.556	0.01163	0.038658	0.2022	0.417	0.322	0.286	0	0.001
BRCA1_OVEREXP_PROSTATE_UP	NO	122	0.38177	1.5293	0.012	0.042042	0.2482	0.443	0.365	0.284	0	0.001
POSITIVE_REGULATION_OF_MAP_KINASE_ACTIVITY	YES	28	0.48034	1.6274	0.01426	0.037837	0.1361	0.464	0.264	0.342	0	0.002
CELL_PROLIFERATION_GO_0008283	YES	307	0.34584	1.5002	0.01765	0.045728	0.2893	0.388	0.324	0.27	0	0.002
CELL_GROWTH_AND_OR_MAINTENANCE	YES	46	0.46253	1.5573	0.02209	0.040646	0.2012	0.326	0.174	0.271	0	0.002
CELL_SURFACE_RECEPTOR_LINKED_SIGNAL_TRANSDUCTION_GO_0007166	YES	323	0.37928	1.5372	0.02231	0.044058	0.2372	0.35	0.287	0.257	0	0.001
REGULATION_OF_MOLECULAR_FUNCTION	YES	184	0.30918	1.4265	0.02245	0.054469	0.3944	0.375	0.345	0.25	0	0
PROLIFERATION_GENES	YES	229	0.35774	1.4399	0.02677	0.052864	0.3784	0.393	0.332	0.268	0	0
CELL_PROLIFERATION	YES	128	0.39426	1.4968	0.0334	0.042917	0.2953	0.398	0.296	0.284	0	0.001
SHEPARD_CELL_PROLIFERATION	YES	128	0.39426	1.4968	0.0334	0.042917	0.2953	0.398	0.296	0.284	0	0.001

KLEIN_PEL_UP	NO	34	0.40858	1.4709	0.04008	0.044725	0.3303	0.412	0.333	0.275	0	0
DRUG_RESISTANCE_AND_METABOLISM	YES	56	0.39119	1.4288	0.04483	0.055736	0.3934	0.429	0.318	0.294	0	0.001
TPA_SENS_MIDDLE_DN	NO	217	0.30057	1.3753	0.054	0.067614	0.4965	0.41	0.394	0.253	0	0

(Significant pathways only; nominal p-value <0.05)

**Table 27: Gene Set Enrichment Analysis; pathways enriched between normal tissue and Barrett's oesophagus**

Gene Set	Contains HER2?	SIZE	Enrichment Score (ES)	Normalised ES	Nominal p-value	False Discovery Rate (FDR) q-val	FWER p-val	Tag %	Gene %	Signal	FDR (median )	glob. p.val
BRCA_ER_POS	NO	334	0.38703	1.7166	0	0.032246	0.04527	0.371	0.292	0.272	0	0.01
CELL_PROLIFERATION_GO_0008283	YES	280	0.34251	1.5959	0	0.024012	0.1348	0.5	0.447	0.285	0	0
POST_TRANSLATIONAL_PROTEIN_MODIFICATION	YES	273	0.31988	1.6258	0	0.023622	0.1076	0.516	0.47	0.282	0	0
PROTEIN_MODIFICATION_PROCESS	YES	354	0.32404	1.6101	0	0.022916	0.1217	0.517	0.47	0.285	0	0
REGULATION_OF_CATALYTIC_ACTIVITY	YES	161	0.31555	1.5358	0	0.02607	0.2183	0.578	0.524	0.28	0	0
REGULATION_OF_MOLECULAR_FUNCTION	YES	181	0.30988	1.5256	0	0.027405	0.2354	0.453	0.423	0.266	0	0



HSC_HSCANDPROGENITORS_ADULT	NO	353	0.31448	1.6321	0.00197 6	0.025468	0.1056	0.227	0.207	0.186	0	0
PROLIFERATION_GENES	YES	207	0.37767	1.5887	0.00200 8	0.024533	0.1459	0.512	0.421	0.303	0	0
TRANSMEMBRANE_RECEPTOR_PROTEIN_TY ROSINE_KINASE_SIGNALING_PATHWAY	YES	47	0.41241	1.6706	0.00206 6	0.03709	0.08249	0.404	0.289	0.289	0	0.008
PHOSPHORYLATION	YES	178	0.30448	1.4936	0.00371 7	0.029863	0.2706	0.517	0.469	0.279	0	0
HSC_HSCANDPROGENITORS_FETAL	NO	345	0.29927	1.5647	0.00394 5	0.020216	0.17	0.214	0.207	0.176	0	0
CELL_SURFACE_RECEPTOR_LINKED_SIGNAL _TRANSDUCTION_GO_0007166	YES	297	0.37034	1.5846	0.00402 4	0.023231	0.1479	0.444	0.372	0.288	0	0
REGULATION_OF_CELL_PROLIFERATION	YES	166	0.37084	1.5742	0.00406 5	0.019073	0.1559	0.494	0.42	0.292	0	0

REGULATION_OF_PROTEIN_KINASE_ACTIVIT Y	YES	100	0.36053	1.6456	0.00583 7	0.025088	0.09457	0.46	0.387	0.285	0	0
REGULATION_OF_KINASE_ACTIVITY	YES	101	0.36433	1.6588	0.00587 1	0.029898	0.08954	0.465	0.387	0.288	0	0.003
REGULATION_OF_KINASE_ACTIVITY	YES	101	0.36433	1.6588	0.00587 1	0.029898	0.08954	0.465	0.387	0.288	0	0.003
REGULATION_OF_MAP_KINASE_ACTIVITY	YES	45	0.44114	1.6918	0.00602 4	0.034542	0.06338	0.6	0.387	0.369	0	0.008
ENZYME_LINKED_RECEPTOR_PROTEIN_SIGN ALING_PATHWAY	YES	84	0.37688	1.577	0.00631 6	0.019792	0.1549	0.452	0.368	0.288	0	0
PROTEIN_AMINO_ACID_PHOSPHORYLATION	YES	163	0.31151	1.4874	0.00763 4	0.029468	0.2817	0.521	0.469	0.281	0	0
REGULATION_OF_TRANSFERASE_ACTIVITY	YES	102	0.36706	1.6585	0.00792 1	0.026326	0.09054	0.471	0.387	0.291	0	0

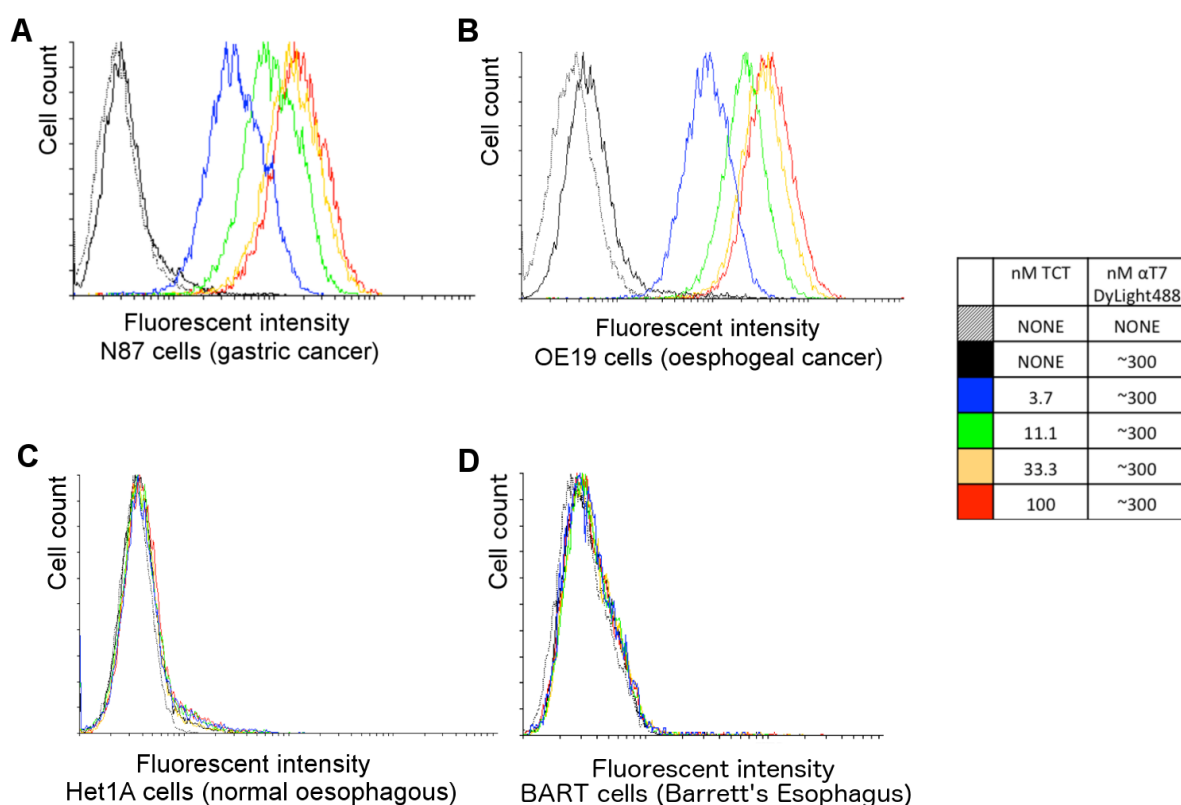
POSITIVE_REGULATION_OF_MAP_KINASE_ACTIVITY	YES	28	0.47933	1.5825	0.01022	0.022252	0.1489	0.607	0.366	0.386	0	0
LEI_MYB_REGULATED_GENES	NO	218	0.41855	1.6212	0.01597	0.022352	0.1097	0.541	0.391	0.337	0	0
CELL_PROLIFERATION	YES	118	0.3645	1.5775	0.018	0.020679	0.1549	0.559	0.451	0.311	0	0
SHEPARD_CELL_PROLIFERATION	YES	118	0.3645	1.5775	0.018	0.020679	0.1549	0.559	0.451	0.311	0	0
CELL_GROWTH_AND_OR_MAINTENANCE	YES	39	0.44008	1.496	0.02	0.030252	0.2656	0.487	0.347	0.32	0	0
TPA_SENS_MIDDLE_DN	NO	187	0.31567	1.4612	0.02037	0.035419	0.326	0.54	0.494	0.278	0	0
FRASOR_ER_DN	YES	47	0.40692	1.4932	0.02204	0.029019	0.2716	0.553	0.394	0.337	0	0
BREAST_CANCER_ESTROGEN_SIGNALING	YES	63	0.41189	1.5035	0.04225	0.029637	0.2515	0.365	0.262	0.271	0	0

Significant pathways only; nominal p-value <0.05)

### 6.3.3. Production of the HER2 targeted phototherapy drug; TCT-Ce6

Using FACS analysis it was demonstrated that the modified C6.5 fragment (TCT) could bind live HER2 positive oesophageal columnar epithelial adenocarcinoma cells (OE19) as well as a known HER2 positive gastric cancer cell line (N87). Negligible binding was seen with an immortalised normal squamous epithelial oesophageal cell line (Het-1A) and an immortalised Barrett's Oesophagus columnar epithelial cell line (BART) (Figure 45).

**Figure 45: Binding of TCT to HER2 in a panel of cell lines derived from gastric adenocarcinoma (A), OA (B), squamous oesophagus (C) and BE (D) *in vitro*.**

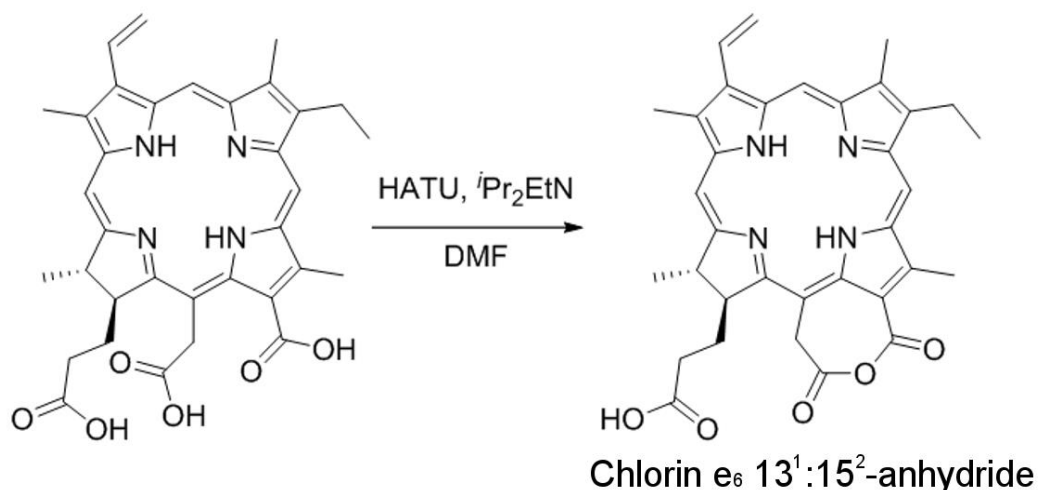


*Flow cytometry showing binding of the HER2 specific ScFv TCT. A fluorescent secondary antibody used to detect the T7 within TCT, an increase in fluorescence represents more TCT has bound to each cell and the saturation of the fluorescent signal indicates cell surface receptor saturation.*

Chlorin e6 (Ce6) is ideal for bio-conjugation as it has high water solubility for a

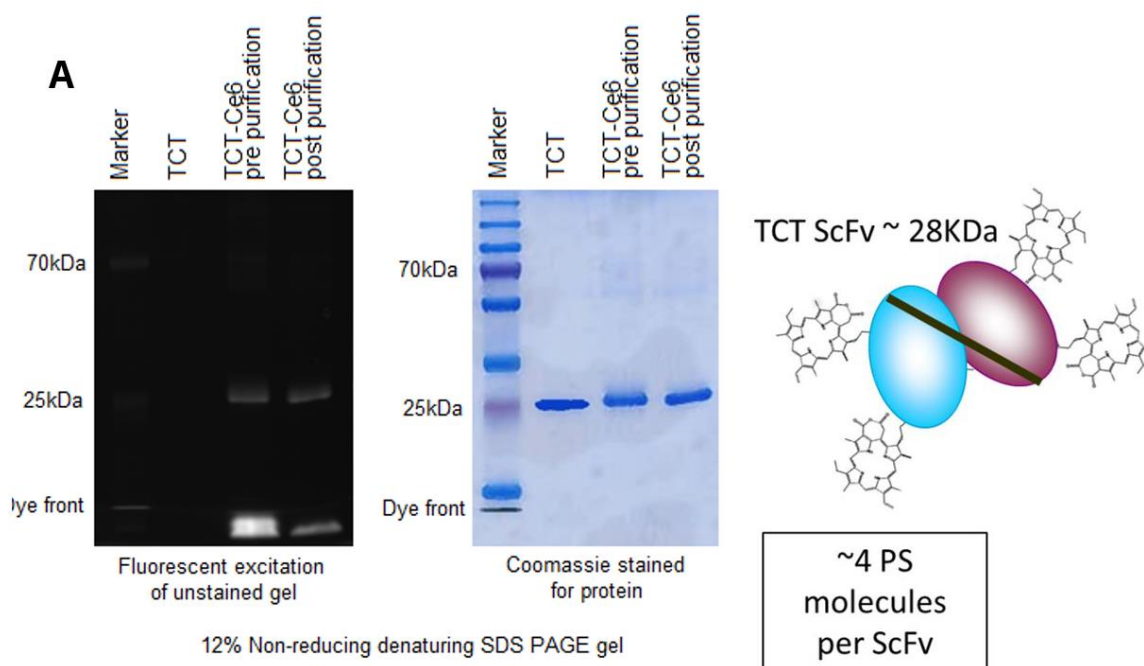
photosensitiser (PS), a high singlet oxygen quantum yield and a strong absorption  $\sim 660$  nm <sup>362</sup>. Ce6 was pre-activated to form an anhydride ring between two carboxyl groups to prevent cross-linking upon bio-conjugation (Figure 46).

**Figure 46: Ce6 pre-activated to form an anhydride ring between two carboxyl groups.**



Reaction conditions were optimised for a product that maintained the best antigen binding with retained aqueous solubility. Samples of the purified antibody–drug conjugate, TCT-Ce6, were analysed by SDS-PAGE and UV-Vis spectroscopy. Unconjugated Ce6 was removed by the purification procedure and the bond formed between the TCT and Ce6 was shown to be covalent (seen at the height of the protein). Almost all unconjugated dye (seen at the dye front with the 10 kDa marker) was removed from the final product, conjugated dye was shown to be covalently bound. The small amount of non-covalent material left in the conjugate was tightly bound and could not be removed with the addition of excipients during the purification process (Figure 47A). Spectroscopic analyses predicted the average drug-to-antibody ratio (DAR) was 4. A product with a DAR  $\sim 4$  was produced reliably and reproducibly between independent experiments. The Ce6 peak at 400nm broadened and the 660nm peak red-shifted upon conjugation (Figure 47B). Despite this the extinction coefficient of the free dye at 400nm was used to determine the dye concentration of the conjugate.

**Figure 47: Analysis of purity and photo-physical spectral properties of TCT-Ce6.**



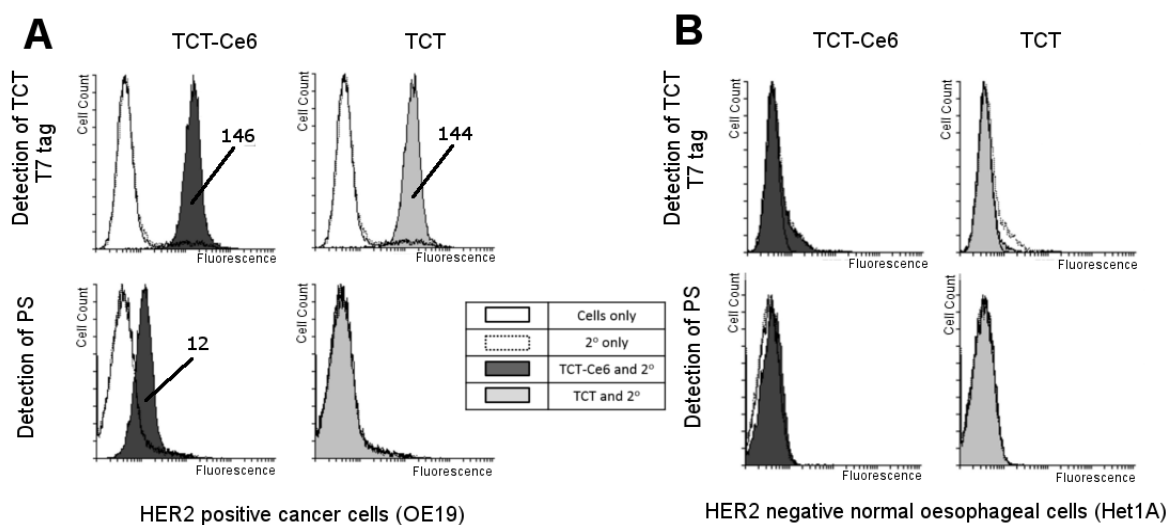
(A) Fluorescent excitation of samples run on non-reducing SDS-PAGE. Gels were Coomassie stained for protein after being imaged for PS fluorescence. (B) TCT-Ce6 was analysed by UV-Vis spectroscopy shown overlaid with a spectrum of free Ce6 (dashed) and free TCT (grey).

#### **6.3.4. Selective binding of TCT-Ce6 to HER2 positive oesophageal cells in vitro**

Binding of the phototherapy agent TCT-Ce6 compared to the binding of unconjugated TCT was studied *in vitro* with human cell lines; the HER2 positive OA cell line OE19

and the HER2 negative normal oesophageal cell line Het1A. Using previously defined cell surface sub-saturation levels (Figure 45) no change in cell surface binding to OE19 was seen with TCT-Ce6 compared to TCT, and neither TCT or TCT-Ce6 bound Het1A (Figure 48). The cells to which TCT-Ce6 bound could be also be detected on flow cytometry by their red fluorescent emission associated with the PS.

**Figure 48: Selective binding of TCT-Ce6 to HER2 positive OA compared to HER2 negative normal oesophagus *in vitro*.**



*Live cell binding of TCT-Ce6 compared to unconjugated TCT was tested on two cell lines (A) OE19; a human oesophageal adenocarcinoma with high HER2 expression and (B) Het1A; a human normal oesophageal cell line with no HER2 expression.*

*Conjugation had no effect on TCT binding to OE19 cells and Ce6 labelled cells could also be detected through PS emission. Neither TCT or TCT-Ce6 bound to Het1A cells. Geometric means of any positive shifts are labelled on the image.*

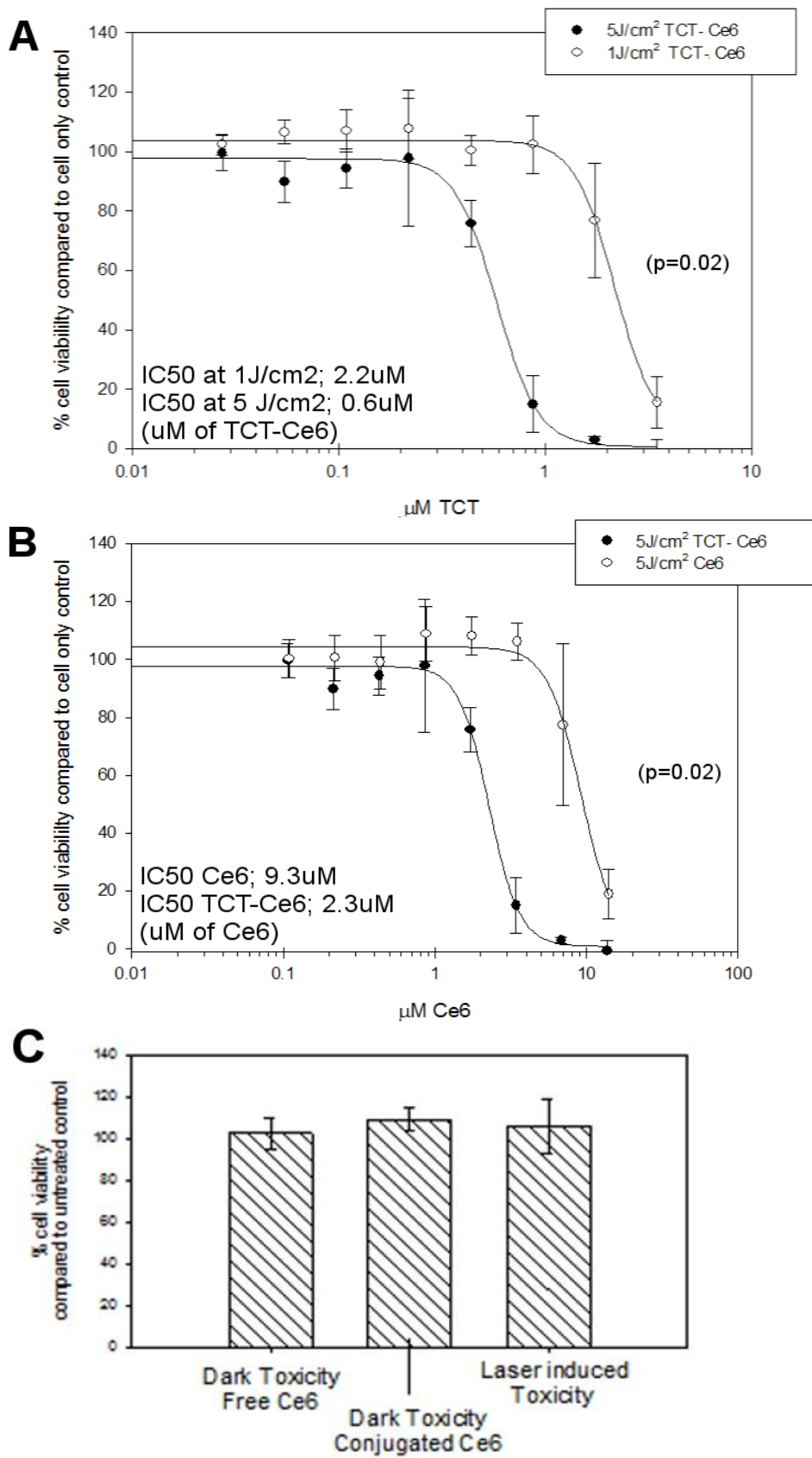
### **6.3.5. Light dependent cytotoxicity of TCT-Ce6 *in vitro***

To determine the activity of TCT-Ce6 for photodynamic therapy (PDT), the HER2 positive OE19 cell line was exposed to increasing equivalent concentrations of TCT-

Ce6 or free Ce6 and exposed to laser light. TCT-Ce6 was significantly more cytotoxic ( $p=0.02$ ) (Figure 49B). The  $IC_{50}$  TCT-Ce6 at  $5J/cm^2$  was  $0.6\mu M$ , with five times less light was  $2.2\mu M$  ( $p=0.02$ ) (Figure 49A). Control samples showed no cytotoxicity of the drug without laser irradiation or from laser irradiation alone (Figure 49C). Upon laser irradiation TCT-Ce6 showed light and dose dependent toxicity with an  $IC_{50}$  of  $0.6\mu M$ . The TCT-Ce6 induced cytotoxicity was significantly higher compared to equivalent amounts of free Ce6 ( $p=0.02$ ).



**Figure 49: Dose and light dependent PDT cytotoxicity of TCT-Ce6 compared to free drug on HER2 positive oesophageal cells (OE19).**

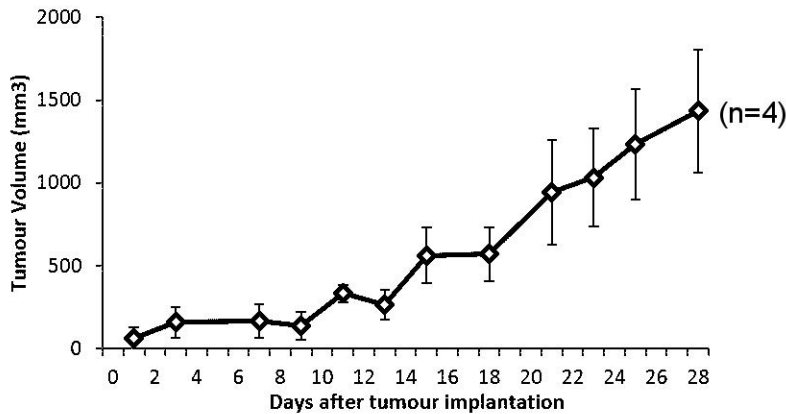


### **6.3.6. Mouse xenograft model of human OA**

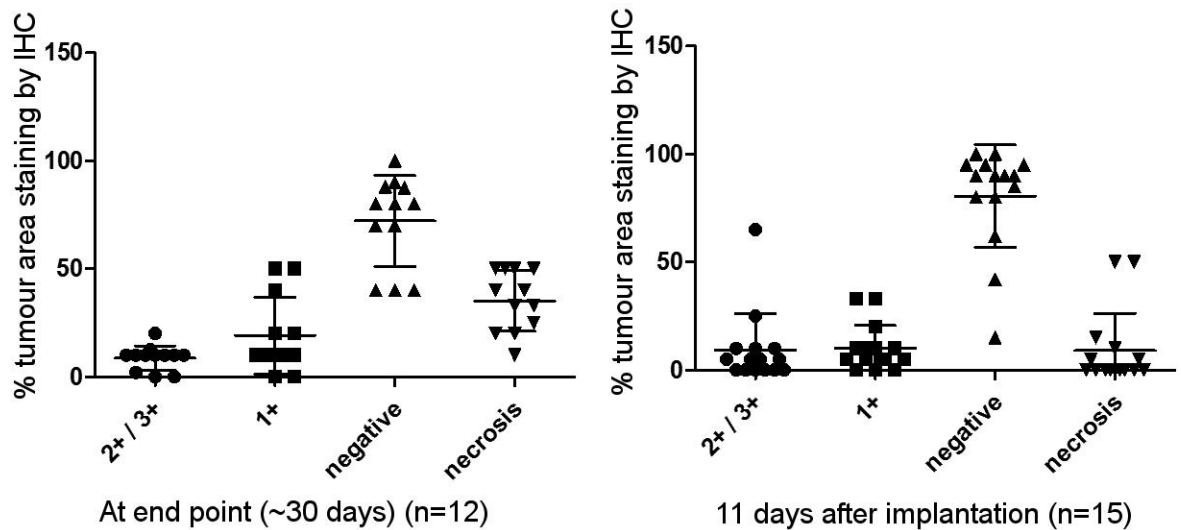
A mouse flank xenograft model was developed from the HER2 positive human OA cell line OE19 subcutaneously injected into the flank of immune compromised mice (Figure 50A). Tumours were harvested as soon as they become measurable (approx. 11 days after inoculation) and at tumour burden (approx. 30 days after inoculation). Tumours were stained and scored for HER2 using clinical parameters (Figure 50B). Although *in vitro* OE19 cells exhibit high levels of HER2 expression by both flow cytometry and IHC, the *in vivo* tumours at day 11 had an average tumour area which was 81% HER2 negative, only 10% HER2 grade 1+ and 9% HER2 grade 2+ or limited 3+. These tumours would be classed as negative according to current guidelines and therefore not qualify for HER targeting therapies. There was no necrosis in these early tumours, but all showed immune cell infiltrate. Tumours at day~30 had no immune cells and demonstrated similar HER2 staining (72% HER2 negative, 19% HER2 grade 1+ and only 9% HER2 grade 2+ or limited 3+) alongside this an average of 30% necrosis was observed in every tumour. In all tumours at both time points 3+ staining was absent or very limited.

**Figure 50: Characterisation of a HER2 positive mouse flank xenograft model of OA.**

**A**



**B**



		Average	SD	
End Point tumours	2+ / 3+ HER2 positive	8.7	5.6	100%
	1+ HER2 positive	19.2	17.8	
	HER2 negative	72.1	21.1	
	Necrosis	35.1	13.9	

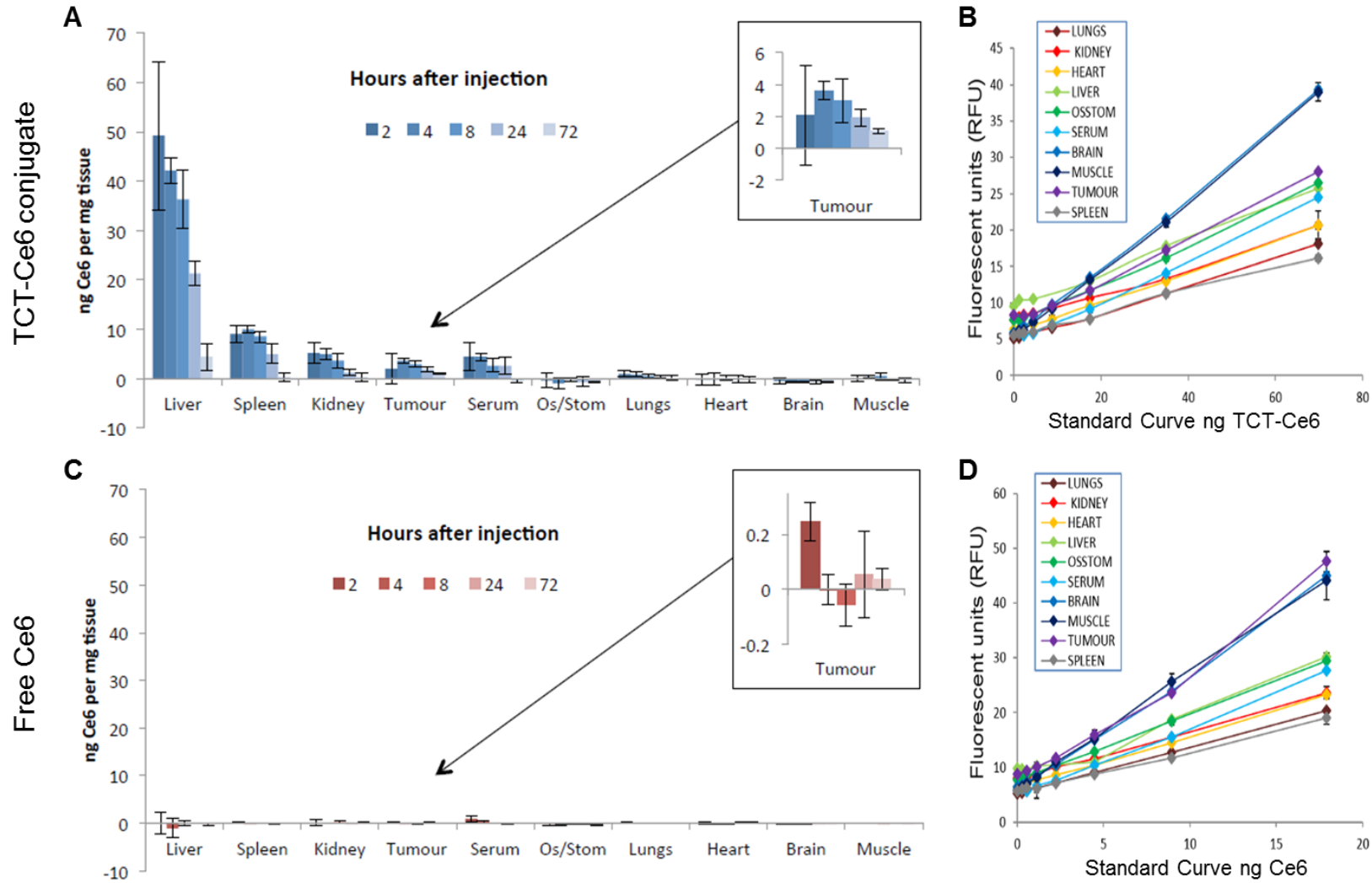
		Average	SD	
Day 11 tumours	2+ / 3+ HER2 positive	9.3	16.8	100%
	1+ HER2 positive	10.1	10.6	
	HER2 negative	80.6	23.7	
	Necrosis	9.0	17.2	

(A) Tumours grew from ~day 10 until between 25-30 days after subcutaneous injection when they reached the size limit. (B) Tumours at day 11 (n=15) and at the experimental endpoint (~day 30) (n=12) underwent IHC investigation for HER2. Bars represent Mean +/- SD. Proportion of tumour area at 100% was divided into negative staining or positive staining either 1+ (low), 2+ or 3+ (high). Proportion of necrosis was separately measured as a percentage of the whole mass.

### **6.3.7. Pharmacokinetics and biodistribution of Ce6 and TCT-Ce6 *in vivo***

The organ distribution of TCT-Ce6 (Figure 51A) or free Ce6 (Figure 51C) *in vivo*, was determined at 2, 4, 8, 24 and 72 hours after drug was injected into the tail vein of the xenograft model. High levels of TCT-Ce6 were found in organs which filter the blood (liver, kidney, spleen), negligible levels of TCT-Ce6 was found in all other organs tested (lung, brain, heart, muscle and oesophagus/stomach). Free Ce6 clears all organs rapidly and within 2 hours. TCT-Ce6 had virtually cleared the body by 72hrs. Peak TCT-Ce6 accumulation in the tumour occurred after 4 hours, while levels of free Ce6 in the tumour and other tissues were negligible.

Figure 51: Biodistribution of free Ce6 at various timepoints after I.V injection

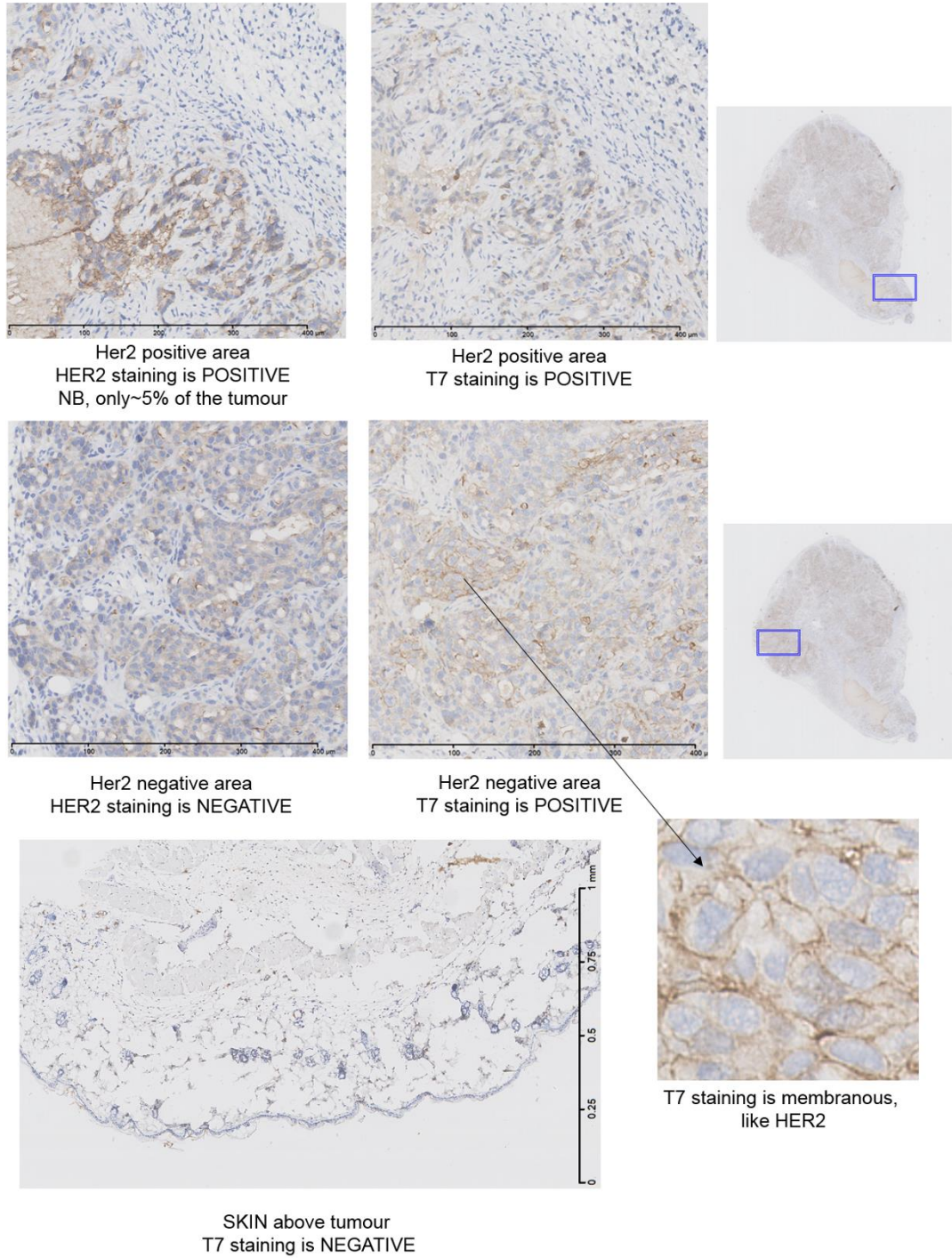


*Distribution of TCT-Ce6 (A) and free Ce6 (C) in dissolved tissue at set time points after I.V injection. Mean data  $\pm$  SEM. Results controlled for tissue specific auto-fluorescence and quenching with standard curves of known concentrations of TCT-Ce6 (B) or free Ce6 (D) dissolved in Solvable™ in each tissue.*

#### **6.3.8. Expression of HER2 in tumour and surrounding skin in vivo**

Xenograft tumours and the skin directly above the tumour, were harvested 4 and 24 hours after TCT-Ce6 and stained by IHC for T7 to detect tagged T7-TCT-Ce6 and HER2. At 4 hours TCT-Ce6 membranous staining was seen specifically in the tumour tissue and not in the surrounding stroma or vasculature, suggesting selective uptake into the tumour. At 24 hours the pattern was similar but the amount of TCT-Ce6 was negligible in many samples. There was no TCT-Ce6 in the skin above the tumour at any time point. At 4 hours TCT-Ce6 and HER2 co-localised in the same areas but TCT-Ce6 was also widely distributed throughout the HER2 negative regions of the tumour (Figure 52).

**Figure 52: IHC distribution of TCT-Ce6 in tumour and overlying skin at 4 hours.**



*IHC images of HER2 or T7 tag (part of TCT-Ce6) staining in harvested tumour and overlying skin at day 11, 4 hours after TCT-Ce6 injection. TCT-Ce6 and HER2 co-localised in the same areas but TCT-Ce6 could also be seen in other tumour areas. TCT-Ce6 could be seen specifically in the tumour in a membranous pattern and not in the stoma or vasculature, suggesting selective uptake.*

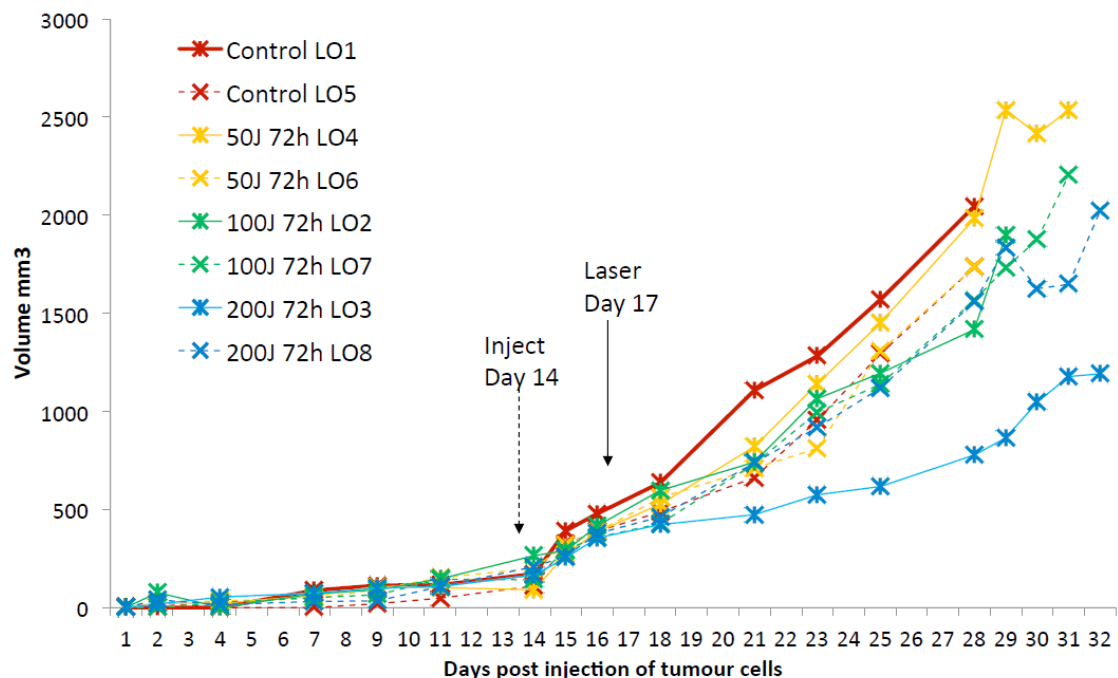


### 6.3.9. Development of laser parameters

#### 6.3.9.1. Laser dose optimisation

The *in vivo* PDT protocol was optimised in small scale experiments (n=2 per variable) with increasing laser doses (50J/cm<sup>2</sup>, 100J/cm<sup>2</sup> and 200J/cm<sup>2</sup>) in mice injected with saline (control) or 200µg TCT-Ce6 72hours prior to lasering. (Figure 53). The highest laser dose was well tolerated, showed no laser induced skin sensitivity or blistering at any time point after drug injection and produced the largest reduction in tumour growth.

**Figure 53: Optimisation of laser dose after fixed injection of TCT-Ce6 vs saline control**



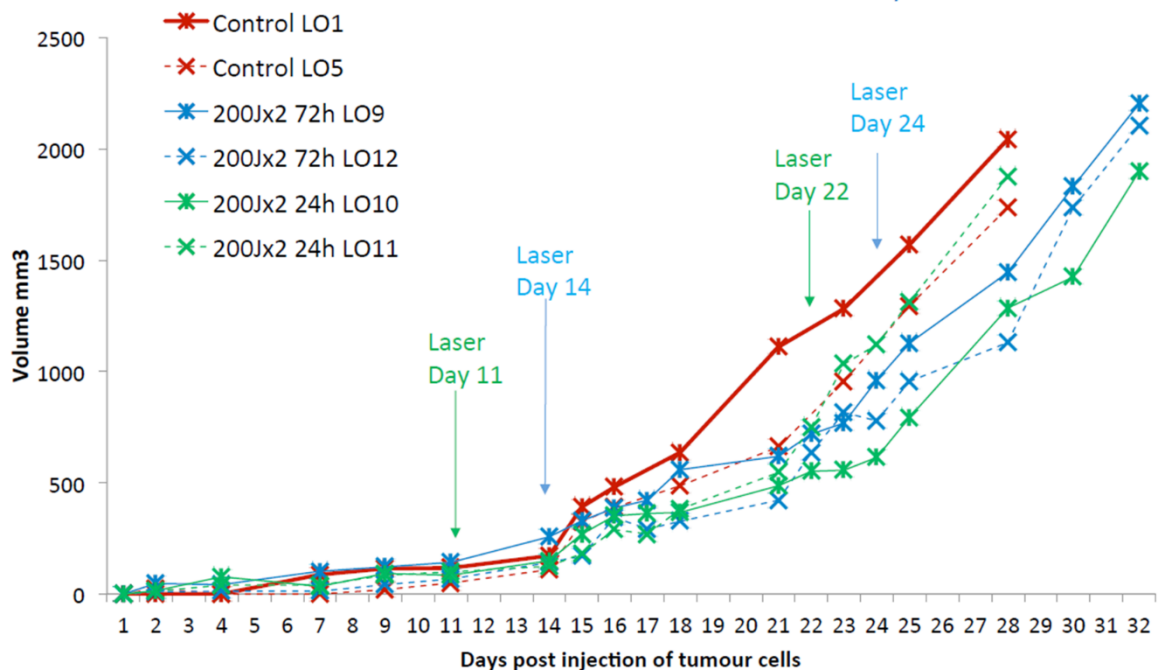
The efficacy of incremental laser light dosage (50J=yellow, 100J=green, 200J=blue) after defined injection of TCT-Ce6 vs saline control was examined (n=2 per variable).

Lines represent tumour growth in individual mice.

### 6.3.9.2. Tolerability of repeated laser illumination

The effect of repeat lasering was examined in concert with evaluating if the drug-light interval would be more effective if reduced from 72hours in the initial experiments to 24hours. Mice were administered 200µg TCT-Ce6 and lasered at 24 or 72 hours, at day 11 post tumour injection. The process was then repeated at day 22. Regardless of drug-laser interval, multiple dosing and lasering was well tolerated. Weight loss was observed with all animals after first PDT, though this remained within accepted parameters and recovered with wet mash. There was no discernible difference between lasering after 24hours or 72hours (Figure 54).

**Figure 54: Effect and tolerability of repeated PDT 10 days apart at 24hour vs 72hour drug light intervals.**

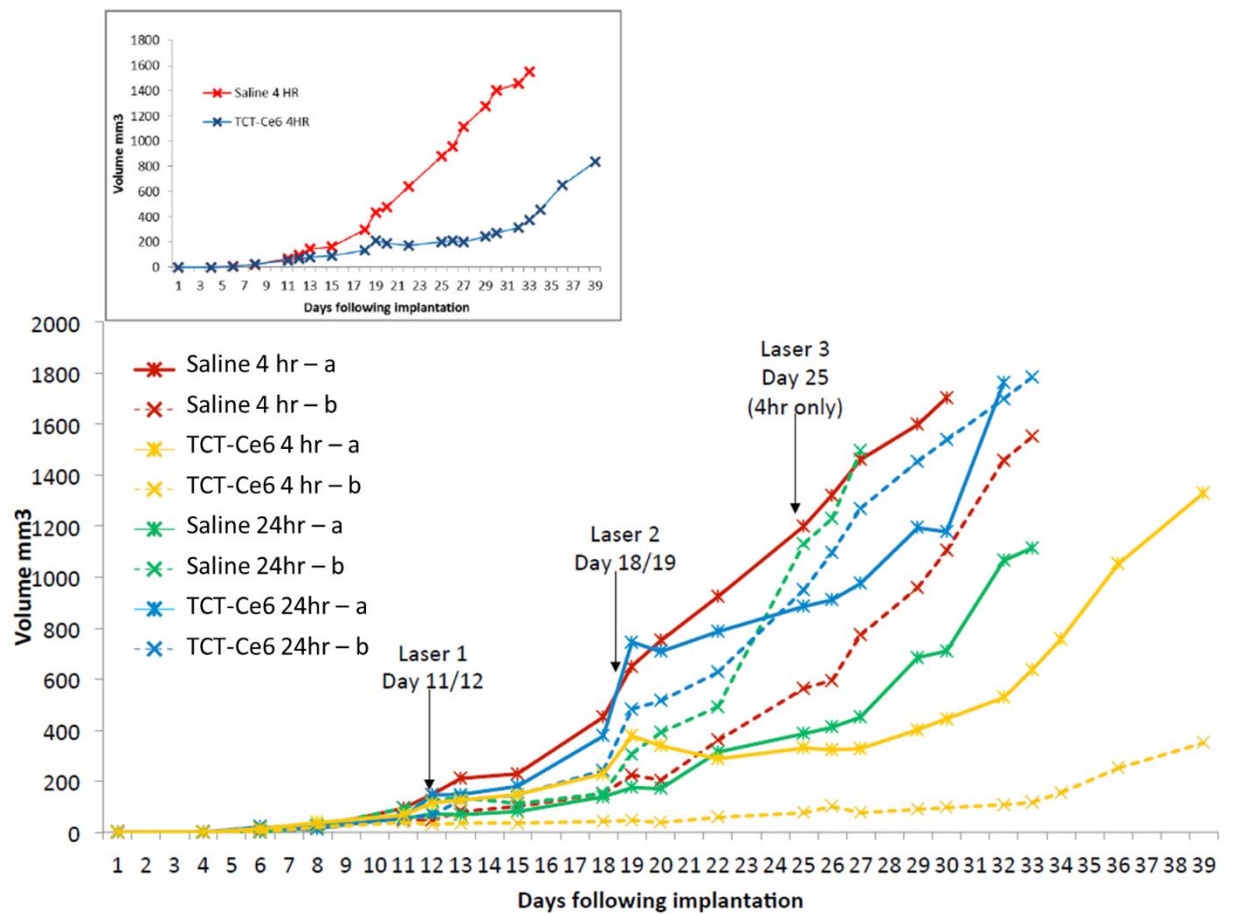


*The efficacy of repeated TCT-Ce6 injection 10 days apart, followed by laser 24 or 72 hours post tail injection was evaluated vs saline (n=2 per variable). Lines represent tumour growth in individual mice.*

### 6.3.9.3. Optimisation of drug – laser interval and tolerability to repeated lasering

The interval between TCT-Ce6 injection and lasering was compared and the tolerance of repeated laser pushed further to repeated injection after 7 days, with three doses of TCT-Ce6 and laser delivered. The 4-hour time point produced the strongest tumour growth reduction and was well tolerated by mice. 1 control tumour grew poorly in this experiment which was due to poor vascular connectivity at the time of dissection (Figure 55).

**Figure 55: Optimisation of drug-laser interval & tolerance to weekly PDT on 3 occasions.**

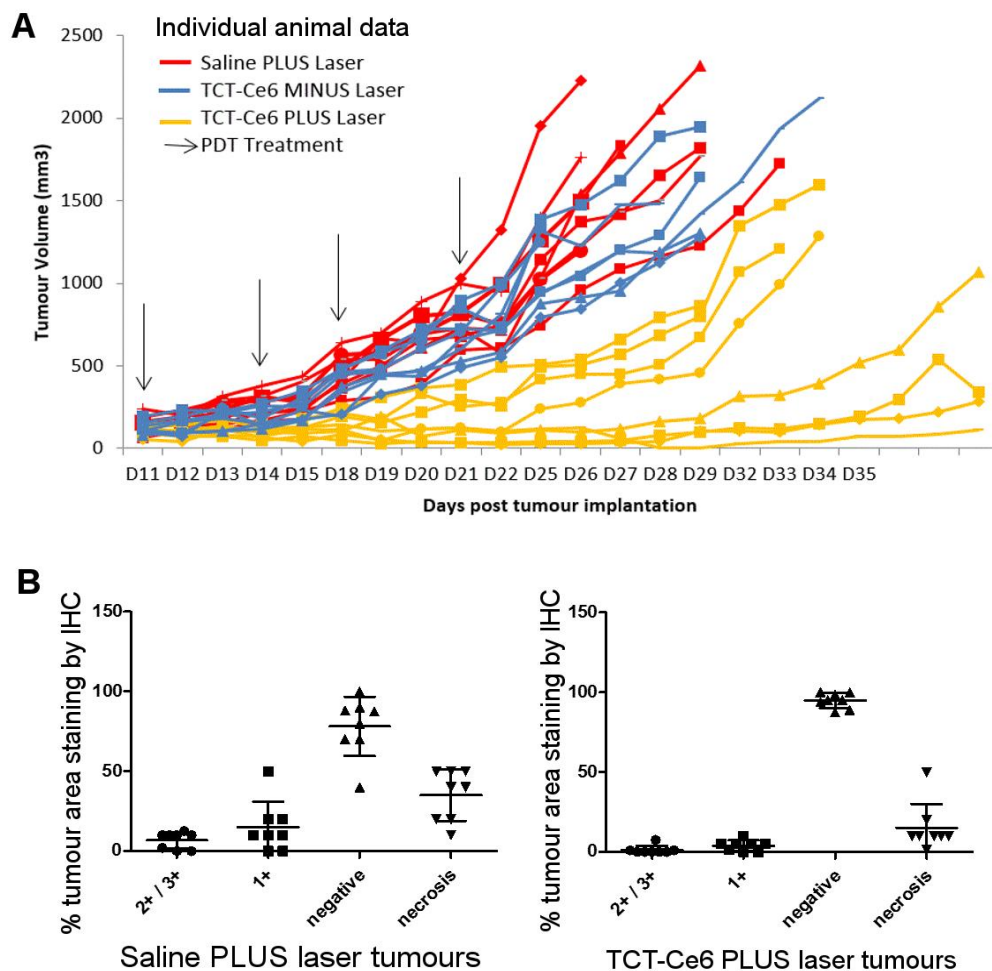


*4 hours post injection was the most effective time point which correlates with previous PK data on maximal TCT-Ce6 levels in the tumour (Figure 51).*

### 6.3.10. Effective photodynamic therapy using TCT-Ce6 *in vivo*

OE19 xenograft tumours of equivalent volume were grown in 24 mice before treating with a single PDT treatment twice weekly for a total of 4 treatments. TCT-Ce6 phototherapy induced tumour growth arrest in all tumours treated. Four of the TCT-Ce6 treated mice with laser irradiation did not reach tumour burden by the end of the study (Figure 56).

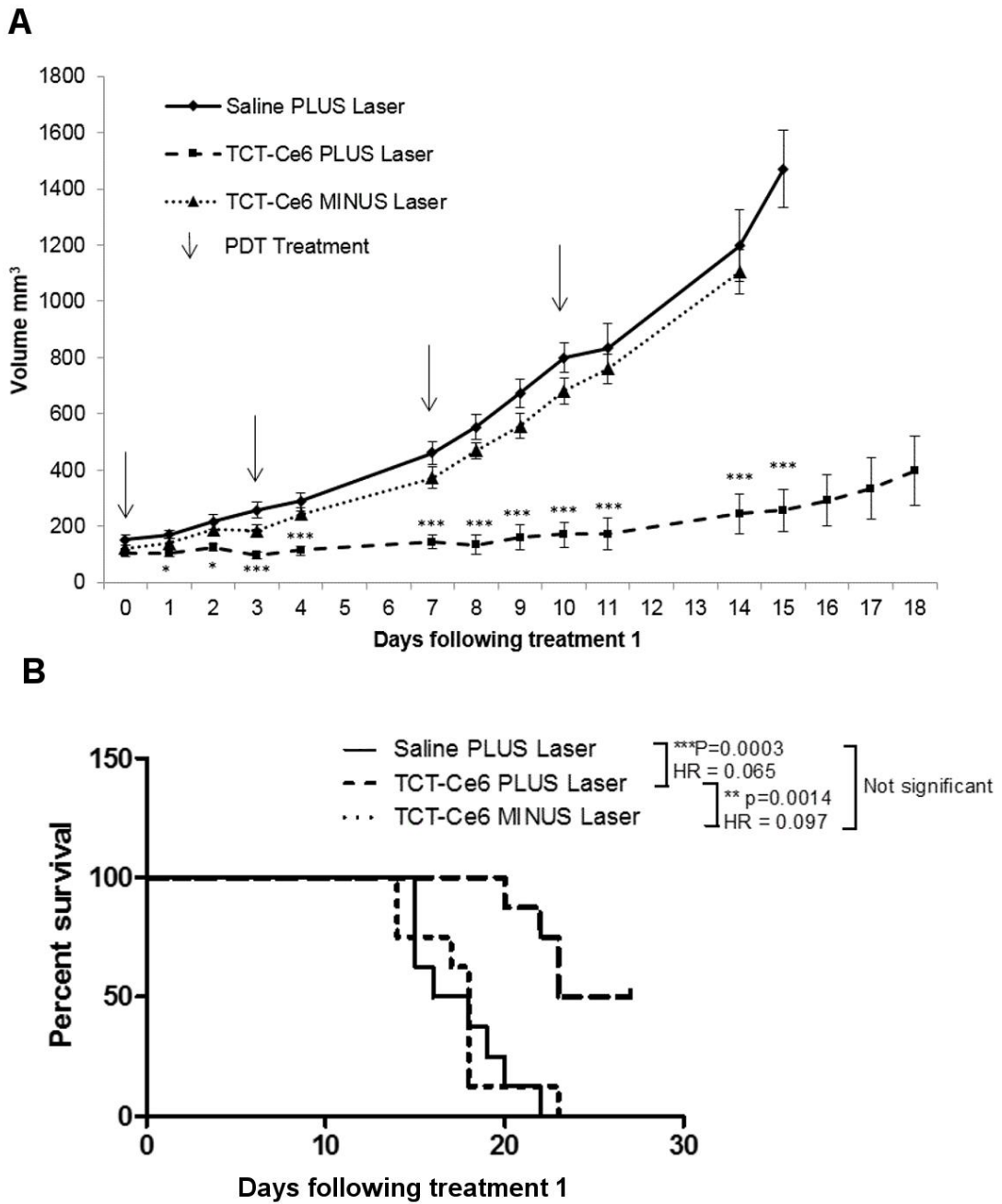
**Figure 56: Effect of TCT-Ce6 PDT on OE19 subcutaneous flank tumours *in vivo*; individual animal data (A) and tumour HER2 characterisation at endpoint (B).**



Each group had 8 animals. Arrows represent PDT treatment time points. Tumours at the end of the experiment were taken for IHC analysis of HER2 staining (B), no differences in HER2 staining were seen between treated and non-treated animals.

Tumour volume was significantly different between TCT-Ce6 treated tumours with and without laser from the third day of treatment (day 3 ( $p < 0.05$ ), day 4 ( $p < 0.01$ ), days 5-14 ( $p < 0.001$ )). Tumour volume was significantly different between lasered tumours +/- TCT-Ce6 from the second day of treatment (day 2:  $p < 0.05$ , days 3-15:  $p < 0.001$ ) (Figure 57).

**Figure 57: Tumour growth arrest in vivo after PDT treatment using TCT-Ce6 on OE19 subcutaneous flank tumours.**



(A) Each group  $n=8$ . Data shown as Mean  $\pm$  SEM. Arrows represent individual i.v./laser treatment time points. Stars represent significant differences between Saline and TCT-Ce6 plus laser treated mice. \*  $p < 0.05$ , \*\*\*  $p < 0.001$ . Kaplan Meier survival curves for each treatment group are shown (B) with log-rank (Mantel-Cox) test; the  $p$  value and hazard ratio (HR) for each pair is shown.

There was a significant survival benefit in mice receiving treatment (hazard ratio of 0.65 between the saline plus laser and TCT-Ce6 plus laser treatment groups ( $p=0.0003$ )) (Figure 57B). At the end of the study tumours were harvested and immunostained for HER2. The intensity and extent of HER2 staining was not significantly different in treated vs non-treated tumours (Figure 52). Dark necrotic patches were observed in some tumours in the area under the skin in treated mice that had demonstrated a greater PDT effect ( $n=4$ ) this was sometimes seen alongside discolouration in small areas of the liver, upon histological analysis of the brown liver sections there was no evidence of cell damage, fat deposition, overt fibrosis or inflammation in these tissues. Some of these mice also exhibited lymph node enlargement that was not seen in the control mice.

#### **6.4. Discussion**

HER2 targeted therapy for cancer is in routine clinical use for breast and gastric tumours<sup>344,363</sup>. In both cancer types, only a subset of patients met criteria for HER2 positivity, rendering HER2 directed therapies inaccessible for the rest. It has been shown however that some of these HER2 negative tumours still have low or heterogeneous HER2 expression<sup>363,364</sup>. In the experiments described in this chapter HER2 expression is examined in a cohort of patients with OA and pre-cancerous oesophageal tissue. HER2 positivity, as defined by NICE guidelines, was shown to occur in 10-15% of patients with either HGD or OA (Figure 43A). This is consistent with previous literature for OA and similar to the levels seen in gastric and breast cancer<sup>223,347,363</sup>. We found an additional 15-18% of OA or HGD patients that classified as HER2 negative still demonstrated low or heterogeneous HER2 staining (Figure 43B), we believe these patients should still be targeted for HER2 therapy. Clinically confirmatory gene amplification testing is suggested for gastric tumours demonstrating weak to moderate (2+) staining in  $\geq 10\%$  of tumour cells, however none of the samples in our cohort would have classified for this<sup>311</sup>. Previously it has been shown that when HER2 negative gastric cancers are reevaluated with either by repeat endoscopic biopsy,

or repeat sampling from metastatic or recurrence sites, in 8.7% and 5.7% respectively tumours could be re-classified as HER2 positive <sup>365</sup>. Often studies examining the impact of HER2 heterogeneity in gastric cancer excluded those expressing HER2 at these low levels and so their impact on prognosis is yet to be established <sup>303,366</sup>. In breast cancer, tumours with this borderline HER2 expression have been shown to have worse disease free survival compared to those which are officially HER2 positive <sup>367</sup>. In breast cancer there is evidence that a subset of HER2-negative patients respond to Trastuzumab and it has been postulated that undetectable sub populations of HER2 positive cells within HER2 negative tumours are responsible for tumour growth re-initiation <sup>368-370</sup>. It has also been shown that histologically HER2 negative breast cancer tumours can still have increased HER2 at the mRNA level compared to normal tissue <sup>368</sup>.

In a mouse flank xenograft model, we replicated the clinical presentation of tumours with both borderline HER2 expression and intratumoural heterogeneity that would be classified as HER2 negative according to current standards (Figure 50). IHC staining techniques and expert pathologist scoring of slices taken throughout the dissected xenograft tumours found similar HER2 expression to the borderline patient samples. Despite the low levels of HER2 expression treatment with a HER2 targeting phototherapy drug (TCT-Ce6) resulted in a rapid and significant effect on tumour volume compared to controls (Figure 57). A novel and sensitive IHC assay for the drug demonstrated that it was tumour specific and cell membrane localised in both HER2 positive and negative areas of the tumour (Figure 52). This supports the evidence from qPCR that HER2 is still expressed in these areas. Modern sequencing techniques have demonstrated the complexity and heterogeneity of all cancers and the validity and utility of all current biomarkers are now being challenged <sup>371,372</sup>.

PDT is already in clinical use to treat certain aspects of OA but wider application has been limited by the sub-optimal pharmacokinetic profile and poor tumour selectivity of



PS drugs<sup>134,139–141</sup>. Antibody targeting of a PS with an antibody aims to remove these limitations. In this work a HER2 targeted PDT drug was developed. The new antibody drug conjugate (Ce6-TCT) confirmed that antibody targeting of a PS improves selective binding and cytotoxicity compared to free PS *in vitro*. It demonstrated good *in vivo* pharmacokinetics e.g. fast serum clearance (days) compared to traditional PDT (weeks) and reduced accumulation in off target organs, particularly the skin, allowing repeated dosing of our drug (Figure 51). The skin is an organ in which drug accumulation in traditional PDT causes particularly bad side effects<sup>336</sup>. PDT has a strong immune component and the requirement of the immune system for prolonged relapse from cancer is becoming evident, *in vivo* tumours will almost always regrow after PDT unless some element of the immune system is reconstituted<sup>340,373–375</sup>. Further testing of this drug in an immune competent system and further modulation in combination therapies alongside better molecular and genetic stratification of patient samples should help define a clear role for drugs like this in clinical practice.

**Chapter 7: Upregulation of MUC1 in the  
progression to oesophageal adenocarcinoma  
and therapeutic potential with a targeted  
photoactive antibody drug conjugate.**

---

## 7.1. Introduction

Despite progress in the treatment of other cancers, the 5-year survival of oesophageal adenocarcinoma (OA) remains low at around 15%<sup>12</sup>. Barrett's epithelium is a premalignant change that increases the risk of developing OA 30-100 fold above that for the general population<sup>4,5</sup>. Eradication of Barrett's epithelium significantly reduces the risk of developing OA<sup>58</sup>. Identifying new therapeutic targets for Barrett's epithelium and OA is of vital clinical importance. Within the field of esophagogastric adenocarcinoma HER2 is the only therapeutic biomarker to be incorporated into widespread clinical practice. The HER2-targeting antibody Trastuzumab when used in combination with chemotherapy has been shown to improve progression-free and overall survival in HER2 positive gastric and gastroesophageal junction cancer patients<sup>229</sup>. HER2 overexpression occurs in approximately 13-23% of esophagogastric cancers but expression can be heterogeneous<sup>321,348</sup>. An ideal therapeutic target would be stable and present in a higher proportion of tumours.

The mucin MUC1 is a densely glycosylated transmembrane protein anchored to the apical surface of many epithelia including the breast, ovary, pancreas, airway and gastrointestinal tract. The extracellular subunit of MUC1 has a 'variable number tandem repeat' (VNTR) region which consists of a repeating 20 amino acid sequence mediating heavy O-linked glycosylation<sup>376</sup>. MUC1 has an important extracellular role in cell surface lubrication and the clearance of debris and pathogens. Its intracellular signalling is linked to the ErbB, fibroblast growth factor receptor 3 and p53 pathways, which are implicated in cancer development<sup>377</sup>. MUC1 is overexpressed in a diverse range of carcinomas. In progression to cancer, MUC1 protein expression generally increases, alters location and is coupled with aberrant glycosylation<sup>376,378</sup>. Previous studies of MUC1 expression in the premalignant changes of OA are inconsistent<sup>249-251</sup>. Up-regulation of MUC1 has been linked to bile acids exposure in gastroesophageal reflux, a condition connected to the development of Barrett's epithelium and OA<sup>379</sup>.

Others have associated a single nucleotide polymorphism in the MUC1 gene to a reduced risk of other upper gastrointestinal cancers<sup>380</sup>.

HuHMFG1 is an antibody against MUC1 that has been tested in clinical trials for breast cancer<sup>252,381,382</sup>. Targeting using HuHMFG1 was ineffective alone but the antibody was well tolerated and had a good safety profile<sup>383</sup>. Later studies used the radiolabelled anti-MUC1 antibody (yttrium-90-AS1402) in ovarian cancer after de-bulking surgery. Administration led to endogenous production of anti-MUC1 IgG in some patients, but there was no survival benefit in those in whom this occurred<sup>253</sup>. HuHMFG1 undergoes cell internalisation<sup>264</sup> and was considered as a vehicle for an antibody-drug conjugate (ADC) approach using the potent cytotoxin, calicheamicin. Reasonable efficacy was seen but in this example the overall therapeutic window was low as calicheamicin was not well tolerated at the higher doses<sup>384</sup>. ADCs are a well-established and clinically-successful approach to cancer therapy, but target and payload selection are key in developing drugs with high efficacy and tolerability, i.e. a high therapeutic index (TI). With the right payload, an anti MUC1 ADC could have great potential.

Photodynamic therapy (PDT) is an ideal modality for application to ADC, particularly where there is some degree of normal tissue expression and hence the TI is low. PDT is already an established treatment modality for dysplastic Barrett's epithelium<sup>134</sup>. It has also shown utility in the treatment of cancers of the prostate, lung, pancreas, bile duct, oral cavity and skin<sup>385,386</sup>. PDT involves the administration of a photosensitiser (PS) and its activation locally using light to cause cellular destruction via intracellular free radicals and/or reactive oxygen species<sup>132,334-336</sup>. As there is little effect on connective tissue, it preserves luminal integrity when used in the digestive tract<sup>132</sup>. Though not inherent to PDT itself, the first-generation photosensitisers approved for clinical use such as porfimer sodium suffered from suboptimal pharmacokinetic / biodistribution profile and poor tumour selectivity. This led to low potency and off target photosensitivity, resulting in severe sunburn and the scarring of internal organs in some patients<sup>134</sup>. These limitations can be inherent to any therapeutic molecule but by

chemical modification and/or combination with other molecules it is now possible to avoid them<sup>387-391</sup>. Photoimmunotherapy is one such approach using a niche ADC where PS are targeted with antibodies called photoimmunoconjugates (PICs)

262,339,340,390,392.

This study aims to highlight the role MUC1 plays in the progression to OA. It further examines how MUC1 expression and glycosylation are altered during oesophageal malignant transformation and later locoregional invasion. Finally, proof of principle data for the mechanism and *in vitro* efficacy of a MUC1 targeting ADC using PDT is shown.

## **7.2. Methods**

### **7.2.1. Gene set enrichment analysis**

Microarray data was obtained from Gene Expression Omnibus data from Wang et al<sup>352</sup>. The data set included 19 normal oesophageal squamous epitheliums, 20 NDBE and 21 OA samples. Gene set enrichment analysis was carried out as previously described on around 4000 cellular pathways using the Kolmogrov-Smirnoff test by Dr Rifat Hamoudi<sup>357</sup>. Recurrent genes in the most important pathways in transition from squamous to NDBE and squamous to OA were identified. The MUC1 gene probe 213693\_s\_at was then used to mine additional gene expression microarray data<sup>352-354,356</sup> for raw mRNA expression levels using Affymetrix, and compared with Mann-Whitney test

### **7.2.2. Tissue panel**

A panel of formalin fixed paraffin embedded (FFPE) oesophageal specimens of varying pathological grades was identified from the University College London Hospital upper gastrointestinal clinical database. The pathology sample chosen was of the highest grade the patient had at the time of sampling. Ethical approval was obtained from the UK Research Ethics Committee (EC13.13; 08/H808/8; 08/H0714/27). Oesophageal tissue samples were selected from 123 patients containing, in order of disease severity; normal squamous tissue (n=15), NDBE (n=29), low grade dysplasia (n=25);

high grade dysplasia (n=34) and invasive OA (n=20). Sections from selected samples were stained with Haematoxylin and Eosin (H&E) to confirm the reported pathological grade by two expert GI pathologists (MN, MRJ). H&E staining was performed using standard protocols.

### **7.2.3. Immunohistochemistry**

To examine MUC1 glycoprotein expression during progression to OA, four antibodies against distinct areas and/or glycoforms were tested.

1. The mouse monoclonal antibody NCL-MUC1 binds a sialylated amino acid attached to a carbohydrate linked to the PDTRPAP region of the VNTR<sup>393</sup>.
2. The humanised monoclonal antibody HuHMFG1 binds a glycan linked PDTR amino acid sequence on the VNTR<sup>394</sup>.
3. The mouse monoclonal antibody NCL-MUC-1-CORE binds directly to the TRPAPG amino acid sequence on the VNTR<sup>393</sup>.
4. The hamster monoclonal antibody CT2 targets the intracellular SSSYTNPAVAATSANL amino acid sequence on the cytoplasmic tail of MUC1<sup>255</sup>. Binding of antibodies to the antigens near or on the VNTR can be sterically hindered in fully glycosylated normal MUC1, but become increasingly exposed in cancer due to aberrant glycosylation<sup>395 396</sup> (Figure 60).

Immunohistochemical (IHC) techniques were optimised to maintain strongly positive tissue staining in the absence of background staining with antibodies at the following primary concentrations. NCL-MUC-1 (1:500; Leica-Novocastra), HuHMFG1 (1:1000 [10µg/mL]; Antisoma, UK) NCL-MUC-1-CORE (1:500; Leica-Novocastra) and CT2 (1:500; gifted by Professor Sandra Gendler, Mayo Clinic, USA). Staining was carried out using heat-induced epitope retrieval in pH 6.0 sodium citrate buffer (Sigma-Aldrich, S4641). Endogenous peroxidase (Leica, RE7157) and non-specific protein activity (Leica, RE7158) were blocked prior incubation with primary antibody. The humanised antibody HuHMFG1 required initial biotinylation (ThermoFisher, 21335) followed by

incubation with ExtrAvidin Peroxidase (Sigma-Aldrich E2886). All other slides were incubated with post-primary block (Leica RE7159) and polymer (Leica RE7161). Slides were then developed with 3,3-diaminobenzadine tetrahydrochloride as a chromogen (Leica RE7162), counterstained with haematoxylin, dehydrated in graded ethanol and mounted in distyrene plasticizer xylene (Sigma Aldrich 06522).

All slides were scored by two expert GI pathologists (MN, MRJ). Positive MUC1 cases were defined as those staining 2+/3+ intensity in  $\geq 10\%$  of the pathology examined, following the established classification adopted for HER2<sup>229</sup>. The Allred system was also used to characterise staining in more detail. Intensity was scored as negative (0), mild (1), moderate (2+) and strong (3+), and proportion of tissues positively stained as negative (0),  $< 1\%$  (1),  $1- < 10\%$  (2),  $10- < 33\%$  (3),  $33- < 66\%$  (4) and  $\geq 66\%$  (5)<sup>261</sup>. Statistical tests including chi squared, Pearson's R and Linear regression analysis were performed using IBM® SPSS® statistics Version 22 (IBM Corporation).

#### **7.2.4. Cell culture**

Het1A obtained from ATCC (October 2014) is a human cell line established from an area of normal oesophageal epithelium that has been SV40 large T antigen-immortalised<sup>397,398</sup>. BAR-T gifted by Prof Rhonda Souza (UT Southwestern, USA) is a human cell line established from an area of non-neoplastic Barrett's that has been telomerase-immortalised<sup>358</sup>. ChTERT (CP-52731) gifted by Dr Stuart McDonald (Barts Cancer Institute, UK) is a human epithelial cell line established from an area of high grade dysplastic Barrett's oesophagus that has also been telomerase-immortalised<sup>399</sup>. OE19, obtained from the ECACC (May 2014) is a human epithelial cell line established from a stage three moderately differentiated oesophageal adenocarcinoma at the oesophageal gastric junction<sup>400</sup>. These cells were compared to human Caucasian colon adenocarcinoma cell line (HT-29) gifted by Prof Marilena Louzidou (Royal Free Hospital, UK) as a negative control, as it does not bind HuHMFG1. All lines were

cultured either according to ECACC/ATCC guidelines or their original publication. All cells were confirmed mycoplasma free.

### **7.2.5. Flow cytometry**

Cell lines were detached with Accutase (Millipore SCR005) or a 0.05% Trypsin/0.02% EDTA/0.5% PVP solution for Het1A cells. Approx. 200,000 cells per sample were washed and incubated in 50ul on ice with varying concentrations of HuHMFG1. After 1-hour cells were again washed and exposed to 300nM  $\alpha$ -Human IgG (FAB specific) FITC conjugate (Sigma-Aldrich F5512) on ice for 30 minutes before two final washes. All steps carried out in FC buffer; PBS + 2% FCS + 1mM EDTA. Flow cytometry was carried out on a Beckman-Coulter Cyan ADP, Cells underwent laser excitation at 488nm and emission was recorded between 510nm and 550nm.

### **7.2.6. Confocal microscopy**

OE19 cells were plated in a Lab-Tek 8 well chambered borosilicate cover glass (NUNC 155411) at 10,000 cells/well and cultured at 37°C / 5%CO<sub>2</sub>. Cells were cultured for 4hrs in media with and without 0.5 $\mu$ M HuHMFG1 (Figure 66B). For the HuHMFG1 ADC, cells were cultured for 2.5hrs in media with either 0.5 $\mu$ M HuHMFG1:PS1 in the ADC conjugated form or 0.5 $\mu$ M unconjugated HuHMFG1 plus the equivalent amount of free PS1 that was present in the ADC (Figure 68A). For sub cellular localisation studies, cells were cultured for 5hrs with 0.3 $\mu$ M HuHMFG1: Cy5.5 with or without additional 0.3 $\mu$ M Transferrin Alexa Fluor 488 (Molecular Probes, Life Technologies) (Figure 68B). Cells were then fixed with 4% formaldehyde (VWR 361387P) in PBS, permeabilised with 0.1% Triton X-100 (Sigma-Aldrich X100) and blocked with 0.05% Triton X-100, 4% goat serum (Sigma-Aldrich G6767) and 1% bovine serum albumin (Sigma-Aldrich 9418) in PBS. HuHMFG1 was labelled with 0.098 mg/ml of anti-human IgG FITC (Sigma F5512), 0.05% Triton X-100 and 4% goat serum. Cells were then washed and co-stained with 300nM 4',6-Diamidino-2-Phenylindole, Dilactate (DAPI) (Invitrogen D3571) in a mounting media made up from 0.5% N-Propyl gallate (Sigma-



Aldrich P3130), 50% glycerol (VWR 24388.295) in 20mM Tris (Sigma-Aldrich T1503) pH 8. Images were collected at x63 magnification on a Perkin Elmer Spinning Disk Microscopy system using Volocity image acquisition software. FITC or Alexa Fluor 488 fluorescence was collected with excitation at 488nm and detection between 500 and 555nm and is shown in green. DAPI fluorescence was collected with excitation at 405nm and detection between 580 and 650nm and is shown in blue. PS1 or Cy5.5 fluorescence was collected with excitation at 640 nm and detection between 485-705 nm and is shown in red. Single stain control wells were included in the experiments and no bleed through was seen for any of the dyes/channels (data not shown).

### ***7.2.7. Production and characterization of HuHMFG1:PS1***

N-Hydroxysuccinimide activated PS1 (PS1-NHS) was produced as previously published<sup>266</sup> and patented<sup>401</sup>. Small volume aliquots of PS1-NHS or a commercially available Cy5.5 NHS Ester (Amersham, GE Healthcare) were dissolved in DMSO were added progressively into a light protected PBS pH7.4 mixture containing 16.7 $\mu$ M HuHMFG1 and organic solvents at a final concentration of 20% DMSO and 6% MeCN, PS1-NHS or Cy5.5-NHS was added until 16 times molar excess over the protein. The reaction was left shaking and protected from light at room temperature for 2 hours. The resulting conjugates were dialyzed extensively into PBS pH 7.4 through a cellulose membrane with pore size MWCO 7kDa (Slide-A-Lyzer Dialysis Cassettes, 66370, Pierce), to remove unreacted or hydrolysed PS1 as well as any organic solvents, neither gentle dialysis with a larger MWCO or size exclusion chromatography in the presence of low detergent concentrations were sufficient to improve the purity. For UV-VIS analyses a sample was diluted to a suitable concentration into PBS in a micro volume 1 cm path length quartz cuvette and absorbance was measured over 190-400nm on an Agilent 8453 UV Visible Spectrophotometer (Agilent Technologies). Spectra were normalised to 900 nm and PBS background removed. Concentrations were calculated using the following equation  $A = \epsilon lc$  where  $A$  is absorbance of the sample,  $\epsilon$  = molar absorptivity,  $l$  = path length in cm and  $c$  = concentration in molar.

Before spectra could be used to calculate conjugation efficiency, Molar extinction coefficient ( $M^{-1} \text{ cm}^{-1}$ ) and the peak absorption were calculated for the free dyes in PBS and used as follows PS1 ( $A_{280}=8896$ ,  $A_{687}=20594$ ) and Cy5,5 ( $A_{280}=22479$ ,  $A_{674}=215826$ ), a generic IgG molar extinction coefficient was used for HuHMFG1 ( $A_{280}=210000$ ). To calculate conjugation ratio; absorbance of the conjugate at its peak absorbance in the red (678nm or 674nm) was used to obtain the concentration of the dye in the conjugate, this concentration could be used to calculate the contribution of the dye to absorption at 280nm. The remaining  $A_{280}$  is then attributed to the antibody and can be used to calculate the protein concentration. For reducing SDS analysis a sample of the conjugate was then denatured in reducing Laemmli Loading buffer that does not contain a loading dye and run through on 12% Acrylamide SDS-PAGE. Fluorescence of the wet gels was visualised by exciting the photosensitisers with a UV-transilluminator (Fujifilm-LAS3000). Gels were then stained with Coomassie Brilliant Blue to visualise protein. Image analysis techniques of the unstained gel images were used to estimate the proportion of covalently coupled to free photosensitiser in the immunoconjugate mixture using AIDA image Analyzer software v3.52.

### **7.2.8. Cytotoxicity studies**

The cytotoxic efficacy of the HuHMFG1-PS1 ADC was compared with both equivalent concentrations of free HuHMFG1, and free equivalent PS1 in the presence or absence of laser “light” activation. MUC1 positive OE19 cells and MUC1 negative HT29 cells were plated in black walled 96 well plates and allowed to adhere over 24 hours. Cells were incubated at  $37^{\circ}\text{C}$  / 5%  $\text{CO}_2$  in the dark with various doses of HuHMFG1, PS1 or HuHMFG1:PS1 ADC in supplemented cell culture media without phenol red (Sigma-Aldrich R7509) plus 2% DMSO. Controls included triton X 100 (100% cell death), culture media with 2% DMSO (vehicle control) and media alone with and without cells. After 2 hours cells were washed and returned to normal media and left at  $37^{\circ}\text{C}$  / 5%  $\text{CO}_2$  for a further hour. Where cells were irradiated laser, light was delivered at 670nm [0.33J/cm<sup>2</sup> over 10seconds] (HPD 7401 laser system, High Power Devices Inc). Dark

controls were not lasered. Cell viability was measured 48 hours later with MTS assay (Promega Cell Titre-96) via absorbance at 490nm. Background absorbance was removed using cells that had been lysed using triton X 100 and % cell viability was calculated using the cells in media only. Cytotoxicity between cell types was compared using the Students T-Test (Microsoft Excel). Dose response curves comparing cytotoxicity of HuHMFG1:PS1 ADC versus equivalent PS1 alone in light and dark were compared using linear regression analysis assigning best fit curves on a log scale (GraphPad PRISM®).

### **7.3. Results**

#### ***7.3.1. Identification of MUC1 as a biomarker in the development of OA***

MUC1 was linked to the progression to OA using gene set enrichment analysis (GSEA). Within the GSEA two groups of upper GI samples were compared; the comparison of non-dysplastic Barrett's oesophagus (NDBE) to normal oesophageal squamous epithelium (Sq) gave 47 pathways that were enriched in NDBE compared to Sq, of which 28 were significant and of these 21% included MUC1. Comparison of OA to Sq gave 49 pathways enriched in OA compared to Sq of which 27 pathways were significant and of these 30% included MUC1 (Figure 58). This recurrent appearance of MUC1 in the significant pathways suggests involvement in the transition of normal oesophageal tissue to malignancy. Some of the most significant pathways included both MUC1 and HER2.

Figure 58: Gene set enrichment analysis highlighting pathways during development of Barrett's oesophagus (A) and oesophageal adenocarcinoma (B) from normal squamous oesophagus and the involvement of MUC1 within them.

**A**

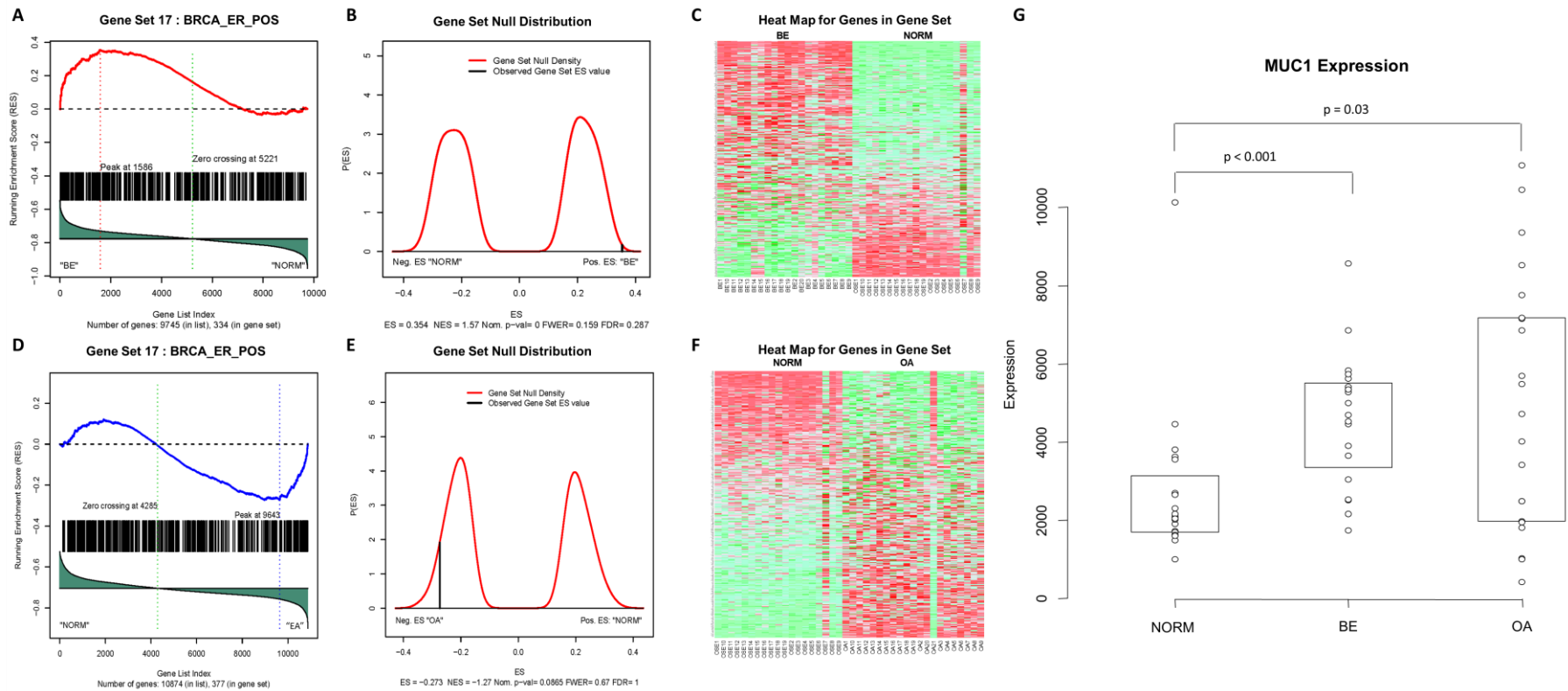
Gene Set	Contains MUC1	SIZE	Enrichment Score (ES)	Normalised ES	Nominal p-value	False Discovery Rate (FDR) q-val	FWER p-val	Tag %	Gene %	Signal	FDR (median)	glob. p.val
BRCA_ER_POS	YES	334	0.38703	1.7166	0	0.032246	0.04527	0.371	0.292	0.272	0	0.01
POST_TRANSLATIONAL_PROTEIN_MODIFICATION	NO	273	0.31988	1.6258	0	0.023622	0.1076	0.516	0.47	0.282	0	0
PROTEIN_MODIFICATION_PROCESS	NO	354	0.32404	1.6101	0	0.022916	0.1217	0.517	0.47	0.285	0	0
CELL_PROLIFERATION_GO_0008283	NO	280	0.34251	1.5959	0	0.024012	0.1348	0.5	0.447	0.285	0	0
REGULATION_OF_CATALYTIC_ACTIVITY	NO	161	0.31555	1.5358	0	0.02607	0.2183	0.578	0.524	0.28	0	0
REGULATION_OF_MOLECULAR_FUNCTION	NO	181	0.30988	1.5256	0	0.027405	0.2354	0.453	0.423	0.266	0	0
HSC_HSCANDPROGENITORS_ADULT	YES	353	0.31448	1.6321	0.001976	0.025468	0.1056	0.227	0.207	0.186	0	0
PROLIFERATION_GENES	NO	207	0.37767	1.5887	0.002008	0.024533	0.1459	0.512	0.421	0.303	0	0
TRANSMEMBRANE_RECEPTOR_PROTEIN_TYROSINE_KINASE_SIGNALING_PATHWAY	NO	47	0.41241	1.6706	0.002066	0.03709	0.08249	0.404	0.289	0.289	0	0.008
PHOSPHORYLATION	NO	178	0.30448	1.4936	0.003717	0.029863	0.2706	0.517	0.469	0.279	0	0
HSC_HSCANDPROGENITORS_FETAL	YES	345	0.29927	1.5647	0.003945	0.020216	0.17	0.214	0.207	0.176	0	0
CELL_SURFACE_RECEPTOR_LINKED_SIGNAL_TRANSDUCTION_GO_0007166	NO	297	0.37034	1.5846	0.004024	0.023231	0.1479	0.444	0.372	0.288	0	0
REGULATION_OF_CELL_PROLIFERATION	NO	166	0.37084	1.5742	0.004065	0.019073	0.1559	0.494	0.42	0.292	0	0
REGULATION_OF_PROTEIN_KINASE_ACTIVITY	NO	100	0.36053	1.6456	0.005837	0.025088	0.09457	0.46	0.387	0.285	0	0
REGULATION_OF_KINASE_ACTIVITY	NO	101	0.36433	1.6588	0.005871	0.029898	0.08954	0.465	0.387	0.288	0	0.003
REGULATION_OF_KINASE_ACTIVITY	NO	101	0.36433	1.6588	0.005871	0.029898	0.08954	0.465	0.387	0.288	0	0.003
REGULATION_OF_MAP_KINASE_ACTIVITY	NO	45	0.44114	1.6918	0.006024	0.034542	0.06338	0.6	0.387	0.369	0	0.008
ENZYME_LINKED_RECEPTOR_PROTEIN_SIGNALING_PATHWAY	NO	84	0.37688	1.577	0.006316	0.019792	0.1549	0.452	0.368	0.288	0	0
PROTEIN_AMINO_ACID_PHOSPHORYLATION	NO	163	0.31151	1.4874	0.007634	0.029468	0.2817	0.521	0.469	0.281	0	0
REGULATION_OF_TRANSFERASE_ACTIVITY	NO	102	0.36706	1.6585	0.007921	0.026326	0.09054	0.471	0.387	0.291	0	0
POSITIVE_REGULATION_OF_MAP_KINASE_ACTIVITY	NO	28	0.47933	1.5825	0.01022	0.022252	0.1489	0.607	0.366	0.386	0	0
LEI_MYB_REGULATED_GENES	YES	218	0.41855	1.6212	0.01597	0.022352	0.1097	0.541	0.391	0.337	0	0
CELL_PROLIFERATION	NO	118	0.3645	1.5775	0.018	0.020679	0.1549	0.559	0.451	0.311	0	0
SHEPARD_CELL_PROLIFERATION	NO	118	0.3645	1.5775	0.018	0.020679	0.1549	0.559	0.451	0.311	0	0
CELL_GROWTH_AND_OR_MAINTENANCE	NO	39	0.44008	1.496	0.02	0.030252	0.2656	0.487	0.347	0.32	0	0
TPA_SENS_MIDDLE_DN	YES	187	0.31567	1.4612	0.02037	0.035419	0.326	0.54	0.494	0.278	0	0
FRASOR_ER_DN	NO	47	0.40692	1.4932	0.02204	0.029019	0.2716	0.553	0.394	0.337	0	0
BREAST_CANCER_ESTROGEN_SIGNALING	YES	63	0.41189	1.5035	0.04225	0.029637	0.2515	0.365	0.262	0.271	0	0
CIS_XPC_UP	YES	98	0.36627	1.5002	0.05758	0.029279	0.2555	0.306	0.27	0.226	0	0
HUMAN_TISSUE_PANCREAS	YES	24	0.40599	1.3091	0.09393	0.10168	0.5875	0.25	0.193	0.202	0.054994	0
TPA_RESIST_EARLY_DN	YES	50	0.35588	1.2717	0.1113	0.12427	0.6398	0.16	0.0938	0.146	0.072983	0
MITOCHONDRIA	NO	183	0.25868	1.2262	0.1717	0.15843	0.7103	0.568	0.551	0.26	0.105	0.001
TPA_RESIST_MIDDLE_DN	YES	70	0.30725	1.1826	0.1738	0.1856	0.7787	0.514	0.506	0.256	0.13462	0.001
FERNANDEZ_MYC_TARGETS	YES	94	0.31121	1.2226	0.1814	0.15796	0.7163	0.574	0.506	0.286	0.1047	0
BRCA1_OVEREXP_PROSTATE_UP	YES	117	0.30584	1.2071	0.1835	0.16934	0.7435	0.65	0.56	0.289	0.12039	0.001
HSA04012_ERBB_SIGNALING_PATHWAY	NO	53	0.28765	1.178	0.2037	0.18444	0.7797	0.472	0.46	0.256	0.13611	0
LINDSTEDT_DEND_8H_VS_48H_DN	YES	51	0.34768	1.2028	0.2153	0.16896	0.7475	0.667	0.512	0.327	0.11722	0.001
BREASTCA_TWO_CLASSES	NO	83	0.29425	1.1702	0.2484	0.18856	0.7867	0.386	0.379	0.241	0.14285	0
DRUG_RESISTANCE_AND_METABOLISM	NO	61	0.31168	1.1463	0.278	0.20944	0.8139	0.508	0.484	0.264	0.16204	0
NfKBinduc_w_MUC1	YES	161	0.314	1.1148	0.2992	0.23881	0.8431	0.255	0.229	0.2	0.18992	0
BROCKE_IL6	YES	106	0.2655	1.0985	0.3314	0.24917	0.8622	0.406	0.442	0.229	0.2084	0
KRETZSCHMAR_IL6_DIFF	YES	106	0.2655	1.0985	0.3314	0.24917	0.8622	0.406	0.442	0.229	0.2084	0
KLEIN_PEL_UP	YES	33	0.29514	1.0633	0.3397	0.28796	0.8833	0.727	0.589	0.3	0.25946	0
HYPOXIA_REG_UP	YES	27	0.33519	0.93025	0.5752	0.52142	0.9678	0.741	0.559	0.327	0.52128	0.004
CHAUHAN_2ME2	YES	30	0.29025	0.90195	0.6055	0.56545	0.9688	0.533	0.528	0.252	0.58333	0.006
RADIATION_SENSITIVITY	NO	15	0.26098	0.77633	0.7752	0.80357	0.9889	0.267	0.326	0.18	0.8524	0.062

# B

Gene Set	Contains MUC1	SIZE	Enrichment Score (ES)	Normalised ES	Nominal p-value	False Discovery Rate (FDR) q-val	FWER p-val	Tag %	Gene %	Signal	FDR (median)	glob. p-val
TPA_RESIST_EARLY_DN	YES	52	0.42742	1.6617	0	0.031003	0.1041	0.269	0.169	0.225	0	0.003
PROTEIN_MODIFICATION_PROCESS	NO	388	0.30516	1.5859	0	0.045142	0.1702	0.309	0.293	0.227	0	0.003
FERNANDEZ_MYC_TARGETS	YES	109	0.39083	1.7664	0	0.015905	0.04404	0.44	0.347	0.291	0	0.002
TRANSMEMBRANE_RECEPTOR_PROTEIN_TYROSINE_KINASE_SIGNALING_PATHWAY	NO	48	0.49821	1.9249	0	0.0038311	0.005005	0.458	0.287	0.328	0	0.001
ENZYME_LINKED_RECEPTOR_PROTEIN_SIGNALING_PATHWAY	NO	87	0.43756	1.8645	0	0.0084891	0.01502	0.356	0.227	0.278	0	0.001
BRCA_ER_POS	YES	377	0.37525	1.7535	0	0.013113	0.04905	0.366	0.302	0.265	0	0.001
POST_TRANSLATIONAL_PROTEIN_MODIFICATION	NO	294	0.29568	1.4925	0	0.042743	0.3073	0.306	0.293	0.222	0	0.001
REGULATION_OF_MAP_KINASE_ACTIVITY	NO	44	0.46894	1.7623	0.001905	0.013432	0.04505	0.477	0.287	0.341	0	0.001
LEI_MYB_REGULATED_GENES	YES	240	0.43097	1.7861	0.002141	0.015645	0.03403	0.454	0.315	0.318	0	0.004
REGULATION_OF_PROTEIN_KINASE_ACTIVITY	NO	101	0.37146	1.5852	0.005714	0.041711	0.1722	0.426	0.322	0.291	0	0.003
HSC_HSCANDPROGENITORS_FETAL	YES	397	0.30164	1.521	0.005859	0.040204	0.2613	0.338	0.336	0.233	0	0
HSC_HSCANDPROGENITORS_ADULT	YES	408	0.30283	1.5266	0.005871	0.040631	0.2502	0.336	0.333	0.233	0	0.001
REGULATION_OF_CELL_PROLIFERATION	NO	184	0.37611	1.6016	0.005952	0.045447	0.1612	0.413	0.329	0.282	0	0.005
REGULATION_OF_KINASE_ACTIVITY	NO	102	0.36812	1.5612	0.007678	0.042096	0.1972	0.422	0.322	0.289	0	0.002
REGULATION_OF_KINASE_ACTIVITY	NO	102	0.36812	1.5612	0.007678	0.042096	0.1972	0.422	0.322	0.289	0	0.002
REGULATION_OF_CATALYTIC_ACTIVITY	NO	165	0.32708	1.5335	0.009881	0.042522	0.2402	0.388	0.345	0.258	0	0.001
REGULATION_OF_TRANSFERASE_ACTIVITY	NO	103	0.36712	1.556	0.01163	0.038658	0.2022	0.417	0.322	0.286	0	0.001
BRCA1_OVEREXP_PROSTATE_UP	YES	122	0.38177	1.5293	0.012	0.042042	0.2482	0.443	0.365	0.284	0	0.001
POSITIVE_REGULATION_OF_MAP_KINASE_ACTIVITY	NO	28	0.48034	1.6274	0.01426	0.037837	0.1361	0.464	0.264	0.342	0	0.002
CELL_PROLIFERATION_GO_0008283	NO	307	0.34584	1.5002	0.01765	0.045728	0.2893	0.388	0.324	0.27	0	0.002
CELL_GROWTH_AND_OR_MAINTENANCE	NO	46	0.46253	1.5573	0.02209	0.040646	0.2012	0.326	0.174	0.271	0	0.002
CELL_SURFACE_RECEPTOR_LINKED_SIGNAL_TRANSDUCTION_GO_0007166	NO	323	0.37928	1.5372	0.02231	0.044058	0.2372	0.35	0.287	0.257	0	0.001
REGULATION_OF_MOLECULAR_FUNCTION	NO	184	0.30918	1.4265	0.02245	0.054469	0.3944	0.375	0.345	0.25	0	0
PROLIFERATION_GENES	NO	229	0.35774	1.4399	0.02677	0.052864	0.3784	0.393	0.332	0.268	0	0
CELL_PROLIFERATION	NO	128	0.39426	1.4968	0.0334	0.042917	0.2953	0.398	0.296	0.284	0	0.001
SHEPARD_CELL_PROLIFERATION	NO	128	0.39426	1.4968	0.0334	0.042917	0.2953	0.398	0.296	0.284	0	0.001
KLEIN_PEL_UP	YES	34	0.40858	1.4709	0.04008	0.044725	0.3303	0.412	0.333	0.275	0	0
DRUG_RESISTANCE_AND_METABOLISM	NO	56	0.39119	1.4288	0.04483	0.055736	0.3934	0.429	0.318	0.294	0	0.001
TPA_SENS_MIDDLE_DN	YES	217	0.30057	1.3753	0.054	0.067614	0.4965	0.41	0.394	0.253	0	0
PHOSPHORYLATION	NO	193	0.27325	1.3428	0.05697	0.078203	0.5495	0.601	0.565	0.266	0.037926	0
POSITIVE_REGULATION_OF_TRANSFERASE_ACTIVITY	NO	52	0.37675	1.4523	0.06012	0.049866	0.3644	0.404	0.322	0.275	0	0
BREAST_CANCER_ESTROGEN_SIGNALING	YES	69	0.37944	1.4049	0.07292	0.058909	0.4424	0.507	0.42	0.296	0	0
BREAST_CANCER_ESTROGEN_SIGNALING	YES	69	0.37944	1.4049	0.07292	0.058909	0.4424	0.507	0.42	0.296	0	0
HSA04012_ERBB_SIGNALING_PATHWAY	NO	53	0.34618	1.3503	0.07407	0.076464	0.5385	0.396	0.339	0.263	0.037838	0
HUMAN_TISSUE_PANCREAS	YES	25	0.4677	1.3793	0.08119	0.06806	0.4925	0.32	0.156	0.271	0	0
FRASOR_ER_DN	NO	56	0.41148	1.405	0.08317	0.062591	0.4424	0.554	0.402	0.333	0	0
NFkBInduc_w_MUC1	YES	177	0.42197	1.468	0.08583	0.046157	0.3373	0.322	0.223	0.254	0	0
PROTEIN_AMINO_ACID_PHOSPHORYLATION	NO	174	0.2653	1.2565	0.1277	0.12926	0.6757	0.598	0.565	0.264	0.083761	0.001
MITOCHONDRIA	NO	193	0.24052	1.203	0.1646	0.16388	0.7638	0.528	0.554	0.24	0.12017	0.001
TPA_RESIST_MIDDLE_DN	YES	78	0.30059	1.1966	0.1798	0.16615	0.7728	0.167	0.13	0.146	0.12661	0
BROCKE_IL6	YES	120	0.30288	1.2202	0.2045	0.15131	0.7297	0.417	0.404	0.251	0.10865	0.001
KRETZSCHMAR_IL6_DIFF	YES	120	0.30288	1.2202	0.2045	0.15131	0.7297	0.417	0.404	0.251	0.10865	0.001
CIS_XPC_UP	YES	109	0.30026	1.184	0.2227	0.17448	0.7898	0.349	0.333	0.235	0.13364	0
BREASTCA_TWO_CLASSES	NO	90	0.26542	1.1385	0.2724	0.21068	0.8218	0.322	0.362	0.207	0.17376	0
HYPOXIA_REG_UP	YES	32	0.374	1.1776	0.2843	0.17691	0.7968	0.625	0.477	0.328	0.13611	0
LINDSTEDT_DEND_8H_VS_48H_DN	YES	53	0.35692	1.1745	0.286	0.17601	0.7968	0.434	0.417	0.254	0.13701	0
CHAUHAN_2ME2	YES	33	0.24302	0.89983	0.6198	0.56762	0.986	0.636	0.625	0.239	0.57939	0.008
RADIATION_SENSITIVITY	NO	16	0.21347	0.63316	0.8934	0.96488	0.998	0.375	0.437	0.212	1	0.606

Significant pathways are highlighted in blue text. Any involvement of MUC1 is shown highlighted by the orange shaded box.

**Figure 59: Gene set enrichment and microarray analysis of MUC1 in the progression to esophageal adenocarcinoma.**



Heat map (A) and an example probability plot (B) of the gene set enrichment analysis (GSEA) for non-dysplastic Barrett's oesophagus (NDBE) vs normal squamous esophageal epithelium (Sq). Heat map (C) and an example probability plot (D) of the GSEA for esophageal adenocarcinoma (OA) vs Sq. GSEA detail in Figure 58 and evaluated with Kolmogrov-Smirnoff test. Microarray analysis (E); raw expression values of MUC1 mRNA in Sq, NDBE and OA tissues. Box plot presented as median and interquartile range.

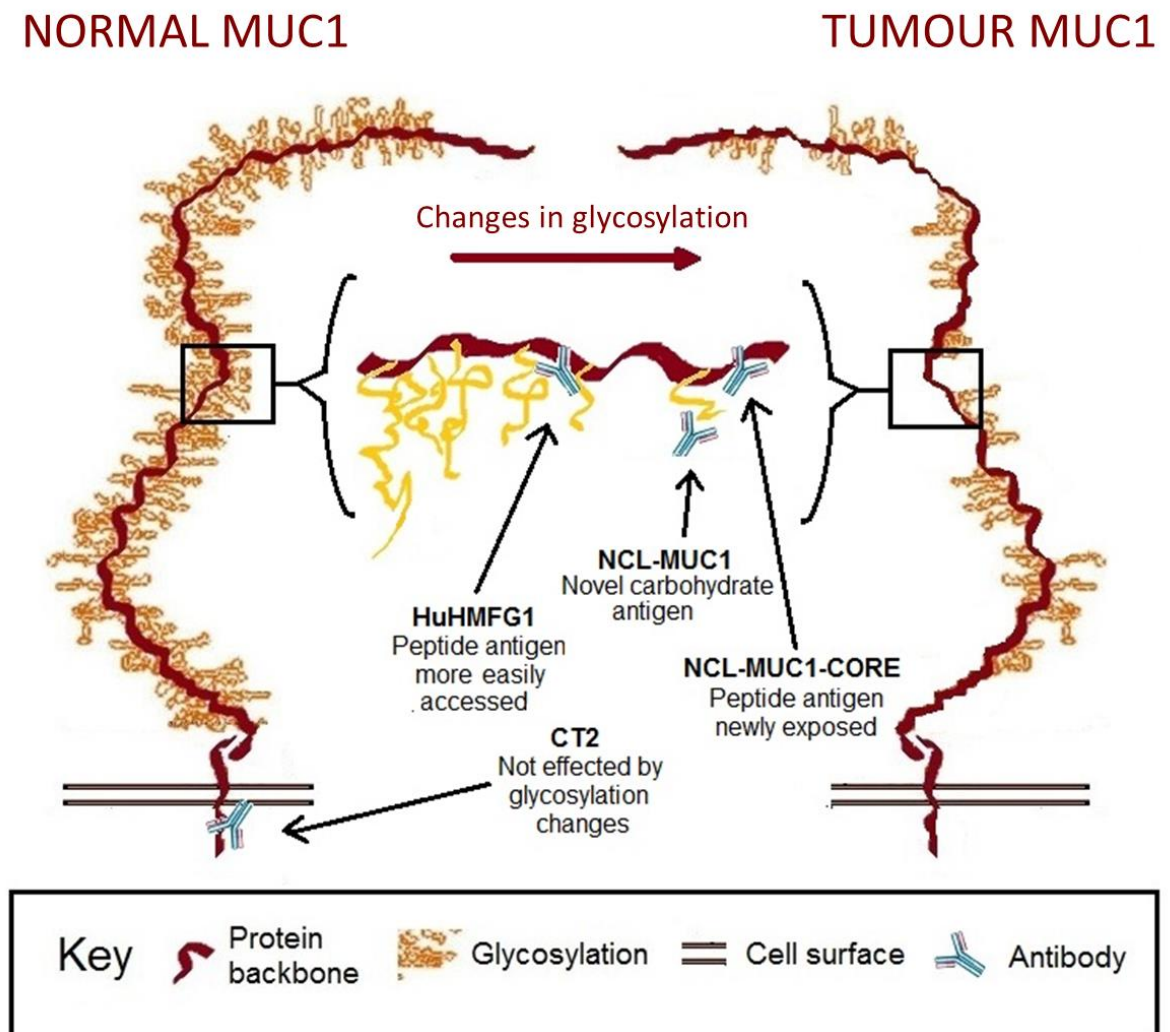
To see if the MUC1 gene was up regulated during cancer progression the data was mined using the Affymetrix probe for MUC1 to retrieve raw gene expression values. When compared to Sq, mRNA levels in NDBE show a 2.3-fold increase in MUC1 expression ( $p < 0.001$ ), while mRNA levels in OA showed an increase in the both the range of expression as well as an overall 2.2-fold increase in MUC1 expression ( $p = 0.03$ ) (Figure 59).

### **7.3.2. MUC1 glycoprotein tissue staining**

#### **7.3.2.1. MUC1 IHC expression by antibodies targeting different epitopes**

Four antibodies were used to stain patient samples representing various stages toward progression to cancer; Sq epithelium, NDBE, low-grade dysplasia (LGD), high grade dysplasia (HGD) and invasive oesophageal adenocarcinoma (OA). Each antibody binds a unique epitope of the MUC1 receptor illustrated in Figure 60. NCL-MUC1 binds a sialic acid on the glycosylated side chain, while NCL-MUC-1-CORE and HuHMFG1 bind the extracellular peptide backbone. The extracellular target antigens can be hidden in fully glycosylated normal tissue but become increasingly exposed in cancer due to aberrant glycosylation. CT2 targets the intracellular cytoplasmic tail of MUC1.

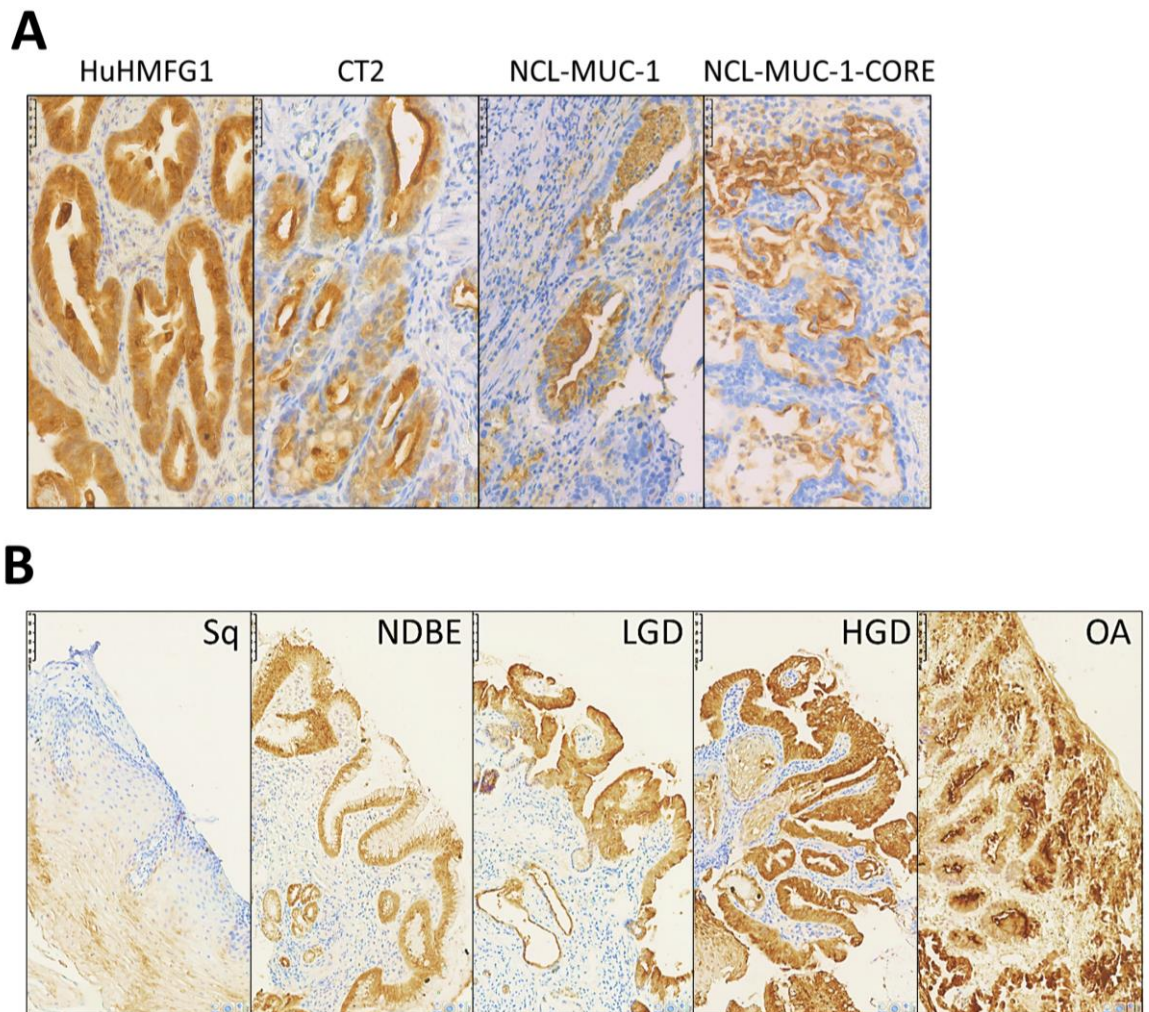
**Figure 60: Representation of MUC1 receptor structure in normal and tumour epithelium with binding sites for selected antibodies.**



HuHMFG1 immunostaining was mostly membranous and cytoplasmic with additional nuclear staining in highly expressing samples. CT2 and NCL-MUC-1 stained predominantly the apical membrane with mild cytoplasmic positivity. NCL-MUC-1-CORE staining was focused on the luminal surface of cells. In all cases binding was limited to the epithelial cell layer. The intensity of HuHMFG1 staining increased in the progression to OA, and towards the more differentiated superficial epithelial cells (Figure 61).



**Figure 61: IHC staining patterns with anti-MUC1 antibodies in high grade dysplasia and HuHMFG1 staining in the squamous-metaplasia-dysplasia-carcinoma sequence.**

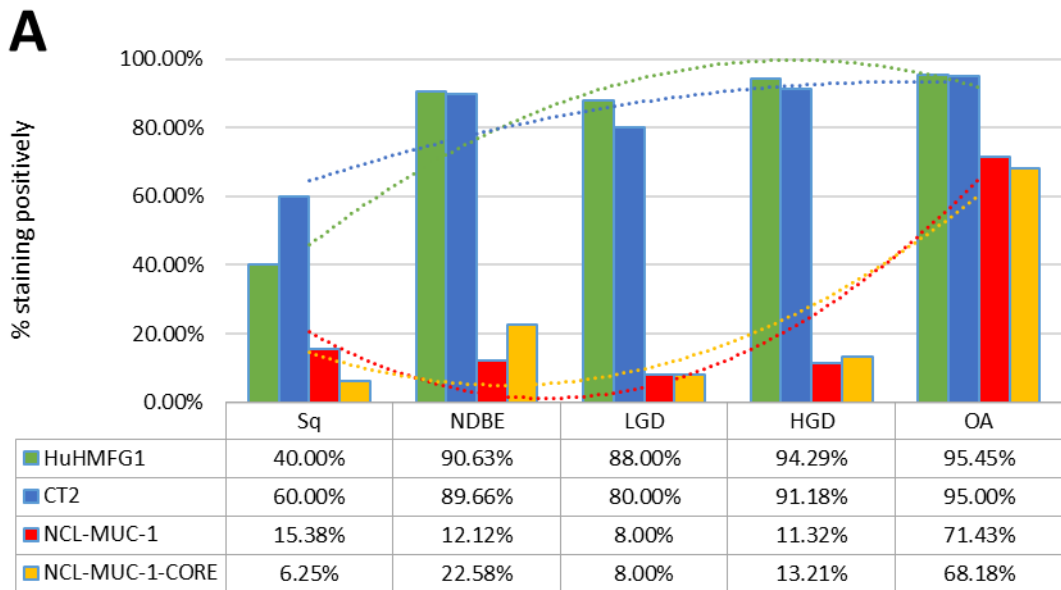


Increasing MUC1 staining intensity and extent accompanies progression to esophageal cancer

*(A) Immunohistochemical images of high-grade dysplasia (HGD) in BE stained with four anti-MUC1 antibodies (brown), and haematoxylin (blue). (B) HuHMFG1 staining in normal oesophageal squamous epithelium (Sq), non-dysplastic BE (NDBE), low-grade dysplasia (LGD), HGD and invasive (OA). An increase in the intensity of staining is seen as pathological grades progress. Staining also follows the direction of epithelial maturation from basement membrane toward the lumen. In higher pathological grades, staining is seen throughout the epithelial layer.*

HuHMFG1 and CT2 binding increased from moderate in squamous mucosa to high levels in NDBE. NCL-MUC-1 and NCL-MUC-1-CORE maintained low binding levels in normal and dysplastic tissue but increased to high levels of binding in OA tissue (Figure 62). An alternative representation (Figure 63) shows the Allred score of individual samples and is presented to show the heterogeneity of all four antibodies across all pathological grades. Due to the recognised OA risk of dysplastic columnar epithelium, and a desire to target it therapeutically<sup>1,58</sup>, HuHMFG1 was selected as the optimum antibody to take forward for therapeutic development over CT2 as the latter is not as suitable for ADC development due to its intracellular location. Since it was shown HuHMFG1 bound some normal epithelium, development as a photoimmunoconjugate was chosen as the use of light to selectively activate the drug in a local area could be used to avoid the majority of normal epithelium which can be distinguished endoscopically.

**Figure 62: Levels of expression of four MUC1 epitopes in the squamous-metaplasia-dysplasia-carcinoma sequence.**

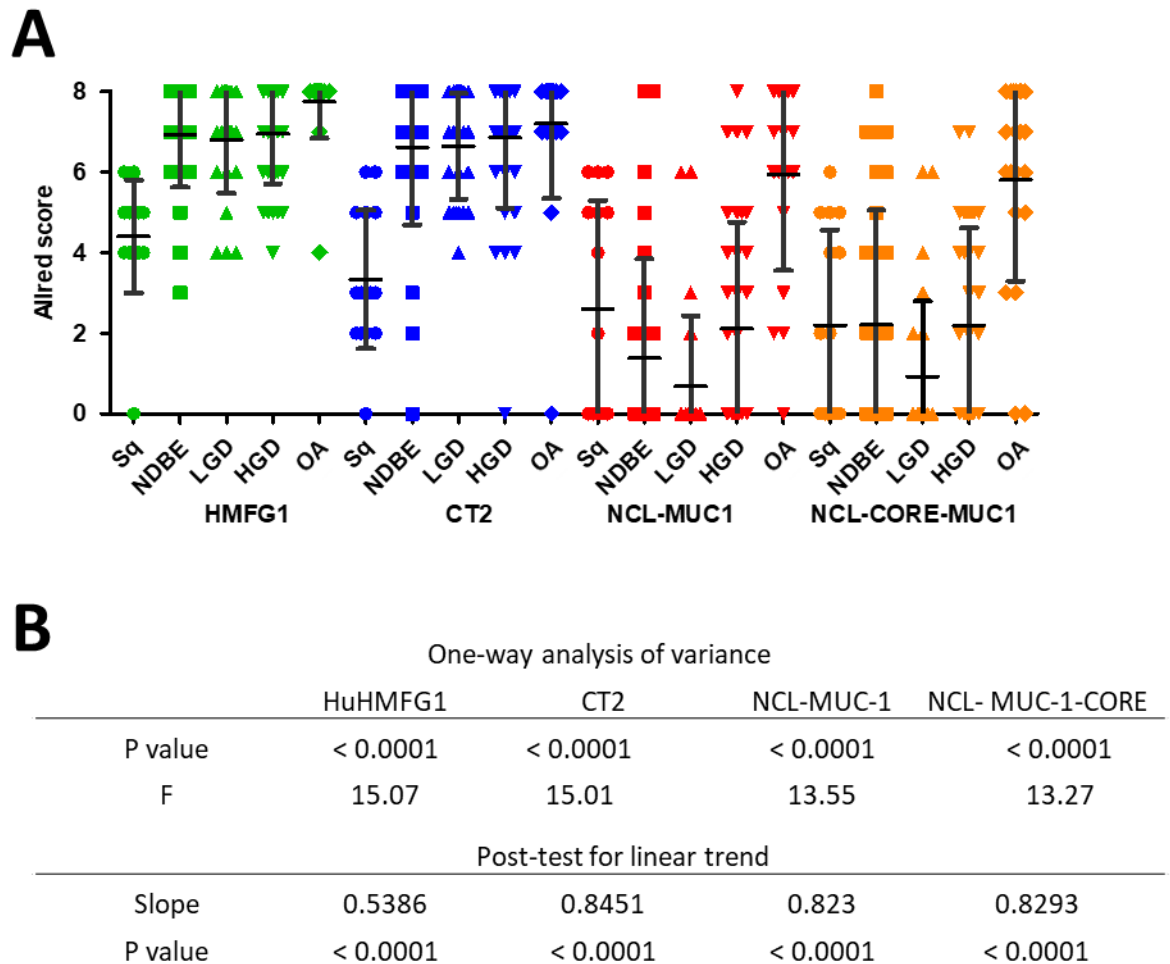


**B**

	$\chi^2$	p	Pearson's R	SE	p
HuHMFG1	74.659	0.0000004	0.4589	0.0722	<0.0001
CT2	83.84	0.0000002	0.4098	0.0933	<0.0001
NCL-MUC-1	70.38	0.0000165	0.3368	0.0892	<0.0001
NCL-MUC-1-CORE	66.882	0.0000501	0.3062	0.0878	0.0010

(A) HuHMFG1, CT2, NCL-MUC-1 and NCL-MUC-1-CORE were evaluated by IHC in oesophageal tissue from incremental pathological grades. The proportion of positive samples for each tissue is shown with respectively coloured polynomial lines of best fit. HuHMFG1 and CT2 staining increase at the metaplastic (NBDE) stage, whereas NCL antibodies increase staining after development of OA. (B) All antibodies showed significant expression differences during progression to cancer ( $\chi^2$  test;  $p < 0.00005$ ), with all having a significant trend of increasing positivity (Pearson's R;  $p < 0.001$ ).

**Figure 63: Scatter plot depicting IHC expression of four MUC1 epitopes in the oesophageal squamous-metaplasia-dysplasia-carcinoma sequence scored by Allred.**



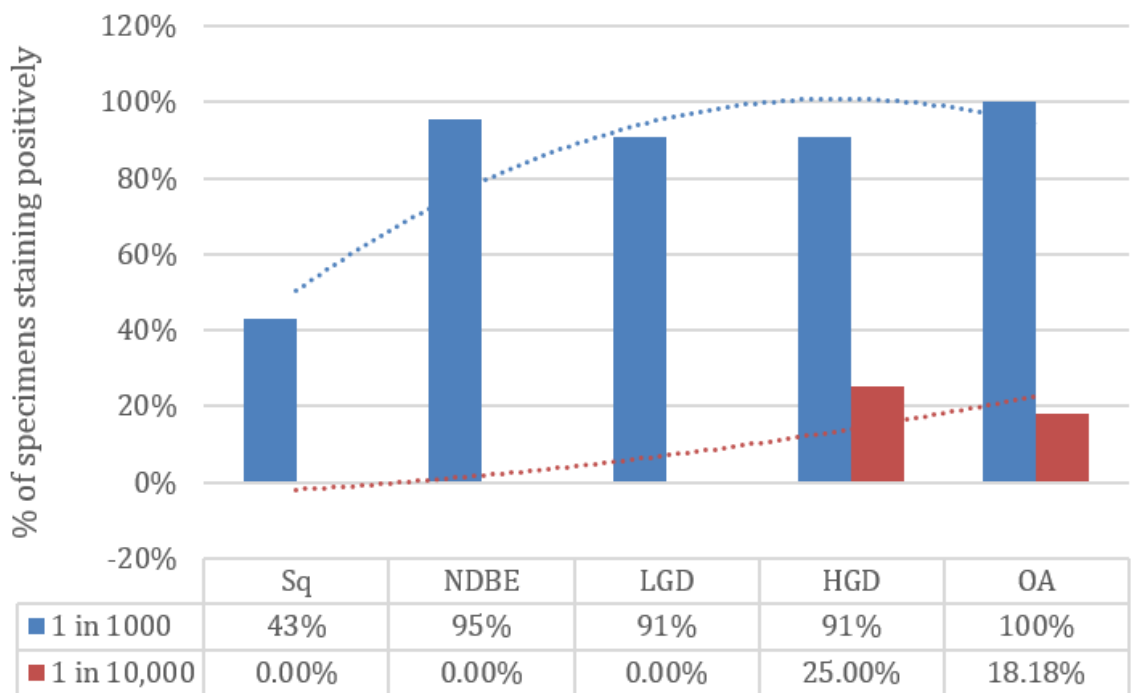
(A) IHC expression of HuHMFG1, CT2, NCL-MUC-1 and NCL-MUC-1-CORE were evaluated with the Allred score in tissue specimens during oesophageal cancer development. The Allred score (0- to 8) combines the proportion of cells that stain positive (on a scale of 0 to 5) with staining intensity (on a scale of 0 to 3). Allred is plotted for each sample with mean and standard deviation. (B) All antibodies show a statistically significant incremental increase in positivity during progression to cancer.

### 7.3.2.2. Improvement in tumour selectivity with HuHMFG1 antibody dilution

HuHMFG1 staining at the optimised concentration was sensitive (95% of cancers were identified as positive) but not specific (40% of normal tissue also stained positive).

Specificity for HGD and OA could be demonstrated by using a less antibody (0% staining in Sq, NDBE and LGD) however this was at the expense of substantially reduced sensitivity (positive staining in HGD and OA fell to ~20%) (Figure 64).

**Figure 64: HuHMFG1 immunostaining optimised to achieve tumour selectivity.**

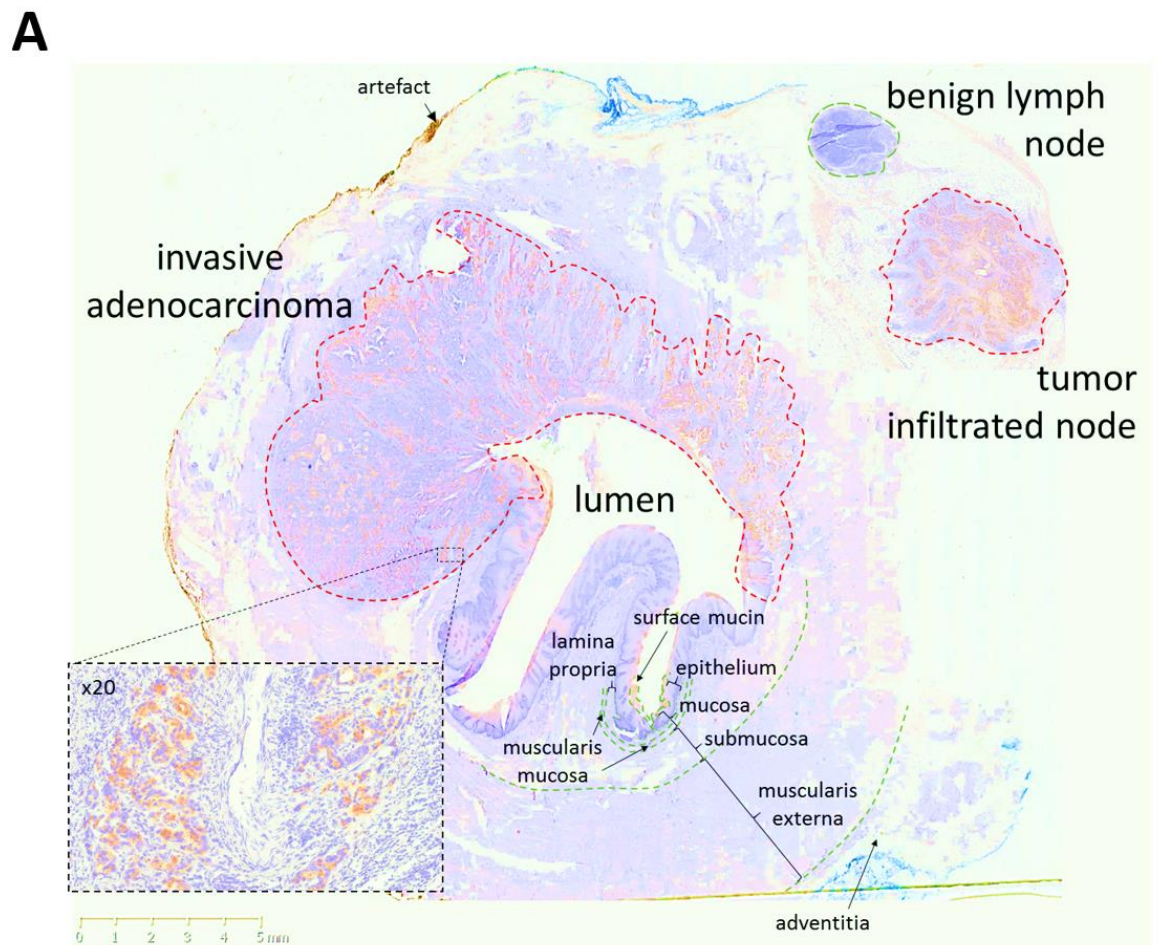


*HuHMFG1 antibody concentration was re-optimised to maintain positivity in higher grade pathologies, whilst excluding normal squamous (Sq) positivity. This concentration was found to be 10x fold less than that used in the original experiment (1:1000 vs 1:10,000). Specificity was achieved for high grade dysplasia (HGD) and oesophageal adenocarcinoma (OA) but at the expense of reduced sensitivity for metaplasia and dysplasia; absent staining in Sq, non-dysplastic Barrett's epithelium (NDBE), and low-grade dysplasia (LGD).*

### 7.3.2.3. MUC1 expression in cancer with locoregional nodal spread

Staining of resection specimens demonstrated that HuHMFG1 does not bind normal connective tissue, vascular or muscular structures of the oesophagus. The epithelial specificity of HuHMFG1 is demonstrated exquisitely in Figure 65 in which a whole oesophagus transverse section taken from a patient with OA was stained with HuHMFG1. This section includes 2 lymph nodes, one infiltrated with cancer and one free of disease. HuHMFG1 selectively stains only the infiltrated node. To confirm this pattern in lymph nodes, staining was extended to a panel of 11 OA resection specimens with 31 associated locoregional nodes. HuHMFG1 staining was positive in all 18 tumour infiltrated lymph nodes and negative in all 13 benign nodes (Fishers exact  $p < 0.0001$ ). This reinforces the choice for HuHMFG1 for therapeutically application as any off target effects in normal areas would spare connective, muscular and vascular tissue and damaged normal squamous mucosa can regrow<sup>402</sup>.

**Figure 65: HuHMFG1 staining MUC1 in invasive oesophageal adenocarcinoma and locoregional lymph node metastases.**



**B**

Node status	MUC1 positive	MUC1 negative
Cancer infiltrated	18	0
Benign	0	13

(A) A oesophagectomy section stained with HuHMFG1 (brown) and haematoxylin (blue). HuHMFG1 stains surface mucin, invasive OA as it invades into muscularis externa and only the local tumour infiltrated lymph node. Normal mucosa and a benign local lymph node did not stain. A x20 magnification from a representative tumour region is inset. (B) Analysis of 31 locoregional nodes resected from 11 patients highlight positive expression of MUC1 by HuHMFG1 in all malignant but no benign lymph nodes (Fishers exact;  $p < 0.0001$ ).

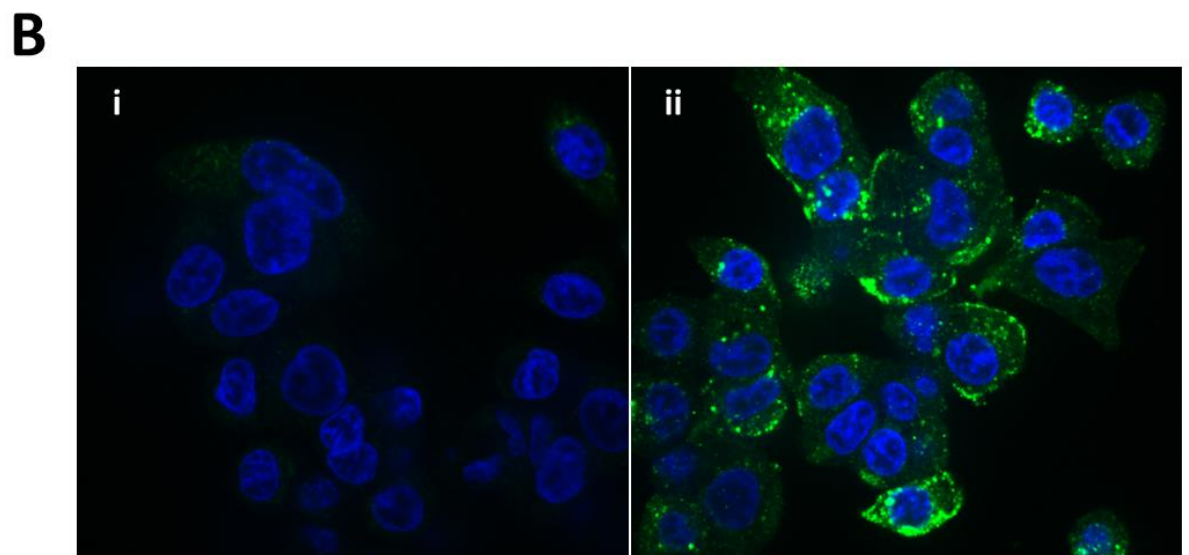
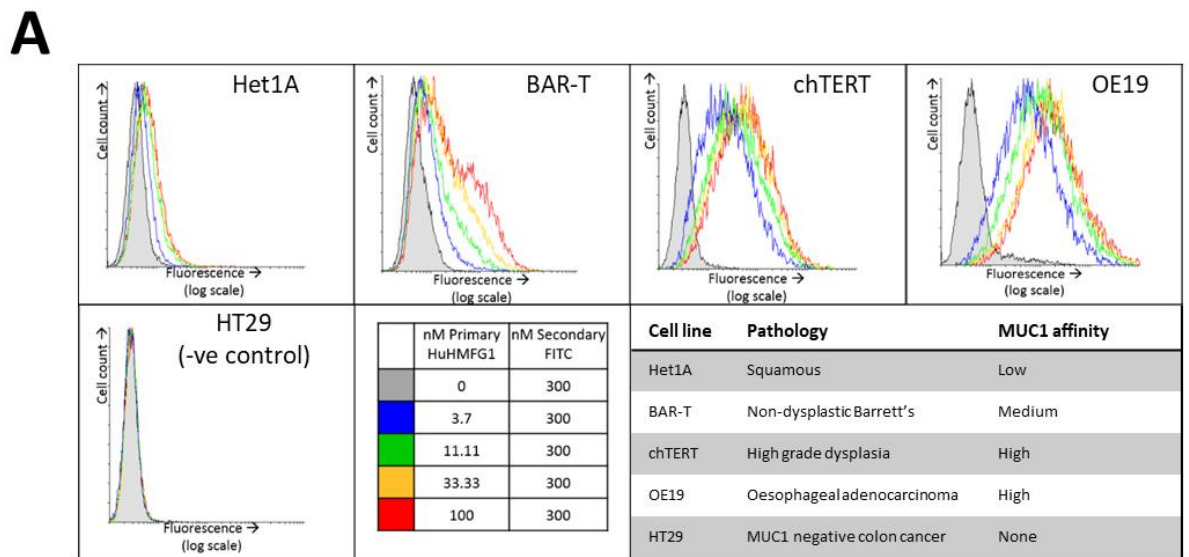
### **7.3.3. HuHMFG1 potential as a therapeutic antibody in living cells**

To confirm binding to native antigen in living cells, HuHMFG1 was tested *in vitro* on a panel of oesophageal cell lines derived from each stage in the squamous-metaplasia-dysplasia-carcinoma sequence. All OA lines showed a dose dependent increase in cell binding of HuHMFG1 to a point of cell surface receptor saturation; HuHMFG1 binding was at a low level in normal squamous cells (Het1A) but then incrementally increased through NDBE cells (BAR-T), HGD cells (chTERT) with the highest level of binding seen in OA cells (OE19) (Figure 66A).

For an effective ADC, it is preferable but not required that it underwent intracellular internalisation after binding. Using confocal microscopy, internalisation of HuHMFG1 into an OA cell line (OE19) was shown (Figure 66B). The punctate intracellular pattern is similar to the pattern seen in previous work where endosomal co-localisation of HuHMFG1 was demonstrated in a breast cancer cell line<sup>264</sup>.



**Figure 66: MUC-1 expression in oesophageal cell lines of various pathological grades and internalisation into oesophageal adenocarcinoma.**



*(A) HuHMFG1 binding in vitro to oesophageal cell lines isolated from various pathological oesophageal grades was carried out using flow cytometry. HuHMFG1 was detected using a FITC conjugated anti-human IgG secondary fluorescent antibody (green) shown alongside nuclei staining with DAPI (blue). An increase in fluorescence represents more HuHMFG1 bound to each cell and the saturation of the fluorescent signal indicates cell surface receptor saturation. HuHMFG1 did not bind the colonic line HT29 (negative control). It bound at a low level in normal squamous and non-dysplastic*

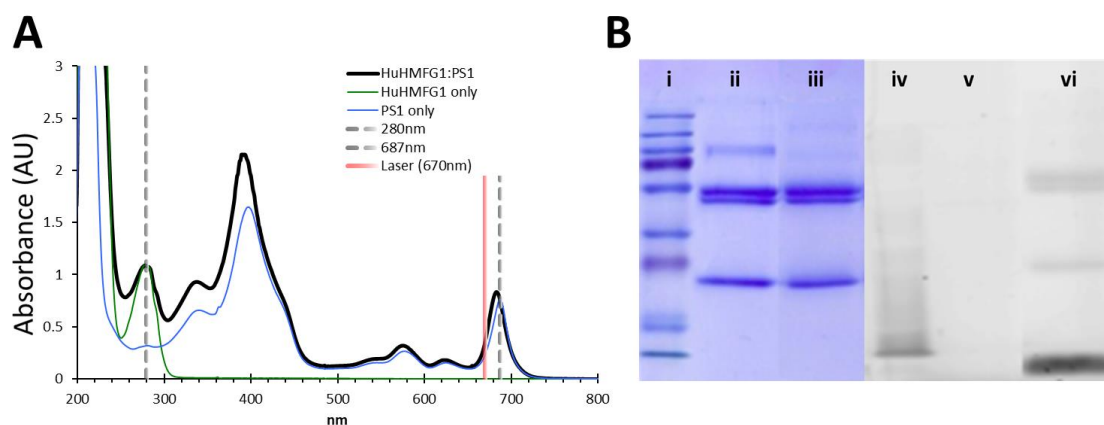
*Barrett's epithelium and a high level in high grade dysplasia and oesophageal adenocarcinoma. (B) Confocal microscopy images showing OE19 cells exposed to HuHMFG1 (i) or media alone (ii). OE19 internalise HuHMFG1 and the intracellular localisation pattern is punctate.*

### **7.3.4. Development of HuHMFG1:PS1 antibody drug conjugate**

#### 7.3.4.1. Photoimmunochemistry and photophysical characterisation of HuHMFG1:PS1

To prove the targetable therapeutic potential of HuHMFG1, an ADC of the antibody was made via NHS ester mediated amide conjugation of photosensitive drug molecules (PS1) to available lysine amino acids<sup>266,401</sup>. UV-VIS spectrometry of the final HuHMFG1:PS1 ADC dissolved in PBS confirmed peak absorption at 683nm for laser activation and approximately 7 PS1 photosensitisers were coupled on average onto each HuHMFG1 antibody (Figure 67). Digital image analysis of reducing SDS-PAGE separation of the conjugate indicated 52% of the PS1 was conjugated to HuHMFG1 via a covalent amide bond, and 48% was conjugated via non-covalent interactions. The non-covalent material in the conjugate was tightly bound and not dissociated in biological buffers or with the addition of low level detergent during the purification process. Upon conjugation small shifts in the absorbance spectra of PS1 were observed; the two main PS1 peaks at 398nm and 687nm shifted 4-5nm into the blue, and the ratio between the two main peaks changed from 2.2 in the free PS1 to 2.6 in the conjugated form. There were no shifts in absorbance observed between the free and conjugated antibody at 280nm (Figure 67).

**Figure 67: Photophysical characterisation of photoactive MUC1 targeting antibody drug conjugates.**



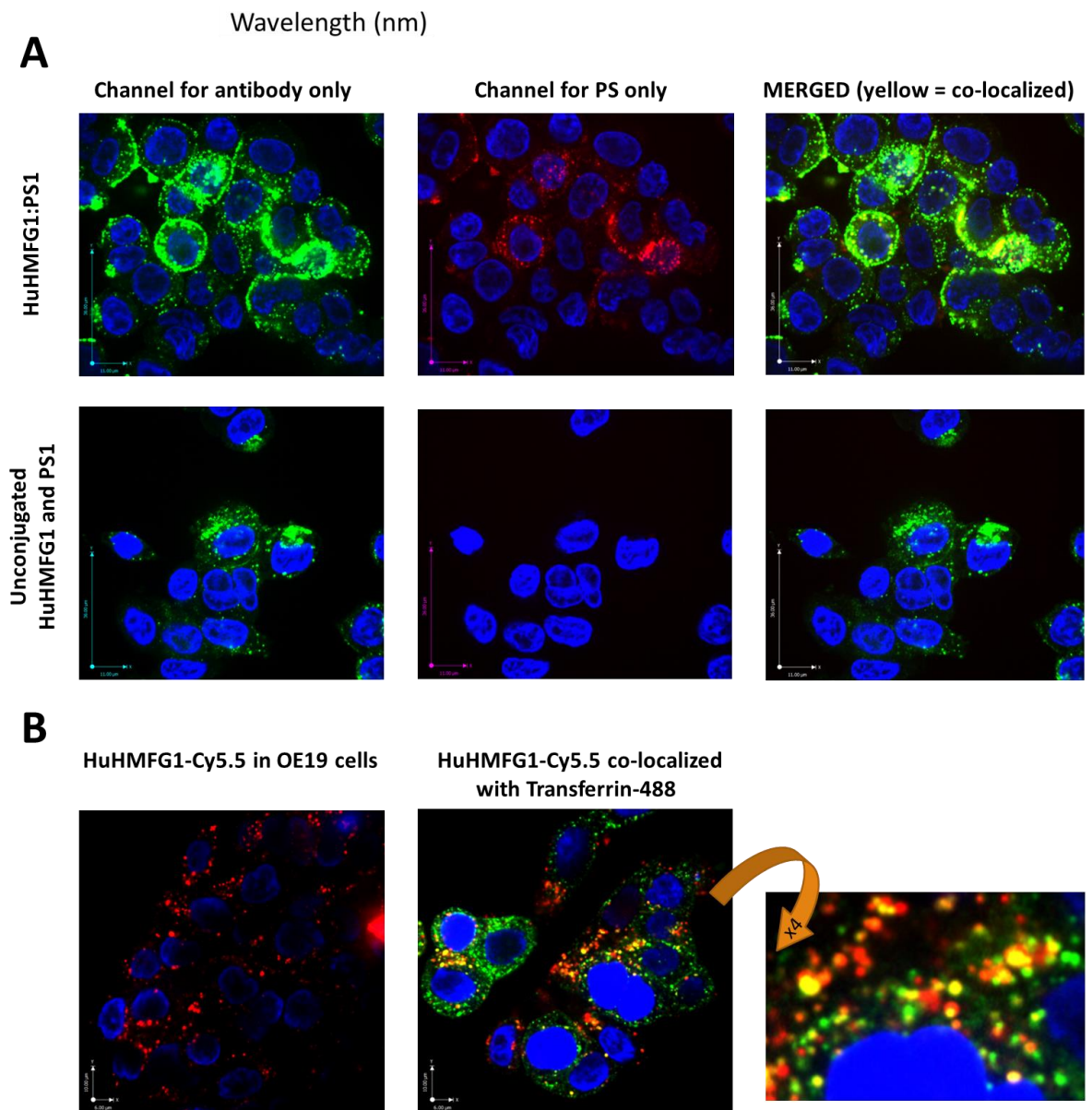
*(A) Absorbance spectra of HuHMFG1:PS1 antibody drug conjugate (ADC) highlights peak absorbance at 683nm (red spectral region) for laser excitation. Shown are any photophysical shifts away from the absorbent spectra of free antibody or free PS1 (spectra normalised to 280nm or 687nm respectively). (B) SDS page gel showing proportion of covalently coupled antibody to free photosensitiser (PS1) in the ADC mixture; (i-iii) Coomassie stained protein gel; (i) molecular weight markers, (ii) HuHMFG1 and (iii) HuHMFG1:PS1 ADC. (iv-vi) Image of the same SDS gel before Coomassie staining for the PS1 dye via UV fluorescence; (iv) molecular weight markers, (v) HuHMFG1 and (vi) HuHMFG1:PS1 ADC. Covalently bound photosensitiser PS1 is that seen at the same height as antibody protein.*

#### 7.3.4.2. Internalisation of HuHMFG1:PS1 and proposed sub-cellular localisation using HuHMFG1: Cy5.5

Confocal microscopy was used to confirm HuHMFG1:PS1 ADC internalisation into OE19 cells. Both the drug (PS1) and antibody (HuHMFG1) parts of the conjugate remain co-localised after internalisation in a similar pattern to that seen with unconjugated HuHMFG1 (Figure 68A). Due to the photoactive nature of the drug, carrying out live cell imaging induces cell death.

To co-localise the ADC with a marker of endosomal localisation, a nontoxic ADC was produced using the same reaction conditions but in which non-toxic Cy5.5 dye molecules were covalently conjugated to HuHMFG1 instead of PS1 by Dr Hayley Pye. Spectral analysis of the new HuHMFG1: Cy5.5 ADC found the antibody had an average of 5 dye molecules covalently bound per antibody and when run on SDS PAGE, the conjugate showed 30% non-covalently bound Cy5.5 (data not shown). Results showed partial co-localisation of the HuHMFG1: Cy5.5 conjugate with transferrin a marker of the recycling endosomal pathway. This could suggest HuHMFG1 conjugates are internalised during endocytosis but then delivered to another compartment, i.e. the lysosome compartment (Figure 68B).

**Figure 68: Internalisation and sub-cellular localisation of photoactive MUC1 targeting antibody drug conjugates.**



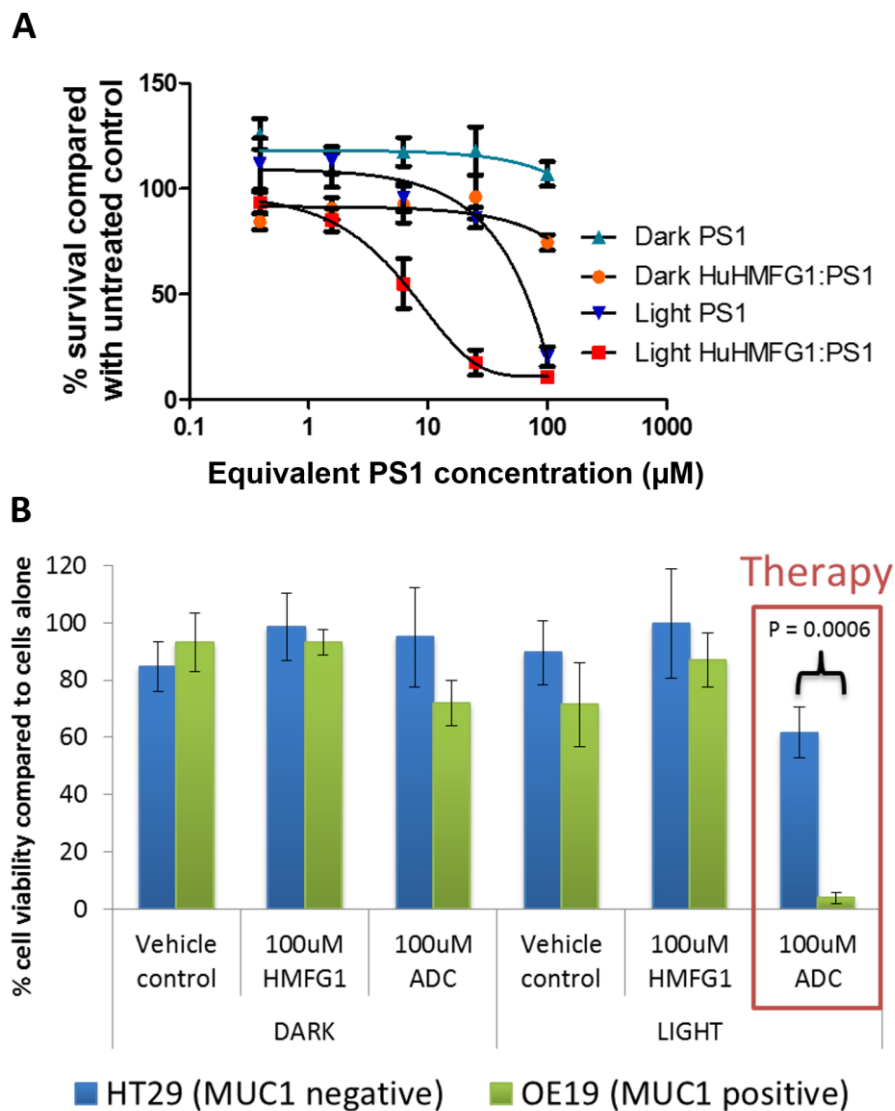
(A) Confocal microscopy images showing OE19 cells exposed to HuHMFG1 and PS1 in either a conjugated form or free un-conjugated form showing the covalently bound photosensitiser and antibody components remain co-localised after internalisation. HuHMFG1 (in green) nuclei staining (in blue) PS1 (in red). (B) HuHMFG1 was conjugated to a non-toxic dye Cy5.5 and OE19 cells exposed to the HuHMFG1: Cy5.5 conjugate with and without a marker of recycling endosomal localisation. Cells were co-stained with the nuclear stain DAPI shown in blue. Cy5.5 fluorescence is shown in red,

*endosomal marker is shown in green and the partial co-localisation of HuHMFG1 and endosomal marker is shown in yellow.*

### **7.3.5. Cytotoxic efficacy of HuHMFG1:PS1 antibody drug conjugate**

The phototoxic ADC HuHMFG1:PS1 was investigated for its light dependent cytotoxicity with an *in vitro* MUC1 positive OA cell line (OE19). OE19 cells were incubated in the dark with a range of doses of either HuHMFG1:PS1 or the equivalent concentration of free PS1 molecules. Cells were then washed and either left in the dark or irradiated with low intensity laser light at 670nm [0.33J/cm<sup>2</sup> over 10seconds] (Figure 69A). Despite the non-covalently bound material, light-dependent cytotoxicity of the HuHMFG1:PS1 ADC was seen to be significantly more potent than equivalent amounts of PS1 alone (linear regression  $p=0.0022$ ,  $F=26.09$ ). No significant cytotoxicity was seen with either drug in the dark (linear regression  $p=0.7335$ ,  $F=0.1273$ ) or between the vehicle control (2% DMSO) and cells in media only ( $p=0.12$ ) (data not shown). The top HuHMFG1:PS1 dose was then used to compare cytotoxicity in MUC1 positive OE19 cells to a MUC1 negative cell line HT29 (Figure 69B). The phototoxic efficacy of the HuHMFG1:PS1 ADC was significantly greater in MUC1 positive OE19 cells than negative HT29 cells (t test  $p<0.0006$ ). No cytotoxicity was seen in either line with the unconjugated antibody or with the ADC in the absence of light.

**Figure 69: Light dependent cytotoxicity and superior efficacy over equivalent free photosensitiser of a MUC1 specific photoactive antibody drug conjugate.**



(A) The cytotoxicity of HuHMFG1:PS1 ADC, was compared with equivalent free photosensitiser (PS1) concentrations in light and dark conditions in OE19 cells. (B) The cytotoxic efficacy of HuHMFG1:PS1 ADC, HuHMFG1 antibody alone and vehicle control were compared in a MUC1 positive line (OE19) and a MUC1 negative line (HT29) with and without light activation.

Light activation was by laser at 0.33J/cm<sup>2</sup> at 670nm over 10 seconds. Light activated ADC cytotoxicity was significantly more effective than light activated PS1 cytotoxicity (linear regression of dose response curves with F test for comparison; p=0.0002;

F=26.09). Light activated ADC cytotoxicity was also significantly more effective in the MUC1 positive line compared to the MUC1 negative control (Students t-test; p=0.0006). No significant cytotoxic effect was seen in either line with the vehicle control, antibody alone or ADC without light activation.

#### **7.4. Discussion**

GSEA looks at cellular pathways focusing on groups of genes that share common biological function, chromosomal location, or regulatory pathways. GSEA found MUC1 was identified as a protein involved with, and up-regulated in, the progression from normal squamous epithelium to invasive OA. To confirm the GSEA results, and to clarify some of the variations in MUC1 IHC profiles previously reported in the literature, 4 different antibodies recognizing different epitopes of MUC1 were tested in a panel of human biopsy samples.

The NCL-MUC-1-CORE antibody binds directly to the VNTR protein backbone where normal mucin glycosylation levels sterically hinder antibody binding. Sagara and colleagues had similar findings with a different MUC1 backbone binding antibody (DF3). They too showed it did not bind normal squamous oesophageal epithelium<sup>403</sup>. Strong binding of this antibody in OA is most likely due to a tumour associated MUC1 reduction in glycan chain length and density similar to that seen in breast cancer<sup>404</sup>. NCL-MUC-1 showed a similar binding pattern to NCL-MUC-1-CORE. NCL-MUC-1 binds a sialylated amino acid attached to a carbohydrate linked to the peptide backbone and like NCL-MUC-1-CORE this epitope was shown to be either exposed or upregulated much later in the progression pathway. Other mucin associated Sialyl-Tn antigens have similarly been associated with the final stages of malignant transformation in squamous cell oesophageal carcinoma<sup>405</sup>. Quantification of these antibodies reflects staining intensity and the amount of antibody bound. With MUC1 this staining intensity will not correlate with MUC1 expression at the molecular level, this is due to variation in the number of tandem repeats between individuals<sup>406</sup>. Though



variation does exist, for the purpose of clinical translation we expect MUC1 will follow the example set by Trastuzumab in HER2 positive oesophagogastric cancer and use a similar IHC staining intensity cut-off to identify which individuals would respond well to antibody treatment<sup>229</sup>.

HuHMFG1 and CT2 demonstrate persistently high levels of binding in all pathological grades from NDBE to OA making them suitable for ADC development for early and locally advanced oesophageal neoplasia. CT2 is an intracellular epitope so further development was focused on HuHMFG1. Though HuHMFG1 bound a proportion of normal epithelium, its specificity to the epithelial layer is important therapeutically. Damaged mucosa can re-grow but serious damage occurs when therapy reaches deeper muscle layers and can cause oesophageal strictures<sup>134,407</sup>. Re-epithelialization with neosquamous epithelium is likely to follow HuHMFG1 treatment strategies in pre-invasive disease, similar to regeneration seen following ablative oesophageal therapies<sup>58</sup>. HuHMFG1 also offers potential to treat a selection of established invasive cancers, including those with locoregional lymph node spread, particularly if a photosensitizing drug is used which is activated by deep red light. At 670nm, light penetrates more deeply into tissue than at 633nm, used to activate first generation PS such as porfimer sodium. Under optimal conditions, depth of necrosis can also extend up to five times the light penetration<sup>408</sup>. In bladder tumours, 673nm light penetrates 5.03mm to create PDT effect up to 25mm from the urothelial surface<sup>409</sup>. When administered into the lumen of the oesophagus, a similar depth of PDT effect is envisaged allowing for treatment of locally infiltrated lymph nodes.

HuHMFG1 was shown to bind a panel of living oesophageal cells throughout the pathological grades in a similar pattern to that observed with IHC. To provide proof-of-concept of HuHMFG1 as an ADC a conjugate with a photoactive-drug was produced. Photodynamic therapy (PDT) is particularly relevant for OA as laser light is easily applied via endoscopy. Targeting photosensitisers with HuHMFG1 would improve PDT selectivity. PS1 (previously developed as compound 1) is a second-generation

photosensitiser based on the chlorophyll derivative PPa. It has been chemically manipulated to include a bioconjugation handle and a series of short PEG-like chains to increase its water solubility<sup>266</sup>. PS1 was conjugated to HuHMFG1 via NHS mediated amide bond formation to exposed lysine amino acid residues. The ADC produced was shown to contain an average of 7 PS1 molecules per antibody but around half of these were non-covalently bound. Since the method for estimating conjugation ratio uses extinction coefficients based on the absorbance spectra of the free PS1 dye, the small shifts in absorbance upon conjugation may compromise the validity of the resulting ratio. Further work would have to be done to address this before the ADC is taken further. The additional non-covalently bound material is a problem seen elsewhere with PDT-ADCs and would hinder further development as it stands. It would likely cause batch-to-batch inconsistencies and make for poor chemical and biological reproducibility alongside a loss of selectivity of the final product<sup>410</sup>. Despite some of the PS1 being non-covalently bound the photosensitiser and antibody seem to remain co-localised *in vitro*. The intracellular localisation of the photoimmunoconjugate is critical to the mechanism of action and would rather be established more fully and where possible done with the final drug, not a non-toxic equivalent as we have shown, if this was to be taken further. For future translation improved purity might be achieved by using smaller antibody fragments with optimised lysine spacing and an alternative conjugation strategy with more hydrophilic PS. This would have advantages from a pharmacokinetic and manufacturing point of view<sup>390</sup>. Our group has successfully applied this technique using a HER2 targeting antibody Fab fragment<sup>411</sup>. Despite these issues with purity, the cytotoxicity results presented offer a promising proof of concept for a MUC targeted ADC. A low dose of laser light, only 0.33J/cm<sup>2</sup>, was used to make it translatable to the lower level of light that can be clinically delivered deeper into tissue. The wavelength of light used was 670nm and so use of a laser closer matched to the peak absorbance of PS1 (Figure 67) would hopefully improve cytotoxicity. HuHMFG1:PS1 demonstrated light dependent cytotoxicity that was significantly more effective for both the MUC1 positive cell line than for the MUC1 negative cell line and

more potent than equivalent free PS1 photosensitiser.

This chapter confirms how MUC1 is upregulated during progression with gene set enrichment analysis, immunohistochemistry and flow cytometry in oesophageal tissues and cell lines taken from discrete histological grades. It clarifies previously conflicting data with regards to the detection of epitopes differentially expressed on MUC1 due to glycosylation changes. It shows how MUC1 expression is maintained by glandular cells throughout the metaplasia-dysplasia-carcinoma sequence, binding only the epithelial layer in early disease. In advanced disease, expression is maintained by glandular cells as they invade the submucosa, muscular layer and into metastases. HuHMFG1 was shown to positively bind a high proportion of cases from non-dysplastic Barrett's epithelium, through degrees of dysplasia to invasive OA. This suggests HuHMFG1 may have excellent therapeutic potential. Indeed, HuHMFG1 binds live cells and the findings presented here offer an in-class proof-of-concept MUC1 targeting photoactive ADCs. The cytotoxic efficacy makes this an interesting approach for the future translation into the clinical arena.

## **Chapter 8: Discussion and future experiments**

---

## **8.1. Future biomarker studies for the risk stratification of BE**

Several strategies for the risk stratification of BE have been evaluated in this thesis. Initial experiments with antibodies to 2 RLF target's, PLK1 and Geminin, have made the case for considering these biomarkers in the prediction of malignant progression in pre-neoplastic oesophageal epithelium, either directly or as surrogates for DNA-CA. DN-CA was also shown to be a better predictor for dysplasia in BE with direct therapeutic implications. These findings support DNA-CA to have a more established role in clinical guidelines.

The audit of the UCH DNA-CA clinical service has laid the foundation for a more robust dataset for future evaluation of risk, as an established service, it would be able to support a phase 4 study as is being proposed. Finally, pilot DIA algorithms have been developed to automate the pathological reporting of slides presently requiring the expertise of specialist GI pathologists.

### ***8.1.1. Validation of DNA-CA in the prediction of dysplasia***

To validate the efficacy of DNA-CA to predict oesophageal dysplasia, evaluation in a larger population of BE patients will be required. In the UK, 3 large collaborative projects exist in which our group has contributed in varying degrees over the years. These cohorts of patients and their relevant samples are based in Queen's University Belfast (Northern Ireland Barrett's Registry), Cambridge University (Oesophageal Cancer Clinical and Molecular Stratification: OCCAMS) and Queen Mary University of London (Chemoprevention of premalignant intestinal neoplasia: ChOPin). The soon to complete ASPECT clinical trial will also potentially have access to a wealth of tissue specimens. The ability of DNA-CA and RLF to examine retrospective tissue specimens opens these tissue repositories if they can be accessed appropriately.

### ***8.1.2. Evaluation of serial RLFs in tissue samples from patients who have progressed during Barrett's screening***

As UCH is a tertiary referral centre for the management of Barrett's dysplasia, most patients are at a late pathological stage on arrival here. The limited local population in Euston means those cases with non-dysplastic Barrett's epithelium that have progressed locally are few and far between. The large categorised cohorts of patients mentioned above will give us access to tissue material that can be evaluated retrospectively from patients known to have progressed within these cohorts.

Following validation and evaluation in Barrett's progressors, the next phase of work would be to translate the findings into clinical use and examine the results of its implementation.

### ***8.1.3. Utility of targeting RLF to prevent malignant progression in Barrett's in high risk populations***

The utility of targeting RLF directly could be further explored in vitro. PLK1 inhibitors are presently undergoing clinical trials in cancer to assess their chemotherapeutic efficacy<sup>412</sup>. In future PLK1 inhibitors may have role to play in those patients in whom RLF are upregulated prior to the development of dysplasia or cancer. It would be interesting to explore this further using PLK1 inhibitors on a range of cell lines in the progression to OA to identify the efficacy of this strategy in preventing progression of BE to cancer.

### ***8.1.4. Validation of RLF immunohistochemistry results and investigation into the relationships between other recently established biomarkers of progression***

To support the potential importance of the RLFs in BE progression it would be of benefit to quantify biomarker positivity with RT-PCR, ISH or next generation sequencing (NGS) technologies.

In addition, it may be useful to broaden this work with further IHC studies and NGS to investigate if new emerging biomarkers hypothesised to be important in the development of BE and OA correlate or interact with PLK1 such as FOXF1<sup>413</sup>, FOXM1<sup>282</sup>, ARID1A<sup>414</sup>, and theoretically STAT3<sup>415</sup>. Screening with PCR and IHC in our currently categorised cohort of patients should technically be feasible.

These final studies may in future form the skeleton of a molecular Barrett's puzzle of carcinogenesis or stasis that researchers have only theorised about to date.

#### ***8.1.5. Expansion of DNA-CA clinical studies***

Interestingly, one conclusion that be ascertained from the analysis in this thesis is how well clinicians predict both pathology and DNA-CA in patients deemed to be at increased risk of progression from clinical history and endoscopic findings.

In future, additional factors such as length of BE segment, distance of DNA-CA sample from the gastroesophageal junction (as most recurrences after failed endoscopic therapy are felt to occur in this region) and age may be added to the datasets. A multivariate regression model to understand the magnitude and relationships between these risk factors is achievable through information accessible through this study. Clinical data on current pathological grade from both ploidy and diploid controls may also be accessed to identify the likelihood and speed of progression to HGD/OA, the most clinically important outcome of DNA CA testing.

#### ***8.1.6. Digital Image Analysis***

Ariol® image analysis has shown how it can be adapted to match pathologists reporting of IHC slides. DIA is of importance as it has potential to be translated into widespread clinical use as a replacement for pathologist reporting, or as a more accurate and time-effective way of quantifying biomarkers than is presently employed.

Strengths of DIA with Ariol® software are that it allows correlation training by individual pixels. This allows selection of ROIs of any shape and size and can analyse entire

tissue scans without the need for smaller tiled images. Slides however must be scanned with a Leica scanner, as the programme does not possess the ability to interpret other software formats.

Limitations include the finding that background tissue staining on stroma surrounding epithelial tissue, on the luminal surface and in blood vessels are often counted as positive nuclei affecting the results in an unpredictable manner. The issue of background staining however is very dependent on the quality of antibody and optimisation of the staining protocols employed. Certain antibodies such as PLK1-L did not have much of an issue when they were analysed with DIA. To overcome this, DIA software able to exclude background staining by training algorithms based on shape as well as pixel colour and intensity will overcome this limitation.

Other limitations include the fact that the program can be slow, taking hours to analyse individual slides on occasion when there is a large amount of tissue in the ROI. For example, oesophageal resection specimens as opposed to biopsies face this issue. Ariol ® also occasionally fails to analyse though this may be hardware/computer related. Finally, the method of analysing intensity may be improved upon. At present Ariol ® gives an intensity score for each area; the program automatically divides ROIs into more manageable smaller areas. This means a weighted average proportional to size of the area must be calculated to get an overall score for the intensity.

A few other image analysis software programmes are available that may be superior to Ariol and able to overcome the limitations described. One such program is Definiens though costs and infrastructure required for its use may limit access to this technology. The next phase of work will therefore aim to compare software programmes to select the best one for clinical use.



## **8.2. Future studies for the translation of biomarkers targeting into clinical practice**

### **8.2.1. Future of HER2 targeting TCT-Ce6**

The characterisation IHC experiments presented here have highlighted the burden of HER2 expressing disease of the upper GI tract that may be targeted. The work demonstrates that certain clinicopathological factors can play a significant role in oesophagogastric cancer prognosis. This will in future better inform clinicians managing these patients.

This thesis presents data on the development of TCT-Ce6 as an effective anti-HER2 antibody drug conjugate. Each antibody fragment is linked with 4 photosensitisers and can be created reproducibly and purified. The inability to purify to a high degree and accurately reproduce conjugation has been the Achilles heel of many previous ADCs. The present anti-HER2 PDT has several potential advantages over its competitors in the HER2 field. It has increased, and immediate potency compared to Trastuzumab. It can also be effective in tumours expressing HER2 heterogeneously and to a lower level would presently be treated in the clinic. This is clear advantages therefore of offering anti-HER2 treatment to a much wider population of patients with oesophagogastric cancer than previously. The direct approach via endoscopy to visualise and kill one of the most difficult to treat tumours also has a bystander effect of destroying adjacent HER2 negative tumour cells.

The in vivo studies have shown the recruitment of the inflammatory cascade and immune system via the confirmation of an inflammatory component within HER2 treated tumours, and the presence of localised lymph nodes in mice at the end of the study protocol. Recruitment of the immune system is a recognised benefit of PDT and works synergistically to provide a double hit for any particularly resistant cancer cells. In addition, this opens the potential for dual therapy immune checkpoint inhibitors in the future.

The anti-HER2 photoactive ADC presented here is rapidly cleared within 3 days and is best activated 4 hours after administration. Though it is difficult to make direct inferences from animal data only, this result may imply that in the clinical arena, TCT-Ce6 can be delivered in an out-patient setting through endoscopy. Avoiding admission would have clear financial benefits for the health service and be more acceptable to patients. Skin photosensitivity was not seen with TCT-Ce6 in animals as hypothesised, with the drug being limited predominantly to more vascular organs, though only transiently, as it was cleared rapidly within 72 hours. The selectivity and rapid clearance should translate to improved tolerance and reduced systemic side effects for a short duration. A major step forward from the current clinically approved photosensitiser for BE and OA, Porfimer sodium which caused protracted side effects that last months in some patients.

Repeated PDT with TCT-Ce6 is safe and well tolerated in rodents, and effective at treating tumours. Further work can look to refine treatment protocols, but this work provides proof on concept to take this project forward into the next phase of drug development. This would include outsourcing the manufacture of the ADC to laboratories working to good laboratory practice (GLP) and good medical practice (GMP) standards. They would repeat these experiments and scrutinise them for batch to batch variability. Once this quality control process has been completed, further therapeutic animal data with other cell lines, will be needed to confirm efficacy and safety of the revised product. The manufacture would have to then be scaled up in preparation for early phase clinical studies to facilitate benefits for OA patients soon.

### **8.2.2. *MUC1 as a therapeutic target in OA***

#### 8.2.2.1. Validation and completion of MUC1 characterisation studies

Based on the tissue expression data presented here, the advantage of MUC1 targeting is that it offers the potential to treat most OA patients. However, the cut off values for MUC1 positivity using IHC were set based upon previous studies scoring membranous

biomarkers such as HER2 and the expertise of our specialist gastrointestinal pathologists. Though our protocol may be correct, further experiments will be needed to more accurately define a IHC protocol to good laboratory practice (GLP) standards to assist in determining which OA patients expressing MUC1 would benefit from anti-MUC1 therapy. It would be interesting to then examine if a threshold of MUC1 positivity exists to correlate with effectiveness of anti-MUC1 therapies.

In future, alternative methods for MUC1 quantification such as ISH or RT-PCR would be useful to validate a selection of cases in the dataset. However, it is noted that this may not mimic the unique binding results of MUC1 antibodies apart from CT2. This is because CT2 is protected from surface glycosylation changes seen in the progression to cancer affecting the antibodies HuHMFG1 and NCL-MUC-1.

#### 8.2.2.2. Characterisation of HuHMFG1 internalisation kinetics

In vitro studies on live oesophageal cells may be further developed. Confocal microscopy identified internalisation of MUC1 within 4 hours. It would be useful to know precisely how rapidly MUC1 is internalised when bound by HuHMFG1 as this would have implications for the in vivo and clinical translation of this work. Furthermore, identification of the cellular compartments where HuHMFG1 is localised post internalisation may be tracked with confocal microscopy providing insights into the mechanism of action of this antibody, and its interaction with oesophageal cancer cells. An attempt was made in this thesis to understand this mechanism with confocal studies but had to rely on the development of another ADC with HuHMFG1 attached to the commercially available dye Cv5.5 (Figure 68B).

#### 8.2.2.3. Evaluation of serum tumour markers in MUC1 positive OA cancers

The utility of using serum MUC1 biomarkers for the prediction and perhaps monitoring of disease should be further examined. Levels of these markers could be evaluated in larger clinical studies of patients with oesophagogastric cancers and compared with MUC1 expression in corresponding tissue specimens.

#### 8.2.2.4. Development of MUC1 targeted therapies against oesophageal adenocarcinoma

This thesis has highlighted the spectrum of MUC1 disease and presents a first in class MUC1 targeting ADC with a whole antibody. This ADC is more effective than free photosensitiser and more effective in MUC1 expressing rather than MUC1 -ve cells.

The initial conjugation experiments have shown a significant quantity of non-covalently bound material remains despite attempts at purification. It may be that of the 7 photosensitiser molecules bound MUC1, up to half may be non-covalently bound. This will have to be addressed before taking this conjugate further. Despite this issue, the confocal studies demonstrated that PS1 does co-localise with HuHMFG1 in vitro, suggesting a significant amount is delivered intracellularly with the antibody vehicle.

To overcome the issue of non-covalent binding of photosensitisers, smaller HuHMFG1 antibody formats such as scFv or Fab antibodies should be considered for. However, this cleaner product may be at the expense of losing effectiveness as a number of lysine residues, relied upon to attach the photosensitiser payload, would be lost. Some pilot studies to produce a HuHMFG1 Fab through direct cleavage with papain were conducted (data not shown), however, the antibody became very low affinity precluding its further development. An attempt to outsource the production of an HuHMFG1 scFv was made, but due to the very low yield delivered, it was not viable to continue. Further experiments with PS1 also had to be limited due an isomer contaminant in the product when its production was scaled up, that made conjugations attempted with the later batches of the drug very poor (data not shown).

#### 8.2.3. Summary

This thesis has detailed experiments to assess disease biomarkers and to take forward the therapeutic management of patients with BE and oesophageal cancer. The biomarkers will help decide which patients should be offered therapy, how their

prognosis will be influenced when they are present and provided proof of concept for 2 light activated ADC's for the future therapeutic intent.

The diagnostic experiments have shown how DNA-CA can play a more significant role in the risk stratification of patients with BE. These decisions will help decide who should be offered endoscopic therapy. Where DNA-CA is not available, the cell cycle marker PLK-1 may be an alternative and more widely available tool to predict this abnormality. We developed DIA protocols to examine PLK1 in tissue, though further development will be needed before these protocols are ready for prime time.

The prognostic role of HER2 in clinical practice was shown and a complete data package on the proof-of-concept of a HER2 targeting photoactive antibody fragment approach for the treatment of future foregut malignancies provided, ready for the final stages of drug development prior to clinical trials.

Finally, previously controversies regarding expression of MUC1 in oesophageal tissue. We provide proof of principle data on the effectiveness of a photoactive ADC targeting MUC1, but further work will be needed in-vitro to improve its purity, and efficacy. Nonetheless, MUC1 remains a promising target for this work as we have shown it is expressed in the vast majority of oesophageal adenocarcinoma and Barrett's patients.

## References

1. Fitzgerald, R. C. *et al.* British Society of Gastroenterology guidelines on the diagnosis and management of Barrett's oesophagus. *Gut* **63**, 7–42 (2014).
2. American Gastroenterological Association, Spechler SJ, Sharma P, Souza RF, Inadomi JM, S. N. American gastroenterological association medical position statement on the management of Barrett'S esophagus. *Gastroenterology* **140**, 1084–1091 (2011).
3. Playford, R. J. New British Society of Gastroenterology (BSG) guidelines for the diagnosis and management of Barrett's oesophagus. *Gut* **55**, 442 (2006).
4. Sharma, P., Falk, G. W., Sampliner, R., Jon Spechler, S. & Wang, K. Management of nondysplastic Barrett's esophagus: where are we now? *Am. J. Gastroenterol.* **104**, 805–808 (2009).
5. Solaymani-Dodaran, M., Logan, R. F. A., West, J. & Card, T. Mortality associated with Barrett's esophagus and gastroesophageal reflux disease diagnoses-a population-based cohort study. *Am. J. Gastroenterol.* **100**, 2616–2621 (2005).
6. Hamilton, S. R., Smith, R. R. & Cameron, J. L. Prevalence and characteristics of Barrett esophagus in patients with adenocarcinoma of the esophagus or esophagogastric junction. *Hum. Pathol.* **19**, 942–948 (1988).
7. Cameron, A. J., Lomboy, C. T., Pera, M. & Carpenter, H. A. Adenocarcinoma of the esophagogastric junction and Barrett's esophagus. *Gastroenterology* **109**, 1541–1546 (1995).
8. Yousef, F. *et al.* The incidence of esophageal cancer and high-grade dysplasia in Barrett's esophagus: a systematic review and meta-analysis. *Am. J. Epidemiol.* **168**, 237–49 (2008).
9. Desai, T. K. *et al.* The incidence of oesophageal adenocarcinoma in non-dysplastic Barrett's oesophagus: a meta-analysis. *Gut* **61**, 970–6 (2012).
10. Bhat, S. *et al.* Risk of malignant progression in Barrett's esophagus patients: results from a large population-based study. *J. Natl. Cancer Inst.* **103**, 1049–57

- (2011).
11. Cancer Research UK. *Oesophageal cancer mortality rates by sex and UK region*. (2012).
  12. Cancer Research UK Cancer Survival Group. *Age-Standardised One-, Five- and Ten-Year Net Survival, Adults (Aged 15-99), England and Wales, 2010-2011*. (2014).
  13. Ronkainen, J. *et al.* Prevalence of Barrett's esophagus in the general population: an endoscopic study. *Gastroenterology* **129**, 1825–31 (2005).
  14. Winters, C. *et al.* Barrett's esophagus. A prevalent, occult complication of gastroesophageal reflux disease. *Gastroenterology* **92**, 118–24 (1987).
  15. Eloubeidi, M. A. & Provenzale, D. Clinical and demographic predictors of Barrett's esophagus among patients with gastroesophageal reflux disease: a multivariable analysis in veterans. *J. Clin. Gastroenterol.* **33**, 306–9 (2001).
  16. Koek, G. H., Sifrim, D., Lerut, T., Janssens, J. & Tack, J. Multivariate analysis of the association of acid and duodeno-gastro-oesophageal reflux exposure with the presence of oesophagitis, the severity of oesophagitis and Barrett's oesophagus. *Gut* **57**, 1056–64 (2008).
  17. Shaheen, N. J. & Richter, J. E. Barrett's oesophagus. *Lancet (London, England)* **373**, 850–61 (2009).
  18. Caygill, C. P. J., Watson, A., Lao-Sirieix, P. & Fitzgerald, R. C. Barrett's oesophagus and adenocarcinoma. *World J. Surg. Oncol.* **2**, 12 (2004).
  19. Sikkema, M. *et al.* Predictors for neoplastic progression in patients with Barrett's Esophagus: a prospective cohort study. *Am. J. Gastroenterol.* **106**, 1231–8 (2011).
  20. Falk, G. W. *et al.* Barrett's esophagus: prevalence-incidence and etiology-origins. *Ann. N. Y. Acad. Sci.* **1232**, 1–17 (2011).
  21. Jacobson, B. C., Chan, A. T., Giovannucci, E. L. & Fuchs, C. S. Body mass index and Barrett's oesophagus in women. *Gut* **58**, 1460–6 (2009).
  22. Vaughan, T. L. *et al.* Nonsteroidal anti-inflammatory drug use, body mass index,

- and anthropometry in relation to genetic and flow cytometric abnormalities in Barrett's esophagus. *Cancer Epidemiol. Biomarkers Prev.* **11**, 745–52 (2002).
23. Lagergren, J., Bergström, R. & Nyrén, O. Association between body mass and adenocarcinoma of the esophagus and gastric cardia. *Ann. Intern. Med.* **130**, 883–90 (1999).
  24. de Jonge, P. J. F. *et al.* Risk factors for the development of esophageal adenocarcinoma in Barrett's esophagus. *Am. J. Gastroenterol.* **101**, 1421–9 (2006).
  25. Moe, G. L., Kristal, A. R., Levine, D. S., Vaughan, T. L. & Reid, B. J. Waist-to-hip ratio, weight gain, and dietary and serum selenium are associated with DNA content flow cytometry in Barrett's esophagus. *Nutr. Cancer* **36**, 7–13 (2000).
  26. Wang, C., Yuan, Y. & Hunt, R. H. Helicobacter pylori infection and Barrett's esophagus: a systematic review and meta-analysis. *Am. J. Gastroenterol.* **104**, 492-500, 501 (2009).
  27. Cook, M. B. *et al.* Cigarette smoking and adenocarcinomas of the esophagus and esophagogastric junction: a pooled analysis from the international BEACON consortium. *J. Natl. Cancer Inst.* **102**, 1344–53 (2010).
  28. Cook, M. B. *et al.* Cigarette smoking increases risk of Barrett's esophagus: an analysis of the Barrett's and Esophageal Adenocarcinoma Consortium. *Gastroenterology* **142**, 744–53 (2012).
  29. Thrift, A. P., Kramer, J. R., Richardson, P. A. & El-Serag, H. B. No significant effects of smoking or alcohol consumption on risk of Barrett's esophagus. *Dig. Dis. Sci.* **59**, 108–16 (2014).
  30. Kubo, A., Corley, D. A., Jensen, C. D. & Kaur, R. Dietary factors and the risks of oesophageal adenocarcinoma and Barrett's oesophagus. *Nutr. Res. Rev.* **23**, 230–46 (2010).
  31. Menke-Pluymers, M. B., Hop, W. C., Dees, J., van Blankenstein, M. & Tilanus, H. W. Risk factors for the development of an adenocarcinoma in columnar-lined (Barrett) esophagus. The Rotterdam Esophageal Tumor Study Group. *Cancer*



- 72, 1155–8 (1993).
32. Avidan, B., Sonnenberg, A., Schnell, T. G. & Sontag, S. J. Hiatal hernia and acid reflux frequency predict presence and length of Barrett's esophagus. *Dig. Dis. Sci.* **47**, 256–64 (2002).
  33. Weston, A. P., Krmpotich, P. T., Cherian, R., Dixon, A. & Topalovski, M. Prospective long-term endoscopic and histological follow-up of short segment Barrett's esophagus: comparison with traditional long segment Barrett's esophagus. *Am. J. Gastroenterol.* **92**, 407–13 (1997).
  34. Weston, A. P. *et al.* Risk stratification of Barrett's esophagus: updated prospective multivariate analysis. *Am. J. Gastroenterol.* **99**, 1657–66 (2004).
  35. Rudolph, R. E. *et al.* Effect of segment length on risk for neoplastic progression in patients with Barrett esophagus. *Ann. Intern. Med.* **132**, 612–20 (2000).
  36. Buttar, N. S. *et al.* Extent of high-grade dysplasia in Barrett's esophagus correlates with risk of adenocarcinoma. *Gastroenterology* **120**, 1630–1639 (2001).
  37. Montgomery, E. *et al.* Are ulcers a marker for invasive carcinoma in Barrett's esophagus? Data from a diagnostic variability study with clinical follow-up. *Am. J. Gastroenterol.* **97**, 27–31 (2002).
  38. Hofstetter, W. L. *et al.* Long-term outcome of antireflux surgery in patients with Barrett's esophagus. *Ann. Surg.* **234**, 532-8-9 (2001).
  39. O'Riordan, J. M., Byrne, P. J., Ravi, N., Keeling, P. W. N. & Reynolds, J. V. Long-term clinical and pathologic response of Barrett's esophagus after antireflux surgery. *Am. J. Surg.* **188**, 27–33 (2004).
  40. Schlemper, R. J. *et al.* The Vienna classification of gastrointestinal epithelial neoplasia. *Gut* **47**, 251–5 (2000).
  41. *Understanding Barrett's Esophagus.* (2013).
  42. Shaheen, N. J., Crosby, M. A., Bozyski, E. M. & Sandler, R. S. Is there publication bias in the reporting of cancer risk in Barrett's esophagus? *Gastroenterology* **119**, 333–8 (2000).

43. Wani, S. *et al.* Patients with nondysplastic Barrett's esophagus have low risks for developing dysplasia or esophageal adenocarcinoma. *Clin. Gastroenterol. Hepatol.* **9**, 220–7; quiz e26 (2011).
44. Hvid-Jensen, F., Pedersen, L., Drewes, A. M., Sørensen, H. T. & Funch-Jensen, P. Incidence of adenocarcinoma among patients with Barrett's esophagus. *N. Engl. J. Med.* **365**, 1375–83 (2011).
45. Riddell, R. H. *et al.* Dysplasia in inflammatory bowel disease: standardized classification with provisional clinical applications. *Hum. Pathol.* **14**, 931–68 (1983).
46. Schlemper, R. J., Kato, Y. & Stolte, M. Diagnostic criteria for gastrointestinal carcinomas in Japan and Western countries: proposal for a new classification system of gastrointestinal epithelial neoplasia. *J. Gastroenterol. Hepatol.* **15 Suppl**, G49-57 (2000).
47. Lim, C. H., Treanor, D., Dixon, M. F. & Axon, A. T. R. Low-grade dysplasia in Barrett's esophagus has a high risk of progression. *Endoscopy* **39**, 581–7 (2007).
48. Skacel, M. *et al.* The diagnosis of low-grade dysplasia in Barrett's esophagus and its implications for disease progression. *Am. J. Gastroenterol.* **95**, 3383–7 (2000).
49. Sharma, P. *et al.* Dysplasia and cancer in a large multicenter cohort of patients with Barrett's esophagus. *Clin. Gastroenterol. Hepatol.* **4**, 566–72 (2006).
50. Weston, A. P. *et al.* p53 protein overexpression in low grade dysplasia (LGD) in Barrett's esophagus: immunohistochemical marker predictive of progression. *Am. J. Gastroenterol.* **96**, 1355–62 (2001).
51. Reid, B. J., Levine, D. S., Longton, G., Blount, P. L. & Rabinovitch, P. S. Predictors of progression to cancer in Barrett's esophagus: Baseline histology and flow cytometry identify low- and high-risk patient subsets. *Am. J. Gastroenterol.* **95**, 1669–1676 (2000).
52. Gatenby, P. *et al.* Routinely diagnosed low-grade dysplasia in Barrett's

- oesophagus: a population-based study of natural history. *Histopathology* **54**, 814–9 (2009).
53. Wani, S. *et al.* Esophageal adenocarcinoma in Barrett's esophagus after endoscopic ablative therapy: a meta-analysis and systematic review. *Am. J. Gastroenterol.* **104**, 502–13 (2009).
  54. Inadomi, J. M., Somsouk, M., Madanick, R. D., Thomas, J. P. & Shaheen, N. J. A cost-utility analysis of ablative therapy for Barrett's esophagus. *Gastroenterology* **136**, 2101–2114–6 (2009).
  55. Phoa, K. N. *et al.* Radiofrequency ablation vs endoscopic surveillance for patients with Barrett esophagus and low-grade dysplasia: a randomized clinical trial. *JAMA* **311**, 1209–17 (2014).
  56. Tham, T. LGD: surveillance or ablation? *Br. Soc. Gastroenterol.* (2015).
  57. Schnell, T. G. *et al.* Long-term nonsurgical management of Barrett's esophagus with high-grade dysplasia. *Gastroenterology* **120**, 1607–1619 (2001).
  58. Haidry, R. J. *et al.* Radiofrequency ablation and endoscopic mucosal resection for dysplastic Barrett's esophagus and early esophageal adenocarcinoma: Outcomes of the UK national halo RFA registry. *Gastroenterology* **145**, 87–95 (2013).
  59. Sharma, P. *et al.* The development and validation of an endoscopic grading system for Barrett's esophagus: the Prague C & M criteria. *Gastroenterology* **131**, 1392–9 (2006).
  60. Endoscopic Classification Review Group. Update on the paris classification of superficial neoplastic lesions in the digestive tract. *Endoscopy* **37**, 570–8 (2005).
  61. Hazewinkel, Y. & Dekker, E. Colonoscopy: basic principles and novel techniques. *Nat. Rev. Gastroenterol. Hepatol.* **8**, 554–64 (2011).
  62. Gerson, L. B., Edson, R., Lavori, P. W. & Triadafilopoulos, G. Use of a simple symptom questionnaire to predict Barrett's esophagus in patients with symptoms of gastroesophageal reflux. *Am. J. Gastroenterol.* **96**, 2005–12 (2001).
  63. Modiano, N. & Gerson, L. B. Risk factors for the detection of Barrett's esophagus

- in patients with erosive esophagitis. *Gastrointest. Endosc.* **69**, 1014–20 (2009).
64. Stoltey, J., Reeba, H., Ullah, N., Sabhaie, P. & Gerson, L. Does Barrett's oesophagus develop over time in patients with chronic gastro-oesophageal reflux disease? *Aliment. Pharmacol. Ther.* **25**, 83–91 (2007).
  65. Zagari, R. M. *et al.* Gastro-oesophageal reflux symptoms, oesophagitis and Barrett's oesophagus in the general population: the Loiano-Monghidoro study. *Gut* **57**, 1354–9 (2008).
  66. Murata, A. *et al.* Prospective randomized trial of transnasal versus peroral endoscopy using an ultrathin videoendoscope in unsedated patients. *J. Gastroenterol. Hepatol.* **22**, 482–5 (2007).
  67. Saeian, K. *et al.* Unsedated transnasal endoscopy accurately detects Barrett's metaplasia and dysplasia. *Gastrointest. Endosc.* **56**, 472–8 (2002).
  68. di Pietro, M., Chan, D., Fitzgerald, R. C. & Wang, K. K. Screening for Barrett's Esophagus. *Gastroenterology* **148**, 912–23 (2015).
  69. Atkinson, M. *et al.* Ultrathin esophagoscopy in screening for Barrett's esophagus at a Veterans Administration Hospital: easy access does not lead to referrals. *Am. J. Gastroenterol.* **103**, 92–7 (2008).
  70. Sharma, V. K., Eliakim, R., Sharma, P., Faigel, D. & ICCE. ICCE consensus for esophageal capsule endoscopy. *Endoscopy* **37**, 1060–4 (2005).
  71. Eliakim, R. *et al.* A prospective study of the diagnostic accuracy of PillCam ESO esophageal capsule endoscopy versus conventional upper endoscopy in patients with chronic gastroesophageal reflux diseases. *J. Clin. Gastroenterol.* **39**, 572–8 (2005).
  72. Lin, O. S. *et al.* Blinded comparison of esophageal capsule endoscopy versus conventional endoscopy for a diagnosis of Barrett's esophagus in patients with chronic gastroesophageal reflux. *Gastrointest. Endosc.* **65**, 577–83 (2007).
  73. Bhardwaj, A., Hollenbeak, C. S., Pooran, N. & Mathew, A. A meta-analysis of the diagnostic accuracy of esophageal capsule endoscopy for Barrett's esophagus in patients with gastroesophageal reflux disease. *Am. J. Gastroenterol.* **104**,

- 1533–9 (2009).
74. Ramirez, F. C., Shaukat, M. S., Young, M. A., Johnson, D. A. & Akins, R. Feasibility and safety of string, wireless capsule endoscopy in the diagnosis of Barrett's esophagus. *Gastrointest. Endosc.* **61**, 741–6 (2005).
  75. Ramirez, F. C., Akins, R. & Shaukat, M. Screening of Barrett's esophagus with string-capsule endoscopy: a prospective blinded study of 100 consecutive patients using histology as the criterion standard. *Gastrointest. Endosc.* **68**, 25–31 (2008).
  76. Moglia, A., Menciassi, A., Schurr, M. O. & Dario, P. Wireless capsule endoscopy: from diagnostic devices to multipurpose robotic systems. *Biomed. Microdevices* **9**, 235–43 (2007).
  77. Jaskiewicz, K., Venter, F. S. & Marasas, W. F. Cytopathology of the esophagus in Transkei. *J. Natl. Cancer Inst.* **79**, 961–7 (1987).
  78. Kadri, S. R. *et al.* Acceptability and accuracy of a non-endoscopic screening test for Barrett's oesophagus in primary care: cohort study. *BMJ* **341**, c4372 (2010).
  79. Ross-Innes, C. S. *et al.* Evaluation of a minimally invasive cell sampling device coupled with assessment of trefoil factor 3 expression for diagnosing Barrett's esophagus: a multi-center case-control study. *PLoS Med.* **12**, e1001780 (2015).
  80. Ross-Innes, C. S. *et al.* Risk stratification of Barrett's oesophagus using a non-endoscopic sampling method coupled with a biomarker panel: a cohort study. *lancet. Gastroenterol. Hepatol.* **2**, 23–31 (2017).
  81. Levine, D. S. *et al.* An endoscopic biopsy protocol can differentiate high-grade dysplasia from early adenocarcinoma in Barrett's esophagus. *Gastroenterology* **105**, 40–50 (1993).
  82. Corley, D. A., Levin, T. R., Habel, L. A., Weiss, N. S. & Buffler, P. A. Surveillance and survival in Barrett's adenocarcinomas: a population-based study. *Gastroenterology* **122**, 633–40 (2002).
  83. Incarbone, R., Bonavina, L., Saino, G., Bona, D. & Peracchia, A. Outcome of esophageal adenocarcinoma detected during endoscopic biopsy surveillance for

- Barrett's esophagus. *Surg. Endosc.* **16**, 263–6 (2002).
84. Ramus, J. R., Gatenby, P. A. C., Caygill, C. P. J., Winslet, M. C. & Watson, A. Surveillance of Barrett's columnar-lined oesophagus in the UK: endoscopic intervals and frequency of detection of dysplasia. *Eur. J. Gastroenterol. Hepatol.* **21**, 636–41 (2009).
85. Inadomi, J. M. *et al.* Screening and surveillance for Barrett esophagus in high-risk groups: a cost-utility analysis. *Ann. Intern. Med.* **138**, 176–86 (2003).
86. Sonnenberg, A., Soni, A. & Sampliner, R. E. Medical decision analysis of endoscopic surveillance of Barrett's oesophagus to prevent oesophageal adenocarcinoma. *Aliment. Pharmacol. Ther.* **16**, 41–50 (2002).
87. Somerville, M., Garside, R., Pitt, M. & Stein, K. Surveillance of Barrett's oesophagus: is it worthwhile? *Eur. J. Cancer* **44**, 588–99 (2008).
88. Old, O. *et al.* Barrett's Oesophagus Surveillance versus endoscopy at need Study (BOSS): protocol and analysis plan for a multicentre randomized controlled trial. *J. Med. Screen.* **22**, 158–64 (2015).
89. Gatenby, P. A. C., Caygill, C. P. J., Watson, A., Murray, L. & Romero, Y. Barrett's esophagus registries. *Ann. N. Y. Acad. Sci.* **1232**, 405–10 (2011).
90. Sarr, M. G., Hamilton, S. R., Marrone, G. C. & Cameron, J. L. Barrett's esophagus: its prevalence and association with adenocarcinoma in patients with symptoms of gastroesophageal reflux. *Am. J. Surg.* **149**, 187–93 (1985).
91. Chey, W. D. *et al.* Primary-care physicians' perceptions and practices on the management of GERD: results of a national survey. *Am. J. Gastroenterol.* **100**, 1237–42 (2005).
92. Hillman, L. C., Chiragakis, L., Shadbolt, B., Kaye, G. L. & Clarke, A. C. Effect of proton pump inhibitors on markers of risk for high-grade dysplasia and oesophageal cancer in Barrett's oesophagus. *Aliment. Pharmacol. Ther.* **27**, 321–6 (2008).
93. Hillman, L. C., Chiragakis, L., Shadbolt, B., Kaye, G. L. & Clarke, A. C. Proton-pump inhibitor therapy and the development of dysplasia in patients with

- Barrett's oesophagus. *Med. J. Aust.* **180**, 387–91 (2004).
94. El-Serag, H. B. *et al.* Proton pump inhibitors are associated with reduced incidence of dysplasia in Barrett's esophagus. *Am. J. Gastroenterol.* **99**, 1877–83 (2004).
  95. Freedberg, D. E., Kim, L. S. & Yang, Y.-X. The Risks and Benefits of Long-term Use of Proton Pump Inhibitors: Expert Review and Best Practice Advice From the American Gastroenterological Association. *Gastroenterology* **152**, 706–715 (2017).
  96. Lazarus, B. *et al.* Proton Pump Inhibitor Use and the Risk of Chronic Kidney Disease. *JAMA Intern. Med.* **176**, 238 (2016).
  97. Haenisch, B. *et al.* Risk of dementia in elderly patients with the use of proton pump inhibitors. *Eur. Arch. Psychiatry Clin. Neurosci.* **265**, 419–428 (2015).
  98. Yang, Y.-X., Lewis, J. D., Epstein, S. & Metz, D. C. Long-term Proton Pump Inhibitor Therapy and Risk of Hip Fracture. *JAMA* **296**, 2947 (2006).
  99. Shah, N. H. *et al.* Proton Pump Inhibitor Usage and the Risk of Myocardial Infarction in the General Population. *PLoS One* **10**, e0124653 (2015).
  100. Lo, W.-K. & Chan, W. W. Proton pump inhibitor use and the risk of small intestinal bacterial overgrowth: a meta-analysis. *Clin. Gastroenterol. Hepatol.* **11**, 483–90 (2013).
  101. Lewis, S. J., Franco, S., Young, G. & O'Keefe, S. J. Altered bowel function and duodenal bacterial overgrowth in patients treated with omeprazole. *Aliment. Pharmacol. Ther.* **10**, 557–61 (1996).
  102. Bavishi, C. & DuPont, H. L. Systematic review: the use of proton pump inhibitors and increased susceptibility to enteric infection. *Aliment. Pharmacol. Ther.* **34**, 1269–1281 (2011).
  103. Crim, S. M. *et al.* Preliminary incidence and trends of infection with pathogens transmitted commonly through food - Foodborne Diseases Active Surveillance Network, 10 U.S. sites, 2006-2014. *MMWR. Morb. Mortal. Wkly. Rep.* **64**, 495–9 (2015).

104. Furuya-Kanamori, L. *et al.* Comorbidities, Exposure to Medications, and the Risk of Community-Acquired *Clostridium difficile* Infection: a systematic review and meta-analysis. *Infect. Control Hosp. Epidemiol.* **36**, 132–41 (2015).
105. Xu, H. B. *et al.* Proton pump inhibitor use and risk of spontaneous bacterial peritonitis in cirrhotic patients: a systematic review and meta-analysis. *Genet. Mol. Res.* **14**, 7490–7501 (2015).
106. Lambert, A. A. *et al.* Risk of Community-Acquired Pneumonia with Outpatient Proton-Pump Inhibitor Therapy: A Systematic Review and Meta-Analysis. *PLoS One* **10**, e0128004 (2015).
107. Lam, J. R., Schneider, J. L., Zhao, W. & Corley, D. A. Proton Pump Inhibitor and Histamine 2 Receptor Antagonist Use and Vitamin B 12 Deficiency. *JAMA* **310**, 2435 (2013).
108. Bailey, R. L. *et al.* Monitoring of vitamin B-12 nutritional status in the United States by using plasma methylmalonic acid and serum vitamin B-12. *Am. J. Clin. Nutr.* **94**, 552–61 (2011).
109. García Rodríguez, L. A., Lagergren, J. & Lindblad, M. Gastric acid suppression and risk of oesophageal and gastric adenocarcinoma: a nested case control study in the UK. *Gut* **55**, 1538–44 (2006).
110. Caldwell, M. T., Lawlor, P., Byrne, P. J., Walsh, T. N. & Hennessy, T. P. Ambulatory oesophageal bile reflux monitoring in Barrett's oesophagus. *Br. J. Surg.* **82**, 657–60 (1995).
111. Sontag, S. J. The medical management of reflux esophagitis. Role of antacids and acid inhibition. *Gastroenterol. Clin. North Am.* **19**, 683–712 (1990).
112. Souza, R. F. *et al.* Gastroesophageal Reflux Might Cause Esophagitis Through a Cytokine-Mediated Mechanism Rather Than Caustic Acid Injury. *Gastroenterology* **137**, 1776–1784 (2009).
113. Nehra, D., Howell, P., Williams, C. P., Pye, J. K. & Beynon, J. Toxic bile acids in gastro-oesophageal reflux disease: influence of gastric acidity. *Gut* **44**, 598–602 (1999).



114. Jenkins, G. J. S. *et al.* Deoxycholic acid at neutral and acid pH, is genotoxic to oesophageal cells through the induction of ROS: The potential role of anti-oxidants in Barrett's oesophagus. *Carcinogenesis* **28**, 136–42 (2007).
115. Jenkins, G. J. S. *et al.* The bile acid deoxycholic acid has a non-linear dose response for DNA damage and possibly NF-kappaB activation in oesophageal cells, with a mechanism of action involving ROS. *Mutagenesis* **23**, 399–405 (2008).
116. Huo, X. *et al.* Deoxycholic acid causes DNA damage while inducing apoptotic resistance through NF- B activation in benign Barrett's epithelial cells. *AJP Gastrointest. Liver Physiol.* **301**, G278–G286 (2011).
117. Onuchina, E. V, Tsukanov, V. V & Osipenko, M. F. [Drug UDCA (Ursosan) in therapeutic management of patients Barrett's esophagus]. *Eksp. Klin. Gastroenterol.* 96–101 (2010).
118. Bozikas, A. *et al.* The effect of oral administration of ursodeoxycholic acid and high-dose proton pump inhibitors on the histology of Barrett's esophagus. *Dis. esophagus Off. J. Int. Soc. Dis. Esophagus* **21**, 346–54 (2008).
119. Banerjee, B. *et al.* Clinical Study of Ursodeoxycholic Acid in Barrett's Esophagus Patients. *Cancer Prev. Res. (Phila)*. **9**, 528–33 (2016).
120. Pearson, J. P. *et al.* Review article: reflux and its consequences--the laryngeal, pulmonary and oesophageal manifestations. Conference held in conjunction with the 9th International Symposium on Human Pepsin (ISHP) Kingston-upon-Hull, UK, 21-23 April 2010. *Aliment. Pharmacol. Ther.* **33 Suppl 1**, 1–71 (2011).
121. Samuels, T. *et al.* Local Synthesis of Pepsin in Barrett's Esophagus and the Role of Pepsin in Esophageal Adenocarcinoma. *Ann. Otol. Rhinol. Laryngol.* **124**, 893–902 (2015).
122. Eberhart, C. E. *et al.* Up-regulation of cyclooxygenase 2 gene expression in human colorectal adenomas and adenocarcinomas. *Gastroenterology* **107**, 1183–8 (1994).
123. Cianchi, F. *et al.* Cyclooxygenase-2 activation mediates the proangiogenic effect

- of nitric oxide in colorectal cancer. *Clin. Cancer Res.* **10**, 2694–704 (2004).
124. Morris, C. D., Armstrong, G. R., Bigley, G., Green, H. & Attwood, S. E. Cyclooxygenase-2 expression in the Barrett's metaplasia-dysplasia-adenocarcinoma sequence. *Am. J. Gastroenterol.* **96**, 990–6 (2001).
125. Heath, E. I. *et al.* Secondary chemoprevention of Barrett's esophagus with celecoxib: results of a randomized trial. *J. Natl. Cancer Inst.* **99**, 545–57 (2007).
126. Triadafilopoulos, G. *et al.* The effects of esomeprazole combined with aspirin or rofecoxib on prostaglandin E2 production in patients with Barrett's oesophagus. *Aliment. Pharmacol. Ther.* **23**, 997–1005 (2006).
127. Omer, Z. B. *et al.* Aspirin Protects Against Barrett's Esophagus in a Multivariate Logistic Regression Analysis. *Clin. Gastroenterol. Hepatol.* **10**, 722–727 (2012).
128. Corley, D. A., Kerlikowske, K., Verma, R. & Buffler, P. Protective association of aspirin/NSAIDs and esophageal cancer: a systematic review and meta-analysis. *Gastroenterology* **124**, 47–56 (2003).
129. Thrift, A. P. *et al.* The use of nonsteroidal anti-inflammatory drugs and the risk of Barrett's oesophagus. *Aliment. Pharmacol. Ther.* **34**, 1235–1244 (2011).
130. Das, D., Chilton, A. P. & Jankowski, J. A. Chemoprevention of oesophageal cancer and the AspECT trial. *Recent Results Cancer Res.* **181**, 161–9 (2009).
131. Dolmans, D. E. J. G. J., Fukumura, D. & Jain, R. K. Photodynamic therapy for cancer. *Nat. Rev. Cancer* **3**, 380–7 (2003).
132. Bown, S. G. & Lovat, L. B. The biology of photodynamic therapy in the gastrointestinal tract. *Gastrointest. Endosc. Clin. N. Am.* **10**, 533–50 (2000).
133. Overholt, B. F. *et al.* Photodynamic therapy with porfimer sodium for ablation of high-grade dysplasia in Barrett's esophagus: international, partially blinded, randomized phase III trial. *Gastrointest. Endosc.* **62**, 488–98 (2005).
134. Overholt, B. F. *et al.* Five-year efficacy and safety of photodynamic therapy with Photofrin in Barrett's high-grade dysplasia. *Gastrointest. Endosc.* **66**, 460–468 (2007).
135. Gray, J. & Fullarton, G. M. Long term efficacy of Photodynamic Therapy (PDT)

as an ablative therapy of high grade dysplasia in Barrett's oesophagus.

*Photodiagnosis Photodyn. Ther.* **10**, 561–5 (2013).

136. Overholt, B. F., Panjehpour, M. & Halberg, D. L. Photodynamic therapy for Barrett's esophagus with dysplasia and/or early stage carcinoma: long-term results. *Gastrointest. Endosc.* **58**, 183–8 (2003).
137. Overholt, B. F. & Panjehpour, M. Barrett's esophagus: photodynamic therapy for ablation of dysplasia, reduction of specialized mucosa, and treatment of superficial esophageal cancer. *Gastrointest. Endosc.* **42**, 64–70 (1995).
138. Wang, K. K. & Nijhawan, P. K. Complications of photodynamic therapy in gastrointestinal disease. *Gastrointest. Endosc. Clin. N. Am.* **10**, 487–95 (2000).
139. National Institute For Health And Clinical Excellence. *NICE interventional procedure guidance [IPG350] Photodynamic therapy for Barrett's oesophagus.* (2010).
140. National Institute For Health And Clinical Excellence. *NICE interventional procedure guidance [IPG200] Photodynamic therapy for early-stage oesophageal cancer.* (2006).
141. National Institute For Health And Clinical Excellence. *NICE interventional procedure guidance [IPG206] Palliative photodynamic therapy for advanced oesophageal cancer.* (2007).
142. Regula, J. *et al.* Photosensitisation and photodynamic therapy of oesophageal, duodenal, and colorectal tumours using 5 aminolaevulinic acid induced protoporphyrin IX--a pilot study. *Gut* **36**, 67–75 (1995).
143. Panjehpour, M. *et al.* Photodynamic therapy using verteporfin (benzoporphyrin derivative monoacid ring A, BPD-MA) and 630 nm laser light in canine esophagus. *Lasers Surg. Med.* **30**, 26–30 (2002).
144. Yano, T. *et al.* Phase I study of photodynamic therapy using talaporfin sodium and diode laser for local failure after chemoradiotherapy for esophageal cancer. *Radiat. Oncol.* **7**, 113 (2012).
145. Yano, T. *et al.* A multicenter phase II study of salvage photodynamic therapy

using talaporfin sodium (ME2906) and a diode laser (PNL6405EPG) for local failure after chemoradiotherapy or radiotherapy for esophageal cancer.

*Oncotarget* (2016). doi:10.18632/oncotarget.14029

146. di Pietro, M., Fitzgerald, R. C. & BSG Barrett's guidelines working group. Revised British Society of Gastroenterology recommendation on the diagnosis and management of Barrett's oesophagus with low-grade dysplasia. *Gut* **67**, 392–393 (2018).
147. Shaheen, N. J. *et al.* Radiofrequency ablation in Barrett's esophagus with dysplasia. *N. Engl. J. Med.* **360**, 2277–88 (2009).
148. Ganz, R. A. *et al.* Circumferential ablation of Barrett's esophagus that contains high-grade dysplasia: a U.S. Multicenter Registry. *Gastrointest. Endosc.* **68**, 35–40 (2008).
149. Haidry, R. J. *et al.* Improvement over time in outcomes for patients undergoing endoscopic therapy for Barrett's oesophagus-related neoplasia: 6-year experience from the first 500 patients treated in the UK patient registry. *Gut* **64**, 1192–9 (2014).
150. Prasad, G. A. *et al.* Significance of neoplastic involvement of margins obtained by endoscopic mucosal resection in Barrett's esophagus. *Am. J. Gastroenterol.* **102**, 2380–6 (2007).
151. Allum, W. H., Griffin, S. M., Watson, a & Colin-Jones, D. Guidelines for the management of oesophageal and gastric cancer. *Gut* **50 Suppl 5**, v1–v23 (2002).
152. Nigro, J. J. *et al.* Occult esophageal adenocarcinoma: extent of disease and implications for effective therapy. *Ann. Surg.* **230**, 433-8-40 (1999).
153. Fernando, H. C., Luketich, J. D., Buenaventura, P. O., Perry, Y. & Christie, N. A. Outcomes of minimally invasive esophagectomy (MIE) for high-grade dysplasia of the esophagus. *Eur. J. Cardiothorac. Surg.* **22**, 1–6 (2002).
154. Rice, T. W. *et al.* Esophageal carcinoma: depth of tumor invasion is predictive of regional lymph node status. *Ann. Thorac. Surg.* **65**, 787–92 (1998).

155. Wani, S. *et al.* Greater interobserver agreement by endoscopic mucosal resection than biopsy samples in Barrett's dysplasia. *Clin. Gastroenterol. Hepatol.* **8**, 783–8 (2010).
156. Mino-Kenudson, M. *et al.* EMR for Barrett's esophagus-related superficial neoplasms offers better diagnostic reproducibility than mucosal biopsy. *Gastrointest. Endosc.* **66**, 660–6, 769 (2007).
157. May, A. *et al.* A prospective randomized trial of two different endoscopic resection techniques for early stage cancer of the esophagus. *Gastrointest. Endosc.* **58**, 167–175 (2003).
158. Pech, O. *et al.* Long-term results and risk factor analysis for recurrence after curative endoscopic therapy in 349 patients with high-grade intraepithelial neoplasia and mucosal adenocarcinoma in Barrett's oesophagus. *Gut* **57**, 1200–6 (2008).
159. Minami, S., Gotoda, T., Ono, H., Oda, I. & Hamanaka, H. Complete endoscopic closure of gastric perforation induced by endoscopic resection of early gastric cancer using endoclips can prevent surgery (with video). *Gastrointest. Endosc.* **63**, 596–601 (2006).
160. Seewald, S. *et al.* Circumferential EMR and complete removal of Barrett's epithelium: a new approach to management of Barrett's esophagus containing high-grade intraepithelial neoplasia and intramucosal carcinoma. *Gastrointest. Endosc.* **57**, 854–9 (2003).
161. Giovannini, M. *et al.* Circumferential Endoscopic Mucosal Resection in Barrett's Esophagus with High-Grade Intraepithelial Neoplasia or Mucosal Cancer. Preliminary Results in 21 Patients. *Endoscopy* **36**, 782–787 (2004).
162. Peters, F. P. *et al.* Stepwise radical endoscopic resection is effective for complete removal of Barrett's esophagus with early neoplasia: a prospective study. *Am. J. Gastroenterol.* **101**, 1449–57 (2006).
163. van Vilsteren, F. G. I. *et al.* Stepwise radical endoscopic resection versus radiofrequency ablation for Barrett's oesophagus with high-grade dysplasia or

- early cancer: a multicentre randomised trial. *Gut* **60**, 765–73 (2011).
164. Ng, T. & Vezeridis, M. P. Advances in the surgical treatment of esophageal cancer. *J. Surg. Oncol.* **101**, 725–9 (2010).
165. Pohl, H., Sonnenberg, A., Strobel, S., Eckardt, A. & Rösch, T. Endoscopic versus surgical therapy for early cancer in Barrett's esophagus: a decision analysis. *Gastrointest. Endosc.* **70**, 623–31 (2009).
166. Treitl, D., Hurtado, M. & Ben-David, K. Minimally Invasive Esophagectomy: A New Era of Surgical Resection. *J. Laparoendosc. Adv. Surg. Tech. A* **26**, 276–80 (2016).
167. Luna, R. A., Gilbert, E. & Hunter, J. G. High-grade dysplasia and intramucosal adenocarcinoma in Barrett's esophagus: the role of esophagectomy in the era of endoscopic eradication therapy. *Curr. Opin. Gastroenterol.* **28**, 362–9 (2012).
168. Biomarkers Definitions Working Group. Biomarkers and surrogate endpoints: preferred definitions and conceptual framework. *Clin. Pharmacol. Ther.* **69**, 89–95 (2001).
169. Ong, C.-A. J., Lao-Sirieix, P. & Fitzgerald, R. C. Biomarkers in Barrett's esophagus and esophageal adenocarcinoma: predictors of progression and prognosis. *World J. Gastroenterol.* **16**, 5669–81 (2010).
170. Morales, C. P., Souza, R. F. & Spechler, S. J. Hallmarks of cancer progression in Barrett's oesophagus. *Lancet (London, England)* **360**, 1587–9 (2002).
171. Spechler, S. J., Fitzgerald, R. C., Prasad, G. A. & Wang, K. K. History, molecular mechanisms, and endoscopic treatment of Barrett's esophagus. *Gastroenterology* **138**, 854–69 (2010).
172. Weaver, B. a. & Cleveland, D. W. The Aneuploidy Paradox in Cell Growth and Tumorigenesis. *Cancer Cell* **14**, 431–433 (2008).
173. Doak, S. H. *et al.* Chromosome 4 hyperploidy represents an early genetic aberration in premalignant Barrett's oesophagus. *Gut* **52**, 623–8 (2003).
174. Chaves, P. *et al.* Chromosomal analysis of Barrett's cells: demonstration of instability and detection of the metaplastic lineage involved. *Mod. Pathol.* **20**,

- 788–796 (2007).
175. Reid, B. J. *et al.* Flow-cytometric and histological progression to malignancy in Barrett's esophagus: prospective endoscopic surveillance of a cohort. *Gastroenterology* **102**, 1212–1219 (1992).
  176. Rabinovitch, P. S., Longton, G., Blount, P. L., Levine, D. S. & Reid, B. J. Predictors of progression in Barrett's esophagus III: baseline flow cytometric variables. *Am. J. Gastroenterol.* **96**, 3071–83 (2001).
  177. Galipeau, P. C. *et al.* NSAIDs modulate CDKN2A, TP53, and DNA content risk for progression to esophageal adenocarcinoma. *PLoS Med.* **4**, 0342–0353 (2007).
  178. Dunn, J. M. *et al.* Image cytometry accurately detects DNA ploidy abnormalities and predicts late relapse to high-grade dysplasia and adenocarcinoma in Barrett's oesophagus following photodynamic therapy. *Br. J. Cancer* **102**, 1608–17 (2010).
  179. Bird-Lieberman, E. L. *et al.* Population-based study reveals new risk-stratification biomarker panel for Barrett's esophagus. *Gastroenterology* **143**, 927–935.e3 (2012).
  180. Oukrif, D. *et al.* PTU-158 Dna Ploidy Abnormalities Correlate with Increasing Degree of Dysplasia in Cases Referred to a Specialist Clinical Image Cytometry Service for the Management of Barrett'S Oesophagus. *Gut* **62**, A113.1-A113 (2013).
  181. Fang, M. *et al.* DNA abnormalities as marker of risk for progression of Barrett's esophagus to adenocarcinoma: image cytometric DNA analysis in formalin-fixed tissues. *Am. J. Gastroenterol.* **99**, 1887–94 (2004).
  182. Vogt, N., Schönegg, R., Gschossmann, J. M. & Borovicka, J. Benefit of baseline cytometry for surveillance of patients with Barrett's esophagus. *Surg. Endosc.* **24**, 1144–50 (2010).
  183. Wong, D. J. *et al.* p16(INK4a) lesions are common, early abnormalities that undergo clonal expansion in Barrett's metaplastic epithelium. *Cancer Res.* **61**,

- 8284–9 (2001).
184. Reid, B. J. *et al.* Predictors of progression in Barrett's esophagus II: baseline 17p (p53) loss of heterozygosity identifies a patient subset at increased risk for neoplastic progression. *Am. J. Gastroenterol.* **96**, 2839–48 (2001).
  185. Murray, L. *et al.* TP53 and progression from Barrett's metaplasia to oesophageal adenocarcinoma in a UK population cohort. *Gut* **55**, 1390–7 (2006).
  186. Skacel, M. *et al.* p53 expression in low grade dysplasia in Barrett's esophagus: correlation with interobserver agreement and disease progression. *Am. J. Gastroenterol.* **97**, 2508–13 (2002).
  187. Kastelein, F. *et al.* Aberrant p53 protein expression is associated with an increased risk of neoplastic progression in patients with Barrett's oesophagus. *Gut* **62**, 1676–83 (2013).
  188. Eads, C. A. *et al.* Fields of aberrant CpG island hypermethylation in Barrett's esophagus and associated adenocarcinoma. *Cancer Res.* **60**, 5021–6 (2000).
  189. Maley, C. C. *et al.* Selectively advantageous mutations and hitchhikers in neoplasms: p16 lesions are selected in Barrett's esophagus. *Cancer Res.* **64**, 3414–27 (2004).
  190. Schulmann, K. *et al.* Inactivation of p16, RUNX3, and HPP1 occurs early in Barrett's-associated neoplastic progression and predicts progression risk. *Oncogene* **24**, 4138–48 (2005).
  191. Wang, J. S. *et al.* DNA promoter hypermethylation of p16 and APC predicts neoplastic progression in Barrett's esophagus. *Am. J. Gastroenterol.* **104**, 2153–60 (2009).
  192. Bryant, J. A. & Aves, S. J. Initiation of DNA replication: functional and evolutionary aspects. *Ann. Bot.* **107**, 1119–26 (2011).
  193. Prasad, G. A., Bansal, A., Sharma, P. & Wang, K. K. Predictors of progression in Barrett's esophagus: current knowledge and future directions. *Am. J. Gastroenterol.* **105**, 1490–1502 (2010).
  194. Lao-Sirieix, P., Brais, R., Lovat, L., Coleman, N. & Fitzgerald, R. C. Cell cycle



- phase abnormalities do not account for disordered proliferation in Barrett's carcinogenesis. *Neoplasia* **6**, 751–60
195. Going, J. J. *et al.* Aberrant expression of minichromosome maintenance proteins 2 and 5, and Ki-67 in dysplastic squamous oesophageal epithelium and Barrett's mucosa. *Gut* **50**, 373–7 (2002).
  196. Sirieix, P. S. *et al.* Surface expression of minichromosome maintenance proteins provides a novel method for detecting patients at risk for developing adenocarcinoma in Barrett's esophagus. *Clin. Cancer Res.* **9**, 2560–6 (2003).
  197. Dunn, J. M. *et al.* PLK-1 is upregulated in barrett's adenocarcinoma and is a surrogate marker of aneuploidy. *Gut* **60**, A172–A172 (2011).
  198. WikiMiMa. Cyclin Expression Cycle. *de.wikipedia* (2011). Available at: [https://commons.wikimedia.org/wiki/File:Cyclin\\_Expression.svg](https://commons.wikimedia.org/wiki/File:Cyclin_Expression.svg).
  199. Bani-Hani, K. *et al.* Prospective study of cyclin D1 overexpression in Barrett's esophagus: association with increased risk of adenocarcinoma. *J. Natl. Cancer Inst.* **92**, 1316–1321 (2000).
  200. Lao-Sirieix, P., Lovat, L. & Fitzgerald, R. C. Cyclin A immunocytology as a risk stratification tool for Barrett's esophagus surveillance. *Clin. Cancer Res.* **13**, 659–65 (2007).
  201. Rodriguez-Acebes, S. *et al.* Targeting DNA replication before it starts: Cdc7 as a therapeutic target in p53-mutant breast cancers. *Am. J. Pathol.* **177**, 2034–45 (2010).
  202. Holtrich, U. *et al.* Induction and down-regulation of PLK, a human serine/threonine kinase expressed in proliferating cells and tumors. *Proc. Natl. Acad. Sci. U. S. A.* **91**, 1736–40 (1994).
  203. Tokumitsu, Y. *et al.* Prognostic significance of polo-like kinase expression in esophageal carcinoma. *Int. J. Oncol.* **15**, 687–92 (1999).
  204. Takai, N., Hamanaka, R., Yoshimatsu, J. & Miyakawa, I. Polo-like kinases (Plks) and cancer. *Oncogene* **24**, 287–291 (2005).
  205. Takaki, T., Trenz, K., Costanzo, V. & Petronczki, M. Polo-like kinase 1 reaches

- beyond mitosis--cytokinesis, DNA damage response, and development. *Curr. Opin. Cell Biol.* **20**, 650–60 (2008).
206. Ito, T. *et al.* Polo-like kinase 1 regulates cell proliferation and is targeted by miR-593\* in esophageal cancer. *Int. J. Cancer* **129**, 2134–46 (2011).
207. Kops, G. J. P. L., Weaver, B. A. A. & Cleveland, D. W. On the road to cancer: aneuploidy and the mitotic checkpoint. *Nat. Rev. Cancer* **5**, 773–85 (2005).
208. Blanchard, Z. *et al.* Geminin overexpression induces mammary tumors via suppressing cytokinesis. *Oncotarget* **2**, 1011–27 (2011).
209. Johnson, K. A. & Brown, P. H. Drug development for cancer chemoprevention: focus on molecular targets. *Semin. Oncol.* **37**, 345–58 (2010).
210. Gardner, L., Malik, R., Shimizu, Y., Mullins, N. & ElShamy, W. M. Geminin overexpression prevents the completion of topoisomerase II $\alpha$  chromosome decatenation, leading to aneuploidy in human mammary epithelial cells. *Breast Cancer Res.* **13**, R53 (2011).
211. Rosenberg, S. A. Development of cancer immunotherapies based on identification of the genes encoding cancer regression antigens. *J. Natl. Cancer Inst.* **88**, 1635–44 (1996).
212. Yao, X.-L., Nakagawa, S. & Gao, J.-Q. Current targeting strategies for adenovirus vectors in cancer gene therapy. *Curr. Cancer Drug Targets* **11**, 810–25 (2011).
213. Paszko, E. & Senge, M. O. Immunoliposomes. *Curr. Med. Chem.* **19**, 5239–77 (2012).
214. Liddy, N. *et al.* Monoclonal TCR-redirectioned tumor cell killing. *Nat. Med.* **18**, 980–7 (2012).
215. Berg, K. *et al.* Photochemical internalization (PCI): a technology for drug delivery. *Methods Mol. Biol.* **635**, 133–45 (2010).
216. Hakama, M. *et al.* Tumour markers and screening for gastrointestinal cancer: a follow up study in Finland. *J. Med. Screen.* **1**, 60–4 (1994).
217. Burford, B. *et al.* Autoantibodies to MUC1 glycopeptides cannot be used as a

- screening assay for early detection of breast, ovarian, lung or pancreatic cancer. *Br. J. Cancer* **108**, 2045–55 (2013).
218. National Institute For Health And Clinical Excellence. *NICE guideline [NG85]. Pancreatic cancer in adults: diagnosis and management.* (2018).
219. O'Reilly, E. M. & Lowery, M. A. Postresection surveillance for pancreatic cancer performance status, imaging, and serum markers. *Cancer J.* **18**, 609–13
220. Vargas, G. M. *et al.* Physician follow-up and observation of guidelines in the post treatment surveillance of colorectal cancer. *Surgery* **154**, 244–55 (2013).
221. [TA208], N. technology appraisal guidance. *Trastuzumab for the treatment of HER2-positive metastatic gastric cancer.* (2010).
222. Tanner, M. *et al.* Amplification of HER-2 in gastric carcinoma: association with Topoisomerase IIalpha gene amplification, intestinal type, poor prognosis and sensitivity to trastuzumab. *Ann. Oncol. Off. J. Eur. Soc. Med. Oncol.* **16**, 273–8 (2005).
223. Hofmann, M. *et al.* Assessment of a HER2 scoring system for gastric cancer: Results from a validation study. *Histopathology* **52**, 797–805 (2008).
224. Gu, J. *et al.* Prognostic significance of HER2 expression based on trastuzumab for gastric cancer (ToGA) criteria in gastric cancer: an updated meta-analysis. *Tumour Biol.* **35**, 5315–21 (2014).
225. Thompson, S. K., Sullivan, T. R., Davies, R. & Ruszkiewicz, A. R. Her-2/neu gene amplification in esophageal adenocarcinoma and its influence on survival. *Ann. Surg. Oncol.* **18**, 2010–2017 (2011).
226. Reichelt, U. *et al.* Frequent homogeneous HER-2 amplification in primary and metastatic adenocarcinoma of the esophagus. *Mod. Pathol.* **20**, 120–129 (2007).
227. Gravalos, C. & Jimeno, A. HER2 in gastric cancer: a new prognostic factor and a novel therapeutic target. *Ann. Oncol. Off. J. Eur. Soc. Med. Oncol. / ESMO* **19**, 1523–1529 (2008).
228. Chua, T. C. & Merrett, N. D. Clinicopathologic factors associated with HER2-positive gastric cancer and its impact on survival outcomes--a systematic review.

- Int. J. Cancer* **130**, 2845–2856 (2012).
229. Bang, Y.-J. *et al.* Trastuzumab in combination with chemotherapy versus chemotherapy alone for treatment of HER2-positive advanced gastric or gastro-oesophageal junction cancer (ToGA): a phase 3, open-label, randomised controlled trial. *Lancet (London, England)* **376**, 687–97 (2010).
230. Rüschoff, J. *et al.* [Her2 testing in gastric cancer. What is different in comparison to breast cancer?]. *Pathologe* **31**, 208–17 (2010).
231. *Trastuzumab (Herceptin), Genentech, Inc., in combination with cisplatin and a fluoropyrimidine (capecitabine or 5-fluorouracil), for the treatment of patients with HER2 overexpressing metastatic gastric or gastroesophageal (GE) junction adenocarcinoma, w.* (2010).
232. Mendelsohn, J. & Fan, Z. Epidermal growth factor receptor family and chemosensitization. *J. Natl. Cancer Inst.* **89**, 341–3 (1997).
233. Lenferink, A. E. *et al.* Differential endocytic routing of homo- and hetero-dimeric ErbB tyrosine kinases confers signaling superiority to receptor heterodimers. *EMBO J.* **17**, 3385–97 (1998).
234. Tzahar, E. *et al.* A hierarchical network of interreceptor interactions determines signal transduction by Neu differentiation factor/neuregulin and epidermal growth factor. *Mol. Cell. Biol.* **16**, 5276–87 (1996).
235. Kwak, E. L. *et al.* Epidermal growth factor receptor kinase domain mutations in esophageal and pancreatic adenocarcinomas. *Clin. Cancer Res.* **12**, 4283–7 (2006).
236. Rygiel, A. M. *et al.* Gains and amplifications of c-myc, EGFR, and 20.q13 loci in the no dysplasia-dysplasia-adenocarcinoma sequence of Barrett's esophagus. *Cancer Epidemiol. Biomarkers Prev.* **17**, 1380–5 (2008).
237. al-Kasspoles, M., Moore, J. H., Orringer, M. B. & Beer, D. G. Amplification and over-expression of the EGFR and erbB-2 genes in human esophageal adenocarcinomas. *Int. J. cancer* **54**, 213–9 (1993).
238. Waddell, T. *et al.* Epirubicin, oxaliplatin, and capecitabine with or without

- panitumumab for patients with previously untreated advanced oesophagogastric cancer (REAL3): a randomised, open-label phase 3 trial. *Lancet. Oncol.* **14**, 481–9 (2013).
239. Lordick, F. *et al.* Capecitabine and cisplatin with or without cetuximab for patients with previously untreated advanced gastric cancer (EXPAND): a randomised, open-label phase 3 trial. *Lancet. Oncol.* **14**, 490–9 (2013).
240. Herbst, R. S., Fukuoka, M. & Baselga, J. Gefitinib--a novel targeted approach to treating cancer. *Nat. Rev. Cancer* **4**, 956–65 (2004).
241. Adelstein, D. J., Rodriguez, C. P., Rybicki, L. A., Ives, D. I. & Rice, T. W. A phase II trial of gefitinib for recurrent or metastatic cancer of the esophagus or gastroesophageal junction. *Invest. New Drugs* **30**, 1684–9 (2012).
242. Iyer, R. *et al.* Erlotinib and radiation therapy for elderly patients with esophageal cancer - clinical and correlative results from a prospective multicenter phase 2 trial. *Oncology* **85**, 53–8 (2013).
243. Li, M. *et al.* Affinity peptide for targeted detection of dysplasia in barrett's esophagus. *Gastroenterology* **139**, 1472–1480 (2010).
244. Horm, T. M. & Schroeder, J. A. MUC1 and metastatic cancer: expression, function and therapeutic targeting. *Cell Adh. Migr.* **7**, 187–98
245. Albrecht, H. & Carraway, K. L. MUC1 and MUC4: switching the emphasis from large to small. *Cancer Biother. Radiopharm.* **26**, 261–271 (2011).
246. von Mensdorff-Pouilly, S., Moreno, M. & Verheijen, R. H. M. Natural and induced humoral responses to MUC1. *Cancers (Basel)*. **3**, 3073–3103 (2011).
247. Kimura, T. & Finn, O. J. MUC1 immunotherapy is here to stay. *Expert Opinion on Biological Therapy* 1–15 (2012). doi:10.1517/14712598.2012.725719
248. Remmers, N. *et al.* Aberrant expression of mucin core proteins and O-linked glycans associated with progression of pancreatic cancer. *Clin. Cancer Res.* **19**, 1981–1993 (2013).
249. Piessen, G. *et al.* Clinical impact of MUC1 and MUC4 expression in Barrett-associated oesophageal adenocarcinoma. *J. Clin. Pathol.* **62**, 1144–1146

- (2009).
250. Arul, G. S. *et al.* Mucin gene expression in Barrett's oesophagus: an in situ hybridisation and immunohistochemical study. *Gut* **47**, 753–761 (2000).
  251. Guillem, P. *et al.* Mucin gene expression and cell differentiation in human normal, premalignant and malignant esophagus. *Int. J. Cancer* **88**, 856–861 (2000).
  252. Pegram, M. D. *et al.* Phase I dose escalation pharmacokinetic assessment of intravenous humanized anti-MUC1 antibody AS1402 in patients with advanced breast cancer. *Breast Cancer Res.* **11**, R73 (2009).
  253. Oei, A. L. M. *et al.* Induction of IgG antibodies to MUC1 and survival in patients with epithelial ovarian cancer. *International journal of cancer. Journal international du cancer* **123**, (2008).
  254. Braga, V. M., Pemberton, L. F., Duhig, T. & Gendler, S. J. Spatial and temporal expression of an epithelial mucin, Muc-1, during mouse development. *Development* **115**, 427–37 (1992).
  255. Pemberton, L., Taylor-Papadimitriou, J. & Gendler, S. J. Antibodies to the cytoplasmic domain of the MUC1 mucin show conservation throughout mammals. *Biochem. Biophys. Res. Commun.* **185**, 167–75 (1992).
  256. Gürbüz, Y., Kahlke, V. & Klöppel, G. How do gastric carcinoma classification systems relate to mucin expression patterns? An immunohistochemical analysis in a series of advanced gastric carcinomas. *Virchows Arch.* **440**, 505–11 (2002).
  257. Cohen, M., Drut, R. & Cueto Rúa, E. SIALYL-Tn antigen distribution in *Helicobacter pylori* chronic gastritis in children: an immunohistochemical study. *Pediatr. Pathol. Mol. Med.* **22**, 117–29
  258. Kang, Y.-H., Lee, H. S. & Kim, W. H. Promoter methylation and silencing of PTEN in gastric carcinoma. *Lab. Invest.* **82**, 285–91 (2002).
  259. Lee, H. S., Lee, H. K., Kim, H. S., Yang, H.-K. & Kim, W. H. Tumour suppressor gene expression correlates with gastric cancer prognosis. *J. Pathol.* **200**, 39–46 (2003).

260. Graham, T. A., McDonald, S. A. & Wright, N. A. Field cancerization in the GI tract. *Future Oncol.* **7**, 981–93 (2011).
261. Phillips, T. *et al.* Development of standard estrogen and progesterone receptor immunohistochemical assays for selection of patients for antihormonal therapy. *Appl. Immunohistochem. Mol. Morphol.* **15**, 325–331 (2007).
262. Hayley, P., Stamati, I., Yahioğlu, G., Butt, M. & Deonarain, M. Antibody-Directed Phototherapy (ADP). *Antibodies* **2**, 270–305 (2013).
263. McCafferty, J., Griffiths, A. D., Winter, G. & Chiswell, D. J. Phage antibodies: filamentous phage displaying antibody variable domains. *Nature* **348**, 552–4 (1990).
264. Pericleous, L. M., Richards, J., Epenetos, a a, Courtenay-Luck, N. & Deonarain, M. P. Characterisation and internalisation of recombinant humanised HMFG-1 antibodies against MUC1. *Br. J. Cancer* **93**, 1257–1266 (2005).
265. Dhillon, S. S. *et al.* A Phase I Study of Light Dose for Photodynamic Therapy Using 2-[1-Hexyloxyethyl]-2 Devinyl Pyropheophorbide-a for the Treatment of Non-Small Cell Carcinoma In Situ or Non-Small Cell Microinvasive Bronchogenic Carcinoma: A Dose Ranging Study. *J. Thorac. Oncol.* **11**, 234–41 (2016).
266. Stamati, I. *et al.* Novel photosensitisers derived from pyropheophorbide-a: uptake by cells and photodynamic efficiency in vitro. *Photochem. Photobiol. Sci.* **9**, 1033–1041 (2010).
267. Garside, R. *et al.* Surveillance of Barrett's oesophagus: exploring the uncertainty through systematic review, expert workshop and economic modelling. *Health Technol. Assess.* **10**, 1–142, iii–iv (2006).
268. Shaheen, N. J., Falk, G. W., Iyer, P. G., Gerson, L. B. & American College of Gastroenterology. ACG Clinical Guideline: Diagnosis and Management of Barrett's Esophagus. *Am. J. Gastroenterol.* **111**, 30–50; quiz 51 (2016).
269. El-Serag, H. B. *et al.* Surveillance endoscopy is associated with improved outcomes of oesophageal adenocarcinoma detected in patients with Barrett's oesophagus. *Gut* **65**, 1252–60 (2016).

270. Nishitani, H. & Lygerou, Z. Control of DNA replication licensing in a cell cycle. *Genes Cells* **7**, 523–34 (2002).
271. Blow, J. J. & Gillespie, P. J. Replication licensing and cancer--a fatal entanglement? *Nat. Rev. Cancer* **8**, 799–806 (2008).
272. Barr, F. a, Silljé, H. H. W. & Nigg, E. a. Polo-like kinases and the orchestration of cell division. *Nat. Rev. Mol. Cell Biol.* **5**, 429–440 (2004).
273. Böcking, A., Giroud, F. & Reith, A. Consensus report of the European Society for Analytical Cellular Pathology task force on standardization of diagnostic DNA image cytometry. *Anal. Quant. Cytol. Histol.* **17**, 1–7 (1995).
274. Hamilton, P. W. *et al.* Digital pathology and image analysis in tissue biomarker research. *Methods* **70**, 59–73 (2014).
275. Haidry, R. J. *et al.* Radiofrequency ablation for early oesophageal squamous neoplasia: Outcomes form United Kingdom registry. *World J. Gastroenterol.* **19**, 6011–6019 (2013).
276. Barrett, M. T. *et al.* Evolution of neoplastic cell lineages in Barrett oesophagus. *Nat. Genet.* **22**, 106–9 (1999).
277. Leitao, M. M. *et al.* Mutation and expression of the TP53 gene in early stage epithelial ovarian carcinoma. *Gynecol. Oncol.* **93**, 301–6 (2004).
278. Butt, M. A. *et al.* 56 Evaluation of TP53 Mutations on Barrett's Epithelium FFPE Specimens With a Novel Next Generation Sequencing Platform Highlights a Discordance With p53 Immunohistochemistry: Analysis of the Barrett's Epithelium Genome Investigation Study (BEGINS). *Gastroenterology* **148**, S-16-S-17 (2015).
279. Zeki, S. S., McDonald, S. A. & Graham, T. A. Field cancerization in Barrett's esophagus. *Discov. Med.* **12**, 371–9 (2011).
280. Barrett, M. T. *et al.* Allelic loss of 9p21 and mutation of the CDKN2/p16 gene develop as early lesions during neoplastic progression in Barrett's esophagus. *Oncogene* **13**, 1867–73 (1996).
281. Sato, F. *et al.* Polo-like kinase and survivin are esophageal tumor-specific



- promoters. *Biochem. Biophys. Res. Commun.* **342**, 465–471 (2006).
282. Dibb, M. *et al.* The FOXM1-PLK1 axis is commonly upregulated in oesophageal adenocarcinoma. *Br. J. Cancer* **107**, 1766–75 (2012).
283. Ando, K. *et al.* Polo-like kinase 1 (Plk1) inhibits p53 function by physical interaction and phosphorylation. *J. Biol. Chem.* **279**, 25549–61 (2004).
284. Degenhardt, Y. *et al.* Sensitivity of cancer cells to Plk1 inhibitor GSK461364A is associated with loss of p53 function and chromosome instability. *Mol. Cancer Ther.* **9**, 2079–89 (2010).
285. King, S. I. *et al.* Immunohistochemical detection of Polo-like kinase-1 (PLK1) in primary breast cancer is associated with TP53 mutation and poor clinical outcome. *Breast Cancer Res.* **14**, R40 (2012).
286. Chao, D. L. *et al.* Cell proliferation, cell cycle abnormalities, and cancer outcome in patients with Barrett's esophagus: A long-term prospective study. *Clin. Cancer Res.* **14**, 6988–6995 (2009).
287. Cancer Research UK Statistical Information [Accessed Jan 2017]. *Worldwide Cancer Statistics.* (2012).
288. Cancer Research UK Statistical Information. *Cancer incidence for common cancers.* (2016).
289. Cancer Research UK Statistical Information [Accessed Jan 2017]. *Oesophageal Cancer Statistics.* (2014).
290. Cancer Research UK Statistical Information [Accessed Jan 2017]. *Stomach Cancer Statistics.* (2014).
291. Chadwick, G. *et al.* National Oesophago- Gastric Cancer Audit 2016. *R. Coll. Surg. Engl.* (2016).
292. Bang, Y. *et al.* Pathological features of advanced gastric cancer: relationship to human epidermal growth factor receptor 2 positivity in the global screening programme of the ToGA trial. *J. Clin. Oncol.* **27**, abstract 4556 (2009).
293. Kunz, P. L. *et al.* HER2 expression in gastric and gastroesophageal junction adenocarcinoma in a US population: clinicopathologic analysis with proposed

- approach to HER2 assessment. *Appl. Immunohistochem. Mol. Morphol.* **20**, 13–24 (2012).
294. Huang, D. *et al.* HER2 status in gastric and gastroesophageal junction cancer assessed by local and central laboratories: Chinese results of the HER-EAGLE study. *PLoS One* **8**, 1–7 (2013).
295. Wang, T. *et al.* Matched biopsy and resection specimens of gastric and gastroesophageal adenocarcinoma show high concordance in HER2 status. *Hum. Pathol.* **45**, 970–975 (2014).
296. Janjigian, Y. Y. *et al.* Prognosis of metastatic gastric and gastroesophageal junction cancer by HER2 status: a European and USA International collaborative analysis. *Ann. Oncol.* **23**, 2656–62 (2012).
297. Sheng, W. Q. *et al.* HER2 status in gastric cancers: a retrospective analysis from four Chinese representative clinical centers and assessment of its prognostic significance. *Ann. Oncol.* **24**, 2360–4 (2013).
298. García, I. *et al.* Clinical significance of the epidermal growth factor receptor and HER2 receptor in resectable gastric cancer. *Ann. Surg. Oncol.* **10**, 234–41 (2003).
299. Yano, T. *et al.* Comparison of HER2 gene amplification assessed by fluorescence in situ hybridization and HER2 protein expression assessed by immunohistochemistry in gastric cancer. *Oncol. Rep.* **15**, 65–71 (2006).
300. Barros-Silva, J. D. *et al.* Association of ERBB2 gene status with histopathological parameters and disease-specific survival in gastric carcinoma patients. *Br. J. Cancer* **100**, 487–93 (2009).
301. Marx, A. H. *et al.* HER-2 amplification is highly homogenous in gastric cancer. *Hum. Pathol.* **40**, 769–77 (2009).
302. Yan, B. *et al.* A study of HER2 gene amplification and protein expression in gastric cancer. *J. Clin. Pathol.* **63**, 839–42 (2010).
303. Lee, H. E. *et al.* Clinical significance of intratumoral HER2 heterogeneity in gastric cancer. *Eur. J. Cancer* **49**, 1448–1457 (2013).

304. Park, Y. S. *et al.* Comprehensive analysis of HER2 expression and gene amplification in gastric cancers using immunohistochemistry and in situ hybridization: which scoring system should we use? *Hum. Pathol.* **43**, 413–22 (2012).
305. Takehana, T. *et al.* Status of c-erbB-2 in gastric adenocarcinoma: a comparative study of immunohistochemistry, fluorescence in situ hybridization and enzyme-linked immuno-sorbent assay. *Int. J. Cancer* **98**, 833–7 (2002).
306. Tanaka, T. *et al.* Clinicopathological characteristics of human epidermal growth factor receptor 2-positive Barrett's adenocarcinoma. *World J. Gastroenterol.* **18**, 6263–8 (2012).
307. Butt, M. A. *et al.* Mo1134 HER2 Positivity in Metastatic Upper Gastrointestinal Tumours in a Large Multi-Centre UK Cohort Identifies Similar Positivity Rates but Different Trends Than Previously Reported and Suggests New Potential Avenues for HER2 Therapies. *Gastroenterology* **144**, S-587-S-588 (2013).
308. Sobin, L. H. & Compton, C. C. TNM seventh edition: what's new, what's changed: communication from the International Union Against Cancer and the American Joint Committee on Cancer. *Cancer* **116**, 5336–5339 (2010).
309. Edge, S. B. & Compton, C. C. The American Joint Committee on Cancer: the 7th edition of the AJCC cancer staging manual and the future of TNM. *Ann. Surg. Oncol.* **17**, 1471–4 (2010).
310. Rüschoff, J. *et al.* HER2 diagnostics in gastric cancer-guideline validation and development of standardized immunohistochemical testing. *Virchows Arch.* **457**, 299–307 (2010).
311. Rüschoff, J. *et al.* HER2 testing in gastric cancer: a practical approach. *Mod. Pathol.* **25**, 637–650 (2012).
312. Singh, K. *et al.* Updated 2013 College of American Pathologists/American Society of Clinical Oncology (CAP/ASCO) guideline recommendations for human epidermal growth factor receptor 2 (HER2) fluorescent in situ hybridization (FISH) testing increase HER2 positive and HER2 e. *Breast Cancer*

- Res. Treat.* **157**, 405–11 (2016).
313. LAUREN, P. THE TWO HISTOLOGICAL MAIN TYPES OF GASTRIC CARCINOMA: DIFFUSE AND SO-CALLED INTESTINAL-TYPE CARCINOMA. AN ATTEMPT AT A HISTO-CLINICAL CLASSIFICATION. *Acta Pathol. Microbiol. Scand.* **64**, 31–49 (1965).
314. Okines, A. F. C. *et al.* Effect of HER2 on prognosis and benefit from peri-operative chemotherapy in early oesophago-gastric adenocarcinoma in the MAGIC trial. *Ann. Oncol.* **24**, 1253–61 (2013).
315. Mcshane, L. M., Altman, D. G., Sauerbrei, W. & Taube, S. E. Reporting Recommendations for Tumor Marker. *Cancer* **97**, 9067–9072 (2005).
316. Chan, D. S. Y., Twine, C. P. & Lewis, W. G. Systematic review and meta-analysis of the influence of HER2 expression and amplification in operable oesophageal cancer. *J. Gastrointest. Surg.* **16**, 1821–9 (2012).
317. Albarello, L., Pecciarini, L. & Doglioni, C. HER2 testing in gastric cancer. *Adv. Anat. Pathol.* **18**, 53–9 (2011).
318. He, C. *et al.* Correlation of human epidermal growth factor receptor 2 expression with clinicopathological characteristics and prognosis in gastric cancer. *World J. Gastroenterol.* **19**, 2171–8 (2013).
319. Shan, L., Ying, J. & Lu, N. HER2 expression and relevant clinicopathological features in gastric and gastroesophageal junction adenocarcinoma in a Chinese population. *Diagn. Pathol.* **8**, 76 (2013).
320. Tse, C. H. *et al.* Determining true HER2 gene status in breast cancers with polysomy by using alternative chromosome 17 reference genes: implications for anti-HER2 targeted therapy. *J. Clin. Oncol.* **29**, 4168–74 (2011).
321. Yoon, H. H. *et al.* Adverse prognostic impact of intratumor heterogeneous HER2 gene amplification in patients with esophageal adenocarcinoma. *J. Clin. Oncol.* **30**, 3932–8 (2012).
322. Koopman, T. *et al.* HER2 positivity in gastric and esophageal adenocarcinoma: clinicopathological analysis and comparison. *J. Cancer Res. Clin. Oncol.* (2014).

323. Li, X. *et al.* Temporal and spatial evolution of somatic chromosomal alterations: a case-cohort study of Barrett's esophagus. *Cancer Prev. Res. (Phila)*. **7**, 114–27 (2014).
324. Butt, M. A. *et al.* PTU-161 Expression of Polo-Like Kinase 1 and Geminin is Up-Regulated in the Squamous-Metaplasia-Dysplasia-Carcinoma Sequence and Correlates with Aneuploidy. *Gut* **62**, A114–A114 (2013).
325. Nobili, S. *et al.* Genomic and genetic alterations influence the progression of gastric cancer. *World J. Gastroenterol.* **17**, 290–9 (2011).
326. Khayat, A. S. *et al.* Interrelationship between TP53 gene deletion, protein expression and chromosome 17 aneusomy in gastric adenocarcinoma. *BMC Gastroenterol.* **9**, 55 (2009).
327. Krishnamurti, U., Hammers, J. L., Atem, F. D., Storto, P. D. & Silverman, J. F. Poor prognostic significance of unamplified chromosome 17 polysomy in invasive breast carcinoma. *Mod. Pathol.* **22**, 1044–8 (2009).
328. Vanden Bempt, I. *et al.* Polysomy 17 in breast cancer: clinicopathologic significance and impact on HER-2 testing. *J. Clin. Oncol.* **26**, 4869–74 (2008).
329. Wang, D. *et al.* Comparison of the prognostic value of various preoperative inflammation-based factors in patients with stage III gastric cancer. *Tumour Biol.* **33**, 749–56 (2012).
330. Crumley, A. B. C., Stuart, R. C., McKernan, M., McDonald, A. C. & McMillan, D. C. Comparison of an inflammation-based prognostic score (GPS) with performance status (ECOG-ps) in patients receiving palliative chemotherapy for gastroesophageal cancer. *J. Gastroenterol. Hepatol.* **23**, e325-9 (2008).
331. Schumacher, K., Haensch, W., Röefzaad, C. & Schlag, P. M. Prognostic significance of activated CD8(+) T cell infiltrations within esophageal carcinomas. *Cancer Res.* **61**, 3932–6 (2001).
332. Teng, F. *et al.* Tumor infiltrating lymphocytes (TILs) before and after neoadjuvant chemoradiotherapy and its clinical utility for rectal cancer. *Am. J. Cancer Res.* **5**,

2064–74 (2015).

333. Allum, W. H. *et al.* Guidelines for the management of oesophageal and gastric cancer. *Gut* **60**, 1449–72 (2011).
334. Castano, A. P., Demidova, T. N. & Hamblin, M. R. Mechanisms in photodynamic therapy: Part two - Cellular signaling, cell metabolism and modes of cell death. *Photodiagnosis Photodyn. Ther.* **2**, 1–23 (2005).
335. Castano, A. P., Demidova, T. N. & Hamblin, M. R. Mechanisms in photodynamic therapy: Part one - Photosensitizers, photochemistry and cellular localization. *Photodiagnosis Photodyn. Ther.* **1**, 279–293 (2004).
336. Castano, A. P., Demidova, T. N. & Hamblin, M. R. Mechanisms in photodynamic therapy: Part three - Photosensitizer pharmacokinetics, biodistribution, tumor localization and modes of tumor destruction. *Photodiagnosis Photodyn. Ther.* **2**, 91–106 (2005).
337. Reginato, E., Wolf, P. & Hamblin, M. R. Immune response after photodynamic therapy increases anti-cancer and anti-bacterial effects. *World J. Immunol.* **4**, 1–11 (2014).
338. Castano, A. P., Mroz, P. & Hamblin, M. R. Photodynamic therapy and anti-tumour immunity. *Nat. Rev. Cancer* **6**, 535–45 (2006).
339. Mitsunaga, M. *et al.* Cancer cell-selective in vivo near infrared photoimmunotherapy targeting specific membrane molecules. *Nat. Med.* **17**, 1685–1691 (2011).
340. Palumbo, a *et al.* A chemically modified antibody mediates complete eradication of tumours by selective disruption of tumour blood vessels. *Br. J. Cancer* **104**, 1106–1115 (2011).
341. Deyev, S. M. & Lebedenko, E. N. Multivalency: The hallmark of antibodies used for optimization of tumor targeting by design. *BioEssays* **30**, 904–918 (2008).
342. Deonarain, M. P., Yahioğlu, G., Stamati, I. & Marklew, J. Emerging formats for next-generation antibody drug conjugates. *Expert Opin. Drug Discov.* 1–19 (2015). doi:10.1517/17460441.2015.1025049

343. Fusco, N. & Bosari, S. HER2 aberrations and heterogeneity in cancers of the digestive system: Implications for pathologists and gastroenterologists. *World J. Gastroenterol.* **22**, 7926–37 (2016).
344. National Institute For Health And Clinical Excellence. *NICE technology appraisal guidance [TA208] Trastuzumab for the treatment of HER2-positive metastatic gastric cancer.* (2010).
345. Schoppmann, S. F. *et al.* Expression of Her-2 in carcinomas of the esophagus. *Am. J. Surg. Pathol.* **34**, 1868–1873 (2010).
346. Butt, M. A. *et al.* PTU-157 Her2 Positivity in upper Gastrointestinal Tumours in a Large Multi-Centre UK Cohort Identifies Similar Positivity Rates but different Trends than Previously Reported and Suggests new Potential Avenues for her2 Therapies. *Gut* **62**, A112–A113 (2013).
347. Yoon, H. H. *et al.* Association of HER2 / ErbB2 Expression and Gene Amplification with Pathologic Features and Prognosis in Esophageal Adenocarcinomas. **18**, 546–555 (2012).
348. Stahl, P. *et al.* Heterogeneity of amplification of HER2, EGFR, CCND1 and MYC in gastric cancer. *BMC Gastroenterol.* **15**, 1–13 (2015).
349. Sheffield, B. S. *et al.* HER2/neu testing in gastric cancer by immunohistochemistry: assessment of interlaboratory variation. *Arch. Pathol. Lab. Med.* **138**, 1495–502 (2014).
350. Cao, Y. *et al.* Single-chain antibody-based immunotoxins targeting Her2/neu: design optimization and impact of affinity on antitumor efficacy and off-target toxicity. *Mol. Cancer Ther.* **11**, 143–53 (2012).
351. Schier, R. *et al.* In vitro and in vivo characterization of a human anti-c-erbB-2 single-chain Fv isolated from a filamentous phage antibody library. *Immunotechnology* **1**, 73–81 (1995).
352. Wang, Q., Ma, C. & Kemmner, W. Wdr66 is a novel marker for risk stratification and involved in epithelial-mesenchymal transition of esophageal squamous cell carcinoma. *BMC Cancer* **13**, 137 (2013).

353. Kimchi, E. T. *et al.* Progression of Barrett's metaplasia to adenocarcinoma is associated with the suppression of the transcriptional programs of epidermal differentiation. *Cancer Res.* **65**, 3146–3154 (2005).
354. Stairs, D. B. *et al.* Cdx1 and c-Myc foster the initiation of transdifferentiation of the normal esophageal squamous epithelium toward Barrett's esophagus. *PLoS One* **3**, (2008).
355. di Pietro, M. *et al.* Evidence for a functional role of epigenetically regulated midcluster HOXB genes in the development of Barrett esophagus. *Proceedings of the National Academy of Sciences* **109**, 9077–9082 (2012).
356. Saadi, A. *et al.* Stromal genes discriminate preinvasive from invasive disease, predict outcome, and highlight inflammatory pathways in digestive cancers. *Proc. Natl. Acad. Sci. U. S. A.* **107**, 2177–2182 (2010).
357. Hamoudi, R. A. *et al.* Differential expression of NF-kappaB target genes in MALT lymphoma with and without chromosome translocation: insights into molecular mechanism. *Leuk. Off. J. Leuk. Soc. Am. Leuk. Res. Fund, U.K* **24**, 1487–1497 (2010).
358. Jaiswal, K. R. *et al.* Characterization of telomerase-immortalized, non-neoplastic, human Barrett's cell line (BAR-T). *Dis. Esophagus* **20**, 256–264 (2007).
359. Cleves, M. A. From the help desk: Comparing areas under receiver operating characteristic curves from two or more probit or logit models. *Stata J.* **2**, 301–313 (2002).
360. Case, L. D., Kimmick, G., Paskett, E. D., Lohman, K. & Tucker, R. Interpreting measures of treatment effect in cancer clinical trials. *Oncologist* **7**, 181–7 (2002).
361. Kim, S. M. S.-B. *et al.* Prognostic biomarkers for esophageal adenocarcinoma identified by analysis of tumor transcriptome. *PLoS One* **5**, e15074 (2010).
362. Redmond, R. W. & Gamlin, J. N. A compilation of singlet oxygen yields from biologically relevant molecules. *Photochem. Photobiol.* **70**, 391–475 (1999).
363. Rakha, E. A. *et al.* Updated UK Recommendations for HER2 assessment in breast cancer. *J. Clin. Pathol.* **68**, 93–9 (2015).



364. Treacy, A. D., Karamchandani, J. R., Streutker, C. J. & Grin, A. HER2 Genetic Heterogeneity in Gastric Cancer: Evaluation According to the College of American Pathologists Breast Cancer Criteria. *Appl. Immunohistochem. Mol. Morphol.* **23**, 628–32 (2015).
365. Park, S. R. *et al.* Extra-gain of HER2-positive cases through HER2 reassessment in primary and metastatic sites in advanced gastric cancer with initially HER2-negative primary tumours: Results of GASTric cancer HER2 reassessment study 1 (GASTHER1). *Eur. J. Cancer* **53**, 42–50 (2016).
366. Kurokawa, Y. *et al.* Multicenter large-scale study of prognostic impact of HER2 expression in patients with resectable gastric cancer. *Gastric Cancer* **18**, 691–7 (2015).
367. Seol, H. *et al.* Intratumoral heterogeneity of HER2 gene amplification in breast cancer: its clinicopathological significance. *Mod. Pathol.* **25**, 938–48 (2012).
368. Paik, S., Kim, C. & Wolmark, N. HER2 status and benefit from adjuvant trastuzumab in breast cancer. *N. Engl. J. Med.* **358**, 1409–11 (2008).
369. Ithimakin, S. *et al.* HER2 drives luminal breast cancer stem cells in the absence of HER2 amplification: implications for efficacy of adjuvant trastuzumab. *Cancer Res.* **73**, 1635–46 (2013).
370. Georgoulas, V. *et al.* Trastuzumab decreases the incidence of clinical relapses in patients with early breast cancer presenting chemotherapy-resistant CK-19mRNA-positive circulating tumor cells: results of a randomized phase II study. *Ann. Oncol.* **23**, 1744–50 (2012).
371. Barber, L. J., Davies, M. N. & Gerlinger, M. Dissecting cancer evolution at the macro-heterogeneity and micro-heterogeneity scale. *Curr. Opin. Genet. Dev.* **30**, 1–6 (2015).
372. McGranahan, N. & Swanton, C. Biological and therapeutic impact of intratumor heterogeneity in cancer evolution. *Cancer Cell* **27**, 15–26 (2015).
373. Shams, M., Owczarczak, B., Manderscheid-Kern, P., Bellnier, D. A. & Gollnick, S. O. Development of photodynamic therapy regimens that control primary tumor

- growth and inhibit secondary disease. *Cancer Immunol. Immunother.* **64**, 287–97 (2015).
374. Zhang, N.-Z., Bai, S., Cai, X.-J. & Li, L.-B. Inhibitory and Immunological Effects Induced by the Combination of Photodynamic Therapy and Dendritic Cells on Mouse Transplanted Hepatoma. *Photodiagnosis Photodyn. Ther.* (2015). doi:10.1016/j.pdpdt.2015.06.009
375. Kleinovink, J. W. *et al.* Combination of photodynamic therapy and specific immunotherapy efficiently eradicates established tumors. *Clin. Cancer Res.* (2015). doi:10.1158/1078-0432.CCR-15-0515
376. Nath, S. & Mukherjee, P. MUC1: A multifaceted oncoprotein with a key role in cancer progression. *Trends Mol. Med.* **20**, 332–342 (2014).
377. Bafna, S., Kaur, S. & Batra, S. K. Membrane-bound mucins: the mechanistic basis for alterations in the growth and survival of cancer cells. *Oncogene* **29**, 2893–2904 (2010).
378. Yonezawa, S., Goto, M., Yamada, N., Higashi, M. & Nomoto, M. Expression profiles of MUC1, MUC2, and MUC4 mucins in human neoplasms and their relationship with biological behavior. *Proteomics* **8**, 3329–3341 (2008).
379. Mariette, C. *et al.* Activation of MUC1 mucin expression by bile acids in human esophageal adenocarcinomatous cells and tissues is mediated by the phosphatidylinositol 3-kinase. *Surgery* **143**, 58–71 (2008).
380. Palmer, A. J. *et al.* Genetic variation in C20orf54, PLCE1 and MUC1 and the risk of upper gastrointestinal cancers in Caucasian populations. *Eur. J. Cancer Prev.* **21**, 541–544 (2012).
381. Royer, B. *et al.* Population pharmacokinetics of the humanised monoclonal antibody, HuHMFG1 (AS1402), derived from a phase I study on breast cancer. *Br. J. Cancer* **102**, 827–832 (2010).
382. Ibrahim, N. K. *et al.* Randomized phase II trial of letrozole plus Anti-MUC1 antibody AS1402 in hormone receptor-positive locally advanced or metastatic breast cancer. *Clin. Cancer Res.* **17**, 6822–6830 (2011).

383. Nicholson, S. *et al.* A phase I trial of idiotypic vaccination with HMFG1 in ovarian cancer. *Cancer immunology, immunotherapy: CII* **53**, (2004).
384. Hamann, P. R. *et al.* A calicheamicin conjugate with a fully humanized anti-MUC1 antibody shows potent antitumor effects in breast and ovarian tumor xenografts. *Bioconjug. Chem.* **16**, 354–60 (2005).
385. Oniszczyk, A., Wojtunik-Kulesza, K. A., Oniszczyk, T. & Kasprzak, K. The potential of photodynamic therapy (PDT)-Experimental investigations and clinical use. *Biomed. Pharmacother.* **83**, 912–929 (2016).
386. Bown, S. G. How mainstream medicine sees photodynamic therapy in the United Kingdom. *J. Natl. Compr. Canc. Netw.* **10 Suppl 2**, S69-74 (2012).
387. Mew, D., Wat, C. K., Towers, G. H. & Levy, J. G. Photoimmunotherapy: treatment of animal tumors with tumor-specific monoclonal antibody-hematoporphyrin conjugates. *J. Immunol.* **130**, 1473–7 (1983).
388. Hemming, A. W., Davis, N. L., Dubois, B., Quenville, N. F. & Finley, R. J. Photodynamic therapy of squamous cell carcinoma. An evaluation of a new photosensitizing agent, benzoporphyrin derivative and new photoimmunoconjugate. *Surg. Oncol.* **2**, 187–96 (1993).
389. Hamblin, M. R., Del Governatore, M., Rizvi, I. & Hasan, T. Biodistribution of charged 17.1A photoimmunoconjugates in a murine model of hepatic metastasis of colorectal cancer. *Br. J. Cancer* **83**, 1544–51 (2000).
390. Bhatti, M. *et al.* Targeted photodynamic therapy with multiply-loaded recombinant antibody fragments. *Int. J. Cancer* **122**, 1155–1163 (2008).
391. Jiang, F. N., Jiang, S., Liu, D., Richter, A. & Levy, J. G. Development of technology for linking photosensitizers to a model monoclonal antibody. *J. Immunol. Methods* **134**, 139–49 (1990).
392. Savellano, M. D. *et al.* Photodynamic tumor eradication with a novel targetable photosensitizer: strong vascular effects and dependence on treatment repetition versus potentiation. *Photochem. Photobiol.* **89**, 687–97
393. Rakha, E. A. *et al.* Expression of mucins (MUC1, MUC2, MUC3, MUC4,

- MUC5AC and MUC6) and their prognostic significance in human breast cancer. *Mod. Pathol.* **18**, 1295–304 (2005).
394. Gendler, S., Taylor-Papadimitriou, J., Duhig, T., Rothbard, J. & Burchell, J. A highly immunogenic region of a human polymorphic epithelial mucin expressed by carcinomas is made up of tandem repeats. *J. Biol. Chem.* **263**, 12820–3 (1988).
395. Spencer, D. I. R. *et al.* Effect of glycosylation of a synthetic MUC1 mucin-core-related peptide on recognition by anti-mucin antibodies. *Cancer Lett.* **100**, 11–21 (1996).
396. Burchell, J. & Taylor-Papadimitriou, J. Effect of modification of carbohydrate side chains on the reactivity of antibodies with core-protein epitopes of the MUC1 gene product. *Epithelial Cell Biol.* **2**, 155–62 (1993).
397. Stoner, G. D. *et al.* Establishment and characterization of SV40 T-antigen immortalized human esophageal epithelial cells. *Cancer Res.* **51**, 365–371 (1991).
398. Underwood, T. J. *et al.* A comparison of primary oesophageal squamous epithelial cells with HET-1A in organotypic culture. *Biol. Cell* **102**, 635–644 (2010).
399. Palanca-Wessels, M. C. *et al.* Genetic analysis of long-term Barrett's esophagus epithelial cultures exhibiting cytogenetic and ploidy abnormalities. *Gastroenterology* **114**, 295–304 (1998).
400. Rockett, J. C., Larkin, K., Darnton, S. J., Morris, a G. & Matthews, H. R. Five newly established oesophageal carcinoma cell lines: phenotypic and immunological characterization. *Br. J. Cancer* **75**, 258–263 (1997).
401. Yahioglu, G., Stamati, I. & Deonarain, M. Compounds and biological materials and uses thereof. (2010).
402. Berenson, M. M., Johnson, T. D., Markowitz, N. R., Buchi, K. N. & Samowitz, W. S. Restoration of squamous mucosa after ablation of Barrett's esophageal epithelium. *Gastroenterology* **104**, 1686–91 (1993).

403. Sagara, M. *et al.* Expression of mucin 1 (MUC1) in esophageal squamous-cell carcinoma: Its relationship with prognosis. *Int. J. Cancer* **84**, 251–257 (1999).
404. Lloyd, K. O., Burchell, J., Yin, B. W. T., Kudryashov, V. & Taylor-papadimitriou, J. Products : Comparison of O -Linked Carbohydrate Chains in MUC-1 Mucin from Normal Breast Epithelial Cell Lines and Breast Carcinoma Cell Lines :: FEWER GLYCAN CHAINS IN TUMOR Comparison of O -Linked Carbohydrate Chains in MUC-1 Mucin from Normal Breast Ep. **271**, 33325–33334 (1996).
405. Ikeda, Y. *et al.* Expression of Sialyl-Tn antigens in normal squamous epithelium, dysplasia, and squamous cell carcinoma in the esophagus. *Cancer Res.* **53**, 1706–1708 (1993).
406. Fowler, J. C., Teixeira, A. S., Vinall, L. E. & Swallow, D. M. Hypervariability of the membrane-associated mucin and cancer marker MUC1. *Hum. Genet.* **113**, 473–9 (2003).
407. Dunn, J. M. *et al.* A randomised controlled trial of ALA vs. Photofrin photodynamic therapy for high-grade dysplasia arising in Barrett's oesophagus. *Lasers Med. Sci.* **28**, 707–15 (2013).
408. Bolin, F. P., Preuss, L. E. & Taylor, R. C. Optimization of photodynamic therapy light dose distribution and treatment volume by multi-fiber insertions. *Photochem. Photobiol.* **46**, 609–17 (1987).
409. Shackley, D. C. *et al.* Light penetration in bladder tissue: implications for the intravesical photodynamic therapy of bladder tumours. *BJU Int.* **86**, 638–43 (2000).
410. Savellano, M. D. & Hasan, T. Targeting cells that overexpress the epidermal growth factor receptor with polyethylene glycolated BPD verteporfin photosensitizer immunoconjugates. *Photochem. Photobiol.* **77**, 431–9 (2003).
411. Pye, H. *et al.* A HER2 selective theranostic agent for surgical resection guidance and photodynamic therapy. *Photochem. Photobiol. Sci.* **15**, 1227–1238 (2016).
412. O'Neil, B. H. *et al.* A phase II/III randomized study to compare the efficacy and safety of rigosertib plus gemcitabine versus gemcitabine alone in patients with

- previously untreated metastatic pancreatic cancer. *Ann. Oncol. Off. J. Eur. Soc. Med. Oncol.* **26**, 1923–9 (2015).
413. Su, Z. *et al.* Common variants at the MHC locus and at chromosome 16q24.1 predispose to Barrett's esophagus. *Nat. Genet.* **44**, 1131–6 (2012).
414. Dulak, A. M. *et al.* Exome and whole-genome sequencing of esophageal adenocarcinoma identifies recurrent driver events and mutational complexity. *Nat. Genet.* **45**, 478–86 (2013).
415. Wang, Z. *et al.* STAT3 is involved in esophageal carcinogenesis through regulation of Oct-1. *Carcinogenesis* **34**, 678–88 (2013).